Heat Assisted Machining of Nickel Base Alloys: Experimental and Numerical Analysis

Dissertation submitted in partial fulfillment

of the requirements of the degree of

Doctor of Philosophy

in

Mechanical Engineering

by

Asit Kumar Parida

(Roll Number: 512ME112)

Based on research carried out

Under the supervision of

Prof. Kalipada Maity

2017

Department of Mechanical Engineering

National Institute of Technology Rourkela

Department of Mechanical Engineering

National Institute of Technology Rourkela

Certificate of Examination

Roll Number: *512ME112*

Name: *Asit Kumar Parida*

Title of Dissertation: Heat Assisted Machining of Nickel Base Alloys; Experimental and Numerical Aanalysis. We the below signed, after checking the dissertation mentioned above and the official record book(s) of the student, hereby state our approval of the dissertation submitted in partial fulfillment of the requirements of the degree of *Doctor of Philosophy* in *Mechanical Engineering* at *National Institute of Technology Rourkela*. We are satisfied with the volume, quality, correctness, and originality of the work.

D.R.K. Parhi	*Kalipada Maity*
Chairman (DSC)	Principal Supervisor

S.K. Sahoo	*D.P. Mohapatra*	*Mithilesh Kumar*
Member (DSC)	Member (DSC)	Member (DSC)

Department of Mechanical Engineering

National Institute of Technology Rourkela

Supervisor's Certificate

This is to certify that the work presented in this dissertation entitled "*Heat Assisted Machining of Nickel Base Alloys: Experimental and Numerical Analysis*" by "*Asit Kumar Parida*, Roll Number 512ME112, is a record of original research carried out by him under my supervision and guidance in partial fulfillment of the requirements of the degree of *Doctor of Philosophy* in *Mechanical Engineering*. Neither this dissertation nor any part of it has been submitted for any degree or diploma to any institute or university in India or abroad.

Supervisor's Signature

Kalipada Maity

Dedication

To

“*My Parents*”

Signature

Declaration of Originality

I, *Asit Kumar Parida*, Roll Number *512ME112* hereby declare that this dissertation entitled "*Heat Assisted Machining of Nickel Base Alloys: Experimental and Numerical Analysis*" presents my originality work carried out as a doctoral student of NIT Rourkela and, to the best of my knowledge, contains no material previously published or written by another person, nor any material presents by me for the award of any degree or diploma of NIT Rourkela or any institution. Any contribution made to this research by others, with whom I have worked at NIT Rourkela or elsewhere, is explicitly acknowledged in the dissertation. Works of other authors cited in this dissertation have been duly acknowledged under the sections "Reference" or "Bibliography". I have also submitted my original research records to the scrutiny committee for evaluation of my dissertation.

I am fully aware that in case of any non-compliance detected in future, the senate of NIT Rourkela may withdraw the degree awarded to me on the basis of the present dissertation.

2017

NIT Rourkela *Asit Kumar Parida*

Acknowledgment

The journey of reaching any milestone is never easy without a determined ambition, sincere dedication and a perfect person who can torch your path of ignorance. I am obliged to Prof. Kalipada Maity for being an embodiment of the constant source of inspiration and knowledge. Under the guidance, I have learnt the art of doing research and the real value of life.

I must thank, Director, NIT Rourkela for his motivational speeches at regular interval of my tenure. At the same time, I am thankful to the teaching staffs of the department, whose valuable suggestion at the right time helped me reaching the goal.

I sincerely acknowledge the helping hand of the laboratory staffs and other non teaching staffs of NIT Rourkela, for their timely help and support. My friends, whose consolation during the bad days and encourage words, helped me maintain the equilibrium during the course of fulfilling my ambition.

Lastly, I must thank the invisible force which we define as the almighty god for giving me patience and driving me towards never ending process of learning.

2017

NIT Rourkela *Asit Kumar Parida*

Abstract

Nickel base alloys are frequently used in aerospace industries, marine, biomedical application and other demanding industries due to their high strength, high hardness, resistant to corrosion and ability to withstand at elevated temperature. But machining of these materials in conventional way impairs severely their machinability due to certain inherent properties like low thermal conductivity, high chemical affinity and presence of hard particles in the microstructure etc. Therefore, tool life is reduced, due to the abrasion wear from the hard particles and high temperature of the tool-chip interface due to diffusion wear during machining of nickel base alloys.

In this work, hot machining is introduced for processing of nickel base alloys like Inconel 718, Inconel 625, and Monel 400. In this technique, heating on the workpiece is combined with conventional turning process was used to enhanced machinability of nickel base alloy without compromise quality and productive. The study revealed that the influence of the workpiece temperature on the workpiece surface enhanced machining performance in terms of better surface finish, MRR, and reduction of forces, wear compared to conventional turning process. The surface integrity has been studied in terms of surface roughness, and microhardness beneath the machined surface in hot machining operation. Finite element modeling was also employed to prediction of cutting force, temperature distribution, stress, in hot turning of Inconel 718. The finite element results were compared with the experimental value and close agreement was found. In any industries production of parts along with tool life, surface finish is the major concern. In order to optimize the machining of nickel base alloys, optimization technique was performed using desirability and principal component analysis. Finally, machinability comparison was made between three materials, in order to understand effect of machining parameters along with workpiece temperature. In the literature, no research studies were found on flame heat machining of nickel base alloys (Inconel 625, Inconel 718 and Monel 400). The research led to various contributions to finding in terms of experimental investigation, optimization and FEM modeling. The contribution of the thesis should be of interest who works in the areas of machining of hard materials.

Keywords: Nickel alloys, Finite element analysis, Cutting force, Tool life, Hot turning, Response surface methodology, Optimization

Contents

List of Figures

List of Tables

Nomenclature

V_c	Cutting speed
f	Feed rate
a_p	Depth of cut
T	Temperature
β	Shear angle
γ_0	Back rake angle
η	Friction angle
t	Uncut chip thickness
t_c	Chip thickness
r	Chip thickness ratio
ξ	Chip reduction coefficient
F_c	Cutting force
F_T	Thrust force
F_s	Shear force
N_S	Normal force perpendicular to shear plane
F	Frictional force along the tool face
N	Normal friction force
μ	Coefficient of friction
w	Width of chip
σ_n	Normal stress
P_c	Cutting power
E_c	Cutting energy
Q_p	Heat generated in primary shear zone
Q_S	Heat generated in secondary zone
Q	Total heat generated during machining
τ	Shear force acting on the rake face
T_{PZ}	Temperature in the primary zone
S	Specific heat
ρ	Density
T_w	Initial workpiece temperature
T_{wd}	Temperature of the heat exchange window
A	Area of heat exchange window

h	Heat convention coefficient
k	Proportion of heat conducted into the workpiece
γ	Gamma phase
$\dot{\gamma}$	Gamma prime phase
$\ddot{\gamma}$	Gamma double phase
D_S	Degree of segmentation ratio
H_{max}	Maximum height of the serrated chip
H_{min}	Minimum height of the serrated chip
L	Undeformed surface length
f_S	Segmentation frequency
R_a	Surface roughness
VB_{max}	Flank wear
d_i	Individual desirability Index
d_G	Composite desirability Index
σ	Flow stress
T_{melt}	Melting temperature
T_{Room}	Room temperature
$\bar{\varepsilon}$	Equivalent plastic strain
$\dot{\bar{\varepsilon}}$	Plastic strain rate
$\dot{\bar{\varepsilon}}_0$	Reference equivalent plastic strain rate
τ_0	Shear yield stress
P	Pressure
V_r	Relative slip velocity
ε_f	Equivalent failure strain
$F-value$	Fisher value
$P-value$	Probability value

Abbreviations

HRC	Rockwell hardness
DOE	Design of experiment
RSM	Response surface methodology
BUE	Built up edge
DoF	Degree of freedom
FEM	Finite element analysis
FCC	Face cubic center
CCD	Central composite design
CRC	Chip reduction coefficient
MS	Mean square
SS	Sum of square
SR	Surface roughness
MRR	Material removal rate
EDM	Electro discharge machining
ECM	Electro chemical machining
WEDM	Wire electro discharge machining
OA	Orthogonal array
PCA	Principal component analysis
DFA	Desirability function analysis
GRA	Grey relational analysis
ANOVA	Analysis of variance
PAM	Plasma assisted machining
GAM	Gas flame assisted machining
IAM	Induction assisted machining
EAM	Electric assisted machining
LAM	Laser assisted machining
LPG	Liquefied petroleum gas
HAZ	Heat affected zone
SHZ	Strain hardening zone
PMZ	Parent metal zone
MPCI	Multiple performance characteristics index

Chapter 1

Introduction

1.1 Introduction

Machining of hard materials like titanium base alloy, nickel base alloys, hardened steels possesses big challenge to the industries nowadays. The excellent mechanical properties, like high wear resistance, high corrosion resistant, ability to withstand at elevated temperature and high hardness under high load allow the application of nickel base alloys in a wide area [1]. Nickel base alloys become popular in the aerospace, bio medical equipment, marine and nuclear sector etc. Nevertheless, these unique mechanical properties of nickel base alloys provide some unfavorable effects on machinability issues. The modern machine tool technologies have given new strategies for machining of hard components. The benefits of advanced technologies are excepted to be substantial in the context of machining cost and time compared to the traditional machining, but there are some difficulties such as high setup cost, low material removal rate, high skilled operators etc., which hurdle to the industries. Nickel components could be machined by using non-conventional techniques like EDM, ECM etc., but the cost of the setup is very much expensive compared to a traditional setup.

The current study is aimed at evaluating good technique that was adopted to improve the machinability of nickel base alloys. Hot machining is a technique, in which the material is heated before or during the machining operation, as a result, there is reduction of shear strength due to thermal softening of the material [2]. Three different types of nickel base alloys have been used for experimental investigation and modeling of hot turning operation. Those alloys include Inconel 718, Inconel 625 and Monel 400. The alloys were machined at different cutting conditions with on line heating to determine tool wear, tool life, surface finish, forces, chip temperature, chip tool contact length and chip morphology etc. Furthermore, FEM analysis was carried out to study the physical parameters such as cutting forces, temperature, tool wear, stresses distribution in machining in conventional and hot conventional turning operation.

The research work also focused on the modeling and optimization of machining of nickel base alloys. Response surface methodology (RSM) has been used for modeling hot

machining of three alloys. Stastically taguchi method, coupled with principal component analysis (PCA) and desirability methods was used to optimize the machining inputs (speed, feed, depth of cut and workpiece temperature) parameters.

1.2 Problem statement

A lot of works on tool wear mechanism, surface finish, and effect of machining parameters on hard machining has been carried out by many researchers. There are so many methods have been used for machining hard materials such as non-traditional (EDM, ECM), grinding, hard turning, hot machining, and cryogenic machining. However, investigations for machinability enhancement have received less attention in machining of nickel base alloys using hot machining method. Machinability of nickel base alloys is poor due to excessive tool wear, high heat generation during machining and poor quality of the machined surface. The proposed hybrid technique i.e. heating of workpiece surface and conventional turning could be a viable means of improving the machinability of the nickel base alloys. Further, no work on numerical simulation of gas assisted hot machining operation has been carried out. A few optimization techniques have been used to optimize the hot machining parameters.

1.3 Objective and aim of the study

The main objective of the present work is to investigate heating combined with conventional turning process of nickel base alloys. The effect of workpiece surface temperature on turning of nickel base alloy (Inconel 718) was simulated using finite element method and the machining parameters were optimized using different optimization techniques. The specific objective of the work can be described as follows:

- To carry out an experimental investigation of hot machining of nickel base alloys such as Inconel 718, Inconel 625 and Monel 400 using flame heating technique and compare with machining at room temperature.
- To study the machinability criteria of nickel base alloys such as tool life, tool wear, cutting forces, surface finish and chip morphology using hot machining operation.
- To determine optimum process parameters to maximize tool life, surface finish and to minimize cutting forces of nickel base alloys.

- To study surface integrity of the workpiece in term of microhardness and microstructure both for hot machining and room temperature.
- To develop FEM of 2D and 3D turning for the analysis of cutting forces, and chip morphology using hot turning operation;
- To determine optimization process parameters to obtain the multi-response objective;

1.4 Structure of dissertation/thesis

The Thesis consists of eight chapters.

Chapter 1 has provided an introduction to research aims, objectives and basic theory of machining. The basic theory of metal cutting, cutting tool and type of chip formations in turning process, analysis of cutting force, and heat generation are discussed.

Chapter 2 has provided a critical review of the current research on the machinability of high strength materials. The literature review concerning the various heating method used in hot machining process like gas flame heating, electric arc, plasma arc, laser etc., followed by chip formation, developments in FEM analysis of machining processes and various optimization techniques used in the machining process have been discussed.

Chapter 3 has described the experimental setup and carrying out investigation. Experimental investigation and modeling of Inconel 718 were carried out in this chapter.

Chapter 4 has highlighted the experimental work and modeling method used in the hot turning of Inconel 625. The effect of heating on forces, chip morphology, surface roughness and tool life has been analyzed.

Chapter 5 deals with the experimental work used in hot turning and conventional turning of Monel 400. Modeling and optimization have been carried out to optimize the machining parameters to achieve the multi-objective response criteria.

Chapter 6 has incorporated the various features of 2D and 3D finite element modeling of turning processes. Both conventional turning and hot turning has been investigated to study the effect of cutting parameters specially workpiece temperature on cutting forces, chip thickness, stress, temperature in chip, tool wear, chip tool contact length etc., during machining of Inconel 718.

Chapter 7 describes the comparison between the machinability of three materials during hot machining has been carried out.

Chapter 8 deals with the conclusion of the present work and future work

1.5 Basic theory of metal cutting and collection of machining variables

Removing material from the parent material in the form of chip and giving a desired shape is called metal machining, is one production process used in industries. There are different metal removal processes to shape the machined component used in industries. Some of the conventional machinings are turning, milling, drilling, broaching etc., and there are non-conventional processes such as EDM, ECM, EBM and LBM etc. Though non-conventional machining processes are having high efficiency, and accuracy, but high investment cost is necessary. The skill of the operator is an obstacle to the above process. Among the conventional processes, turning operation is widely used to machine workpiece materials. In turning operation, the cutting tool is fixed to the tool post and workpiece revolves in axial direction and feed is given to shape the materials is shown in Fig 1.1. There are some parameters to be set in lathe machine for carrying out turning operation.

Cutting speed: Cutting speed in turning operation is defined as the speed at which the workpiece moves with respect to the tool. It is related to the spindle revolution, and workpiece diameter through the formula

$$V_c = \frac{\pi DN}{1000} \qquad (1\text{-}1)$$

where, *Vc*: Cutting speed (m/min), *D*: Diameter (mm), *N*: Spindle speed (rpm)

The temperature generation in the cutting zone rises rapidly as cutting speed increases and reach a maximum value at the cutting edge. A thermo-plastic shear band is formed at the tool rake face in critical speed range.

Feed rate: Feed rate in turning operation is the axial movement of tool per one revolution of work piece. Feed rate may be as low as 0.0125 mm/rev and with very high up to 2.5 mm/rev. Cutting forces, cutting temperature, and tool wear are larger at larger feed.

Depth of Cut: It is the distance that the tool bit moves into the workpieces. The depth of cut in machining operation may vary for different workpiece and tool material. An increase of depth of cut reduces the tool life.

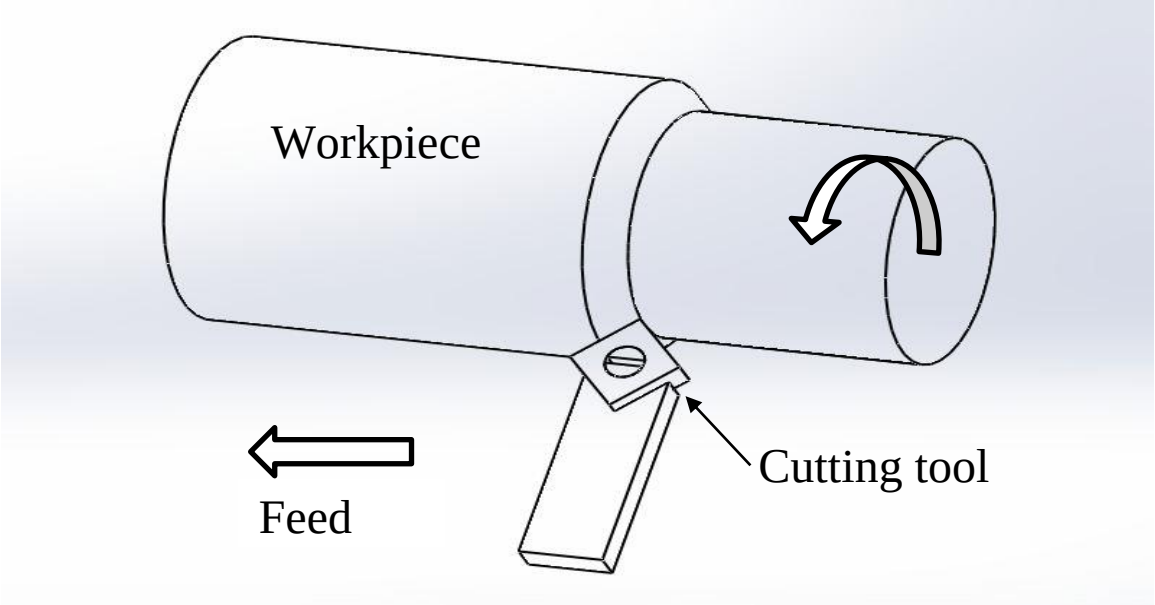

Figure 1.1 Schematic diagram of turning operation

In machining operation, there are two types of cutting operation used to analyse the mechanics of machining. The angle of cutting edge with cutting velocity direction is the main difference between the two processes. In orthogonal cutting, the cutting edge of the tool is perpendicular to the cutting velocity direction, whereas cutting edge of the tool make some angle with cutting velocity in oblique cutting (in Fig 1.2) [3].

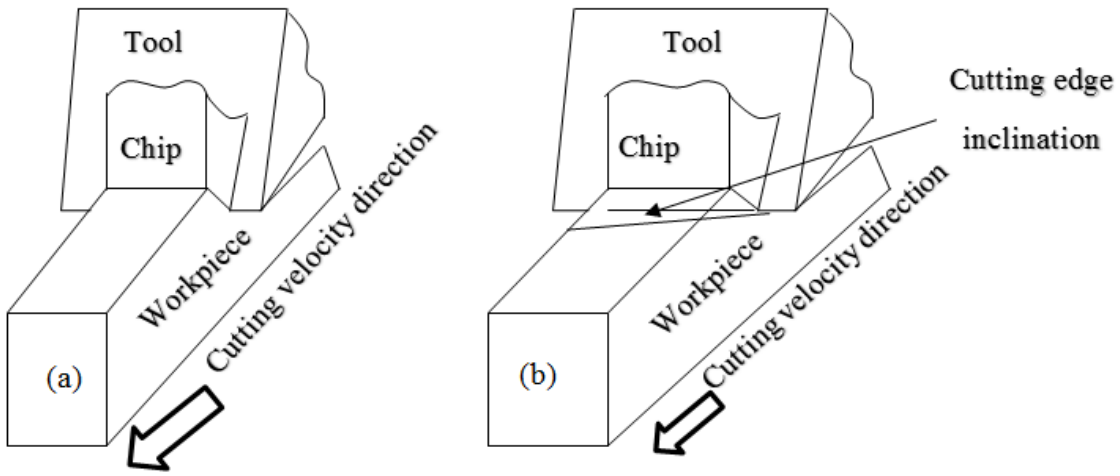

Figure 1.2 Types of cutting operation (a) Orthogonal (b) Oblique

1.5.1 Types of chips produced during machining

In metal removal process, the unwanted material is removed from the workpiece surface in the form of chips. Basically, there are four types of chips formed in any machining processesas shown in Fig 1.3.

Discontinuous chip

The discontinuous chip is formed while machining of hard and brittle materials. The main reason is the deformation due to repeated fracture. This type of chip formation is considered to be ideal for machining system as it does not harm to the operator. The disposal is good compared to continuous chips. Factors affects the formation of discontinuous chips are non-ductile/brittle materials, low cutting speed, small rake angle, large feed, large depth of cut and high friction at the chip tool interface etc.

Continuous chip

Machining of ductile material at high cutting speeds with large rake angles produce continuous chip formation. Although the continuous chip is not always desirable because it may harm to the operator, but generally it produces a better surface finish. Continuous chips tend to become wound around the workpiece, tool post, and disposal system is not good. Factors affecting formation of continuous chips are high cutting speed, large rake angle, ductile material, low friction between tool chip interface, low feed, and low depth of cut etc.

Continuous chip with built-up edge

In machining of ductile material at low cutting speed, layers of material from the workpiece attached to the tip of the tool during machining. It became as cutting edge instead of actual cutting edge. Although the formation of built-up-edge (BUE) enhanced the tool life but it decreased the surface finish of the job. The chips are very similar to the ribbon type's chips and it protects the cutting edge from wear. Factors affecting the formation of continuous chip with built-up-edge are low cutting speed, high friction at the chip-tool interface, small rake angle and ductile material.

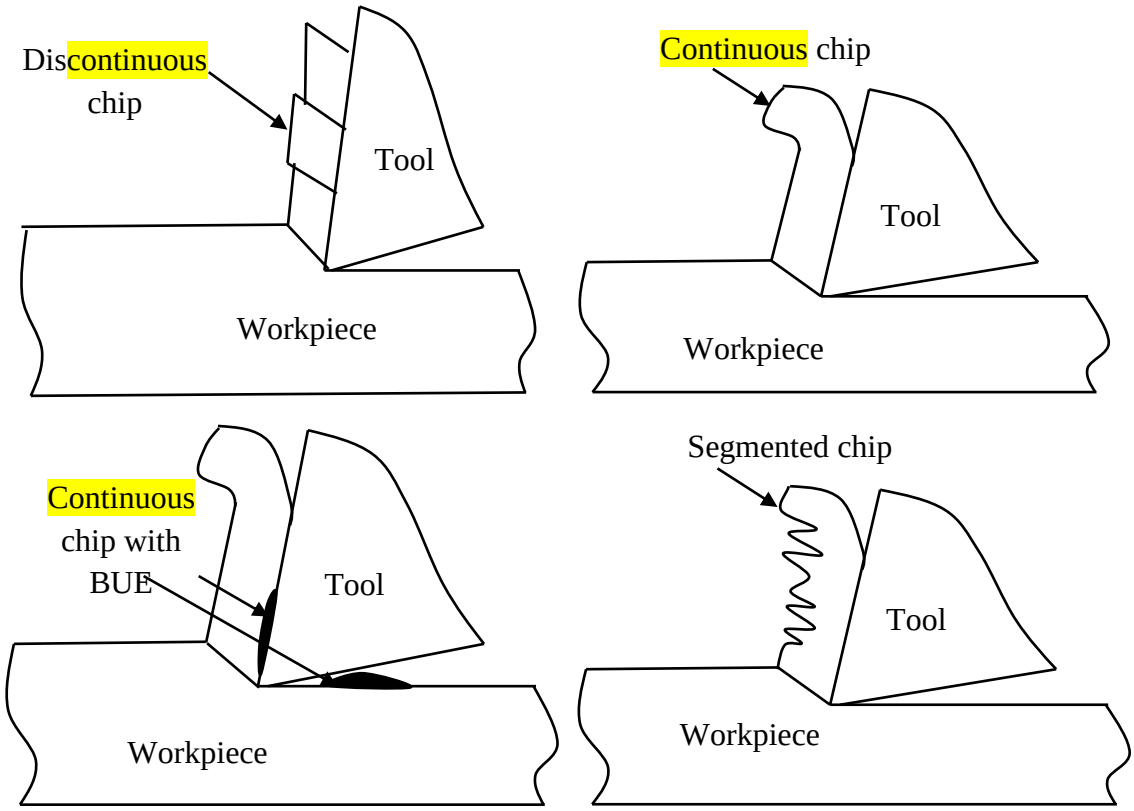

Figure 1.3 Different modes of chip formation in metal cutting [4]

Although generally above three types of chip formation are observed in machining operation, but in machining hard materials like nickel and titanium base alloys, there is the formation of segment types of chips due to low thermal conductivity of the materials. The chip variation in thickness and continuous form is called a segmental chip. It depends upon the microstructure and material composition of the workpiece. The segment chip is normally formed within the certain range and machining condition. The same type of chip is also formed due to vibration. Due to self-excited vibration or chatter, there is a cyclic variation of undeformed chip thickness in the chips and formed wavy structure. The wavy chip is resembling a harmonic wave and symmetrical in nature. This type of chip is formed due to low rigidity and damping of the machine tool system.

1.5.2 Cutting tool

It is wedge shape that has one or more cutting edges used in the metal cutting operation. The selection of cutting tool for a particular operation is a crucial part of any operation. High hot hardness, strong mechanical properties are the main characteristics of any cutting tool. Although a cutting tool should have above properties, but based on requirement and operation conditions, different types of tool are used in the different operation.

Cutting tool geometry

A cutting tool is defined by its geometry. Various angle of cutting tool is shown as Fig.1.4. An angle between a line parallel and passing the tip of cutting tool and rake face is called back rake angle.

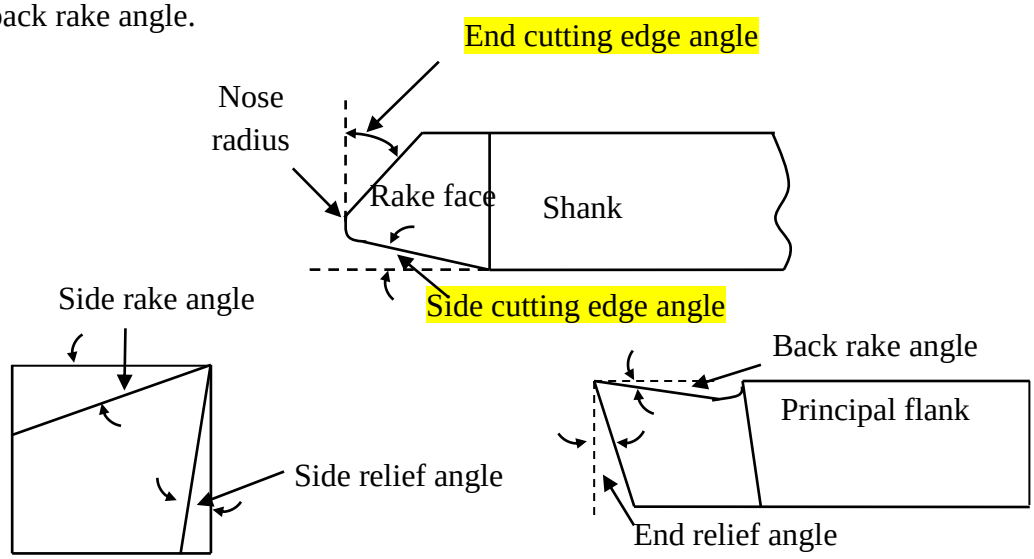

Figure 1.4 Cutting tool geometry [4]

The angle of rake face may be positive, negative, or zero. Negative rake angle is usually recommended for machining hard material as it strengthened the cutting tool. Generally, low nose radius tool generates less chatter compared to higher nose radius tool.

1.5.3 Cutting forces in machining

The shear deformation during machining was analyzed by merchant and it was based on principle of minimum energy. Angle of shear is determined as follows

$$Cot\beta = \frac{\xi - \sin\gamma_0}{\cos\gamma_0} \qquad (1\text{-}2)$$

where, β – shear plane angle, γ_0 – orthogonal rake angle, and ξ – chip reduction coefficient and it can be calculated as

$$\xi = \frac{t_c}{t} \qquad (1\text{-}3)$$

Merchant force equilibrium diagram is given in Fig.1.5.

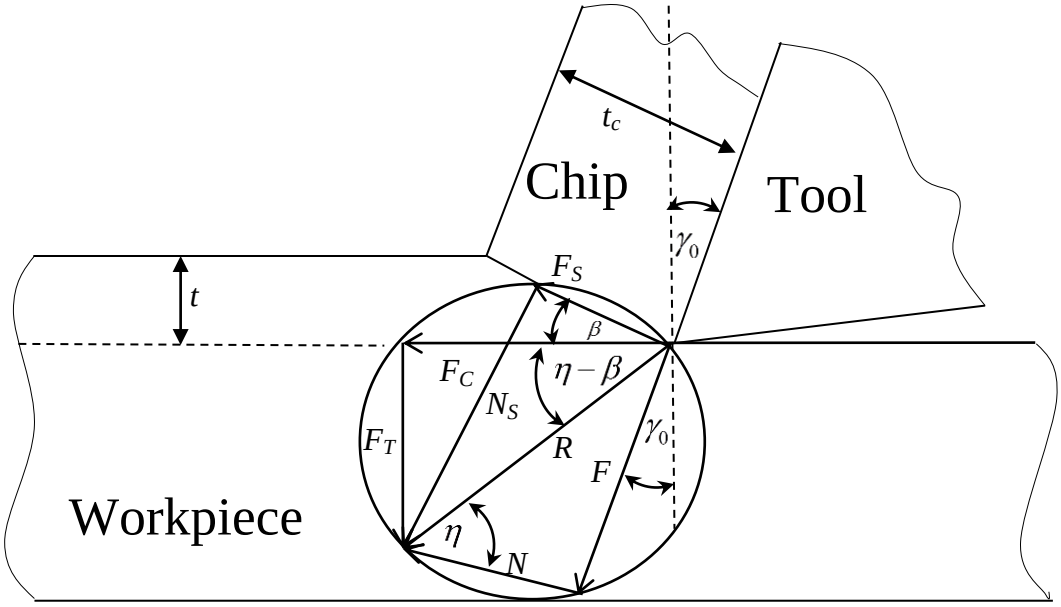

Figure 1.5 Merchant's force equilibrium diagram [4]

F_c = Cutting force measured during machining

F_T = Thrust force measured during machining

F_s = Shear force along the shear plane

N_S = Normal force perpendicular to the shear plane

F = Frictional force along the tool face

N = Normal friction force

τ_S = Shear stress

t_c = Chip thickness

μ = Coefficient of friction

t = Uncut chip thickness

w = Width of chip

The force component in the shear plane and tool faces are related to the cutting forces and thrust force

$$F_s = F_c \cos\beta - F_T \sin\beta \quad (1\text{-}4)$$

$$N_s = F_T \cos\beta + F_c \sin\beta \quad (1\text{-}5)$$

$$F = F_c \sin\gamma_0 + F_T \cos\gamma_0 \quad (1\text{-}6)$$

$$N = F_c \cos\gamma_0 - F_T \sin\gamma_0 \quad (1\text{-}7)$$

The coefficient of friction μ can be determined as

$$\mu = \frac{F}{N} = \frac{F_c \sin\gamma_0 + F_T \cos\gamma_0}{F_c \cos\gamma_0 - F_T \sin\gamma_0} = \frac{F_T + F_c \tan\gamma_0}{F_c - F_T \tan\gamma_0} \quad (1\text{-}8)$$

The normal stresses can also be determined as

$$\sigma_n = \frac{N_S}{wt}\sin\beta \quad (1\text{-}9)$$

When the shear angle is predicted and the geometry is fixed, the cutting force and thrust force can be determined from the geometry for certain shear flow stress of material

$$F_c = \frac{\tau_S wt \cos(\eta - \gamma_0)}{\sin\beta\cos(\beta + \eta - \gamma_0)} \quad (1\text{-}10)$$

$$F_T = \frac{\tau_S wt \sin(\eta - \gamma_0)}{\sin\beta\cos(\beta + \eta - \gamma_0)} \quad (1\text{-}11)$$

The cutting power P_c can be calculated as

$$P_c = F_c V_c \quad (1\text{-}12)$$

It is the energy required for plastic deformation of the workpiece material, during metal cutting operation per unit time.

1.5.4 Heat generation during machining processes

There are three zones heat generated in machining process, (i) primary zone in the shear plane, (ii) secondary zone at the chip tool interface (iii) tertiary zone at the tool and machined surface.The heat generated from three zones is shown in Fig 1.6. Heat generated

in machining can be determined by measuring the cutting forces. The rate of energy consumption in machining is given by

$$E_c = F_c V_c \qquad (1\text{-}13)$$

F_c is the cutting force in newton and V_c is the cutting velocity in m/min

In machining processes, it is assumed that mechanical work done is converted into heat. So amount of heat generated in primary zone may be calculated from the energy consumption

$$Q_p = E_c = F_c V_c \qquad (1\text{-}14)$$

where Q_p = Heat generated in the primary shear zone

In secondary shear zone, the heat generated due to work calculated from the friction is given by

$$Q_s = \left(\tau_S . V_c / r\right) \qquad (1\text{-}15)$$

where τ is the shear force acting on the rake face and *r* is the chip thickness ratio

Total heat generated in machining is calculated by

$$Q = Q_p + Q_s \qquad (1\text{-}16)$$

80-85% heat is transferred to the chip. The temperature of the tool was the highest at some distant from the tip and the temperature of the chip was the highest at the exit point of the secondary deformation zone. So, the temperature of the chip can be the sum of the initial temperature of the workpiece, the temperature rises in the primary deformation zone and secondary zone respectively.

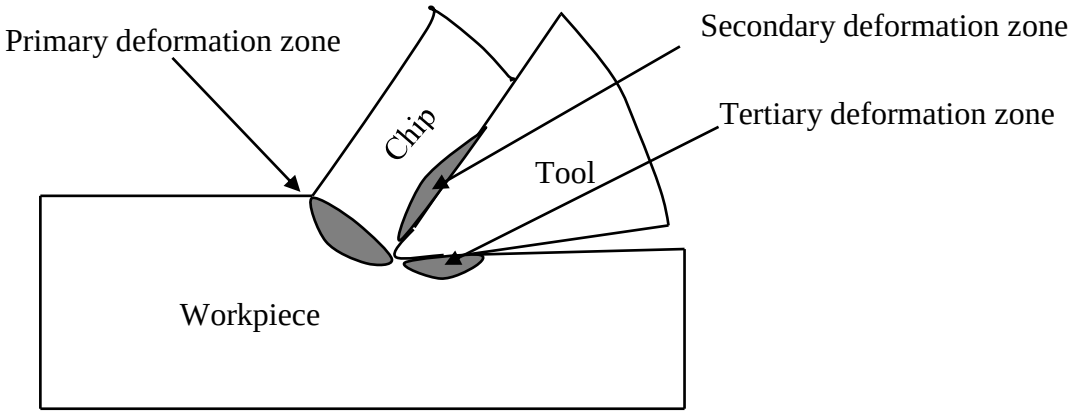

Figure 1.6 Heat generation in machining process [5]

1.5.5 Cutting temperature

The cutting temperature in machining affects the tool life, part quality, chip morphology, etc. During machining high temperature is generated in the shearing zone, which influence on the rate of wear of the cutting tool. When material is deformed elastically, the energy required for the operation is stored in the material as strain energy, and no heat is generated. However, when the material is deformed plastically, the energy is converted into heat [5]. There are three zones, where energy is accumulated. These are primary shear zone, chip-tool interface region, and tool-work interface region. It is noticed that each of these three zones lead to the ascent of temperature at the chip tool interface. It is found that the most extreme temperature happens somewhat far from the cutting edge. This temperature causes formation crater on the tool face. The rise in temperature in cutting tool and chip-tool interface are due to heat generated in both primary and secondary shear zone. In machining different methods like analytical, numerical and finite element analysis were used to model the temperature distribution of the process zone. Tay et al. [6] calculated temperature distribution from force and shear angle measurements in machining. The average temperature in the primary zone $\left(T_{pz}\right)$ is given by Eq. (1-17)

$$T_{pz} = T_w + \frac{1 - kF_s \cos\gamma_0}{\rho Stw \cos(\beta - \gamma_0)} \tag{1-17}$$

where T_w is the initial workpiece temperature, k is the proportion of heat conducted into the workpiece, ρ is the density and S is the specific heat of the workpiece.

The average temperature rise in the chip is given by Eq. (1-18)

$$\Delta T_c = \frac{F \sin\beta}{\rho Stw \cos(\beta - \gamma_0)} \tag{1-18}$$

where F is the friction force at the interface and w is the width of the chip

Both experimentally and theoretically, study of temperature at the cutting zone were studied by Childs et al. [7]. The investigating on coolant effect on temperature distribution in machining has been carried out and observed that the tool temperature was sensitive to heat transfer coefficient and effect of coolant was the least on the rake face, where maximum rake face temperature reduced. Sumer et al. [8] compared the temperature

distribution in the cutting zone using two different type of drill types (stainless steel and ceramic). The stainless steel drill bit generated less heat compared to ceramic drill at the depth of 3 mm but no significant difference when compared to 6 and 9 mm depths. There has beenlot of investigations on temperature distribution in the cutting zone using finite element method. The temperature in orthogonal machining was studied using the photographic technique. Workpiece material, and machining variables greatly influence the heat generation in the cutting zone [9]. There are different methods for calculating temperature measurement. Some of methods are radiation pyrometers, embedded thermocouples, metallographic techniques, calibration of chip-tool thermocouple

Among all above methods, the tool work thermocouple technique is the most widely used for the measurement of the average chip-tool interface temperature. Though all other methodsare quite good for measurement of temperature, but they fail to determine like, slow response, indirectness, and complications in measurement.

Chapter 2

Literature Review

2.1 Introduction

In this chapter a general review of nickel base alloy, classification, application, mechanical and metallurgical properties of alloys are studied. A brief review of the machinability of nickel base alloys, different heating process used in hot machining, and different modeling and optimization techniques used in machining of hard materials has also been discussed.

2.2 Classification of nickel base alloys

1. Commercially pure nickel alloys- Three-digit number (2xx, 3xx) are used as trade's names of commercial nickel. They are characterized by very good corrosion resistance and high ductility;
2. Non-heat-treatable nickel chromium iron alloys- (15-22% chromium and up to 46% iron) form a solid solution with nickel. The alloys are identified by their trade name: Inconel, Incoloy and Hastelloy. The alloys are hardened by cold work;
3. Heat treatable nickel chromium iron alloys- Nimonic, Inconel X-750, Astroloy, Waspaloy, are some example of this categories. This alloys are hardened by precipitation hardening due to presence of additional alloying element like aluminum, titanium, silicon;
4. Nickel-Copper alloys contain 30% copper, which forms a solid solution with nickel and accepted trade name of nickel copper alloys is called Monel;

2.3 Application of nickel base alloys

In recent years, the application of nickel base alloys are the most important development made in material engineering due to its excellent properties like light weight, high strength, high stiffness, high corrosion resistance and ability to withstand at elevated temperature. Nickel base alloys are now used in various engineering applications such as aerospace, marine, automotive, biomedical, and nuclear sector. Commercially available nickel-base superalloys include Inconel, Nimonic, Pyromet, Monel, and Hastalloy. Due to

their high specific stiffness, strength and light weight it is used in aerospace parts like (combustion chambers, exhaustive systems and blade etc. Nickel base alloy are used in a variety of parts in aerospace sectors like disks, combustion chambers, casings, exhaust systems, blades, vanes, burners stack gas reheater [10]. The overall application in different fields is shown in Fig 2.1. It is used in many parts in reciprocating engines (Turbochargers, exhaust valves, hot plugs, and heat treating equipment's). Due to its ability to withstand at elevated temperature, is used in furnace mufflers, nuclear power plants, heat exchangers, and conveyor belts etc., and due to its high corrosion resistance, it is often used in marine sectors and making biomedical equipment's, and automobile.

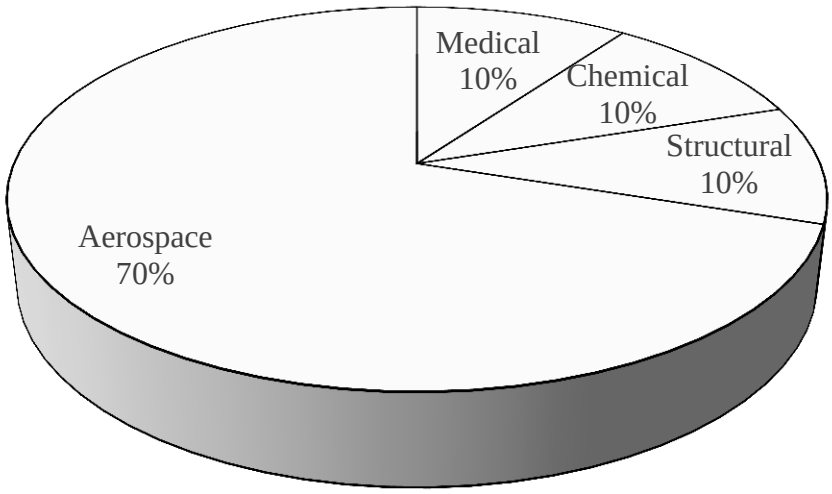

Figure 2.1 Superalloy consumption [10]

2.4 Mechanical and metallurgical properties

Nickel base superalloy has high temperature mechanical properties like high resistance, corrosion, ability to retain at elevated temperature. Nickel base alloys have density 8 g/cm^3, melting point above 1300ºC, coefficient of thermal expansion above 10 (µm/mºC) and thermal conductivity above 10 (W/mK). Nickel base alloy consists of gamma phase (γ), gamma prime phase ($\dot{\gamma}$), and gamma double phase ($\ddot{\gamma}$). The γ phase is a continuous matrix of an FCC nickel-base non-magentic phase. $\dot{\gamma}$ phase is addition of aluminum and titanium in amounts required to precipitate FCC. This phase is required for high temperature strength and creep resistance. Formation of second phase ($\ddot{\gamma}$) makes nickel base alloys stronger, abrasive and make more difficult to machine [11]. Generally,

nickel–base alloys are composed of 10 to 12 elements. Nickel base alloy contains chromium, aluminum, titanium, cobalt and molybdenum in varying quantities to give better performance [2]. Amount of alloy element, method of production, and heat treatment control the properties of nickel base alloys. There is large no of elements whose combinations produce desire effect in the superalloy. Some elements mix into solid solution to provide different strength; oxidation resistance (chromium and aluminum); hot corrosion resistance (titanium); phase stability (nickel) etc. By adding titanium and niobium, the γ' gamma phase formed, which is responsible for strength. The precise microstructural effects produced are function of processing and heat treatment. The strength of nickel base alloys has not only been a function of composition, it is also associated with method of melting, hot working conditions and heat treatment processes [2]. Nickel and titanium alloys increase hardness upon heat treatment and hence called age hardenable [10]. There are different mechanisms used to strengthen the nickel base alloy.

(a) Solid solution and precipitation hardening

Degree of mismatch between precipitate and matrix, precipitate order, precipitate size are some factor for strengthening the nickel base alloy. The principal precipitate phase in super alloys is γ'. Other types of intermetallic phases like δ orthorhombic Ni_3Nb have been observed increase the strength of nickel base super alloy.

(b) Carbide strengthening

Depending on the alloying elements and processing, there may be chance of formation of various carbides in the microstructure of superalloys like nickel based alloys.

(c) Oxide dispersion strengthening

The advantages of this method are to develop a protective oxide layer.

The variation of strength of Inconel 718 with respect to temperature is shown in Fig 2.2.

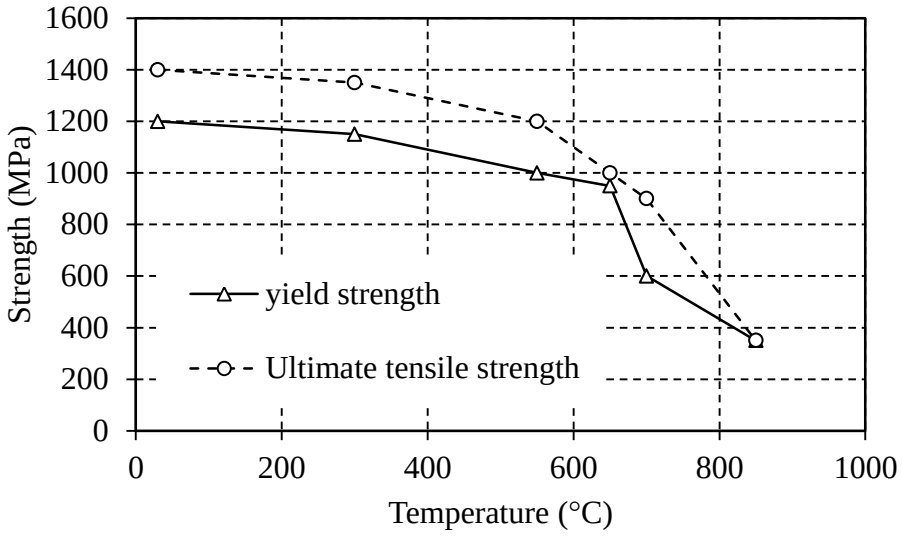

Figure 2.2 Temperature vs Strength of Inconel 718 [12]

2.5 Machining of high strength materials

Machining of high strength materials create a big challenge to machining industries due to excellent properties like high corrosion resistance, high hardness, ability to withstand to elevated temperature, low thermal conductivity and low thermal diffusivity [2]. So machining of these hard materials in conventional way is not possible due to rapid tool wear [13]. Machinability of nickel base alloy can be enhanced by taper turning, high pressure coolant, hot machining, cryogenic machining, self-rotary tooling etc. [11]. Fig 2.3 shows the different techniques used for machining hard materials. Though modern techniques can be used to machine hard materials and have many advantages, but due to high setup cost, skilled operator requirement, and low material removal rate production, which is not reliable to many industries. Many investigators studied machining of hard material using different techniques.

Wang et al. [14] studied machining of different hard materials using new technique called cryogenic machining. The application of liquid nitrogen coolant was applied in cutting region to reduce heat generation and friction. It was observed that surface roughness improved compared to without cryogenic machining. Khan and Ahmed [15] investigated the tool wear and mechanism in machining of stainless steel using cryogenic cooling and low cutting speed. It was observed that high tool wear occurred compared to high speed under cryogenic machining. The other researchers work on cryogenic machining to investigate other aspects of materials [16–18]. Machining of hard material using non-

conventional machining processes were studied by Ay et al. [19]. The effect of cutting parameters like pulse current and pulse duration on electro discharge machining of Inconel 718 was studied and found that compared to pulse duration, the pulse current was having more influence on the machining characteristics. Talla and Gangopadhayay [20] studied critical review of powder mixed electric discharge machining. It was observed that compared to conventional electro discharge machining process, powder mixed electro discharge machining gave better results in terms of better surface finish, and material removal rate.

Similarly, hard turning is another process used for machining hard material by different researchers. Tang et al. [21] studied the effect of cutting parameters on hard turning of AISI D2 steel using PCBN cutting tool. Different level of hardness of AISI D2 steel was taken and found that ploughing, and elastic deformation was the most prominent to surface roughness whereas depth of cut was not sensitive to the surface roughness. Aouici et al. [22] analyzed the effect of machining parameters on cutting force, power, and specific cutting force by ceramic insert on machining of AISI D3 steel. The experimental result was compared with the predicted surface response methodology (RSM) method and good agreement was observed. Karpat and Srivastava [23] analyzed the effect of different geometry of cutting tool in hard turning process. The variable geometry of tool reduced heat, plastic deformation and tool wear compared to uniform edge preparation. Pal et al. [24] measured the hardness of AISI 4340 steel for investigating machinability. Cutting forces decreased with decrease in hardness, feed and depth of cut was noticed.

Tamizharasan et al. [25] analyzed tool wear, tool life, material removal rate on hard turning process using of work material as PCBN tool. At larger depth of cut, and feed, white layer formation occurred when cutting edge radius is increased. Other investigators studied hard turning of high strength materials [26,27]. FEM of hard turning have been studied [28,29] in order to find cutting forces and other responses. Machining by hard turning gives better surface finish, high MRR, flexibility, no coolant or lubrication necessary, but only the disadvantage is the cost of tool is generally 10 to 20 times more than the conventional cutting tool. The oldest process for machining of hard materials is grinding. The disadvantage is with low material removal. The coolant and lubrication is needed for finishing operation in grinding operation, which is not environment friendly. The grinding performance like specific cutting force, grinding energy, etc. were studied by ZhenZhen et al. [30] for grinding of Inconel 718 on the basis porosity of wheel. Other

researchers work on grinding of high strength materials such as nickel base alloys, titanium base alloys [31–34].

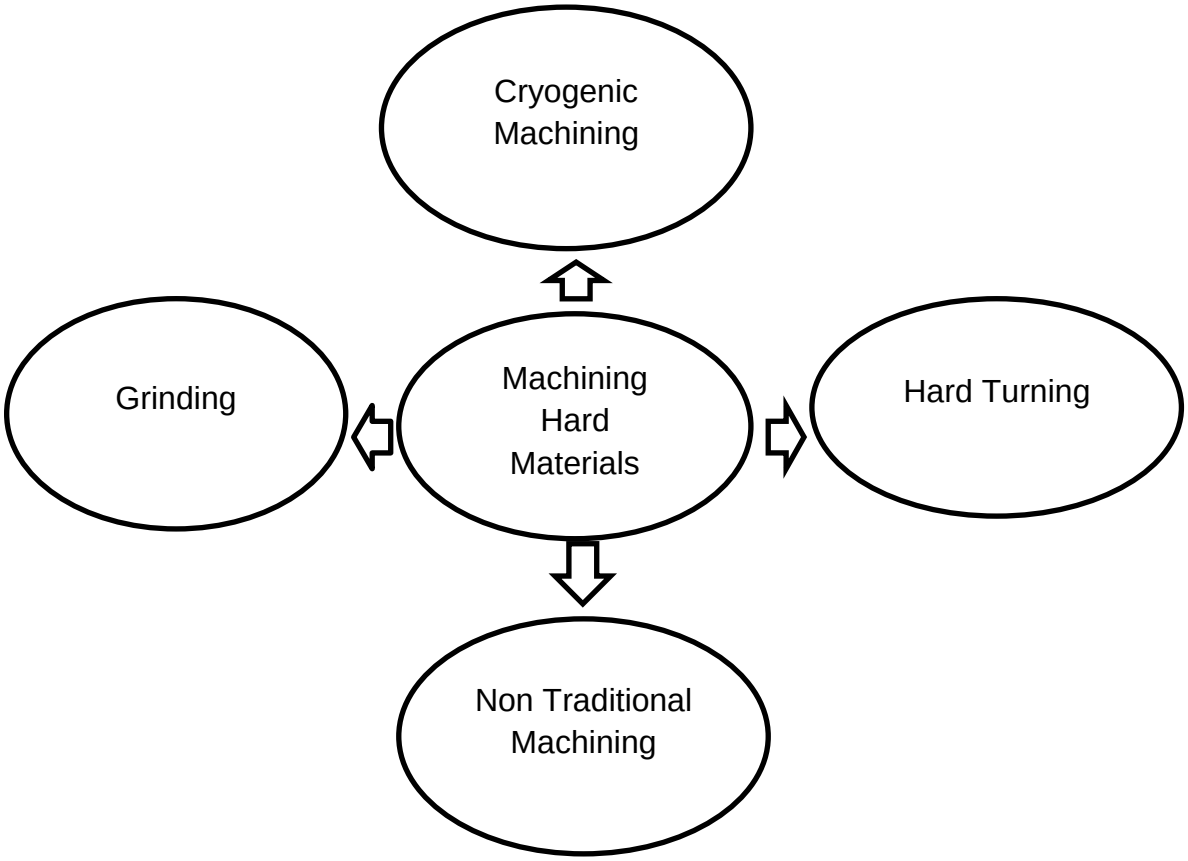

Figure 2.3 Different approaches in machining high strength material

2.6 Machinability issues of nickel base super alloys

The investigation on the machinability characteristics of nickel base super alloy such as cutting force, temperature generation, surface roughness, tool wear and surface integrity etc., were carried out by many researchers. Many investigators carried out experimental investigation during turning of nickel based super alloys like Inconel 718, Inconel 625, nimonic 75, hastelloy, nimonic C-263 etc., to determine machining characteristics. The main obstacles for machining nickel-base alloys are rapid tool wear due to high temperature generation at chip-tool interface, high strain hardening behavior, high tendency to weld with the cutting tool and formation of built-up-edge formation etc.

2.6.1 Tool performance aspects in machining hardened materials

In machining nickel base alloys, tool wear is affected by machining parameters, workpiece and cutting tool properties, cutting tool geometry, application of metal working fluid, etc. [2]. Tribological parameters like tool-chip and tool–workpiece interfaces are the different ways to correlate the tool wear. The dimension of tool life can be represented by the tool operating time, number of machine parts, overall area of the machined surface etc. There are many literatures on tool wear formation in machining of high strength materials. Kadirgama et al. [35] investigated the tool wear, tool life and surface finish using different types of coated cutting tools (PVD & CVD). The PVD coated tool performed better than CVD and was validated using FEM analysis. Fusova et al. [36] studied tool wear mechanism on high speed machining of nickel based alloy. The tool life of cutting tool was affected by increase of cutting speed. Abrasion, fracture, built-up edge and tribo-chemical effects are the main mechanism for tool wear. Kivak et al. [37] studied the effect of machining parameters on the drilling tests with uncoated different drill bits. A gradual tool wear increased with increase in cutting speed. Bushlya et al. [38] studied the wear mechanism of silicon carbide-whisker-reinforced alumina cutting tools on machining of Inconel 718 alloy. The notch wear was the most prominent wear for tool and chemical wear mechanism found for the degradation and decomposition of whiskers and formation of tribolayer on tool surfaces. Cracking of tool face and localized plastic deformation were observed for the tool deterioration.

2.6.2 Tool failure modes and wear mechanism

Due to low thermal conductivity, diffusivity, and high hardness characteristics of nickel base alloys, severe stress and temperature are generated in the cutting zone. The notch wear, diffusion wear, abrasion and adhesion wear are the dominant wear in machining of nickel base alloys.

Adhesion wear

Adhesion wear caused due to adhesion of workpiece material to the tool surfaces due to high temperature and stresses. At low speed, the generation of temperature is not too high to plastically deform material. Hence causes adhesion, but at high speed, diffusion and chemical wear mechanism become the main factor for tool wear [39]. Compared to low or high speed, the medium cutting speed is the favorable condition for adhesive wear. Qiao et

al. [40] studied the formation of adhesive layer and its effect on the wear of PVD (TiAlN) coated cemented carbide tool while machining Inconel 718 super-alloy in wet condition. They found that flank wear and notching wear was the main failure modes, and the main wear mechanism was adhesive wear. They observed that although adhesive wear did not occur on rake and flank faces of the tool but, its occurrence on the depth of cut location was the most severe. Many investigators reported this types of wear in machining of nickel base alloys [2,41,42]. A SEM image of adhesion wear in machining of nickel base alloys is shown in Fig 2.4.

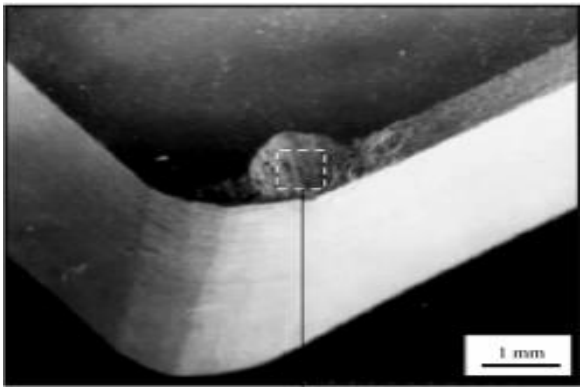

Figure 2.4 SEM image of adhesion wear formation [39]

Abrasive Wear

The presence of hard particles and plucking off particles from the tool material generally termed as abrasive wear. Qiao et al. [40] investigated machining of nickel base alloys at low speed and observed that flow of chips and work hardening properties of the material caused tool wear rapidly. Abrasive wear was found by other researchers in machining of nickel base alloys [43,44].

Chemical wear

Chemical reaction between the tool and workpiece material occurs at high temperature in modern alloys like nickel and titanium base alloys. This type of wear occurs generally at high temperature. The tool material starts soften due to wear and lose its properties. Chemical wear of cutting tool on machining nickel base alloys is shown in Fig 2.5. The discussion of chemical wear is less mentioned in the literature because correlations in diffusion wear with chemical wear mostly discussed by many researchers.

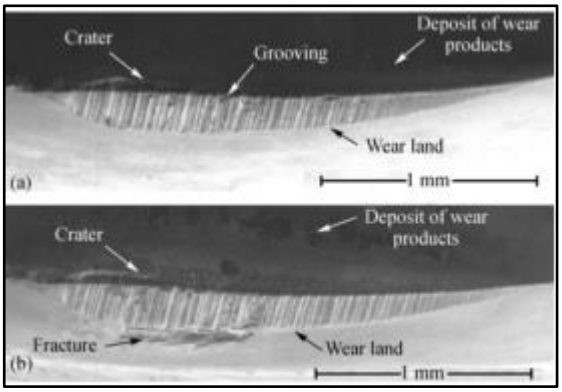

Figure 2.5 Chemical wear in machining of nickel base alloys [39]

Diffusion wear

Machining at high speed, some elements of tool melt and diffuse from the tool material due to high temperature and evaporate [39]. Many investigators have studied the mechanism of diffusion wear. Ezugwu et al. [2] studied the diffusion wear on machining of nickel and titanium base alloys. Bermingham et al. [45] studied that tool life obtained in thermal assisted machining compared to cryo-machining was less because of diffusion wear. All material cannot be machined using thermal enhancing machining process. The use of cryogenic fluid to the cutting zone can avoid diffusion and adhesion in the cutting tool explained by Venugopal et al. [46], but crater wear may be dominant compared to diffusion. Other researchers studied diffusion wear on machining of nickel and titanium alloys [47–49].

Plastic deformation

Formation of micro-cracks in the tool surface and chipping due to stress acting on the tool at high temperature is the sign of plastic deformation of the tool as shown in Fig 2.6.

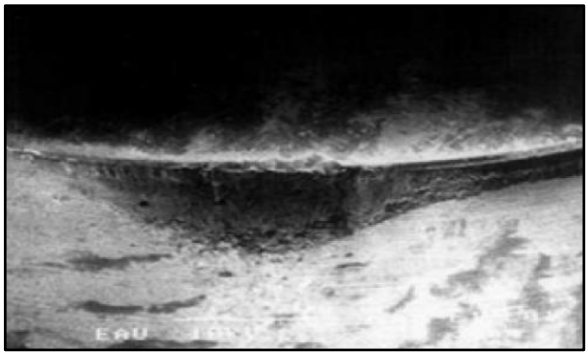

Figure 2.6 Tool wear due to plastic deformation [39]

Generation of tool-workpiece interface temperature on machining of nickel base alloy that causes bonding and chipping on the tool due to high temperature and form tool failure. The plastic deformation of the cutting edge was studied by Ezugwu et al. [50]. Prengel et al. [51] studied the abrasive wear due to plastic deformation of different coated tool in dry machining of Inconel 718.

2.6.3 Cutting force on machining of nickel base alloys

Cutting force generation is of greatly importance in machining high strength materials as it directly affects the tool wear and tool life of the cutting tool. Euan et al. [52] studied the modeling of the static and dynamic cutting forces, vibrations for inserted ceramic milling tools. Ceramic inserts can be used in higher cutting speeds as compared to carbide inserts. They have used a time-domain model to develop dynamic cutting force coefficients, which are needed to calculate cutting forces. Machinability of three materials in terms of tool wear, forces, and chip formation was studied by Bakkal et al. [53]. Shi et al. [54] reported the effect of machining parameters on cutting force in machining of Nickel base alloys on three different materials. It was observed that with increase of cutting speed, the cutting force decreased and with the increased of feed rate the cutting force increased. Forces and vibrations of machining of Inconel 718 was studied [52] and titanium alloys [55]. Cutting coefficient were used for calculation of cutting force and validated with the experiment. Different types of tool wear and mechanism has been explained by Zhu et al. [56] in machining of superalloys.

2.6.4 Surface integrity of machining of nickel base alloys

Surface integrity is the surface and subsurface characteristics produced in a machining process. It tells many aspect of machined surface like metallurgical aspect, surface topography, residual stress, micro hardness etc., generated in machining process. Nickel base alloys are very sensitive to microstructure changes. Surface integrity conducted in terms of surface topography which include optical observation of machined surface, second subsurface microstructure, micro hardness, and residual stress was observed in machined subsurface. Khidhir and Mohamed [57] reported the surface roughness and chip formation of Hastelloy C-276. At low cutting speed, the burr formation took place and disappeared at high cutting speed. They also studied the surface finish of nickel alloy highly affected by cutting speed. Kadirgama et al. [35] studied effect of dry

cutting on force and tool life on machining of nickel based alloy using two different types of coated carbide cutting tools. The optimal results were obtained using particle swam optimization technique. Pusavec et al. [58] investigated the surface integrity of Inconel 718 using cryogenic machining. The results show that cryogenic machining process gives better result on all surface integrity characteristics. Ulutan et al. [59] investigated the friction and surface integrity of modern alloys using FEM. It was noticed that friction severely affected the residual stress generated in the machined surface. Jin and Liu [60] investigated the high speed machining of nickel base alloys and to study on surface integrity. Both residual stress and micro hardness were affected drastically with increased of cutting speed. Cai et al. [61] presented surface integrity in term of surface topography, surface roughness, residual stress, subsurface microstructure and microhardness of end milling of Inconel 718. They also found that residual stress and micro hardness increased with increase in cutting speed. Peng et al. [62] analyzed the surface integrity and tool wear on high speed machining of Inconel 718 alloy machined by whisker reinforced alumina ceramic inserts and cutting fluid. High surface tensile residual stresses, and recrystallization of surface layer were induced by tool wear which significantly affected the fatigue strength of machined part. Umbrello [63] investigated the effect of machining parameters on surface integrity in dry machining of Inconel 718. Saoubi et al. [64] reviewed the surface integrity in machining and its impacts of functional performance i.e. life of machined products. They studied surface alternations, phase transformations, micro hardness, and residual stress.

2.7 Heat assisted machining

2.7.1 Principle of hot machining

Though there are different techniques for machining hard materials, but because of high investment cost, and high skilled operator, it is not economically satisfying for every industry to use above methods. Another way to enhance the machinability of hard material is use of heat source to the surface of the materials before or during the machining process without changing any change of metallurgical properties [2]. Depending on the mechanical properties of the work materials, the material is heated below recrystallization temperature to reduce shear strength. Hot machining is one of the key manufacturing techniques with high productivity [65]. The benefits of heat assisted machining are the reduction of forces, chatter, cutting power, energy and increase material removal rate (MRR), chip tool contact length and surface finish etc. Heat assisted machining also

decrease the chance of chip segregation, chatter formation, and thereby increase tool life. The effectiveness of hot machining is depending upon the type of heat source with optimum temperature; otherwise it will damage the machined surface. Various types of heat assisted machining have been studied by different investigators.

2.7.2 Electric arc machining (EAM)

In electric heat machining the tool and workpiece are connected to a power source as shown in Fig 2.7. The tip of the tool and shear plane are the major contribution to the resistance. Generally, 0-5V power is supplied to the workpiece and tool for both A.C or D.C. Though electric heat resistance is simple equipment to heat the workpiece, but the disadvantage is to control temperature precisely and it is limited by cutting speeds.

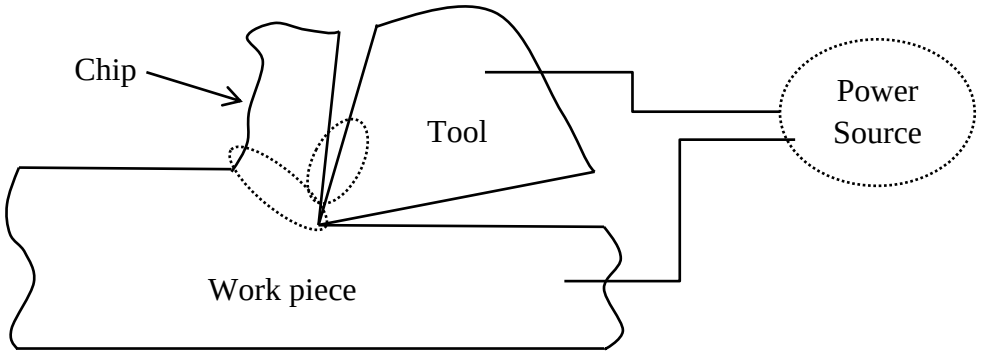

Figure 2.7 Structure of tool and workpiece in electric arc machining [66]

Chen and Lo [67] used localized heating technique i.e. DC current as a heat source for hot machining. Machining tests were carried out with different tool polarities over wide range of speeds and D.C. heating current. Investigating the tempering of the workpiece from hot machining, the influence of tool polarity on the interface temperature was studied by cutting workpiece in transverse wise and hardness across the section was determined using a micro hardness tester. Tool life in D.C. machining was 19 times more than conventional machining tool life. The electric heat machining was used by Kainth and Chaturvedi [68] to heat up the workpiece in machining of EN-24 steel. The temperature distribution was calculated using resistance heating. They stated that the total electric resistance is sum of chip material resistance, resistance at shear, and contact resistance at chip-tool interface. With increase of cutting speed above 26.4 m/min, there was increase of chip-tool temperature and decrease of tool-chip contact length.

Lo and Chen [69] used direct current to heat the alloys to predict the tool life using response surface methodology. Raghuram and Muju [70] used magnetic field to heat the material by supplying 0-5V voltage, 0-600A current and thermocouple was used to measure the tool workpiece temperature. The application of heat reduced the wear for a particular heating current.

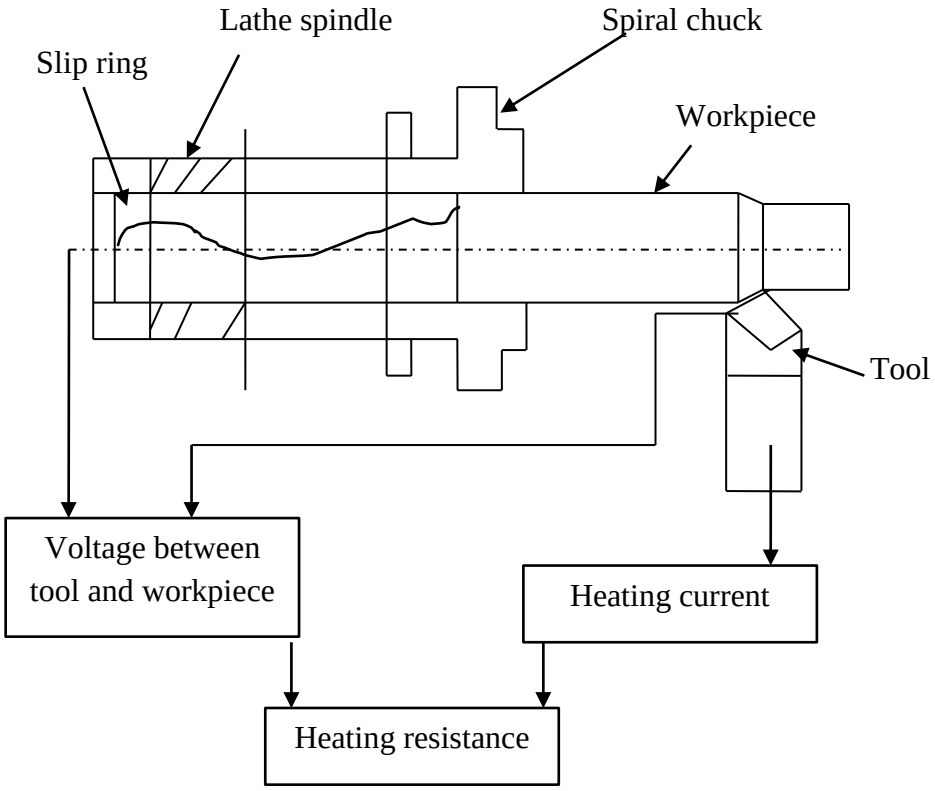

Figure 2.8 Scheme for measuring the heating resistance [71]

An empirical formula was used by Xu et al. [71] in electric hot machining of AISI 52100 steel. The scheme for measuring the heating resistance is shown in Fig 2.8. 3D finite element model was used to verify the experimental results. It was found that the value of heating resistance increased with cutting speed but decreased with increase of feed rate and depth of cut. Optimum heating current in different cutting conditions can be achieved by changing current and temperature. Ulutan et al. [72] used electric sources for machining of high strength materials. The cutting force decreased with increase of certain current limit and decreased if further increased of current.

2.7.3 Induction assisted machining (IAM)

The induction heating system consists of three parts (1) Inventors (2) Transformer and condenser (3) Cooling unit. In induction heating system, induction coils become the

electrical source that induces a high-frequency alternating electrical current into the workpiece to be heated as shown in Fig 2.9.

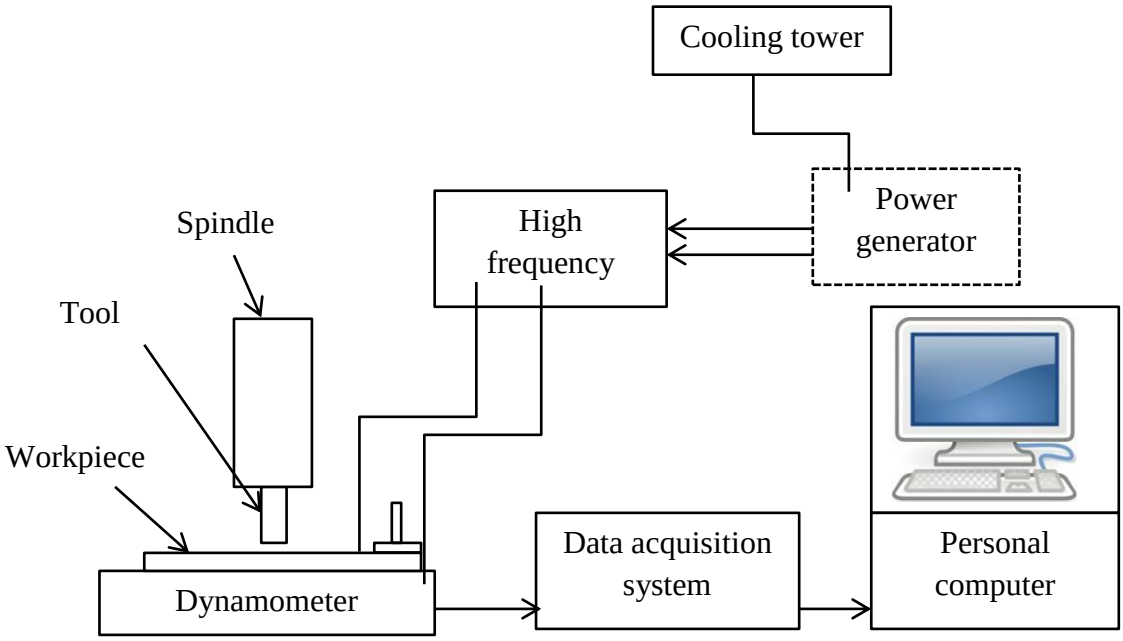

Figure 2.9 Schematic diagram for induction heat machining setup [73]

The alternating current in the induction coil has a magnetic flux around it which is restricted to localized areas or surfaces zones immediately adjacent to the coil. So in this process there is no contact between the workpiece and coil. The workpiece is heated up due to the resistance to the flow of this induced high frequency alternating electric current. In the workpiece the opposing A.C. current is equal to the induction coil induced force. Specific heat of the material, magnetic permeability of the material, frequency and the induced current are the factors which affects the rate of workpiece heating.

The improvement of machinability of Ti-5553 alloy using heat induction machining was studied by Bali et al. [74]. There was 13% reduction of specific cutting force compared to room temperature, but tool life reduced due to change in the microstructure of the workpiece material. Hossain et al. [75] studied end milling of titanium alloys by TiAlN coated inserts using induction heating. They heated the workpiece up to 420ºC so that no phase changes occurred. They found that, there was significant influence of preheating on tool life compared to the room temperature. Higher cutting speed gave better advantage in preheating while lower cutting speed somewhat suppressed the benefit of preheating. They also studied cutting force and vibration chatter reduced due to preheating. Chips produced

during machining in room temperature conditions are quite thick and strong, while elongated and thinner chips are observed during hot machining.

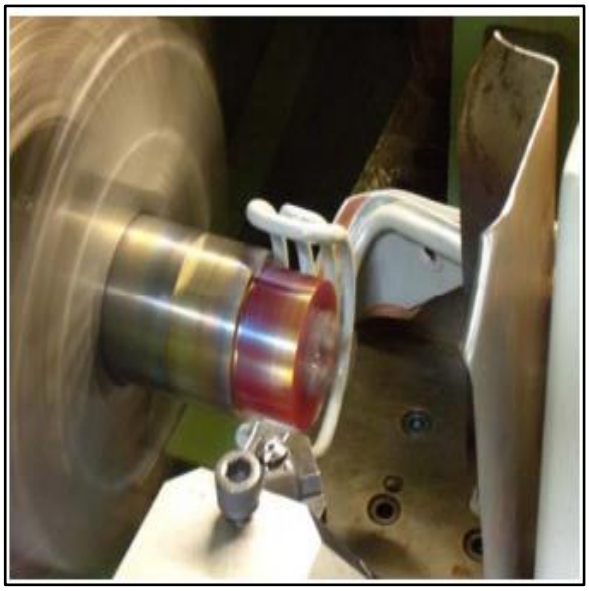

Figure 2.10 Induction heat machining [74]

The use of induction hot machining was carried out by Ginta et al. [76] to study machinability of titanium alloy in milling operation. The tool life increased 169.4% in hot machining compared to room temperature machining conditions. Surface integrity of Ti-6Al-4V and AISI D2 steel in term of micro hardness, surface finish, microstructure were studied using induction heat assisted machining process [77]. Luo et al. [78] investigated Induction based hot machining of elastomers. They observed that, there was formation of smoke and better surface finish at high cutting speed due to low frequency vibration on the soft elastomer material. They also analyzed the simulation and experimental validation on induction based machining process. The machinability of a nickel base alloy was reported by Hossain et al. [75] using induction heat assisted machining process using TiAlN coated carbide inserts. It was observed that 80% of increase of tool life in preheating condition was observed compared to room temperature. Tool wear and vibration/chatter also reduced significantly in induction heat machining.

It is necessary to avoid coolant during heat assisted machining to preserve the material temperature at the cutting zone. It was reported in the literature that the cutting tool having lower entry angle 45° was having lower cutting force compared to entry angle as 95°. The advantages of induction heating system are easy to use, cleanliness, but high concentration heating is not possible and limited tool mobility are the disadvantages.

2.7.4 Plasma assisted machining (PAM)

The successful of plasma assisted machining is the use of intense heat locally in the cutting zone, softening the workpiece material for machining of high strength material. This technique not only reduces the hardness of the workpiece, but also changes the discontinuous chip to continuous one. Plasma consists of high velocity, high temperature stream of ionized gas capable of supporting a high current, low voltage electric arc. Depending on current carrying capacity, the workpiece materials are designed as anode [79]. Fig 2.11 shows the principle of plasma assisted machining. Hinds and Almeida [80] used plasma arc heating for hot machining of EN31. They used split plate calorimeters to measure the heat transfer density within the plasma arc. Both insulated and non-insulated thermocouple were used the record the temperature. Madhavulu and Ahmed [81] used plasma arc for increasing material removal rates in turning operations. They used SS 410 of hardness 300BHN as workpiece material. The use of plasma has many advantages like softening and weakening of materials at high temperatures, or avoiding the transformation of metastable materials. It was observed that tool gain in hot machining was better compared to room temperature.

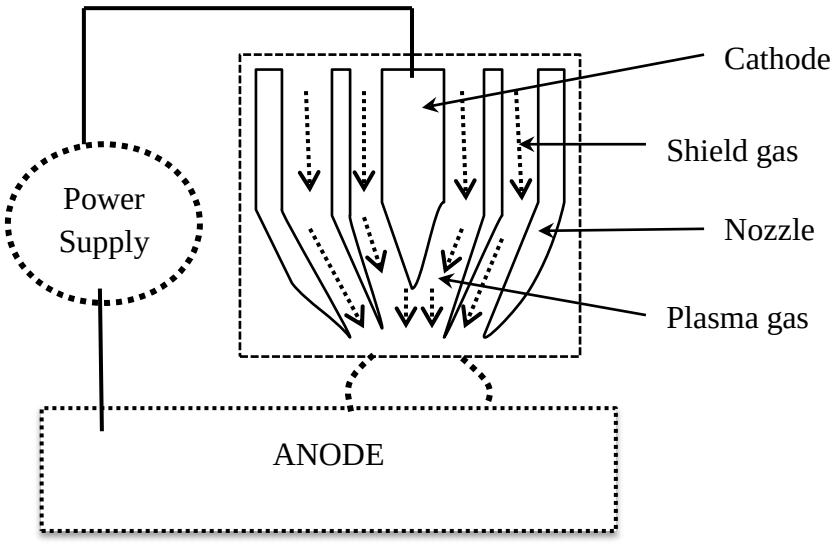

Figure 2.11 Plasma arc generator [79]

Leshock et al. [82] studied experimental and numerical analysis of machining of Inconel 718. A finite difference method was used for temperature calculation considering three modes of heat transfer i. e. conduction, convention and radiation. A plasma setup was used as shown in Fig 2.12.

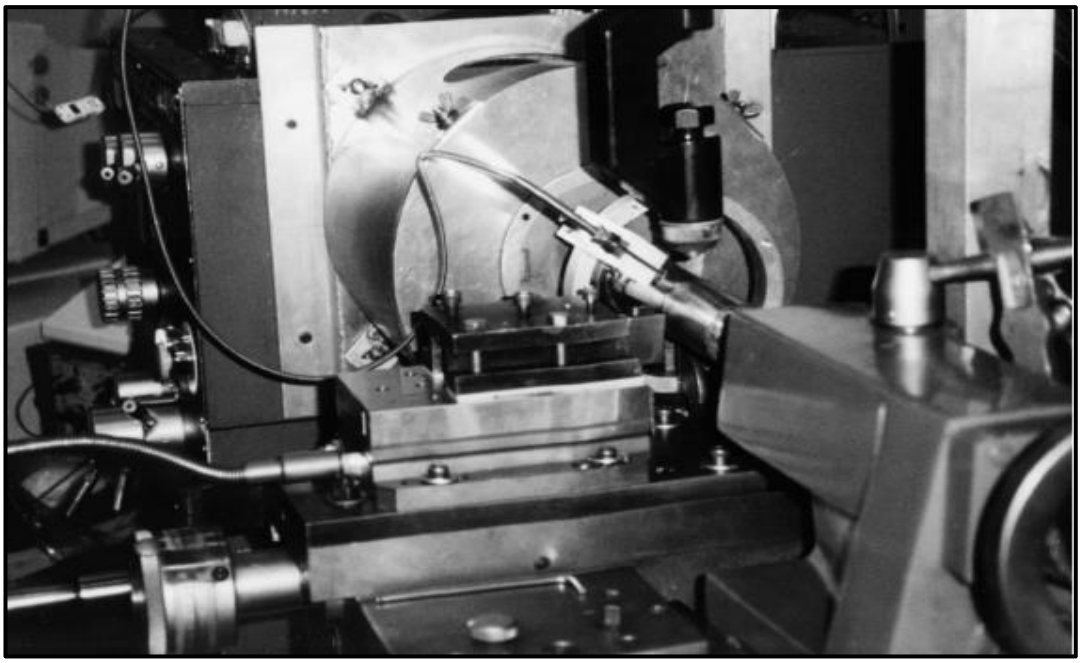

Figure 2.12 Experimental setup for plasma assisted machining [82]

A sensitivity analysis was used to examine the effect of machining conditions on temperature distribution. PAM reduced 30% cutting force, 40% enhancement in tool life, and improvement in surface finish.Hot machining of different materials was studied by Kitagawa and Maekawa [83]. It was found that plasma hot machining was responsible for catastrophic failure of the workpiece of alumina and zirconia.The thermal stress generated in the surface of the workpiece is compressive during the machining as thermal expansion is constrained by the rest of the material. The mild heating and cooling conditions was given to machined surface in order to avoid the thermal damage. Popa [84] studied jet of heat plasma for machining difficult-to-machine materials. There was reduction of 60-70% of tensile strength with 40-50% of cutting force and increase of 10-15 times of productivity. Lacalle et al. [85] studied the machinability of three nickel base alloy i.e. Inconel 718, a cobalt base alloy Haynes 25 and titanium base alloy with ceramic tool. The tool life of whisker reinforced ceramic tools increased 300% in PAM compared to conventional machining. Novak et al. [86] used plasma heat assisted machining of Inconel 718.They found that with plasma heating, cutting forces were reduced by 20% and surface finish improved as much as a factor of 4 but severe notching wear was found in the tool. It was found that although plasma arc heating was one best method for heating the material but over heating the machined workpiece surface caused oxidation and burning.

2.7.5 Laser assisted machining (LAM)

Laser is the localized source of heat, alternative to plasma. In this section both laser assisted turning and milling is discussed. Some investigators have carried out hot machining which are difficult-to-machine using laser as heat source. Laser assisted turning is method in which workpiece is preheated using laser. The schematic and actual setup for laser assisted turning is shown in Fig 2.13. Bejjani et al. [87] studied the effect of laser heating on, tool life, tool particle interaction and surface finish of titanium metal matrix composite. They observed that the tool life and surface finish increased 180% and 15% respectively compared to conventional machining at same cutting conditions.

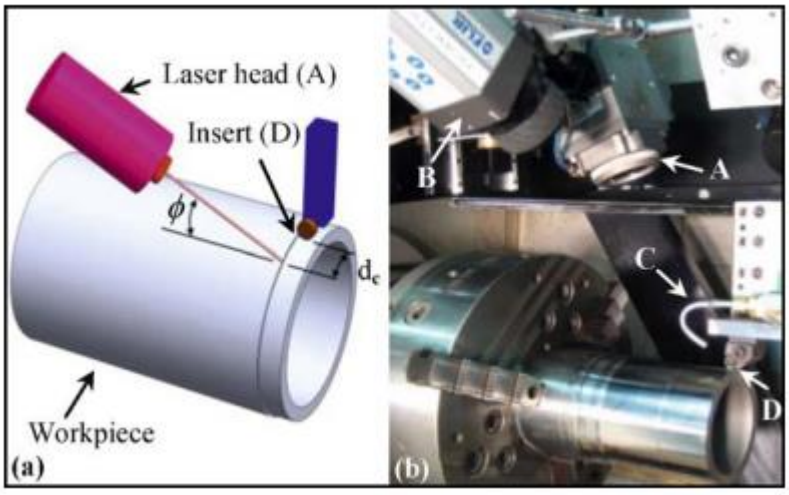

Figure 2.13 LAM Experimental setup: (a) Schematic diagram, (b) Actual setup [87]

Abdulghani et al. [88] analyzed the modeling and simulation of laser assisted turning of hard steels using finite volume software. The verified model was used for simulation of laser assisted turning of 20 mm diameter with workpiece of AISI D2 tool steel. Prediction of the cutting depth was done as a function of different lasers and machining parameters. They studied the laser shock peening of aluminum 7075-T7351 and laser assisted turning compact graphite iron. They observed that laser assisted turning gave more environmental benign compared to conventional process. Dumitrescu et al. [89] studied high power laser assisted hard turning of AISI D2 tool steel. The use of high power diode has potential laser being compact and feasibility of fiber optic beam transport. It was found that laser assisted machining avoid catastrophic fracture of the carbide tools, improved tool life, suppression machining chatter, saw tooth chip formation, and reduced the thrust component of the cutting force. It was observed that laser heating was no significant thermal

detrimental to the machined surface. Bejjani and Balazinski [90] studied laser assisted turning of Titanium MMC. LAM can significantly increase tool life by up to 180%. At high speeds and high surface temperature, LAM had abrasion wear which was still the dominant wear mode. An explanation of the increased tool life with LAM has been related to the tool-particle interaction.

Similar to laser assisted turning, laser assisted milling have been reported in literature by many investigators. Zhuang et al. [91] studied preheating and cooling assisted in machining of Inconel 718 with ceramic cutting tools to analyze tool wear and surface integrity. They observed that less tool wear and better surface finish were obtained in preheating compared to dry machining. Flank wear and notch were observed within the Plasma and dry cutting conditions but adhesion wear was the main mechanism of flank wear in cryogenic cooling. A thermal enhancing milling process was used by Kim and Lee [92] to analyze the cutting force and workpiece temperature in laser assisted milling process using two materials Inconel 718 and AISI 1045 were taken for modeling using response surface methodology and results were found to be good agreement with the experiment. Woo and Lee [93] developed three dimensional laser assisted milling (AISI 1045 and Inconel 718) to study the effectiveness (cutting force, tool wear, specific cutting energy, and surface roughness) and compared to the conventional machining method. Cutting force decreased and surface roughness was improved as compared to conventional machining while machining of AISI 1045. But for Inconel 718, the surface roughness was improved for both conventional and laser assisted milling. It was found that the application of laser heating reduced cutting force, tool wear and increase material removal rate. Sun et al. [94] investigate the laser assistant milling of titanium alloy. Chips were studied in both compressed and without compressed air conditions. The feed force decreased due to increase of laser temperature and edge chipping was the dominant wear mode in machining of titanium alloy. Ding and Shin [95] studied the laser assisted machining of hardened steel parts with surface integrity analysis. They developed three-dimensional transient thermal model to predict the temperature field in the hollow shaft of varying thickness undergoing laser-assisted turning. LAM produced the parts of a good surface finish less than 0.3 mm, and no microstructure change. Cutting force during LAM dropped about 20% as the temperature increased to above 300˚C compared to hard turning conditions. Yang et al. [96] carried out investigation of heat affected zone during laser assisted machining of Ti6Al4V alloy with FEM simulation. It was noticed that the depth

and width of the heat affected zone were strongly dependent on the laser parameters (laser power, laser scan speed, the angle of incidence and the diameter of the laser spot) and material properties (thermal conductivity, specific heat and density). They found five different type of microstructures dendritic microstructure, needle-shaped zone, a fine needle-shaped zone, a lamellar zone and an equiaxed zone. Pfefferkorn et al. [97] explained heat transfer model of semi-transparent ceramics undergoing laser assisted machining. They developed three-dimensional, unsteady heat transfer model developed for predicting the temperature field in partially-stabilized zirconia in LAM. The PSZ is treated as optically thick within a spectral band from approximately 0.5 to 8 μm.

Rashid et al. [98] studied the effect of laser power on the machinability of the Ti-6Cr-5Mo-5V-4Al beta titanium alloy during laser assisted machining. No significant reduction of cutting force was observed with a low laser temperature of 600ºC. There was effective reducing of cutting forces at laser power range of 1300-1600W during heat assisted machining with moderate high cutting speeds. Anderson and Shin [99] investigated the laser assisted machining of an austenitic stainless steel (P550). Reduction of strain hardening of the workpiece materials, caused a significant reduction in the tool-chip interface temperature during LAM. LAM of P550 decreased the overall time required to machine one part by 20-50% when compared with both carbide and conventional ceramic machining at higher machining speeds and longer tool life. Though laser assisted machining have many advantages like cleanliness, high penetration of heat, dimensional accuracy, local heating but the disadvantages are consumption of large amount of energy and high cost of setup.

2.7.6 Gas flame assisted machining (GAM)

In flame heating machining method, the workpiece is heated using gas flame during or before the machining process up to recrystallization temperature. Usually liquefied petroleum gas (LPG) combined with oxygen is used. The distance between the flame and workpiece should be maintained for proper heating; otherwise it may damage the workpiece. Gas flame heating method is simple in design, with low initial investment cost. There is difficulty in having high concentration of heat to the materials. The titanium alloys cannot be machined due to formation of carbide on the machined surface [100].

Pal and Basu [101] used oxy-acetylene gas to heat austenitic manganese steel on shaping operation. The surface roughness, cutting force and tool life were measured using different

cutting speed, feed and depth of cut. The equation for tool life, thrust force and cutting force were determined. Davami and Zadshakoyan [102] investigated the tool temperature and surface quality in hot machining of AISI 1060 using uncoated carbide insert. The experiment was carried out in two cases. They finally concluded that surface roughness in hot machining was better compared to room temperature. Tool temperature variation was measured by placing thermocouple on the opposite side of tool tip. The temperature in each cutting speed increased exponentially with time at the beginning of machining, and then it reached the steady state. Maity and Swain [103] studied the tool life of hot turning of high manganese steel using carbide insert. They used liquid petroleum gas and oxygen as heating agent. They investigate chip reduction coefficient and non-dimensional cutting force along with flank wear and tool life.

Thandra and Choudhary [104] studied the effect of cutting speed, feed and depth of cut on responses using gas flame heat machining shown in Fig 2.14. With application of heat, the surface finish improved, with decrease of cutting and thrust force. It was also found that there was decrease of 33.95% flank wear compared to conventional machining. Tosun and Ozler [105] studied optimization for hot turning operation with performance characteristics i.e. to see the level of importance of machining parameters on and tool life in hot turning of high manganese material with M20 sintered carbide tool, using LPG (liquefied petroleum gas) and oxygen as heating medium. Both S/N and ANOVA were used for the optimization tool life and surface roughness. Ravi et al. [106] studied that influence of tool temperature on cutting forces when high chrome white cast iron was machined. It was found that tool tip temperature and cutting force decreased as cutting speed increased with constant depth of cut and surface temperature. The effect of cutting parameters on response was tested by Taguchi L_9 orthogonal array. Upadhaya et al. [107] studied machinability of Ti alloy using hot machining. The workpiece was heated up to 300°C and the effect of heating to cutting forces, flank wear, and surface roughness was discussed. They also studied chip analysis.

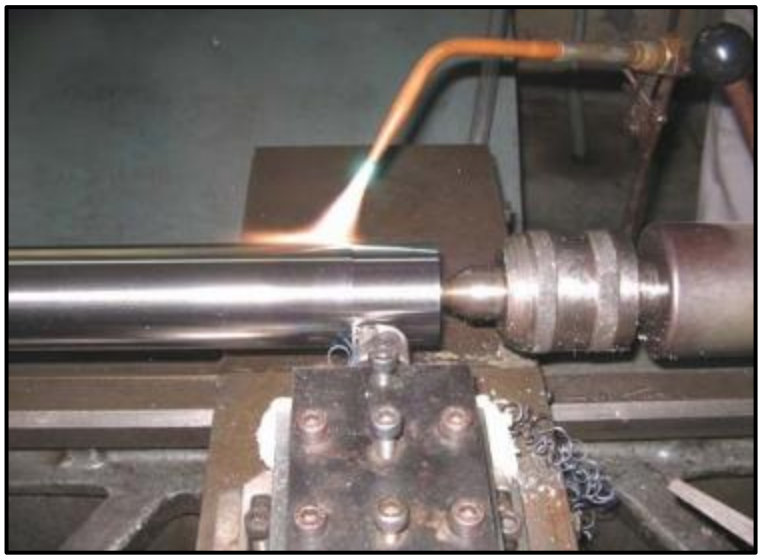

Figure 2.14 Experimental set up for flame heat machining [104]

The tubular chips were formed at room temperature whereas ribbon type of chips was observed at heated conditions. Atomic force microscope was used to study surface morphology and roughness. Reduction in surface roughness with preheating was due to lower chip rupture stress at elevated temperature. Other researchers used gas flame for machining hard material [108–111].

2.7.7 Others assisted machining

Hot ultrasonic assisted machining (UAT)

Muhammad et al. [112] studied an advanced way of machining where vibration was provided along with heating of beta-titanium base alloys. It was observed that there were reduction of tangential and radial force in conventional hot turning and ultrasonic assisted hot turning compared to conventional machining. Other researchers investigated the thermally enhanced ultrasonic studied assisted machining of Ti alloy [113,114].

Hybrid machining processes

Other researchers in the past, combined two different machining processes and called hybrid machining process studied by Wang et al. [14]. In this hybrid machining process, two types of process i.e. plasma and cryogenic were used for machining Inconel 718. It was observed that, compared to single plasma machining; all responses performancewere better in hybrid machining process. The advantages of hybrid machining was studied by investigators [91,115,116]. Although there are many advantages on hybrid machining,

but combined processes may affect the surface finish studied by Lauwers [117]. The use of hybrid machining in micro components and development were studied by some investigators [118,119]. The advantage and disadvantage of different type of heating process in machining is shown in Table 2.1.

Table 2.1 Advantages and disadvantages of different type of heating sources [120]

Heat Source	Advantages	Disadvantages
Electric arc machining	Simple equipment	Not possible to control
Induction assisted machining	Easy to use High capacity preheating	Not possible to high concentration preheating
Plasma assisted machining	High concentration of preheating	Not possible to control
Laser assisted machining	Easy to control to heat High concentration of heat	Costly equipment
Gas assisted machining	Low investment cost	Not high concentration preheating

2.8 Modeling and optimization in hot machining process

Hot machining is one of the alternative choices for machining of high strength materials. Due to the complexity, cost, time consuming, safety to operator and uncertainty of the machining processes, the optimization of the process is necessary for smooth operation. So optimization techniques are needed. Both traditional and non-traditional optimization tools have been applied for machining hard material at high temperature. Tosun and Ozler [121] presented a study of tool life in hot machining of high manganese steel using artificial neural network and regression analysis method. They used LPG flame as heating agent and machined with different cutting conditions of cutting speeds, feed rates, depth of cuts and temperature. The experimental run was trained and tested using artificial neural network with back propagation algorithm and experimental data were compared with both regression analysis and ANN. Tosun and Ozler [122] studied the machining parameters with multiple performance characteristics on hot turning of high manganese steel and found that cutting speed and feed were the more dominant variables on tool life and roughness. Using the Taguchi method, Ranganathan and Senthivelan [123] presented a

study on optimization of input parameters (cutting speed, feed rate and depth of cut and workpiece temperature) on tool wear of tungsten carbide. The optimum results were achieved by using Taguchi method and ANOVA method was carried out to determine significant parameter.

Ranganathan and Senthilvelan [109] utilized a multi-response optimization of machining parameters of hot turning of AISI-316 using grey-taguchi analysis to obtain a desire. Multi-responses are mostly affected by Feed rate and cutting speed. Analysis of variance (ANOVA) and confirmation test also were carried out to validate the predicted values. Patil et al. [124] used grey relational analysis (GRA) for multi-response of hot machining of EN 36 with carbide inserts. This technique gives the combination of factors and respective levels. Finally, a mathematical model was built using multiple linear regression analysis to establish a relation between response and process parameter. Modh et al. [125] optimized the process parameters on hot machining of AISI D2 steel. They had taken 27 runs with machining parameters along with different workpiece temperature to optimize responses. ANOVA test was carried out to obtain the significance parameter. Optimization of multi-responses parameters using desirability function analysis [126–131] coupled with taguchi were carried out in machining operation. Kilickap and Huseyinoglu [132] studied the effect cutting parameters of burr height in the drilling operation. They used surface response methodology along with genetic algorithm and observed the optimum results were obtained at lower cutting speed, feed rate, and higher point angle. Noordin et al. [133] studied the effect of cutting parameters on cutting force and surface finish on turning of AISI 1045 steel using surface response methodology. They noticed that feed was the significant parameters affecting the surface roughness and cutting force comparing to cutting speed and cutting edge. Thangavel et al. [134] investigated the effect of cutting parameters on flank wear in machining of mild steel using high-speed steel. Regression analysis was carried out using surface response methodology to check the individual parameter on the response. Asiturk et al. [135] conducted as a study where they used Co28Cr6Mo metal for turning operation. They observed that tool tip radius is the most significant parameters compared to cutting sped, feed rate and depth of cut.

Chapter 3

Experimental Investigation and Modeling of Hot Machining of Inconel 718 Alloy

3.1 Introduction

Inconel 718 is a nickel base alloy widely used in aerospace sectors due to its excellent characteristics such as high mechanical strength, ability to retain strength at elevated temperature, high corrosion resistance etc. But machining of Inconel 718 is a big challenge to industry due to some other characteristics like low thermal conductivity, low elastic modulus, tendency to weld to the cutting tool etc. The above characteristics of Inconel 718 create rapid tool wear during machining. To avoid tool wear and improve surface finish, investigators used different thermal assisted machining.

Woo and Lee [93] developed 3D laser assisted milling (AISI 1045 and Inconel 718) to study the cutting force, tool wear, specific cutting energy, surface roughness and compared to the conventional machining method. Thermal analysis was also carried out to determine the effective depth of cut. Cutting force decreased and surface finish improved as compared to conventional machining while machining of AISI 1045. But for Inconel 718, the surface finish was improved for both conventional and laser assisted milling. Laser assistant milling of silicon nitride ceramic was studied by Yang and Lei [136]. Similarly, laser assisted machining of Inconel 718 was reported by Tian et al. [137]. From the both observation, it was observed that thermal assisted machining have better machinability characteristics compared to room temperature machining conditions. Germain et al. [138] investigated reduction in force and tool life in LAM of Inconel 718 using two types of cutting tools: carbide and ceramic inserts. With both insert types the authors observed that force reduced up to 40%. The life of ceramic inserts in LAM increased by 25% whereas tool life of carbide inserts was considerably lower in LAM than in conventional machining. Shi et al. [139] studied numerical and experimental investigation of LAM of Inconel 718. Prediction of cutting force and chip thickness

was done using DEFORM 3D software and were validated with experiments. The error in cutting force was due to the rotation movement of the workpiece simplified as the translation in the simulation, and temperature effect in the friction model was not considered. Attia et al. [140] studied laser assisted high speed finish turning of superalloy Inconel 718 under dry conditions.Though machining of Inconel 718 using laser assisted machining were carried out by many investigators due to high cost, lack of skilled operator create obstacles for wide applications in the industries. On the other hand, flame heating technique is easy to design, simple, easily available and less expensive.

In the present investigation, the experimental investigation of Inconel 718 using flame heating has been carried out using oxygen and liquefied petroleum gas. Effect of cutting variables on tool life, tool wear, chip-morphology and surface finish has been studied. The optimization of process parameters has been carried out to satisfy different response criteria. Experiments have been carried out using response surface methodology. Result predicted by RSM method agreed well with the experimentation with acceptable limit.

3.2 Experimental investigation

The experiments (both at room temperature and heated condition) were performed on a center lathe having spindle speed range of (88-1200 rpm), feed ranges (0.07-2 mm/rev), and motor power (6hp). Inconel 718 (diameter 50 mm and 300 mm length) in the form of round bar was taken as workpiece material (420 *HV*). The chemical composition of Inconel 718 is given in Table 3.1. The insert SNMG120408 was fitted with PSBNR 1616M12 tool holder with -6° normal rake angel, 6° clearance angle and 75° principal cutting angle for machining. The physical properties of Inconel 718 and cutting tool (*WC*) are shown in Table 3.2. For heating the workpiece, liquefied petroleum gas (*LPG*) combined with oxygen was used. The temperature of workpiece surface was measured with the help of thermocouple (*K*-type). The flow of oxygen (110 ml/min) and liquefied petroleum gas (30 ml/min) from the cylinder was kept constant, so that there was no interruption in heating on the workpiece surface. The distance between the workpiece and heating nozzle was maintained at 40 mm apart, so that heating was maximum on the surface of the workpiece. The workpiece was kept rotating during heating to ensure uniform heating on the surface. The temperature of the workpiece was controlled by automatic movement of the flame torch by setting the required temperature in

temperature controlling unit. As soon as the desired temperature reached the machining was carried out.

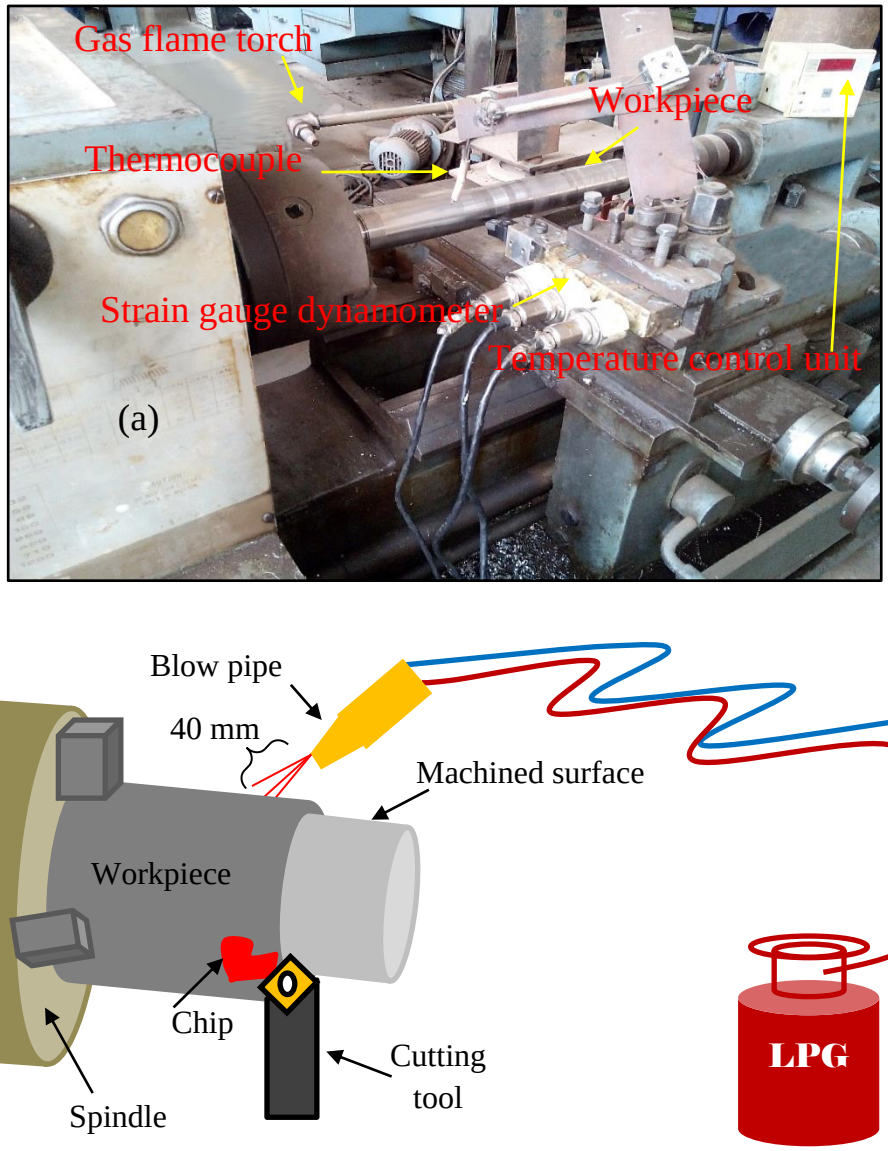

Figure 3.1(a) Hot machining setup (b) Schematic diagram of hot machining

Table 3.1 Chemical composition of inconel 718 (weight %) [141]

Ni	Fe	Cr	B	C	Co	Cu	Mn	Mo	Nb	P	S	Si	Ti	Al
53	18	19	0.006	0.08	1	0.3	0.35	3	5.1	0.015	0.015	0.35	0.9	0.5

Table 3.2 Physical properties of inconel 718 and cutting tool (WC) [142]

Properties	Inconel 718	WC
Density (kg/m^3)	8080 (kg/m^3)	15000
Thermal conductivity (W/m/ $^\circ$C)	10.5 (W/m/$^\circ$K)	46
Specific heat (J/Kg/)	515 (J/kg$^\circ$K)	203
Melting temperature (°C)	1336	2870
Thermal expansion (mm.mm$^{-1^\circ}$/C)	13	4.7x10^{-6}

The machining was carried out with varying cutting speed, feed rate, depth of cut and workpiece temperature tabulated in Table 3.3. The selection of machining parameters was based from the machinability of nickel base high temperature alloys reported by Arunachalam and Mannan [143]. The experimental setup and schematic diagram for hot machining is illustrated in Fig. 3.1 (a-b).

Table 3.3 Machining parameters used in experiments

Cutting parameters	Magnitude
Cutting speed (m/min), $V\,c$	40,60,100
Feed rate (mm/rev), f	0.1,0.13,0.15
Depth of cut (mm), a_p	0.5, 1, 1.5
Workpiece temperature (°C), T	30, 300, 600

3.2.1 Measurement of forces

The cutting force data was recorded by strain gauge dynamometer during all the experiments. Before recording the cutting data, the dynamometer was calibrated properly with the application of different loads. SYSCON strain gauge dynamometer was connected with center lathe tool holder post to measure the forces.

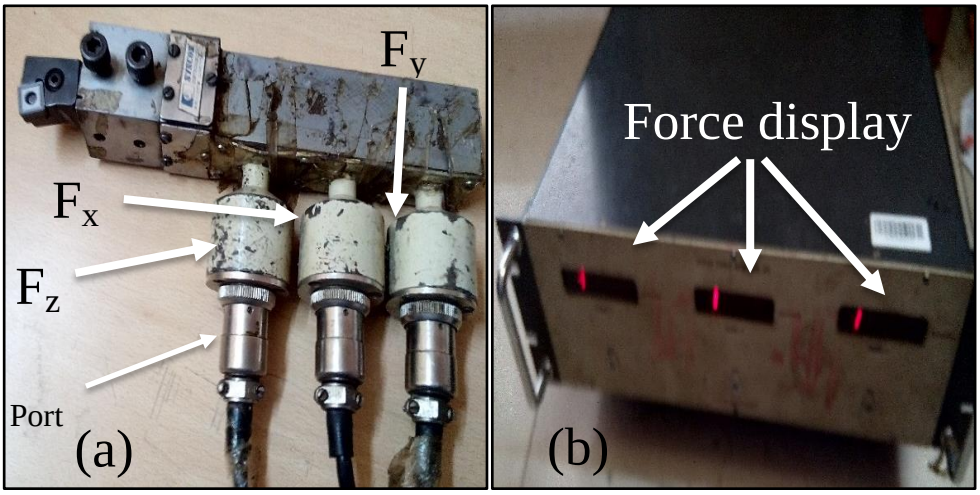

Figure 3.2 Strain gauge dynamometer system, (a) Strain gauge transducer, and (b) Digital force measuring device

The acquired data from transducer got collected through port available in the instrument as shown in Fig 3-2 (a-b). The specification and calibration range of dynamometer is tabulated in Table 3.4.

Table 3.4 Specification of strain gauge dynamometer

Model	Strain gauge dynamometer (SYSCON)
Calibration range	
Force	F_x, F_y, and F_z
Capacity	1000 kg
Indicator	Digital

3.2.2 Workpiece surface temperature measurement

Nickel-base alloys are not temperature-sensitive materials. Their mechanical properties does not change even the temperature varies up to certain temperature [2]. There are two heat sources during nickel machining process, i.e. due to external heating on the workpiece and other heat is created by friction at the workpiece/tool interface and workpiece material. A *k*-type of thermocouple is used have to sense the temperature of workpiece which is displayed in temperature meter as shown in Fig 3.1. *K*-type thermocouple consists of alumel and chromel wire and it has capacity to measure the temperature within the range of (200-1200 ºC).

3.2.3 Measurement of cutting and chip temperature

Various methods are used for measurement of cutting temperature in the machining processes. Thermocouple, embed thermocouple, Infrared pyrometer are some of the instruments used for measurement of temperature. In this work infrared pyrometer has been used for measurement of chip temperature (Fig 3.3). The specification of pyrometer is shown in Table 3.5.

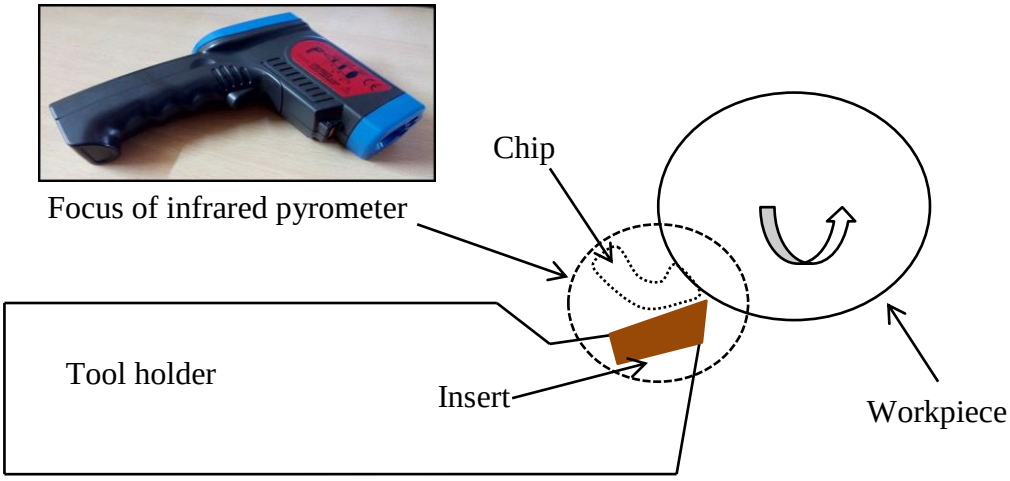

Figure 3.3 Schematic diagram of measurement of temperature using infrared pyrometer

Table 3.5 Specification of infrared pyrometer

Model	EUROLAB 1250
Temperature range	-30 to 1250 °C
Storage temperature	-20-60°C
Response time	500 m.sec, 95% response
Relative humidity	10-95% RH noncondensing

3.2.4 Tool wear, chip thickness and chip tool contact length measurement

Due to friction between the machined surface and flank face of the cutting tool, wear appears on the tool. A uniform and maximum tool wear land values were taken for measurement for tool wear. Flank wear height of 0.3 mm was used as tool life criteria. For each turning operation, a new cutting edge of the insert has been used in all experiment. The tool wear, chip thickness and chip-tool contact length were measured with different magnifications with the help of optical microscope (Fig 3.4). The specification of optical microscope is given in Table 3.6.

Table 3.6 Specification of optical microscope

Model	Zeiss axio imager M2
XY range	100 x 50 mm
Total magnification	2.5-100
Features	• Universal stand-transmitted light • Light and contrast manager

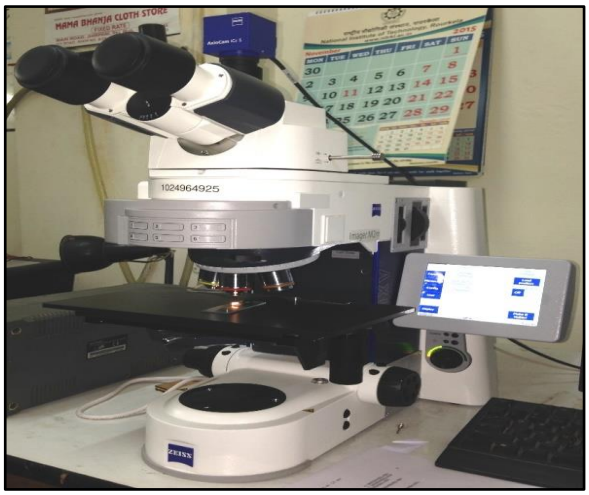

Figure 3.4 Optical microscope (Model: Zeiss axio imager m2)

3.2.5 Scanning electron microscope

The microstructure of the workpiece and tool before and after machining, serration formation in the chips, chip segment, and tool wear, were examined under scanning electron microscope as shown in Fig 3.5. The specification of SEM is shown in Table 3.7.

Figure 3.5 Scanning electron microscope (SEM)

Table 3.7 Specification of scanning electron microscope

Model	JSM-6480LV
Features	• Low vacuum mode • Can accommodate a specimen of up to 8” in diameter • Auto gun (Saturation & alignment)

3.2.6 Surface roughness measurement

For measurement of surface roughness, Taylor hobson profile meter was used in all experiment (Fig 3.6). The profile meter measures the arithmetical mean deviation value of the profile (R_a). The workpiece was allowed to cool after set of operation and the experimental runs were marked with marker for easy measurement. All machined surfaces were measured three times in all the experiments and average value was taken. The specification and model of profile meter is shown in Table 3.8.

Figure 3.6 Taylor hobson roughness profile meter

Table 3.8 Specification of taylor hobson profile meter

Model	Taylor hobson profile meter
Gauge range	±150µm
Traverse length and speed	25.4 mm (Max) and 0.25 mm (Min), 1 mm/sec
Cut off value	0.8 mm

3.2.7 Microhardness tester

The surface and subsurface of the machined surface before and after machining were measured with the help of microhardness tester (Fig. 3.7). The specification of

microhardness tester is tabulated in Table 3.9. The load (150 gm) and dwell time (10 sec) was kept constant for all measurement.

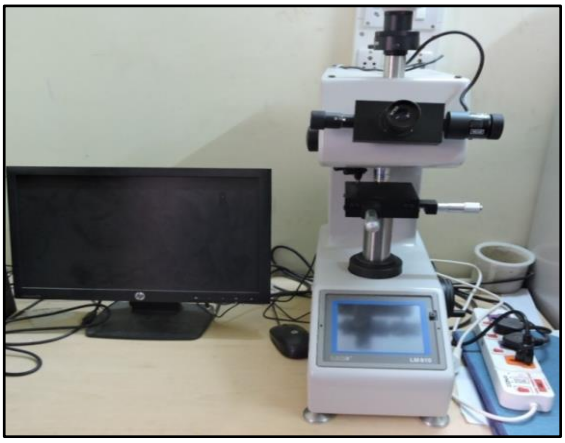

Figure 3.7 Microhardness tester

Table 3.9 Specification of microhardness tester

Model	LECO LM 810
Magnification	2.5 X to 100 X
Indenter	Diamond made pyramid shaped
Features	Advanced full-color touch panel, fracture toughness value (K_c) holds up to three objectives, light load model available,

3.2.8 Measurement of cutting power

A Power data logger or power meter was used to measured energy or power consumed during each cutting (Fig 3.8). Table 3.10 shows the specification of the power meter used in the experiment.

Figure 3.8 Power analyzer/logger

Table 3.10 Specification of power logger/analyzer

Model	VERITEX (VIPS 808)
Operating range	90-270V AC/DC
Sensing : V:	440 VAC (L-L); A: 5 Amps
System	3 Phase 4 wire, Accuracy: Class 1.0

3.3 Results and discussion

The machining was carried out at different machining conditions for room and high temperature condition to study forces (cutting, feed and radial), tool life, and surface roughnessand results are tabulated in Table 3.11. Microhardness, chip-tool contact length, chip geometry, chip geometry etc., have also been studied.

Table 3.11 Responses obtained at various cutting conditions in room and heated condition

Cutting conditions			Force (N)									Tool life (min)			Surface roughness (µm)		
			30°C			300°C			600°C								
V_c(m/min)	f(mm/rev)	a_p(mm)	Feed	Radial	Cutting	Feed	Radial	Cutting	Feed	Radial	Cutting	30° C	300 °C	600° C	30° C	300° C	600° C
40	0.13	0.5	215	18	423	211	16	412	209	12	357	11	16	21	2.7	2.5	2.3
60			214	15	388	208	14	378	192	8	349	8	12	17	2.2	1.9	1.7
100			210	13	359	197	11	343	187	7	323	5	7	13	1.7	1.5	1.3
100	0.10	0.5	192	15	391	152	13	346	136	12	259	8	11	18	2.3	2.1	1.7
	0.13		229	18	397	227	15	358	189	13	264	6	9	15	2.4	2.2	1.9
	0.15		254	20	438	229	17	378	201	16	312	5	9	12	2.6	2.5	2
100	0.13	0.5	175	9	324	147	7	303	128	5	284	10	12	13	2.1	1.8	1.7
		1	199	11	337	162	8	316	135	5	295	8	9	10	2	1.7	1.6
		1.5	216	12	346	169	9	322	146	6	305	5	6	7	1.9	1.5	1.4

3.3.1 Force

Variation of Cutting, feed and radial force with respect to cutting speed and workpiece temperature

The variation of cutting, feed and radial force with respect to cutting velocity and workpiece temperature is shown in Fig 3.9 (a-c). It was observed that there was a reduction of (15, 10, and 10%) of cutting force, (31, 36 and 48%) feed force and (33, 46 and 46%) radial force at cutting speed of 40, 60, and 100 m/min respectively, when machining Inconel 718 was carried outat 600ºC workpiece temperature. The reduction of forces is due to application of heat on the surface of the workpiece which reduce the shear strength due to thermal softening of the workpiece material. But when increase the cutting speed from 40 to 100 m/min, there was reduction (15, 16 and 9%) of cutting force, (15, 19 and 35%) feed force and (27, 31 and 41%) radial force at 30, 300 and 600°C workpiece temperature respectively. Decrease of cutting force with increasing cutting speed was due to increase of heat generation at the interface area because of friction. But in heat assisted machining, there was decrease in time for heat transfer with increase of cutting velocity, hence less reduction of cutting force. Similar case was reported by investigator [105] in hot machining of high manganese steel using flame heating.

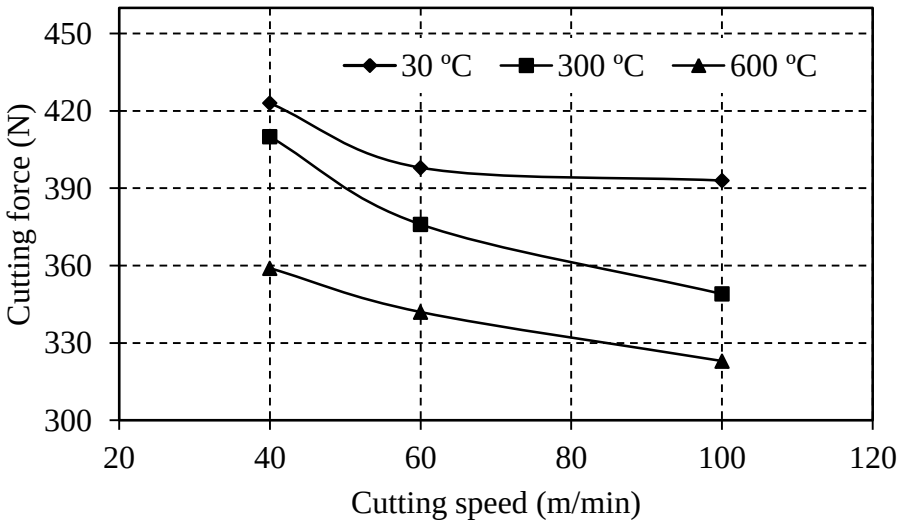

(a)

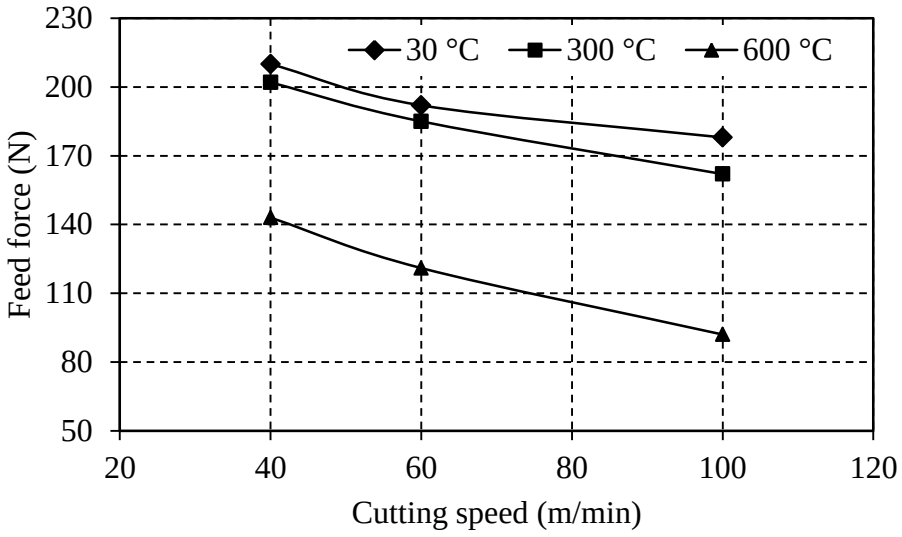

(b)

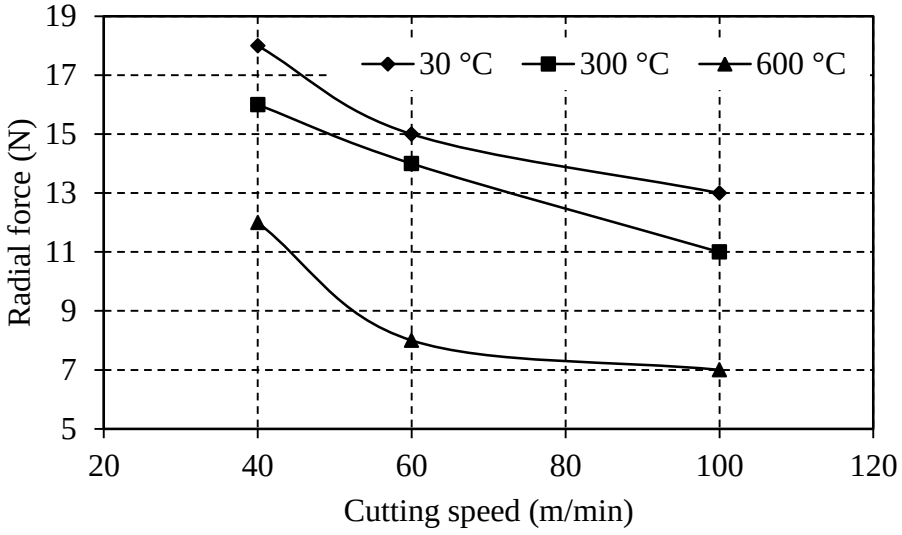

(c)

Figure 3.9 Variation of (a) Cutting force (b) Feed force (c) Radial force with respect to workpiece tempeature and cutting speed at feed rate 0.13 mm/rev and depth of cut 0.5 mm

Variation of cutting, feed and radial force with respect to feed rate and workpiece temperature

The variation of cutting, feed and radial force with respect to feed rate and workpiece temperature is shown in Fig.3.10 (a-c). It was evident that, there was reduction of (33, 33 and 28% (Fig.3.10 (a)) of cutting force, (29, 17 and 20% (Fig.3.10 (b)) feed force and (20, 27 and 20% (Fig.3.10 (c)) of radial force at feed rate 0.1, 0.13 and 0.15 mm/rev respectively, when machining was performed from 30ºC to 600ºC workpiece temperature. Reduction of forces was mainly due to decrease the strength of Inconel 718 at high

temperature in hot turning operation. With increase in the feed rate from 0.1 to 0.15 mm/rev, there was increased of cutting force (12, 9 and 20%), feed force (32, 50 and 47%) and radial force (33, 30 and 33%), at 30, 300 and 600°C temperature respectively.

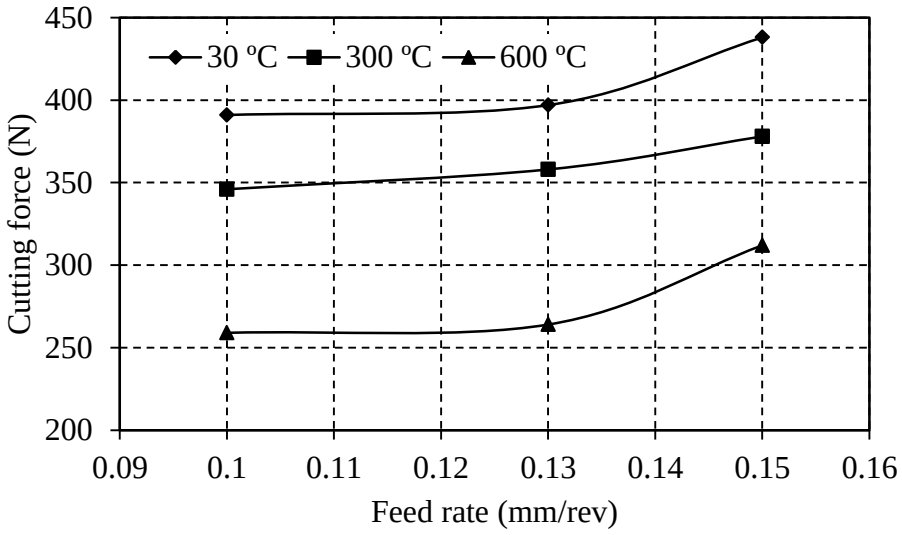

(a)

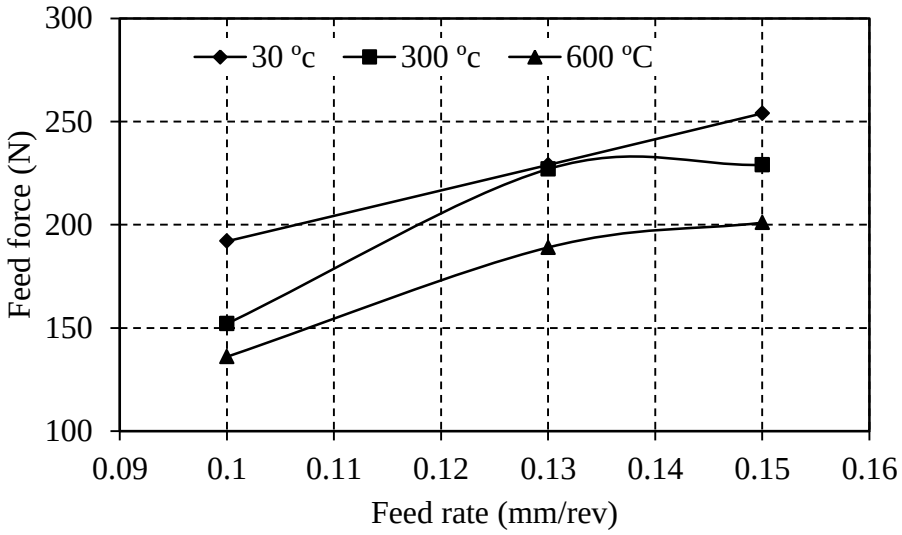

(b)

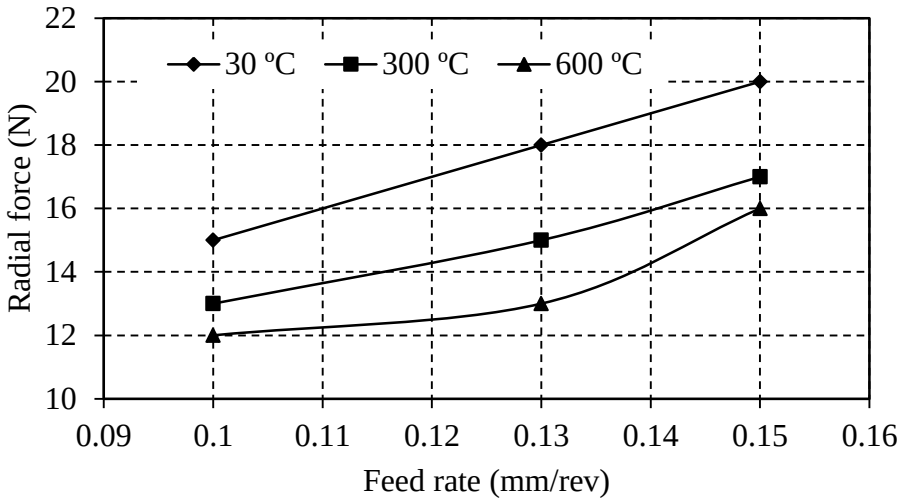

(c)

Figure 3.10 Variation of (a) Cutting force (b) Feed force (c) Radial force with respect to workpiece tempeature and feed rate at cutting speed 100 m/min and depth of cut 0.5 mm

Variation of cutting, feed and radial force with respect to depth of cut and workpiece temperature

Variation of cutting, feed and radial force with respect to depth of cut and workpiece temperature was also studied and presented in Fig. 3.11 (a-c). Machining from room temperature to 600°C workpiece temperature, there was reduction of (12, 12, and 11% (Fig.3.11 (a)) cutting force, (26, 32 and 32% (Fig.3.11 (b)) feed force and (44, 54 and 50% (Fig.3.11 (c)) radial force at 0.5, 1 and 1.5 mm depth of cut respectively. There was increase of (6, 6 and 7%) of cutting force, (23, 14 and 14%) feed force and (33, 28 and 20%) radial force at 30, 300 and 600°C workpiece temperature respectively, when depth of cut increased from 0.5 to 1.5 mm.

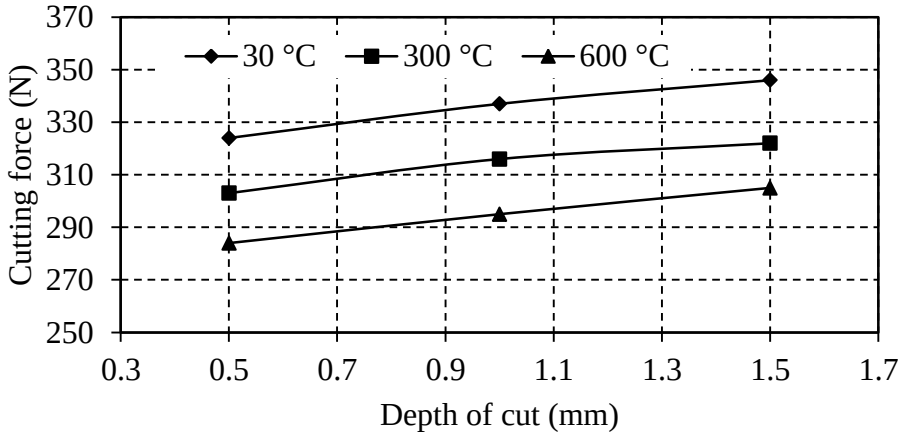

(a)

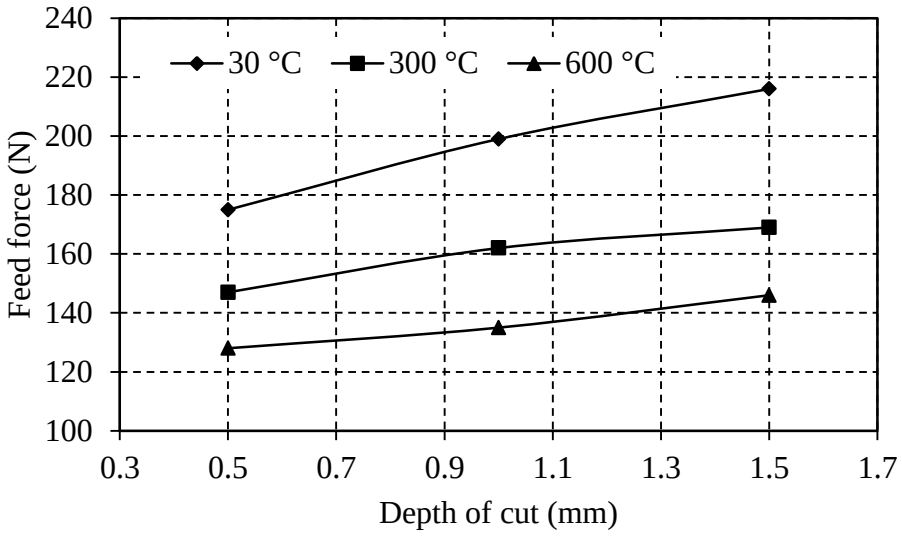

(b)

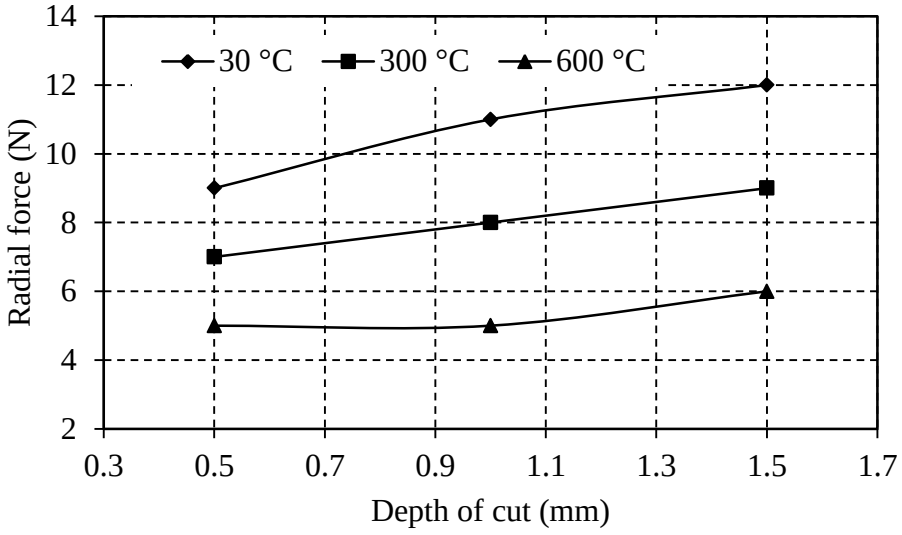

(c)

Figure 3.11 Variation of (a) Cutting force (b) Feed force (c) Radial force with respect to workpiece temperature and depth of cut at cutting speed 100 m/min and feed rate 0.13 mm/rev

3.3.2 Surface roughness and microhardness

Effect of cutting speed on surface roughness

Variation of surface roughness of the machined surface was measured at different cutting speed, and workpiece temperature as presented in Fig.3.12.

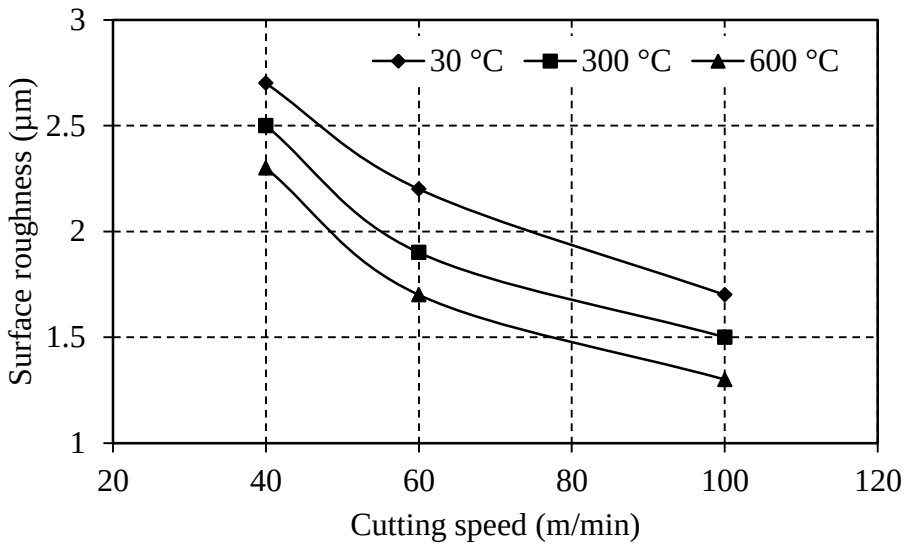

Figure 3.12 Variation of surface roughness with respect to cutting speed and workpeice temperature at feed rate 0.13 mm/rev and depth of cut 0.5 mm

The surface roughness was measured with the help of surface profile meter on three different locations on the machined surface and average value was taken. It was observed that surface roughness decreased by 14, 22 and 23% at 40, 60 and 100 m/min cutting speed respectively, when machining was carried out from room temperature to 600°C. With increase in the cutting speed from 40 to 100 m/min, the surface roughness again decreased (37, 40 and 43%) at 30, 300 and 600°C workpiece temperature respectively.

Effect of feed rate on surface roughness

The surface roughness decreased (26, 20 and 23%) at 0.1, 0.13 and 0.15 mm/rev feed rate respectively, machining at 600°C workpiece temperature compared to room temperature. But surface roughness increased (13, 19 and 17%) at 30, 300 and 600°C temperature respectively, when feed rate increase from 0.1 to 0.15 mm/rev as shown in Fig.3.13.

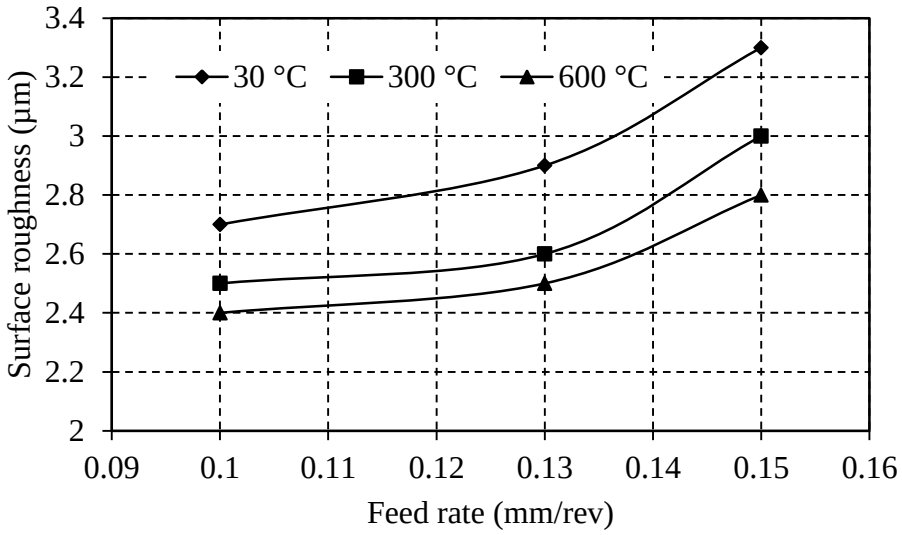

Figure 3.13 Variation of surface roughness with respect to feed rate and workpeice temperature at cutting speed 100 m/min and depth of cut 0.5 mm

Effect of depth of cut on surface roughness

Likewise, the surface roughness decreased (19, 20 and 26%) at 0.5, 1 and 1.5 mm depth of cut respectively, from room temperature to 600°C temperature. When depth of cut increased from 0.5 to 1.5 mm, the surface roughness again decreased (9, 16, and 17%) at 30, 300 and 600°C temperature respectively as shown in Fig.3.14.

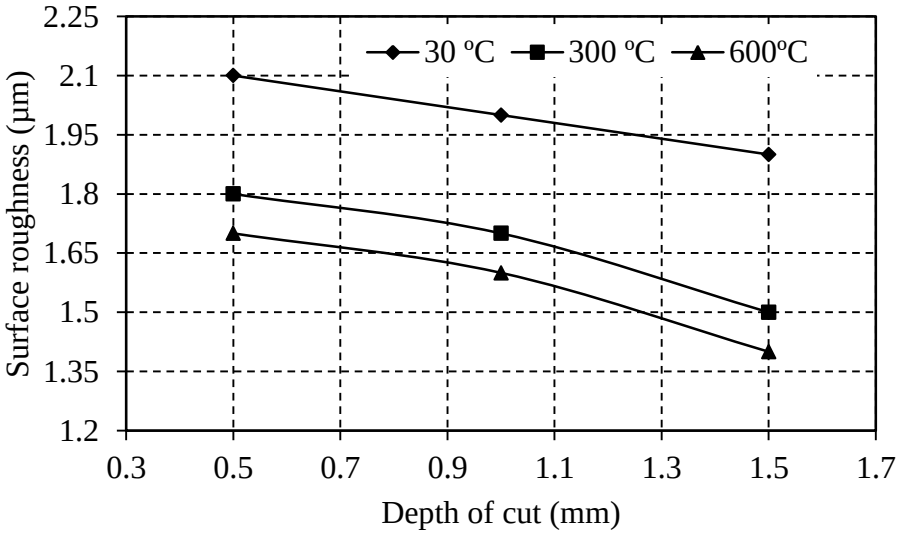

Figure 3.14 Variation of surface roughness with respect to depth of cut and workpeice temperature at cutting speed 100 m/min and feed rate 0.13 mm/rev

Measurement of microhardness

The use of hot machining might have affected the mechanical propertieson the surface of Inconel 718 alloy. So for analyzing the effect of heating on the machined surface and subsurface, the workpiece was cut into cross section with the help of wire-EDM machine and grond with grinding machine for finishing. Finally, it was polished with different types of grade polishing paper. The cutting sample, grinding and polishing machine are shown in Fig 3.15 (a-c).

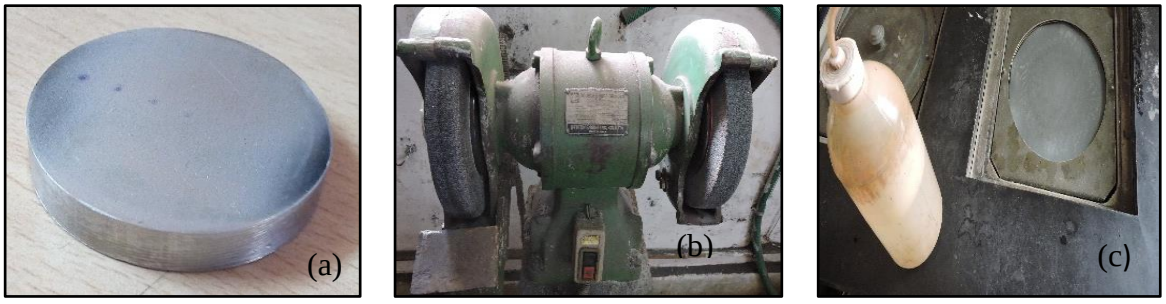

Figure 3.15 (a) Cutting sample (b) Grinding machine (c) Polishing operation

The method of measuring microhardness of sample specimen and corresponding distribution of microhardnessgraph beneath the machined surface is shown in Fig 3.16 (a-b). The microhardness from machined surface was measured toward the center with 20µm equal distance. It was observed that up to 40 µm the hardness value decreased due to softening of material because of heating. Moving from 40 to 140 µm, the hardness value increased due to strain hardening effect. After moving from 140 µm towards to the center, the hardness again decreasedto the hardness of the parent metal. Due to heating, the density of dislocation become lower and which reduce the strain hardening and decrease the hardness. Similar type of observation was observed by Amin and Ginta [79] using induction heat machining of titanium alloys.

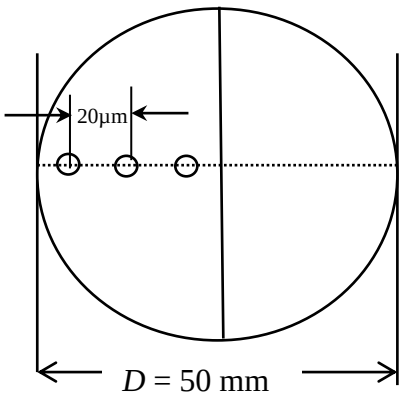

(a)

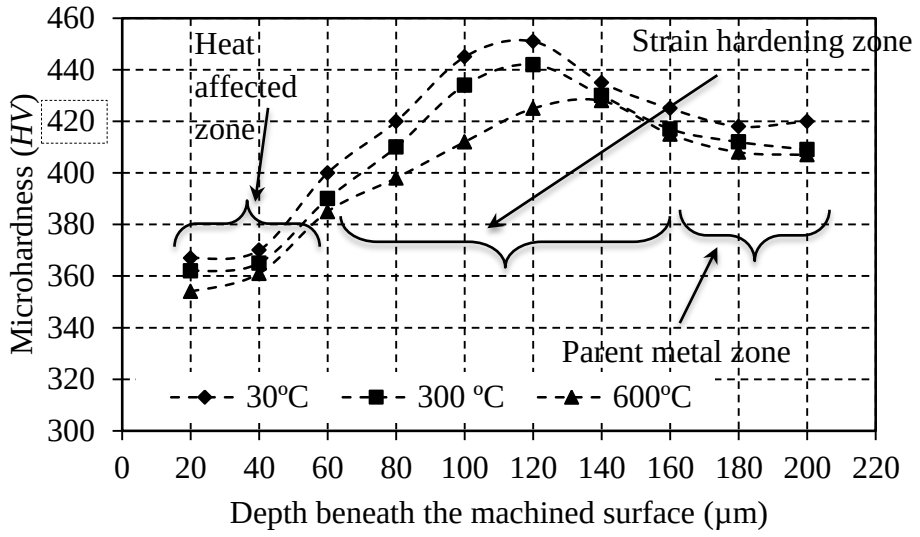

(b)

Figure 3.16 (a) Method of measurement of microhardness sample (b) Microhardness beneath the machine surface of the workpiece at room and hot turning operation

3.3.3 Tool life analysis

During hot machining, the tool life of cutting tool increased due to softening of the workpiece material. The effect of cutting variables and workpiece temperature on tool life and tool wear has been studied in this section.

Effect of cutting speed on tool life

It is important to understand the effect of cutting speed on tool wear as it is the most dominant factor that affects tool life. The flank wear of the cutting tool was measured at 2 min interval to determine the tool life using optical and scanning electron microscope.

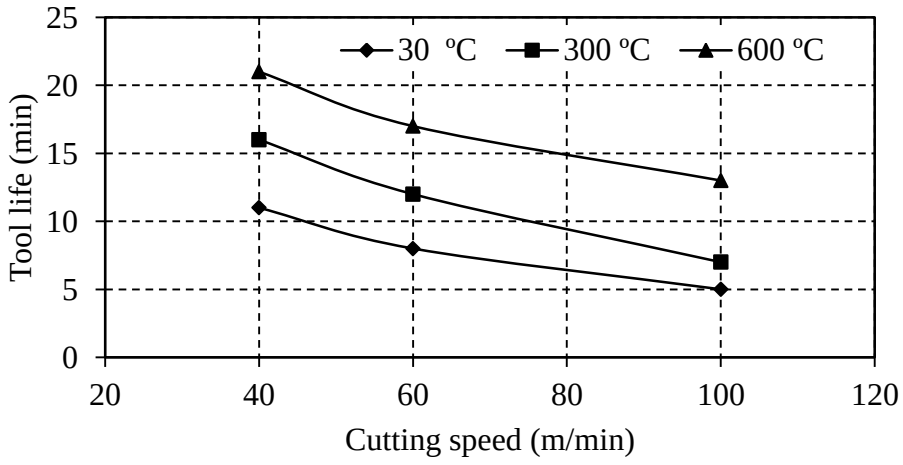

(a)

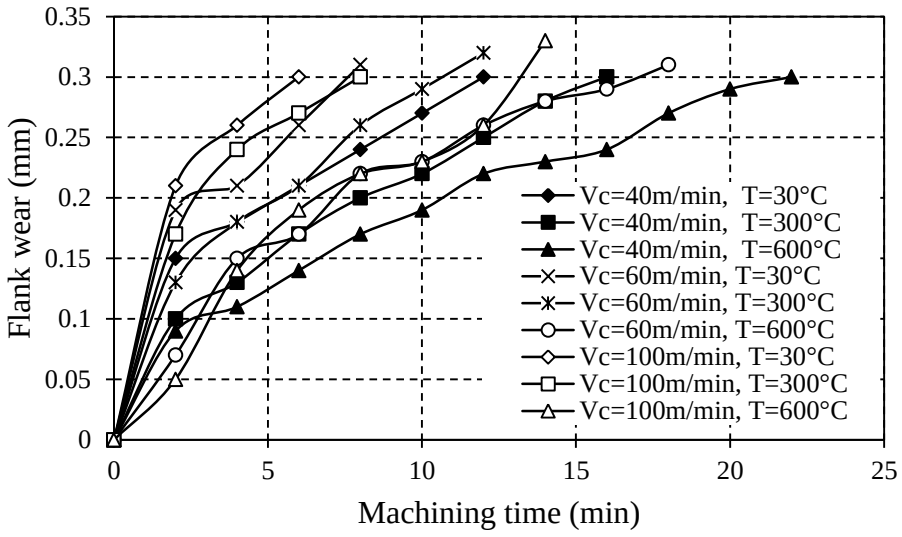

(b)

Figure 3.17 Variation of (a) Tool life (b) Flank wear with respect to cutting speed and workpiece temperature at feed rate 0.15 mm/rev and depth of cut 0.5 mm

The height of flank wear was taken 0.3 mm as criteria of tool life. There was increase of (90, 112 and 160%) of tool life at 40, 60 and 100 m/min cutting speed respectively, when workpiece was heated from room temperature to 600°C temperature. This was due to at high temperature, the material became softened and stress acting on the tool was less. Hence, tool wear reduced. With increase of the cutting speed from 40 to 100 m/min, there was decrease in tool life (42, 60 and 42%) at 30, 300 and 600°C workpiece temperature. This is due to, at high cutting speed, there was increase of cutting zone or process zone temperature which again reduced the shear strength of material, hence increase the tool life. The variation of tool life and corresponding flank wear with respect to cutting speed and workpiece temperature is shown in Fig.3.17 (a-b).

Effect of feed rate on tool life

The variation of tool life and flank wear with respect feed rate and workpiece temperature is shown in Fig 3.18 (a-b). Increasing workpiece temperature from 30°C to 600°C, the tool life increased (125, 150 and 140%) at 0.1, 0.13 and 0.15 mm/rev feed rate respectively.

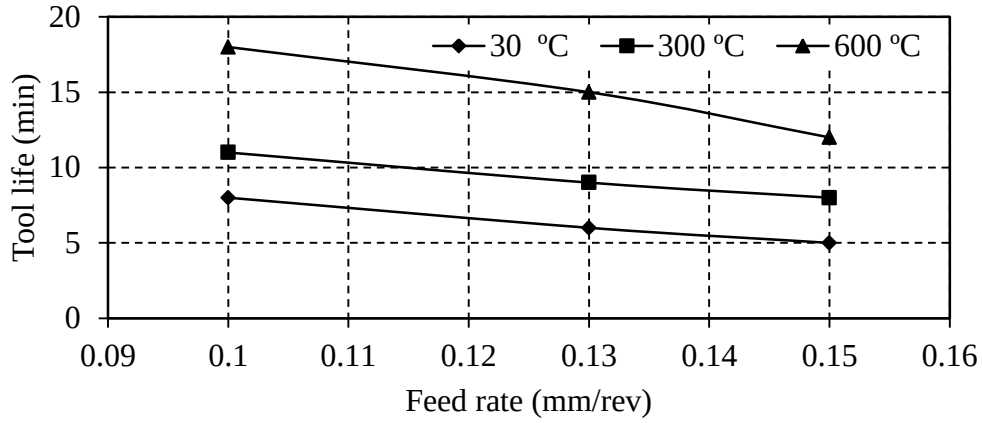

(a)

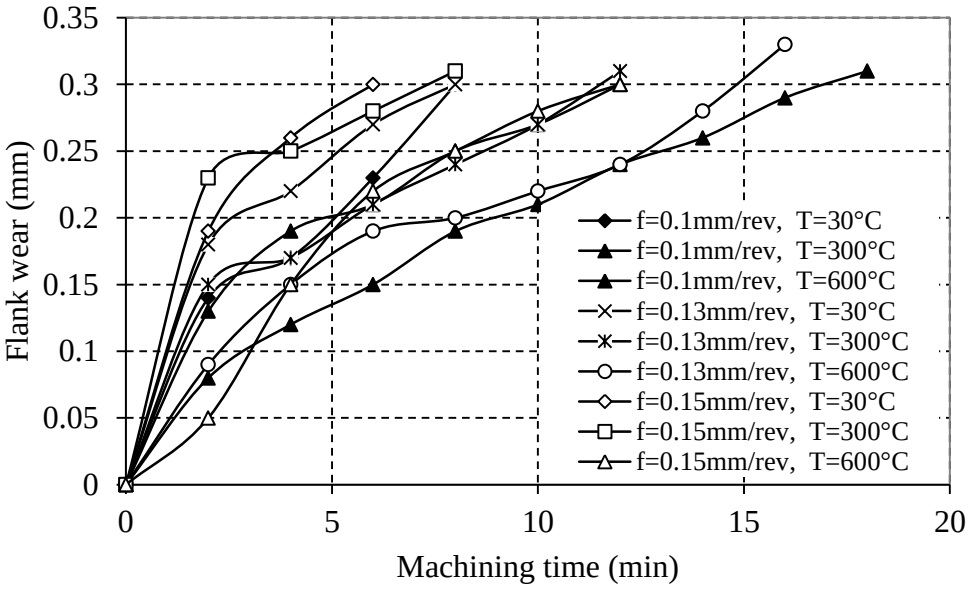

(b)

Figure 3.18 Variation of (a) Tool life (b) Flank wear with respect to feed rate and workpiece temperature at cutting speed 100 m/min and depth of cut 0.5 mm

But with increase the feed rate from 0.1 to 0.15 mm/rev, there was decrease in tool life 37, 27 and 33% at 30, 300 and 600ºC workpiece temperature respectively. This may be during hot machining at high feed rate, there is not sufficient heat transfer to the cutting zone. Hence the reduction of shear strength in the workpiece material is not possible.

Effect of depth of cut on tool life

The variation of tool life and flank wear with respect to depth of cut and temperature of the workpiece is shown in Fig 3.19 (a-b). There is increase of tool life 30, 25 and 40% at 0.5, 1 and 1.5 mm depth of cut respectively, machining from room temperature to 600°C

workpiece temperature. But with increase the depth of cut from 0.5 to 1.5 mm, the tool life decreased (37, 27 and 33%) at 30, 300 and 600ºC temperature respectively. The variation of flank wear with respect to time is shown in Fig. 3.19 (b) for different condition of depth of cut and temperature.

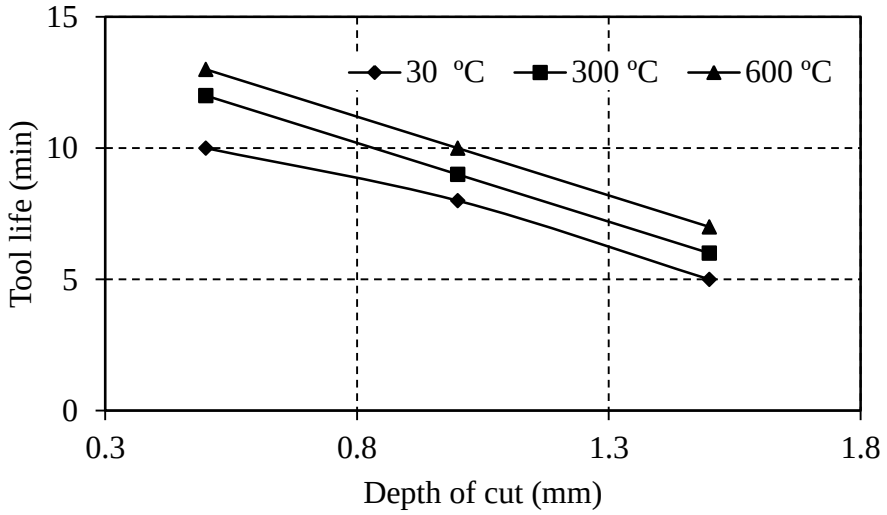

(a)

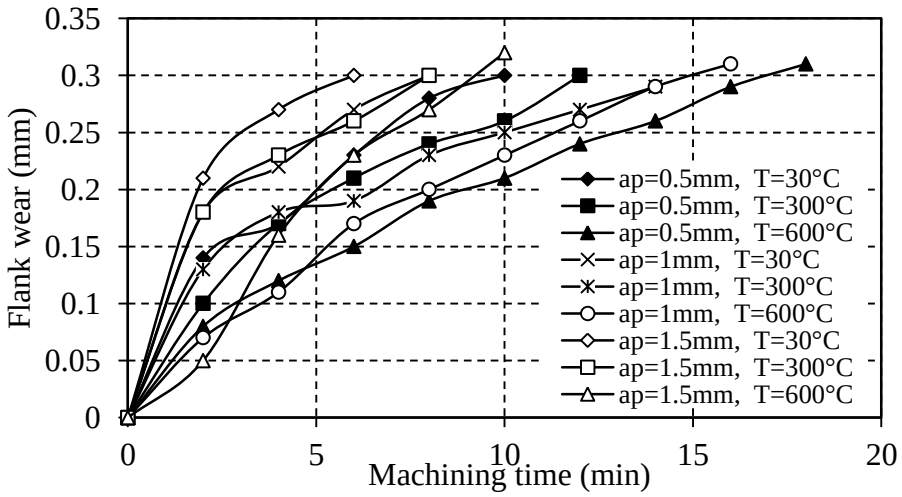

(b)

Figure 3.19 Variation of (a) Tool life (b) Flank wear with respect to depth of cut and workpiece temperature at cutting speed 100 m/min and feed rate 0.13 mm/rev

3.3.4 Tool wear analysis

The images of worn tool at room and high temperature of the workpiece during hot machining using optical microscope are shown in Fig 3.20. The experimental runs with different cutting speed, feed and workpiece temperature were selected for this purpose to

analyze and verify. It is clearly shown that the wear is reduced to different degree after heat assisted machining, but increase of cutting speed and feed rate at constant depth of cut increase tool wear. It is observed that at room and 300ºC temperature, both attrition and abrasion wear are found more dominant. While heating 600ºC, the tool softens and diffusion wear is the more dominant. Due to application of heating, the cutting force, dynamic loads acting on the tool is less. This reduced the tool wear.

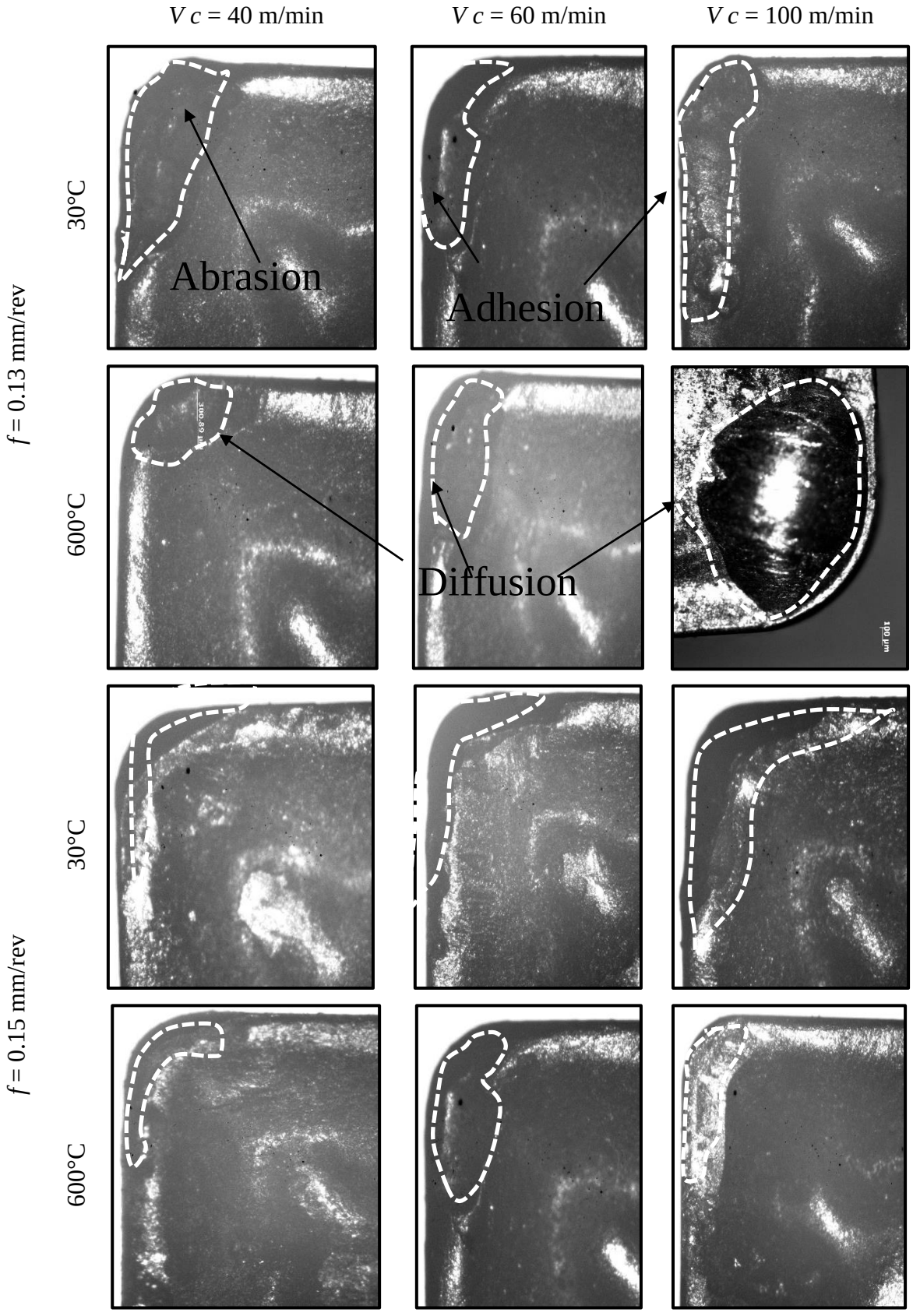

Figure 3.20 Tool wear at different conditions of machining of Inconel 718

3.3.5 Chip morphology analysis

The chip morphology was observed which were machined at room temperature and heated conditions.

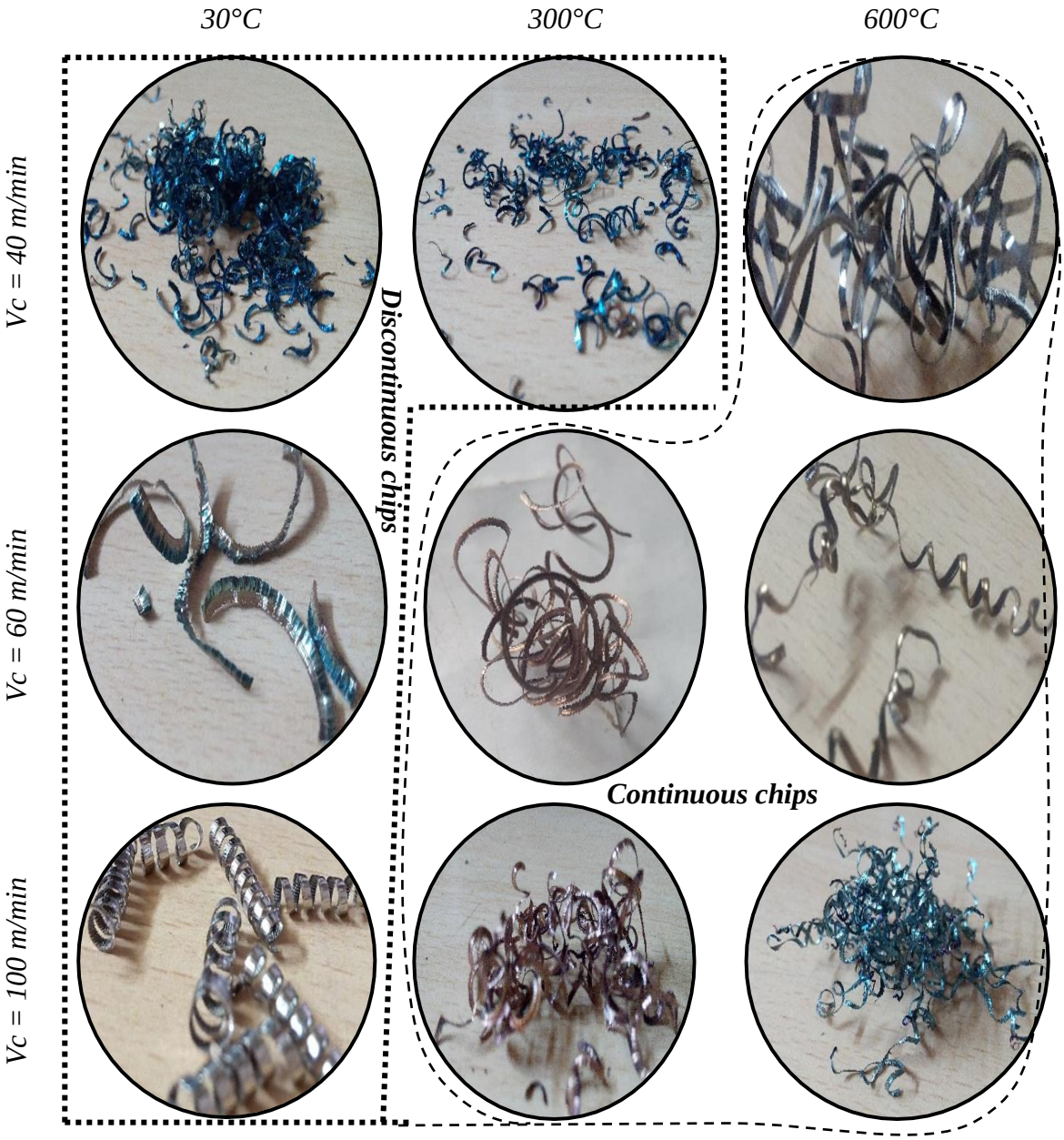

Figure 3.21 Chip morphology with respect to cutting speed and workpiece temperature at *f=0.13* mm/rev and a_p*=0.5* mm

The chips formed during room temperature are wavy structure and have high strain rate. But at heated conditions the chips formed are of continuous type, due to thermal softening of the workpiece (Fig 3.21). The chips are discontinuous type at low cutting speed and low temperature. At high temperature, the ductility of the workpiece increases. As a result, the

formation of continuous chip takes place. In each experiment, the chips were collected and put on the plastic bag and marked with the corresponding cutting conditions.The chip thickness was measured with the help of optical microscope and was observed that the chip thickness decrease with the increase of workpiece temperature compared to room temperature.The chips from the experiment were collected to study the chip serration and chip geometry. For this the chips were mounted, polished properly and etched with kronel reagent (2% of hydrochloric acid, 2% of hydrofloric acid, and water). The chips were examined with the help of scanning electron microscope (SEM) with different magnification. At cutting speed of 100 m/min, segmented type of chip was formed at room temperature and with an increase of workpiece temperature the segmented chips gradually converted into almost continuous chips. As the workpiece temperatureincreases, chip serration decreased and finally disappeared as shown in Fig.3.22 (a-c).

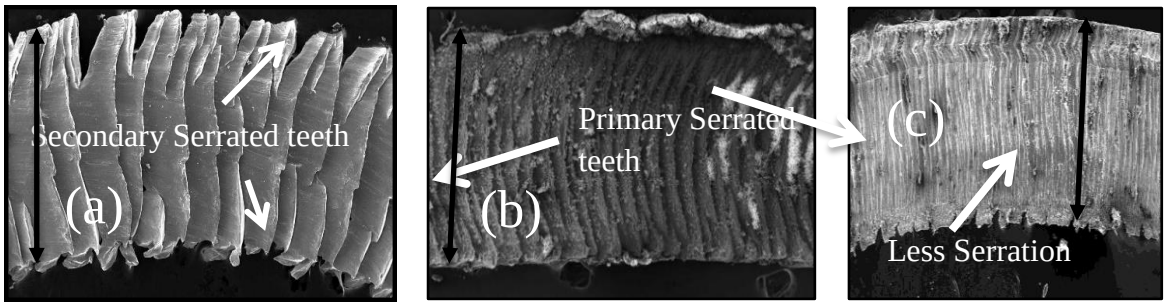

Figure 3.22 SEM view of chip serration at (a) 30°C (b) 300°C (c) 600°C

The chip parameters such as tooth spacing or chip pitch, peak, valley of the chip was taken from the SEM image of the chip segment (Fig 3.23). Generally, chip geometry of segmented chip characterized by three parameters such as Degree of segmentation ratio, segmentation frequency and chip pitch.

The degree of segmentation ratio is defined as [144].

$$D_s = (H_{\max} - H_{\min}) / H_{\max} \qquad (3\text{-}2)$$

where, D_s is the degree of segmentation, $H_{\max}, H_{\min}$ are the maximum and minimum height of the serrated chip. Similarly, the frequency of segmentation can calculated using Eq.(3-3) [144]. It is defined as the number of saw tooth chip formed per second during the machining process.

$$Segmentation\ frequency\ (f_s) = \frac{Cutting\ speed}{Undeformed\ Surface\ Length} \qquad (3-3)$$

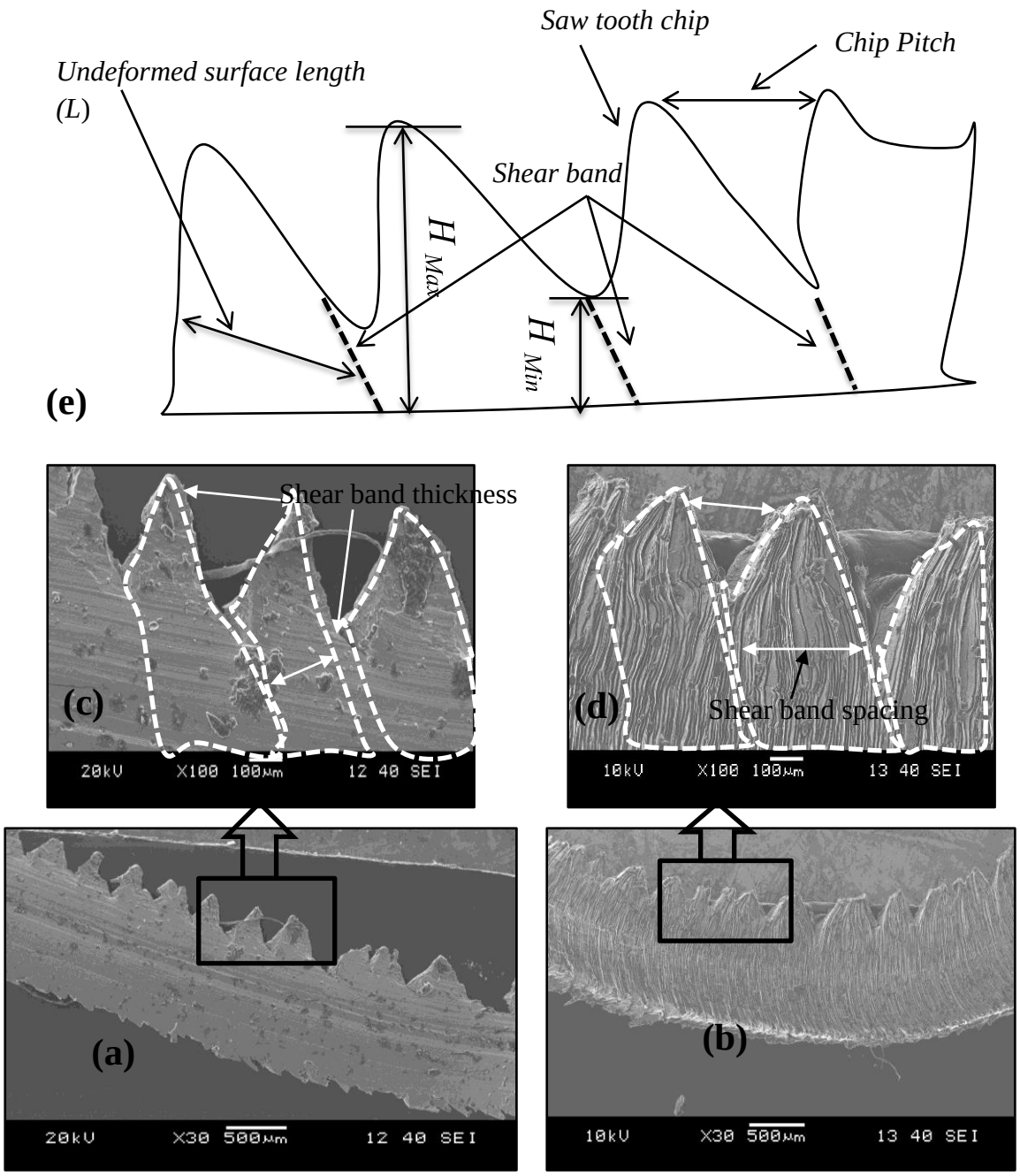

Figure 3.23 Cross section of chip obtained at different machining environment (a) at 30ºC (b) at 600ºC at cutting speed of 100 m/min (c) magnification view of 30°C (d) magnification view of 600°C (e) Schematic diagram for evaluation of segmentation frequency, chip pitch

It was observed that with the increase of workpiece temperature, the degree of segmentation ratio, frequency of serration, tooth spacing or chip pitch decreases compared to room temperature as shown in Fig.3.24, Fig.3.25 and Fig.3.26 respectively. All the measurement was done with the help of imageJ software. With the increase of temperature of workpiece, during hot machining, serration disappeared with formation of continuous chip.

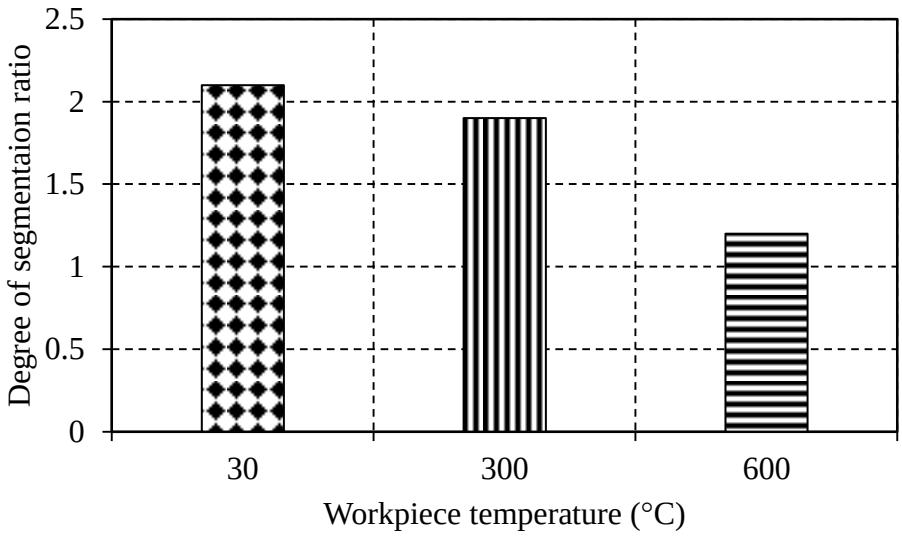

Figure 3.24 Degree of segmentation ratio at different workpiece temperature at cutting speed of 100 m/min, feed 0.13 mm/rev and depth of cut 0.5 mm

At room temperature, higher segmentation frequencywas observed compared to high temperature 600°C. With increase inworkpiece temperature, the undeformed surface length increases, this reduces segmentation frequency. It is also observed that with the increase of workpiece temperature the shear band spacing increases, but shear band thickness decreases. Similar observation was observed in machining titanium alloy different environment i.e. cryogenic, room and heated conditions [145].

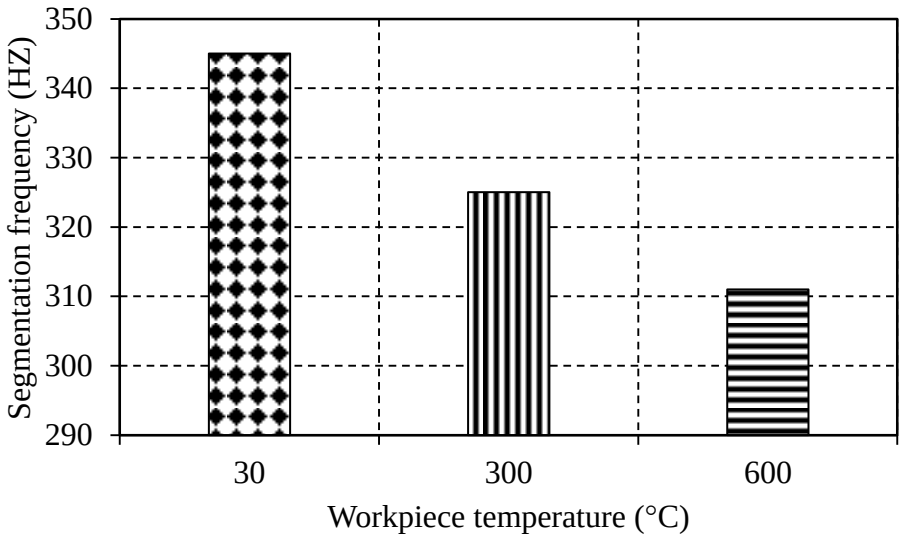

Figure 3.25 Segmentation frequency at different workpiece temperature at cutting speed of 100 m/min, feed rate 0.13 mm/rev and depth of cut 0.5 mm

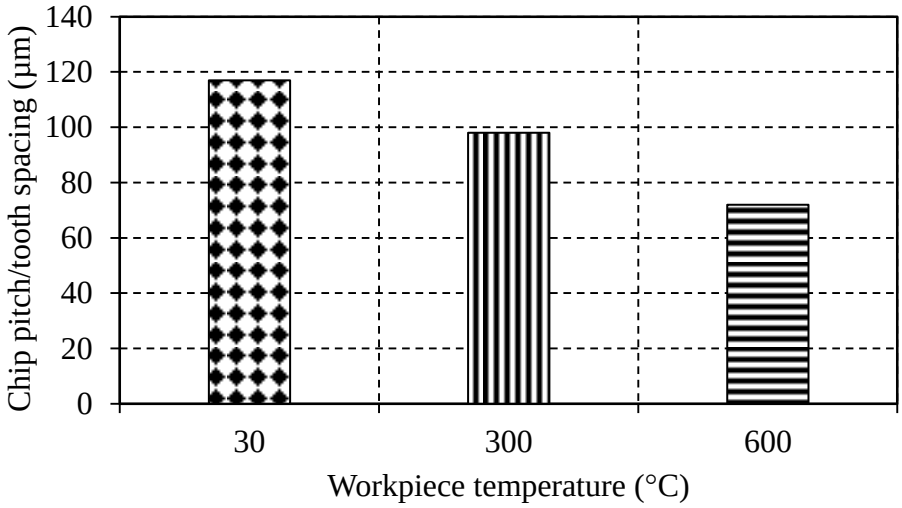

Figure 3.26 Chip pitch/ tooth spacing at different workpiece temperature at cutting speed of 100 m/min, feed rate 0.13 mm/rev and depth of cut 0.5 mm

3.3.6 Natural contact length of chip

The optical view of natural chip-tool contact length and variation with workpiece temperature is shown in Fig 3.27. It is clearly seen that natural chip-tool contact length increased 95.52 µm to 360.41 µm with increase of workpiece temperature from 30°C to 600°C. The benefit of longer chip-tool contact length may lower the normal stress acting on tool [79].

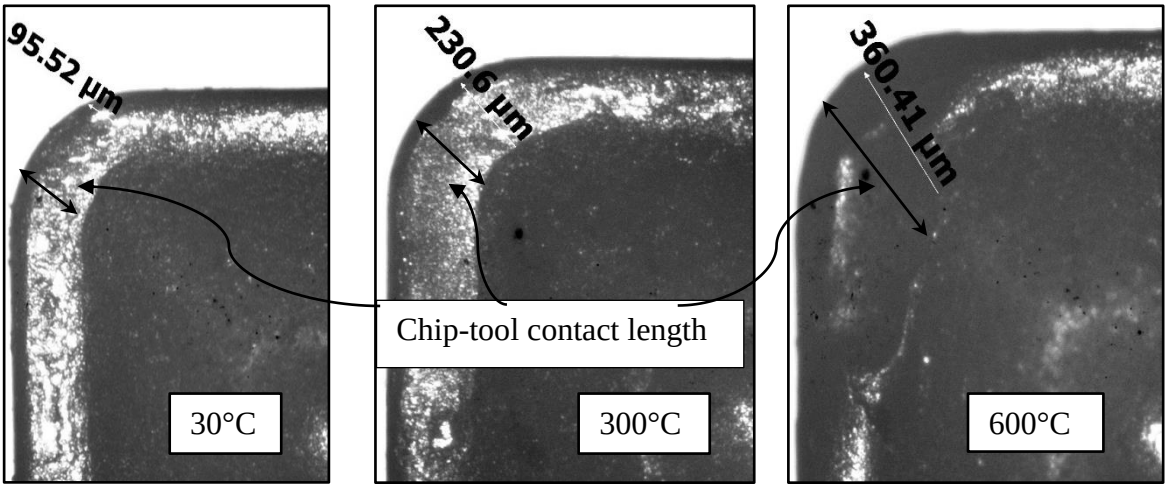

Figure 3.27 Optical view of chip-tool contact length at room and heated conditions at cutting speed of 100 m/min, feed 0.13 mm/rev and depth of cut 0.5 mm

3.4 Modeling of hot turning of Inconel 718 using response surface methodology

3.4.1 Introduction

The relationship between the cutting parameters (cutting speed, feed rate and depth of cut) and workpiece temperature on surface roughness and tool wear in hot machining of Inconel 718 has been statistically evaluated using surface response methodology in this section. The experimental plan was based on the central composite design and significance of the cutting parameters was evaluated using analysis of variance (ANOVA). The predicted results from the regression equation were found to be in good agreement with the experimental results. Basically, surface response methodology is the collection mathematical model which determines the relationship between the process parameters and responses. To develop the response surface methodology (RSM) base for surface roughness and flank wear mode, it is necessary to plan the experiment. The experiments were conducted with four factor, 3-level and two responses variables. MINITAB software was used to obtain the sequential set of the experimental run.

The relation between the inputs or machining parameters such as cutting speed (V_c), feed rate (f), depth of cut (a_p) and temperature (T) and the responses (flank wear and surface roughness) Y is defined as

$$Y = \phi\left(V_c,\ f, a_p\ T\right) + e \qquad (3\text{-}4)$$

The function ϕ is called response function and e is experimental errors. The approximation of Y is proposed by using quadratic second-order mathematic model. The quadratic model can be expressed as

$$Y = c_0 + \sum_{i=1}^{3} c_i x_i + \sum_{i=1}^{3} c_{ii} x_i^2 + \sum_{i<j}^{3} c_{ij} x_i x_j \qquad (3\text{-}5)$$

3.4.2 Modeling and discussion

Cutting parameters along with workpiece temperature were taken as input parameters with each three level (low, medium and high). The medium value was chosen by average of low and high input values and tabulated in Table 3.12. The experimental results of surface roughness and tool wear along with design matrix are tabulated in Table 3.13.

Table 3.12 Machining parameters and their levels

Parameters	Unit	Levels		
		-1	0	+1
Cutting speed (V_c)	m/min	40	70	100
Feed rate (f)	mm/rev	0.1	0.125	0.15
Depth of cut (a_p)	mm	0.5	1	1.5
Temperature (T)	°C	30	315	600

Table 3.13 Design layout with responses for Inconel 718

Run	Coded factors				Actual factors				Response variables	
	X_1	X_2	X_3	X_4	V_c	f	a_p	T	VB_{max}, mm	R_a, µm
1	0	0	0	0	70	0.125	0.75	315	0.348	2.164
2	-1	+1	-1	+1	40	0.15	0.5	600	0.352	2.566
3	-1	-1	-1	-1	40	0.1	0.5	30	0.342	2.301
4	0	-1	0	0	70	0.1	0.75	315	0.384	2.312
5	+1	0	0	0	100	0.125	0.75	315	0.359	2.114
6	-1	0	0	0	40	0.125	0.75	315	0.332	2.774
7	0	0	0	0	70	0.125	0.75	315	0.347	2.101
8	+1	-1	+1	+1	100	0.1	1	600	0.442	2.192
9	+1	-1	+1	-1	100	0.1	1	30	0.408	2.053
10	+1	-1	-1	-1	100	0.1	0.5	30	0.353	2.053
11	0	0	+1	0	70	0.125	1	315	0.374	2.37
12	0	0	0	0	70	0.125	0.75	315	0.348	2.162
13	-1	+1	-1	-1	40	0.15	0.5	30	0.388	2.411
14	0	+1	0	0	70	0.15	0.75	315	0.368	2.349
15	+1	+1	+1	-1	100	0.15	1	30	0.433	2.237

16	0	0	0	+1	70	0.125	0.75	600	0.382	2.4
17	+1	+1	-1	-1	100	0.15	0.5	30	0.408	2.128
18	-1	-1	+1	+1	40	0.1	1	600	0.393	2.485
19	0	0	0	0	70	0.125	0.75	315	0.346	2.16
20	0	0	0	0	70	0.125	0.75	315	0.347	2.164
21	0	0	0	-1	70	0.125	0.75	30	0.370	2.256
22	-1	-1	+1	+1	40	0.1	1	600	0.354	2.408
23	-1	+1	+1	+1	40	0.15	1	600	0.356	2.664
24	+1	+1	+1	+1	100	0.15	1	600	0.45	2.103
25	+1	-1	-1	+1	100	0.1	0.5	600	0.418	2.128
26	+1	+1	-1	+1	100	0.15	0.5	600	0.433	2.163
27	-1	-1	-1	+1	40	0.1	0.5	600	0.387	2.645
28	0	0	-1	0	70	0.125	0.5	315	0.337	2.223
29	-1	+1	+1	-1	40	0.15	1	30	0.39	2.512
30	0	0	0	0	70	0.125	0.75	315	0.346	2.165

The experimental plans are developed for establishing the quadratic model of tool wear and surface roughness. The fitted ANOVA model for flank wear and surface roughness are shown in Table 3.14. For flank wear the determination of coefficient (R^2) is 93.26%, R^2 adjusted 86.40% and predicted R^2 62.65%. Whereas for surface roughness the value of the coefficient of determination, R^2 adjusted and predicted R^2 are 92.45%, 85.40%, and 74.45% respectively. When the coefficient of determination approaches to unity, then predicted model fits to the actual data.

The ANOVA tables for the reduced quadratic model for flank wear and surface roughness are shown in Table 3.15 and Table 3.16 respectively. When *P* values in Table 3.15 and Table 3.16 is less than 0.05, the corresponding term is considered to be significant. The significant terms for flank wear are cutting speed, depth of cut, temperature and square of cutting speed, temperature, product of temperature and speed, and product of feed and temperature as these values are less than 0.05.

Table 3.14 ANOVA table for the fitted models

Source	DoF	SS	MS	*F*-Value	*P*-Value
Flank wear					
Model	14	0.030804	0.002200	14.83	0
Error	15	0.002226	0.000148		
Lack-of-fit	9	0.001461	0.000162	1.27	0.397
Pure error	6	0.000765	0.00127		
Total	29	0.033029			
R^2-93.26					
R^2 Adjusted-86.97					
Prediction R^2-62.65					

Surface roughness					
Model	14	0.96986	0.069275	13.12	0
Error	15	0.07922	0.005282		
Lack-of-fit	9	0.06697	0.007441	3.64	0.065
Pure error	6	0.053120	0.008853		
Total	29	1.04908			
R^2-92.45					
R^2 Adjusted-85.40					
Prediction R^2-74.45					

Similarly, for surface roughness the significant terms are cutting speed, depth of cut and square of cutting speed. The insignificant parameters can be eliminated by selecting backward elimination procedure.

Table 3.15 Analysis of variances (ANOVA) for the flank wear (VB_{max})

Source	DoF	SS	MS	*F*-Value	*P*-Value	Remarks
Model	14	0.030804	0.002200	14.83	0	
V_c	1	0.008502	0.008502	57.29	**0.000***	Significant
f	1	0.000465	0.000465	3.13	0.097	
a_p	1	0.001715	0.001715	19.70	**0.000***	Significant
T	1	0.000639	0.000639	11.55	**0.004***	Significant
Vc^2	1	0.000108	0.000108	0.73	0.406	
f^2	1	0.001494	0.001494	10.07	**0.006***	Significant
a_p^2	1	0.00032	0.00032	0.22	0.648	
T^2	1	0.001494	0.001494	10.07	**0.006***	Significant
V_c* f	1	0.000506	0.000506	3.41	0.085	
V_c* a_p	1	0.000518	0.000518	3.49	0.085	
V_c* T	1	0.001700	0.001700	11.46	**0.004***	Significant
f* a_p	1	0.000250	0.000250	2.23	0.156	
f* T	1	0.001350	0.001350	9.10	**0.009***	Significant
a_p*T	1	0.000478	0.000478	3.22	0.093	
Residual	15	0.002226	0.000148			
Total	29	0.033029				

Table 3.16 Analysis of variances (ANOVA) for the Surface roughness (R_a)

Source	DoF	SS	MS	*F*-Value	*P*-Value	Remarks
Model	14	0.96986	0.069275	13.12	0	
V_c	1	0.67446	0.674455	127.70	**0.000***	Significant
f	1	0.01209	0.012094	2.29	0.151	
a_p	1	0.00049	0.000487	0.09	0.766	
T	1	0.02738	0.027381	0.09	0.766	
Vc^2	1	0.06240	0.062402	11.82	**0.004***	Significant

f^2	1	0.00002	0.000019	0	0.953	
a_p^2	1	0.02106	0.021055	3.99	0.064	
T^2	1	0.00015	0.000154	0.03	0.867	
$V_c * f$	1	0.00104	0.001038	0.20	0.664	
$V_c * a_p$	1	0.00195	0.001947	0.37	0.553	
$V_c * T$	1	0.03513	0.035133	6.65	**0.021***	Significant
$f * a_p$	1	0.00330	0.003301	0.63	0.441	
$f * T$	1	0.00001	0.000007	0	0.971	
$a_p * T$	1	0.02273	0.022731	4.30	0.056	
Residual	15	0.02273	0.005282			
Total	29	1.04908				

In terms of coded factors, the final quadratic models of flank wear and surface roughness equation are equated in Eq. (3-6) and Eq.(3-7) respectively.

$$\textit{Flank wear} = 0.34949+0.02270\ X_1+0.00531\ X_2+0.01019\ X_3+0.00640\ X_4-0.00647\ X_1\ X_1+0.02403\ X_2\ X_2+0.00353\ X_3\ X_3+0.0203\ X_4\ X_4+0.00590\ X_1\ X_2+0.00597\ X_1\ X_3+0.01117\ X_1\ X_4-0.00315\ X_2\ X_3-0.00995\ X_2\ X_4-0.00592\ X_3\ X_4 \quad (3\text{-}6)$$

$$\textit{Surface roughness} = 2.4152-0.2022\ X_1+0.0271\ X_2+0.0054\ X_3+0.0419\ X_4+0.1553\ X_1\ X_1-0.0027\ X_2\ X_2-0.0902\ X_3\ X_3-0.0077\ X_4\ X_4-0.0085\ X_1\ X_2+0.0116\ X_1\ X_3-0.0508\ X_1\ X_4+0.0151\ X_2\ X_3+0.0007\ X_2\ X_4-0.0408\ X_3\ X_4 \quad (3\text{-}7)$$

In terms of actual factors, the final quadratic models of response equation (flank wear and surface roughness) are as follows Eq. (3-8) and Eq.(3-9):

$$\textit{Flank wear} = 0.876-0.00023Vc-9.13f-0.010\ a_p-0.000018*T-0.000007\ Vc*Vc+38.4\ f*f+0.056\ a_p*a_p+0.000000\ T*T+0.00787\ Vc*f+0.000796\ Vc*a+0.000001\ Vc*T-0.505\ f*a_p-0.001397\ f*T-0.000083\ a_p*T \quad (3\text{-}8)$$

$$\textit{Surface Roughness} = 2.78-0.0198\ Vc-0.5\ f+0.61\ a_p+0.001169\ T+0.000123\ Vc*Vc+4\ f*f-0.56\ a_p*a_p-0.000000\ T*T\ 0.0199\ Vc*f+0.00074\ Vc*a_p\ 0.000006\ Vc*T+3.45\ f*a_p-0.00127\ f*T-0.000611\ a_p*T \quad (3\text{-}9)$$

The actual factors, final quadratic models of flank wear and surface roughness is used to predict within the factors studied. The comparison between predicted and measured flank wear and surface roughness are shown in Fig. 3.28 and Fig. 3.29 respectively. An average of 4% error for flank wear and 3% for surface roughness were observed between the predicted and measured values.

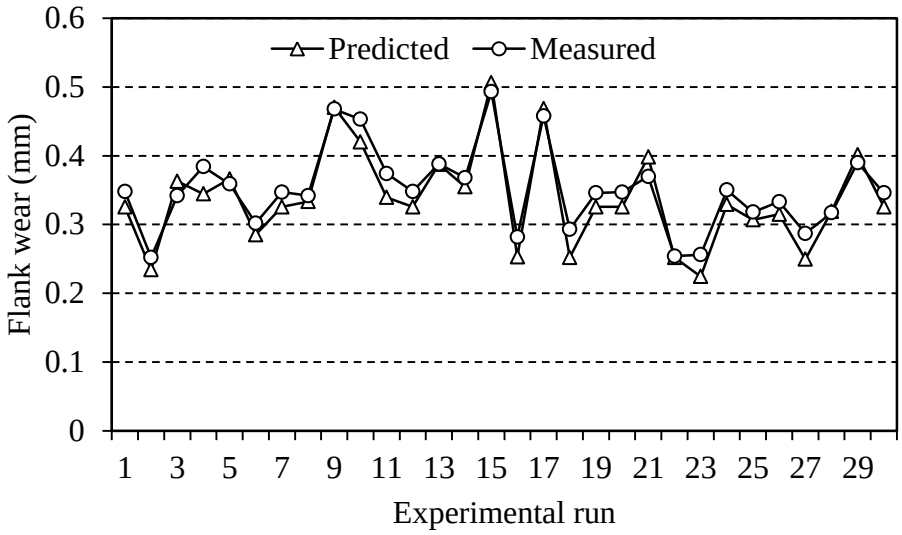

Figure 3.28 Comparison between measured and predicted value for the flank wear

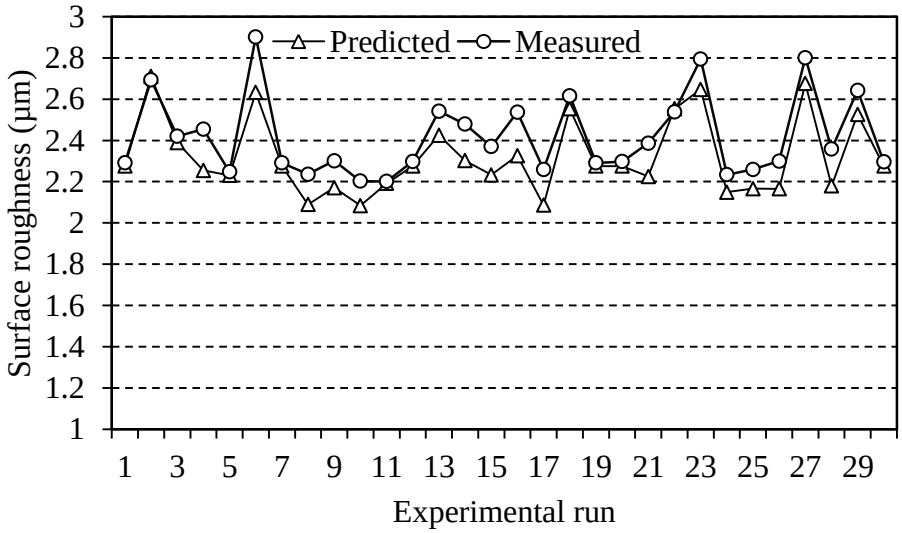

Figure 3.29 Comparison between measured and predicted value for the surface roughness

Three-dimensional surface and corresponding contour plot are drawn, to evaluate the effect of machining parameters on surface roughness and flank wear shown in Fig. 3.30 (a-b) and Fig. 3.31 (a-b) respectively. The estimated response surface for the surface roughness is made at the variation of cutting speed and feed while the depth of cut and temperature is kept at the middle level. Surface roughness decreases with the increase of cutting speed. The increase of temperature and depth of cut with at the middle level of cutting speed and feed rate enhance the surface roughness for a certain value of the depth of cut. After an increase of depth of cut, the surface roughness decreases.

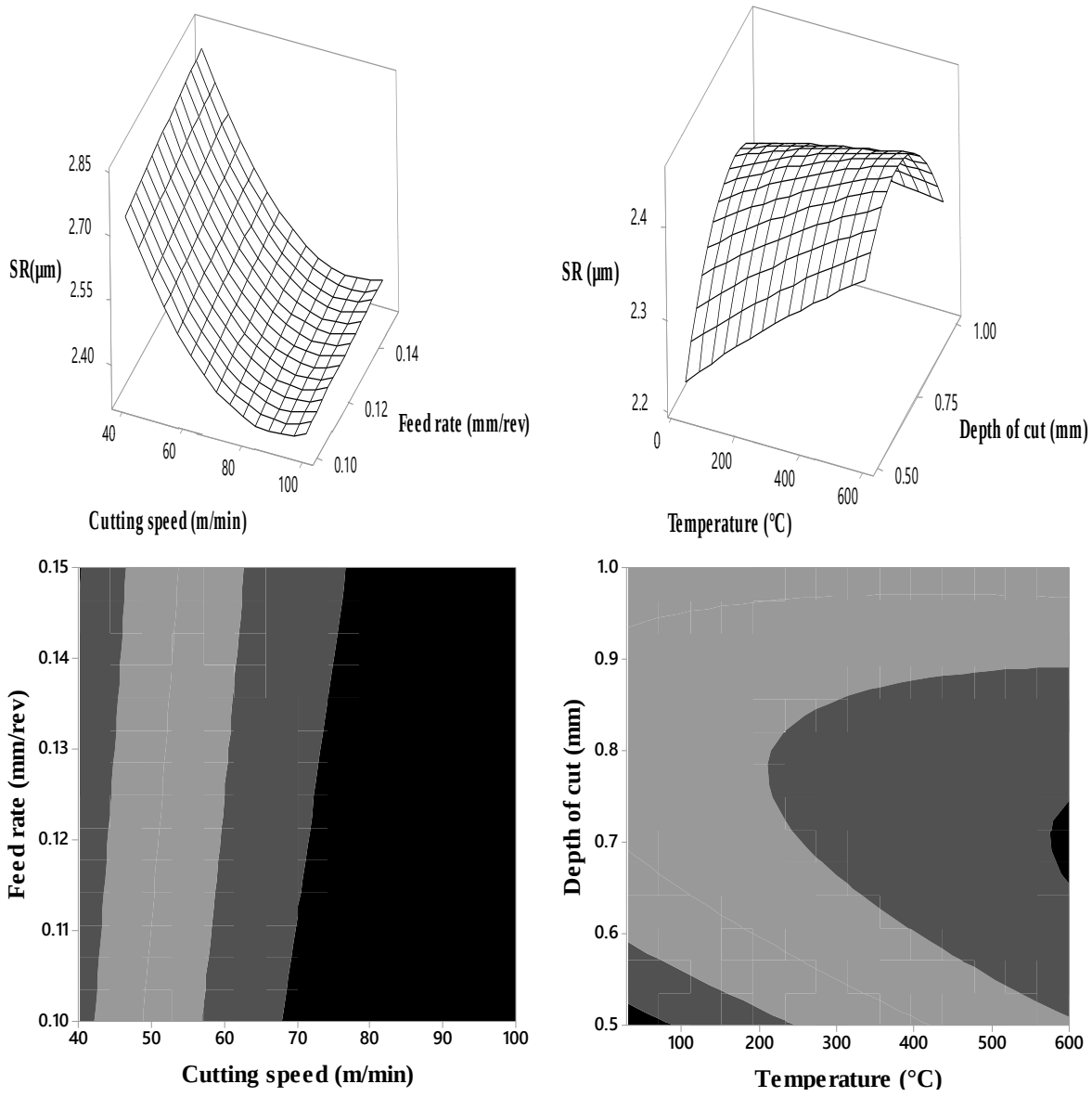

(a) (b)

Figure 3.30 Surface and contour plot for surface roughness with respect to (a) Cutting speed and feed rate (b) Temperature and depth of cut

The surface and contour plot for flank wear shows that with increase of feed rate and cutting speed, flank wear increases while the depth of cut and temperature are kept at the middle level. With the increase of depth of cut there is an increase of flank wear. Increase in temperature reduces flank wear up to certain limit. Increase in temperature enhances flank wear when cutting speed and feed are kept at the middle level.

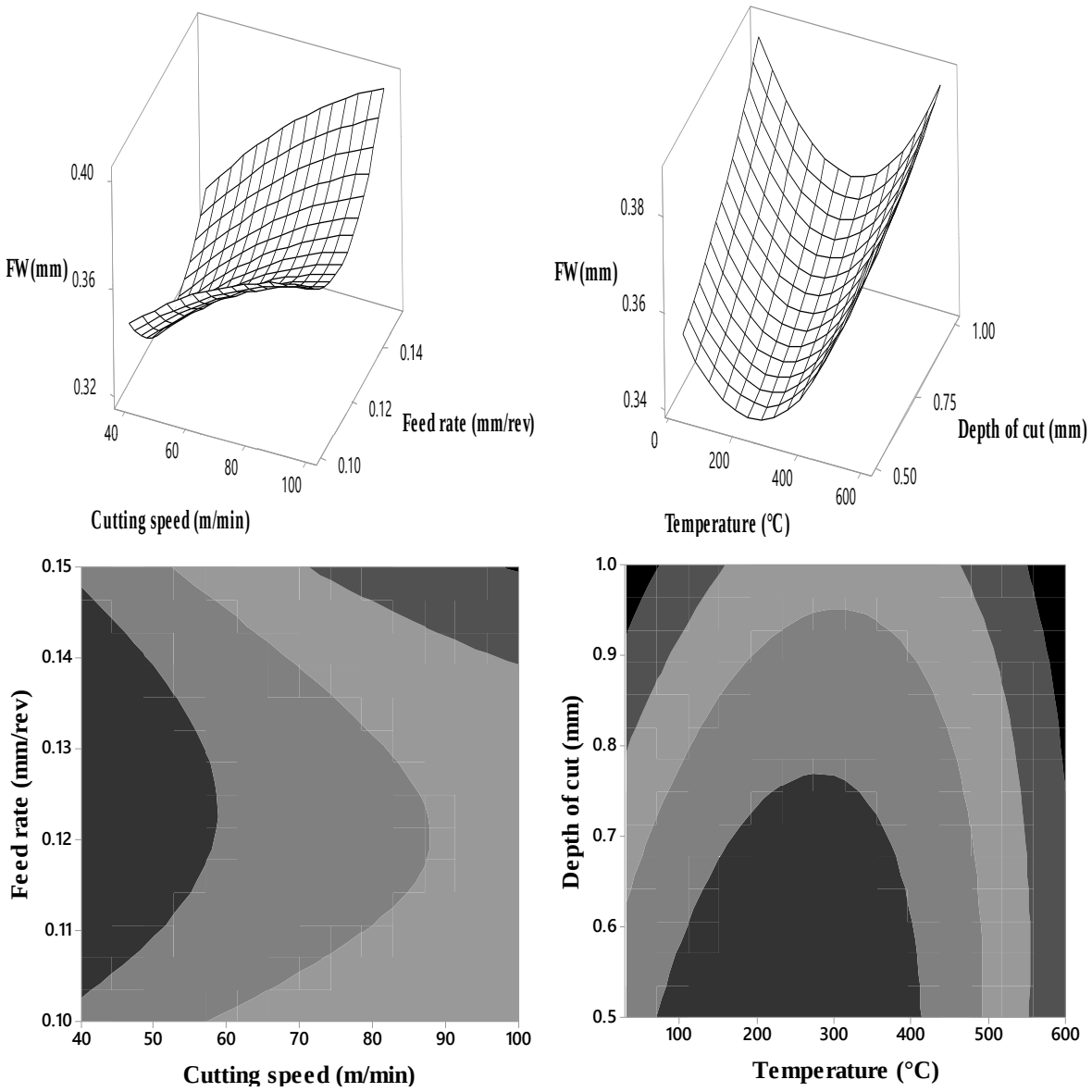

(a) (b)

Figure 3.31 Surface and contour plot for flank wear with respect to (a) Cutting speed and feed rate (b) Temperature and depth of cut

3.5 Optimization of hot machining parameters of Inconel 718 using desirability-taguchi and PCA-taguchi method

3.5.1 Introduction

In this section, the optimization of machining parameters in hot turning of Inconel 718 has been studied. L_9 orthogonal array has been selected for design of experiment. Surface roughness, chip reduction ratio and flank wear were the outputs. Two optimization technique such as Principal component analysis (PCA) and desirability function analysis (DFA) along with Taguchi's method have been used to optimize the multi-responses in hot turning of Inconel 718.

3.5.2 Experimental Procedure

The experiment was carried out at various cutting speed, feed rate, depth of cut and workpiece temperature. The machining parameters are tabulated in Table 3.17. L_9 orthogonal array has been taken for design of experiment (DOE). The experiments were performed according to the DOE and the results are tabulated in Table 3.18.

Table 3.17 Input parameters and levels

Process parameters	Level (1)	Level (2)	Level (3)
Cutting speed (m/min)	40	60	100
Feed (mm/rev)	0.1	0.13	0.15
Depth of cut (mm)	0.5	1	1.5
Temperature (°C)	30	300	600

3.5.3 Principal component analysis

Principal Component Analysis (PCA) is a way of identifying patterns in the correlated data, and expressing the data in such a way so as to highlight their similarities and difference. The main advantage of PCA is that once the patterns in data have been identified, the data can be compressed, i.e. by reducing the number of dimensions, without much loss of information. The steps involved in PCA are discussed below:

1. Getting some data

2. Normalization of data

3. Calculation of covariance matrix.

4. Interpretation of covariance matrix.

The outputs of the design of experiment data are normalized according to higher the better or lower the better criterion. Normalized data are calculated using Eq. (3-10), Eq. (3-11) and tabulated in Table 3.18. In this case, surface roughness (*Ra*), flank wear (*VB*) and chip reduction coefficient (ξ) were chosen as lower the better the criteria.

(1) The higher is the better

$$x_i^*(y) = \frac{x_i^{(0)}(y) - \min\ x_i^{(0)}(y)}{\max\ \mathrm{x}_i^{(0)}(y) - \min x_i^{(0)}(y)} \tag{3-10}$$

(2) The lower is the better

$$x_i^*(y) = \frac{\max\ x_i^{(0)}(y) - x_i^{(0)}(y)}{\max\ \mathrm{x}_i^{(0)}(y) - \min x_i^{(0)}(y)} \tag{3-11}$$

wherex_i is the current response, *max* x_i, and *min* x_i, are the maximum and minimum output in the layout. The normalized data have then been utilized to construct a covariance matrix *E*, which is illustrated as below:

$$E = \begin{bmatrix} E_{1,1}\ E_{1,2}\ E_{1,3}.\ldots.E_{1,n} \\ E_{2,1}\ E_{2,2}\ E_{2,3}.\ldots.E_{2,n} \\ .\quad .\quad .\quad .\ .\ . \\ E_{c,1}\quad E_{c,2}\quad E_{c,3}\ .\ .\ E_{c,n} \end{bmatrix} \tag{3-12}$$

The correlation coefficient array can be calculated as

$$E_{p,q} = \frac{Cov\left(Y^*_{i,p}, Y^*_{i,q}\right)}{\sqrt{Var\left(Y^*_{i,p}\right)Var\left(Y^*_{i,q}\right)}} \tag{3-13}$$

$where,\ p = 1,2,3.....,c$ and $q = 1,2,3.....,n$

Number of quality characteristics and experimental runs are denoted as *c* and *n* respectively. Then, eigenvectors and eigenvalues of matrix *E* can be computed from the correlation coefficient array.

$$(E - \lambda_k B_m)C_{ik} = 0 \tag{3-14}$$

where λ_k is the eigenvalues $\sum_{k=1}^{n} \lambda_k = n,$ k=1,2,.....n; and

$C_{ik} = [d_{k1} d_{k2} ..... d_{kn}]$ is the eigenvectors corresponding to the eigenvalue λ_k and the values are tabulated in Table 3.19. The principal component value was calculated using Eq.3.15 and tabulated in Table 3.20. The principal uncorrelated component or multiple performance characteristics index (MPCI) can be determined using Eq. 3.16 and tabulated in Table 3.21.

$$Y_{mk} = \sum_{i=1}^{n} E_{c,n} . C_{ik} \qquad (3\text{-}15)$$

$$X_m = \sum_{i=1}^{n} Y_{mk} e(k) \qquad (3\text{-}16)$$

where, $e(k) = \dfrac{eig(k)}{\sum_{k=1}^{n} eig(k)}$

Table 3.18 Responses with normalized values (Inconel 718)

Run	Input data				Output data			Normalized data		
	Vc	*f*	a_p	*T*	*Ra (μm)*	*ξ*	*VB (mm)*	*Ra*	*ξ*	*VB*
1	40	0.1	0.5	30	2.84	2.203	0.301	1.00	0.35	1.00
2	40	0.13	1	300	1.98	2.422	0.258	0.56	0.43	0.53
3	40	0.15	1.5	600	1.97	2.362	0.297	0.55	0.40	0.96
4	60	0.1	1	600	1.16	2.712	0.248	0.14	0.53	0.42
5	60	0.13	1.5	30	1.48	3.032	0.25	0.30	0.65	0.45
6	60	0.15	0.5	300	1.95	4.01	0.275	0.54	1.00	0.72
7	100	0.1	1.5	300	1.14	1.245	0.209	0.13	0.00	0.00
8	100	0.13	0.5	600	1.18	2.267	0.211	0.15	0.37	0.02
9	100	0.15	1	30	0.89	3.156	0.254	0.00	0.69	0.49

Table 3.19 Eigen values and eigen vectors of the covariance matrix

Eigen value	1.8734	0.9770	0.1496
Eigen vector	0.636	0.425	-0.642
	0.317	-0.905	-0.285
	0.702	0.022	0.712
Proportion	0.624	0.326	0.050
Cumulative	0.624	0.950	1

Table 3.20 Principal components in all L_9 OA experimental observations

Run	Principal 1	Principal 2	Principal 3
1	1.449832	0.13344	-0.0287
2	0.865457	-0.136	-0.101
3	1.152893	-0.1092	0.21034
4	0.554113	-0.412	0.06172
5	0.710759	-0.4465	-0.0611
6	1.167419	-0.6582	-0.1232
7	0.081795	0.05449	-0.0823
8	0.227313	-0.2708	-0.1853
9	0.562461	-0.6147	0.15129

Table 3.21 Multiple performance characteristics index (MPCI) and SN ratio

Run	MPCI	SN ratio
1	0.947	-0.4752
2	0.491	-6.18412
3	0.694	-3.16865
4	0.215	-13.3696
5	0.295	-10.6066
6	0.508	-5.88719
7	0.065	-23.7836
8	0.044	-27.0743
9	0.158	-16.0191

Table 3.22 Response table for signal to noise ratio

Level	Cutting speed (m/min)	Feed (mm/rev)	Depth of cut (mm)	Temperature (°C)
1	-3.276	-10.699	-9.651	-9.034
2	-9.954	-14.622	-11.858	-10.256
3	-18.011	-8.358	-12.520	-14.538
Max-Min	14.735	6.263	2.868	5.504
Rank	1	2	4	3

Referring to Table 3.22, cutting speed is the most influential parameter which affects the outputs followed by feed rate, temperature and depth of cut respectively. Fig. 3.32 shows the main effect plots for SN ratio and the maximum value of SN ratio is considered to be optimal setting parameters. The optimal setting was obtained at 40 m/min cutting speed, 0.15 mm/rev feed rate, 0.5 mm depth of cut and 30°C workpiece temperature.

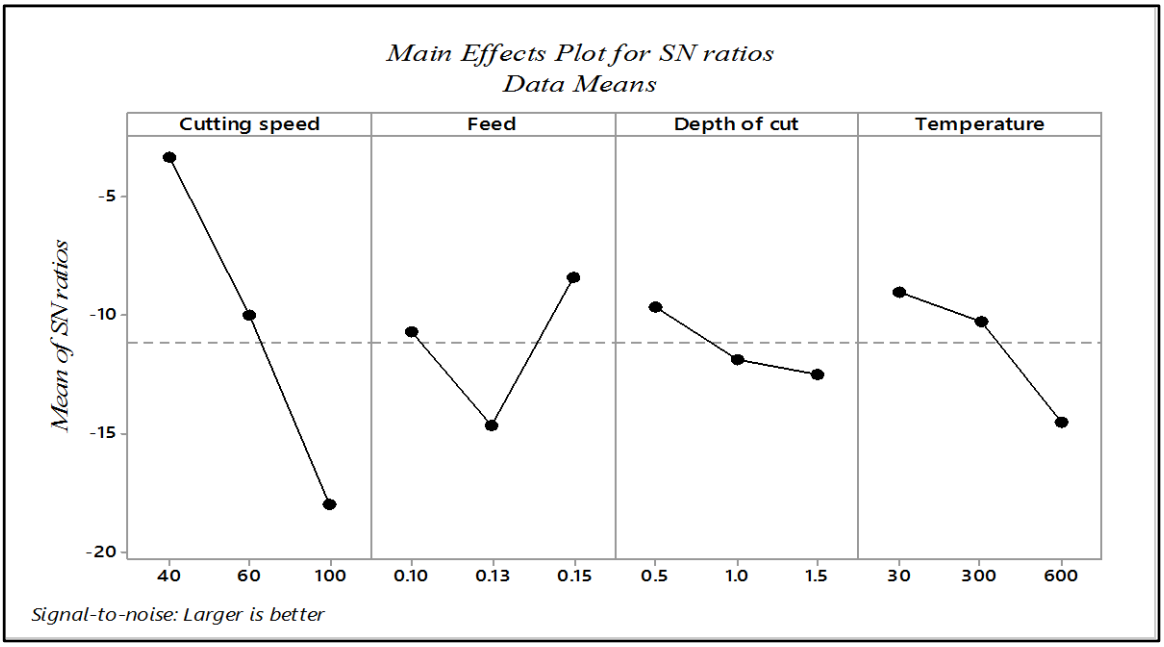

Figure 3.32 Main effects plot for SN ratios

3.5.4 Desirability function analysis

Multi-response optimization problem can be solved by desirability function, where all the objectives are attaining a definite goal simultaneously. The desirability ranges vary from zero to one and the factors setting with maximum desirability are considered to be the optimal parameter conditions. Desirability optimization was proposed by Derringer and Suich in 1980. In this method each response is first converted into an individual desirability function (d_i) with over the range of $0 \le d_i \le 1$. The simultaneous objective function is a geometric mean of all converted responses [128]. Derringer and Suich defined the three type's desirability function depending on the type of response characteristics. Individual desirability index according to the response characteristics i.e. Nominal-the-better, larger-the-better, smaller-the-better which are shown in Eq. (3-16) and Eq. (3-17) respectively are to be calculated.

The higher-the-better can be written as

$$d_i = \begin{cases} 0, & \hat{y} \le y_{\min} \\ \left(\dfrac{\hat{y} - y_{\min}}{y_{\max} - y_{\min}} \right)^r, & y_{\min} \le \hat{y} \le y_{\max},\ r \ge 0 \\ 1, & \hat{y} \ge y_{\min} \end{cases} \qquad (3\text{-}16)$$

Smaller-the-better

$$d_i = \begin{cases} 1, & \hat{y} \le y_{\min} \\ \left(\dfrac{\hat{y} - y_{\max}}{y_{\min} - y_{\max}} \right)^r, & y_{\min} \le \hat{y} \le y_{\max},\ r \ge 0 \\ 0, & \hat{y} \ge y_{\min} \end{cases} \qquad (3\text{-}17)$$

where, $y_{\min}$ represents the lower tolerance limit of $\hat{y}$, $y_{\max}$ represent the upper tolerance limit of $\hat{y}$, and r refers to the weight.In this study, smaller-the-better characteristic is applied to determine the individual desirability index values for flank wear, power and higher the better for material removal rate.The higher the composite desirability (d_G) value implies better product quality and the optimal parameter and its level combination as shown in Eq. (3-18).

$$d_G = \left(d^{w_1}{}_1 d^{w_2}{}_2 \cdots\cdots\cdots d^{w_n}{}_n \right)^{\frac{1}{w}} \qquad (3\text{-}18)$$

where d_n is the individual desirability of the property Y_i, w_i is the weight of the property Y_i in the composite desirability and w is the sum of the individual weight. The weight assigned to flank wear; MRR and power are 3, 3 and 4 respectively according to importance of responses.

The same value of machining input parameters and output are taken for optimization analysis using desirability function analysis. As all the output are the lower the better criteria and individual desirability index of surface roughness and chip reduction coefficient and flank wear are calculated using Eq. (3-17) and tabulated in Table.3.23. From the individual desirability index, the composite desirability index can be calculated using Eq. (3-18). The composite desirability index which is closer to one and corresponding machining variables is considered to be optimal setting for this operation. The variation of composite desirability with respect to experimental run is shown in Fig.3.33. It is observed that the experimental run 7 has highest composite desirability and the highest value of composite desirability is the setting of the corresponding machining operation. The optimal values lie at cutting speed 100 m/min, feed rate 0.1 mm/rev, depth of cut 1.5 mm and workpiece temperature 300°C.

Table 3.23 Calculation of individual desirability index and composite desirability index

Expt. Run	Individual desirability Index (d_i)			Composite desirability d_G
	Surface roughness	Chip reduction ratio	Flank wear	
1	0	0.653526	0	0.000
2	0.441025641	0.574322	0.467391	0.499
3	0.446153846	0.596022	0.043478	0.249
4	0.861538462	0.469439	0.576087	0.599
5	0.697435897	0.353707	0.554348	0.496
6	0.456410256	0	0.282609	0.000
7	0.871794872	1	1	**0.960**
8	0.851282051	0.63038	0.978261	0.787
9	1	0.308861	0.51087	0.511

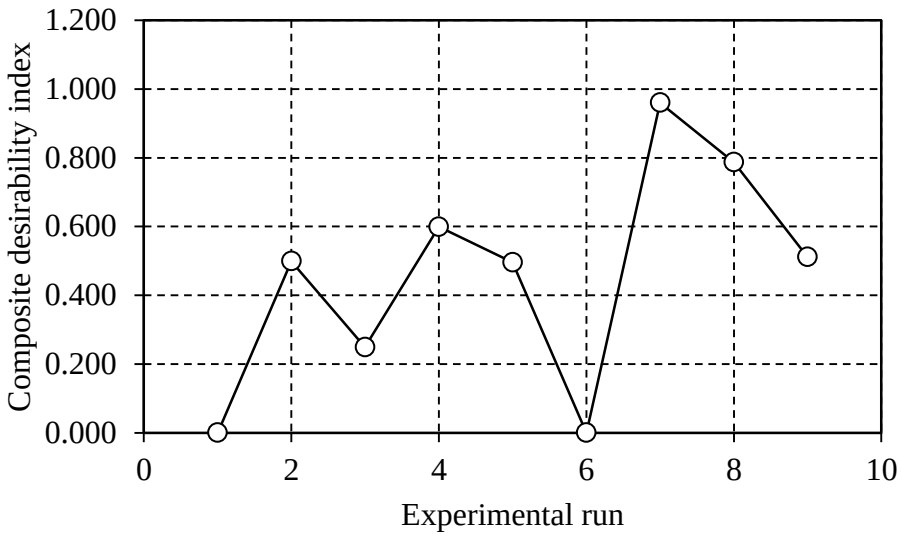

Figure 3.33 Variation of composite desirability with respect to experimental run

As the two optimization techniques have two different optimal setting, so it is difficult to say which optimal setting has beneficiary. In order to shot out this problem, a confirmation test was carried out with the value of obtained optimal setting of two optimization techniques and best results obtained is considered as the best optimal setting. It is clearly seen that the obtained results in DFA gave better results compared to PCA as tabulated in Table 3.24.

Table 3.24 Comparison of experimental results between two optimization techniques

Method	*Vc*	*f*	a_p	*T*	*Ra*	ξ	*VB*
PCA	40	0.15	0.5	30	1.36	1.461	0.313
DFA	100	0.1	1.5	300	1.14	1.245	0.209

3.6 Conclusion

In this chapter, machining of Inconel 718 was carried out at room and elevated temperature. The machining trials were carried out at different cutting conditions and workpiece temperature. Response surface methodology has been used to predict the experimental data such as flank wear and surface roughness. Principal component and desirability function analysis have been used to optimize the machining parameters to achieve multi-response criteria. Following conclusions was derived from this chapter.

- The maximum reduction of cutting, feed and radial force was 33%, 48% and 54% observed in hot turning (600°C) of Inconel 718 compared to room temperature.There was improvement of 43% surface and increase 150% of tool life in hot condition (600°C) compared to room temperature conditions
- The chip geometry characteristics such as degree of segmentation ratio, frequency of serration, and chip tooth spacing decreased with the increase of workpiece temperature (600°C).
- There was decreased of shear band thickness and increase of shear band spacing with the increase of heating compared (600°C) to room temperature.
- There was an increase of chip tool contact length and decrease of chip thickness with the increase of workpiece temperature.
- The predicted flank wear and surface roughness using surface response methodology were having good correlation with the experimental results. An average 4% error for flank wear and 3% for surface roughness were observed between the predicted and measured responses.
- The optimal settings were obtained at 100 m/min cutting speed, 0.1 mm/rev feed rate, 1.5 mm depth of cut and 300°C temperature using desirability function analysis to minimize flank-wear, surface roughness and chip reduction ratio.

Chapter 4

Experimental Investigation and Modeling of Hot Machining of Inconel 625

4.1 Introduction

In this chapter, another nickel base alloys i.e. Inconel 625 is used for machining at room and elevated temperature conditions. This nickel-base alloy (Inconel 625) is generally used in themarine sector due to high corrosion resistance. Other applications include nuclear plant, power plant, biochemical sector and automobile sector etc. Inconel 625 belongs to austenitic nickel-chromium-molybdenum alloys. It is usually used in the range of corrosion conditions like jet engine and chemical processes and marine application where stainless steel cannot be applicable [146]. Similar to Inconel 718 nickel alloy, Inconel 625 alloy is difficult-to-machine due to high hardness, presence of hard particles in the microstructure of the material, and low elastic modulus etc.

Ramanujam et al. [147] studied optimization of machining parameters on dry turning of Inconel 625. They used L_9 orthogonal array as design of experiment and fuzzy based principal component analysis for optimization. ANOVA model was carried out. It was observed that feed rate was the most significant parameter affecting the responses such as surface roughness, power consumption, and material removal rate. Lotfi et al. [148] studied the wear mechanism of nickel base alloys i.e. Inconel 625 using two different cutting tool in finite element analysis. The depth of cut was significantly affecting the tool wear and selection of usui's parameters was necessary for abetter result. Jemielniak et al. [149] investigated the tool condition monitoring system using wavelet packet transform from cutting forces and acoustic emission signal in therough turning of Inconel 625. They observed that skewness did not produce any signal features whereas the effective type of wavelet coefficient feature appeared to be kurtosis. In another study multi-feature fusion based tool condition monitoring was studied [150]. Kashaev et al. [151] investigated the mechanical properties of standard and micro specimens of two different nickel alloy i.e.

Inconel 625 and Inconel 718 and another mostly used titanium alloy (Ti-6Al-4V) by performing electro discharge machining to obtain the tensile and fatigue test. It was observed that micro tensile specimen was having higher elongation to failure compared to standard specimens. Maurotto et al. [152] compared machinability characteristics of nickel and titanium alloy using ultrasonic assisted turning operation. They used Ti-5-3-3-3 and Inconel 625 as workpiece materials. It was observed that for both metals the average cutting force decreased by 70% at ultrasonic assisted turning compared to conventional turning operation. Dhanabalan et al. [153] have analyzed the form tolerances in EDM for two nickel base alloys i.e. Inconel 718 and Inconel 625. It was observed that material removal rate increased with theincrease of peak current.

Though machining of Inconel 625 alloy was carried out using electro discharge machining, ultrasonic assisted machining, still no work has been carried out on hot machining. So, in this present chapter, an attempt has been taken to study machinability of another nickel base alloys i.e. Inconel 625 using hot machining operation using uncoated carbide tool. The machinability in terms of tool life, tool wear, cutting force, surface roughness, Chip morphology analysis were analyzed in both conditions (room and high temperature) at different machining conditions. RSM has been applied to model the hot turning of Inconel 625 and optimization has been carried out to optimize the machining parameters. Both desirability function analysis (DFA) and principal component analysis (PCA) have been used to optimize the multi-response optimal parameters. The selection of machining parameters for machining Inconel 625 was taken same as of Inconel 718 for room temperature and hot turning process. The chemical composition and mechanical properties of Inconel 625 are tabulated in Table 4.1 and Table 4.2 respectively.

Table 4.1 Chemical composition of Inconel 625 (weight %) [154]

Ni	Cr	Mo	Nb	Ta	Fe	Al
58	20	8	3.15	4.15	5	0.4

Table 4.2 Physical properties of Inconel 625 [148]

Name of properties	Value
Density	8.4 g/cm^3
Hardness	320 *HV*
Melting point	1290 to 1350 °C
Modulus of rigidity	79 KN/mm^2
Modulus of elasticity	205.8 KN/mm^2

4.2 Results and discussion

The experimental investigation of hot machining of Inconel 625 has been studied. The effect of workpiece temperature, cutting speed, feed and depth of cut on forces (cutting, feed and radial), tool life, surface roughness have investigated and the results tabulated in Table 4.3. Microhardness, chip morphology, and tool wear mechanism also has been studied.

Table 4.3 Responses obtained at various cutting conditions in room and heated conditions

Cutting conditions			Force (N)									Tool life (min)			Surface roughness (µm)		
			30°C			300°C			600°C								
V_c(m/min)	f (mm/rev)	a_p(mm)	Feed	Radial	Cutting	Feed	Radial	Cutting	Feed	Radial	Cutting	30° C	300° C	600° C	30° C	300° C	600° C
40	0.13	0.5	213	18	287	205	16	261	183	12	201	21	28	65	2.01	1.74	1.2
60			192	15	262	186	14	248	150	8	185	18	26	47	1.47	1.36	1.07
100			184	11	235	164	11	211	132	7	166	13	25	44	1.12	1.1	0.64
100	0.1	0.5	138	15	197	132	13	152	112	10	125	21	30	38	1.27	1.26	0.75
	0.13		168	18	208	145	15	183	121	12	137	17	23	30	1.57	1.52	1.27
	0.15		172	20	231	168	17	211	144	16	149	16	20	26	2.09	1.86	1.31
100	0.13	0.5	143	9	312	128	7	278	113	5	256	15	17	33	1.27	1.23	1.05
		1	162	11	325	141	8	294	138	5	276	13	15	27	1.32	1.3	1.01
		1.5	201	12	304	161	9	317	142	6	287	12	14	21	1.45	1.36	1.25

4.2.1 Cutting force

Variation of cutting, feed and radial force with respect to cutting speed and workpiece temperature

The variation of cutting force, feed force and radial force with respect to cutting speed and temperature of the workpiece is shown in Fig 4.1(a-c). There was (29.96, 29.38 and 29.36 %) reduction of cutting force, (14, 21, and 28%) feed force and (33, 46 and 36%) radial

force with cutting velocity 40, 60 and 100 m/min respectively, machining at 600ºC compared with room temperature. But with increase in the cutting speed from 40 to 100 m/min, there was again reduction of (18, 19 and 17%) cutting force, (13, 20 and 27%) feed force and (38, 31 and 41%) radial force at 30, 300 and 600°C temperature respectively.

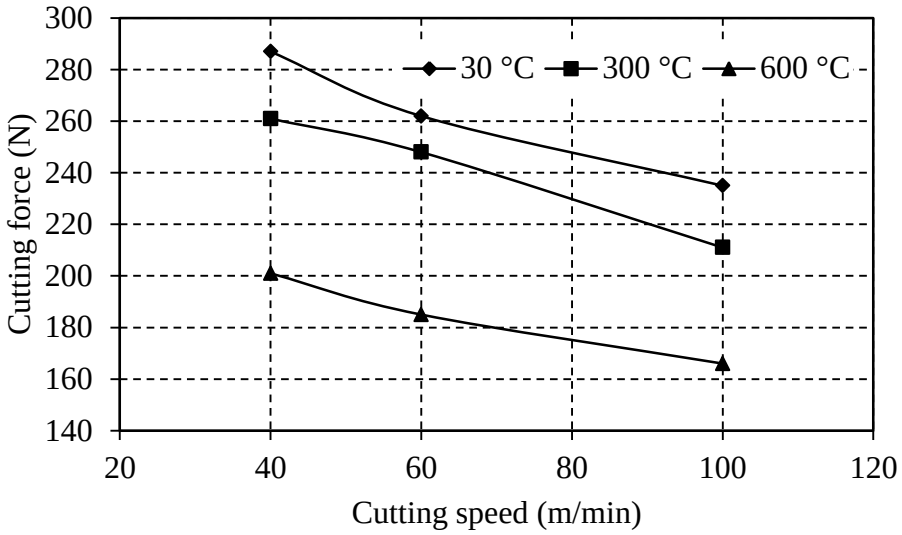

(a)

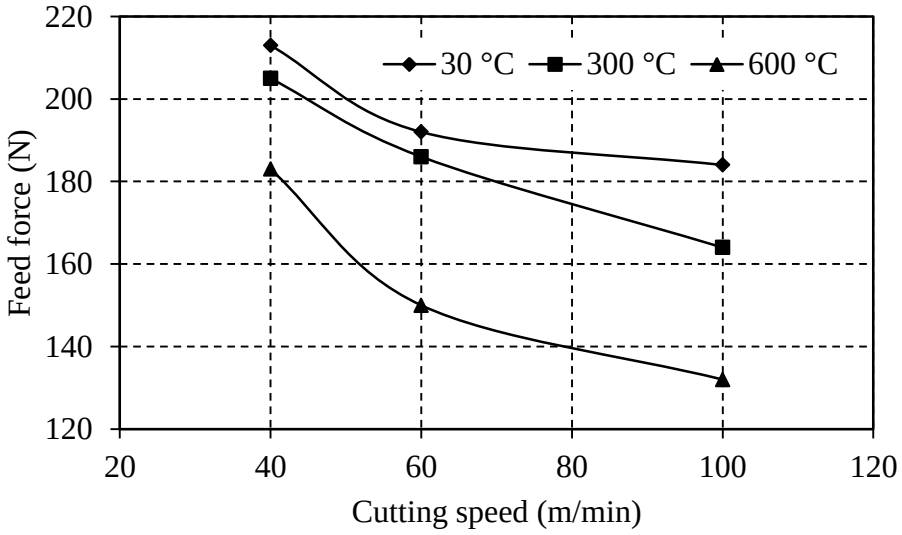

(b)

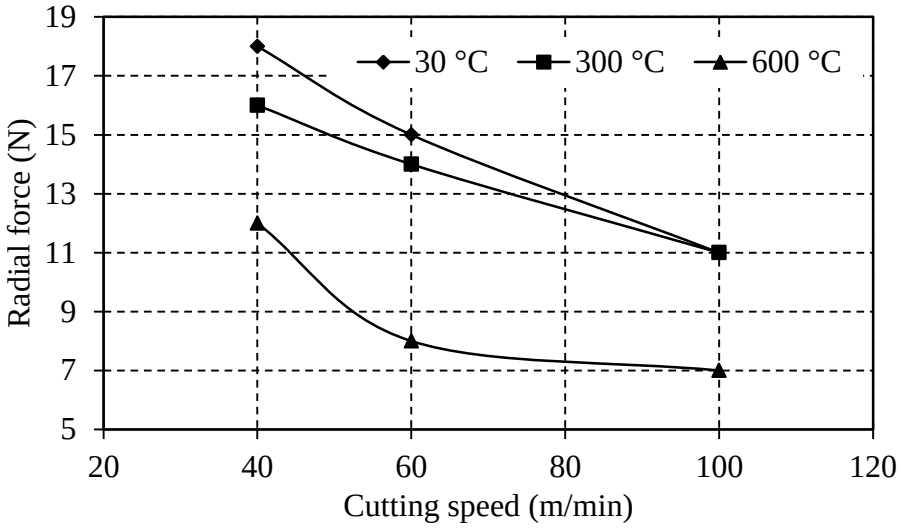

(c)

Figure 4.1 Variation of (a) Cutting force (b) Feed force (c) Radial force with respect to cutting speed and workpiece temperature at feed rate 0.13 mm/rev and depth of cut 0.5 mm

Variation of cutting, feed and radial force with respect to feed rate and workpiece temperature

The effect of feed rate on cutting force, feed force, and radial force during room and hot machining operation is shown in Fig 4.2 (a-c). Machining at 600°C, there wasreduction of (36, 34 and 35%) cutting force, (18, 27 and 16%) feed force and (33, 46 and 36%) radial force at cutting speed 40, 60 and 100 m/min respectively, compared to room temperature. With increased of feed rate from 0.1 to 0.15 mm/rev, there was increase of (17, 38 and 19%) cutting force, (24, 27 and 28%) feed force and (33, 28 and 20%) radial force at 30, 300 and 600ºC temperature respectively. It was observed that all forces increased with the increase of feed rate for all range of temperature of the workpiece.

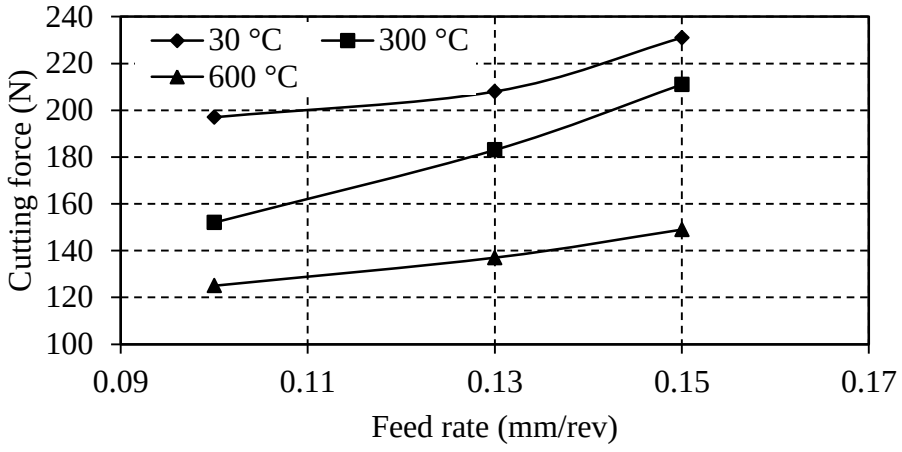

(a)

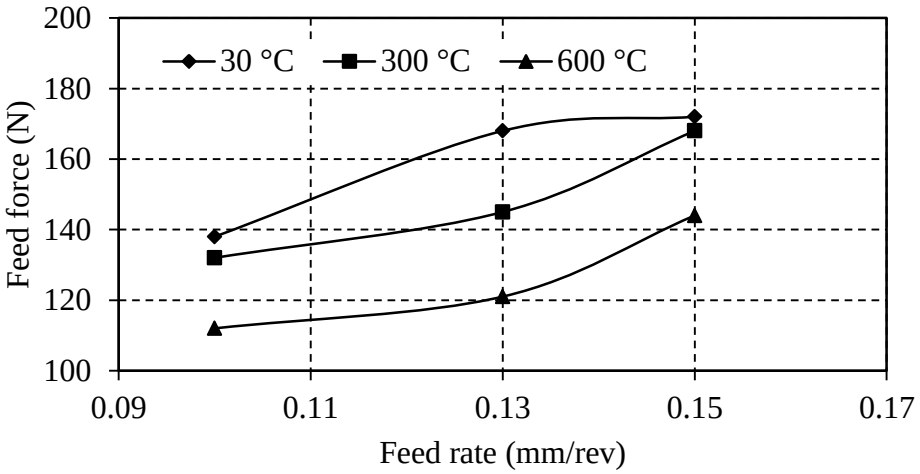

(b)

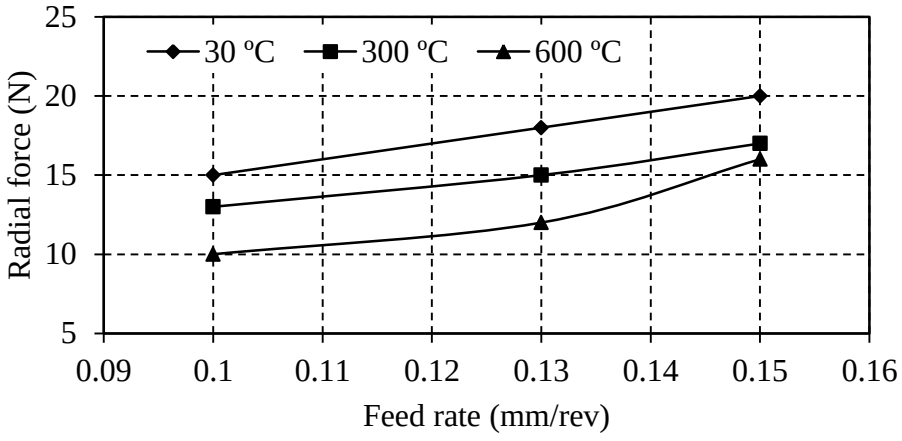

(c)

Figure 4.2 Variation of (a) Cutting force (b) Feed force (c) Radial force with respect to feed rate and workpiece temperature at cutting speed 100 m/min and depth of cut 0.5 mm

Variation of cutting, feed and radial force with respect to depth of cut and workpiece temperature

The variation of cutting, feed and radial force with respect to thedepth of cut and workpiece temperature is presented as Fig.4.3 (a-c). Machining from room temperature to 600°C temperature, there was areduction of (17, 15 and 15%) cutting force, (20, 14 and 29%) feed force and (44, 54 and 50%) radial force at 0.5, 1 and 1.5mm depth of cut respectively. But with increase of the depth of cut from 0.1 to 1.5 mm, there was anincrease of (9, 14 and 12%) cutting force, (40, 25 and 25%) feed force, and (33, 28 and 20%) radial force at 30, 300 and 600°C temperature respectively.

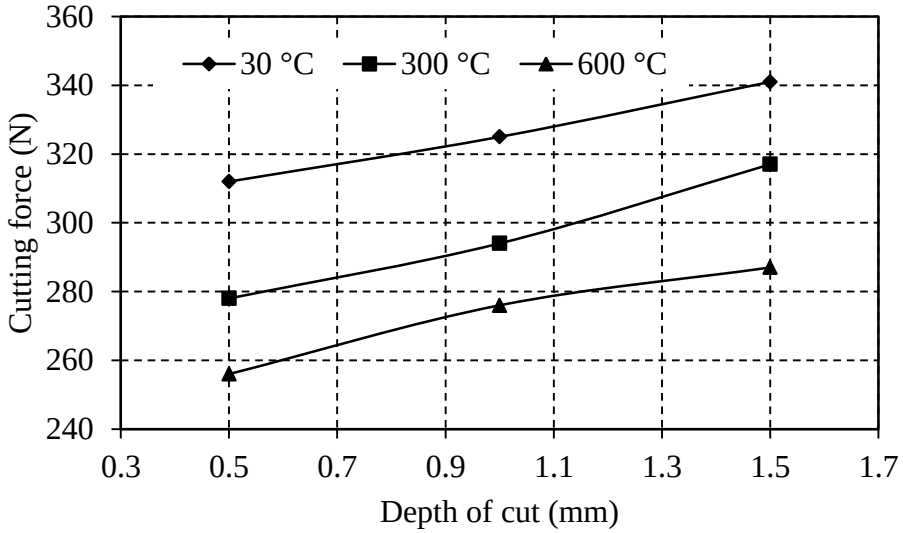

(a)

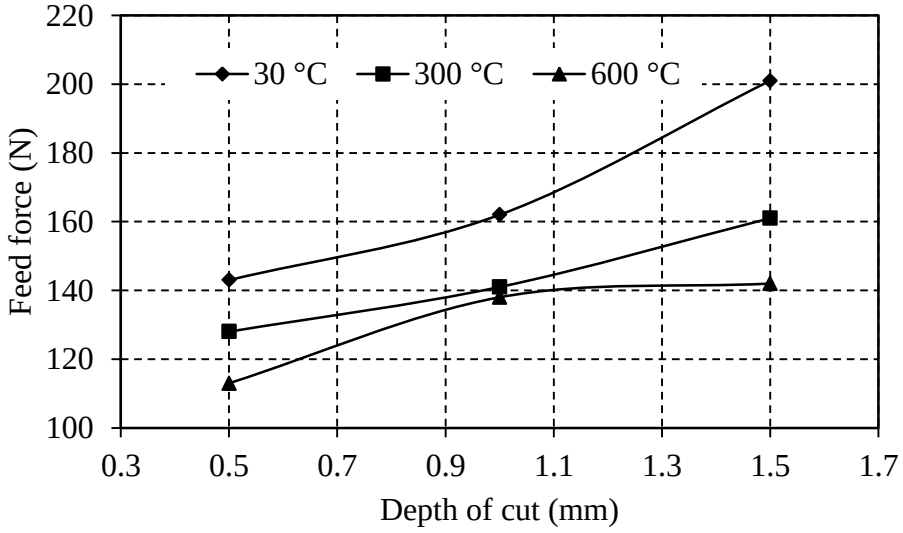

(b)

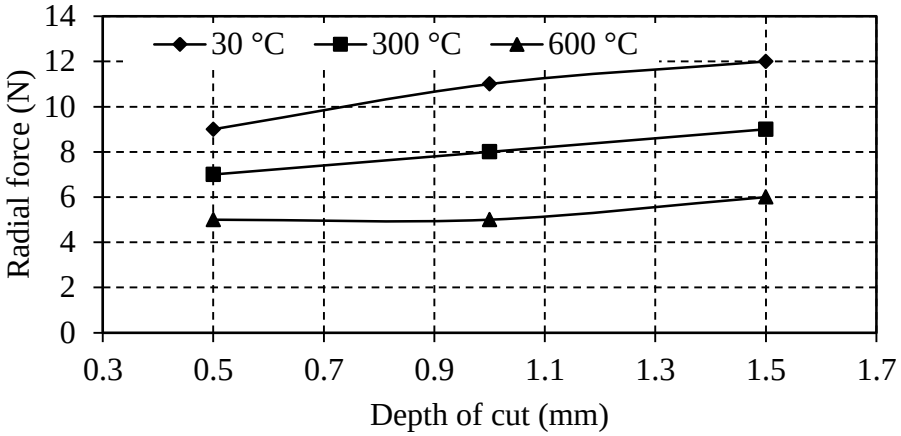

(c)

Figure 4.3 Variation of (a) cutting force (b) feed force (c) Radial force with respect to depth of cut and workpiece temperature at cutting speed 100 m/min and feed rate 0.13 mm/rev

4.2.2 Surface roughness and microhardness

Variation of Surface Roughness with respect to cutting speed and workpiece temperature

The improvement of surface finish with respect to cutting speed and workpiece temperature was studied (Fig 4.4). The surface roughness value decreased with theincrease of workpiece temperature. There was animprovement in thesurface finish at high temperature compared to room temperature.

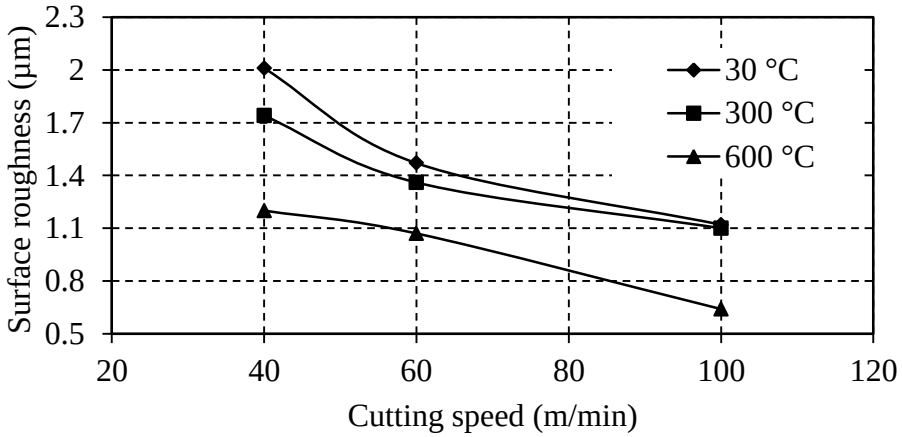

Figure 4.4 Variation of surface roughness with respect to cutting speed and workpiece temperature at feed rate 0.13 mm/rev and depth of cut 0.5 mm

It was observed that there was 40, 27 and 42% reduction of surface roughness at 600ºC compared to room temperature at 40, 60 and 100 m/min cutting speed respectively. When cutting speed increased from 40 to 100 m/min, the surface finishes value increased, by reducing surface roughness (44, 36 and 46%) at 30, 300 and 600ºC temperature respectively.

Variation of Surface Roughness with respect to feed rate and workpiece temperature

The effect of workpiece temperature on thesurface roughness of Inconel 625 was studied at different feed rate (Fig 4.5). Machining Inconel 625 at 600ºC, the surface roughness decreased (40, 19 and 37%) at feed rate of 0.1, 0.13 and 0.15 mm/rev respectively, compared to room temperature machining. While increase in feed rate from 0.1mm/rev to 0.15 mm/rev, the surface roughness increased (64, 47 and 74%) at 30, 300 and 600ºC temperature respectively. The surface roughness increased in the room and high temperature for all range of feed rate.

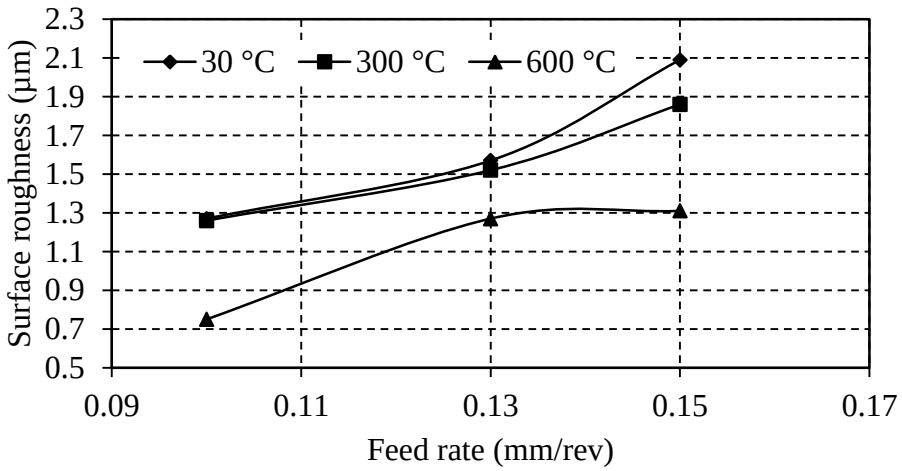

Figure 4.5 Variation of surface roughness with respect to feed rate and workpiece temperature at cutting speed 100 m/min and depth of cut 0.5 mm

Variation of surface roughness with respect to depth of cut and workpiece temperature

The effect of depth of cut on surface roughness at different workpiece temperature of Inconel 625 has been studied (Fig. 4.6). There was an improvement of surface finish at 600ºC compared to room temperature by reducing surface roughness (17, 23 and 13%) at depth of cut of 0.5, 1 and 1.5 mm respectively. But with increase in the depth of cut from 0.5 to 1.5 mm, surface roughness increased 14, 10 and 32% at 30, 300 and 600ºC temperature of the workpiece respectively.

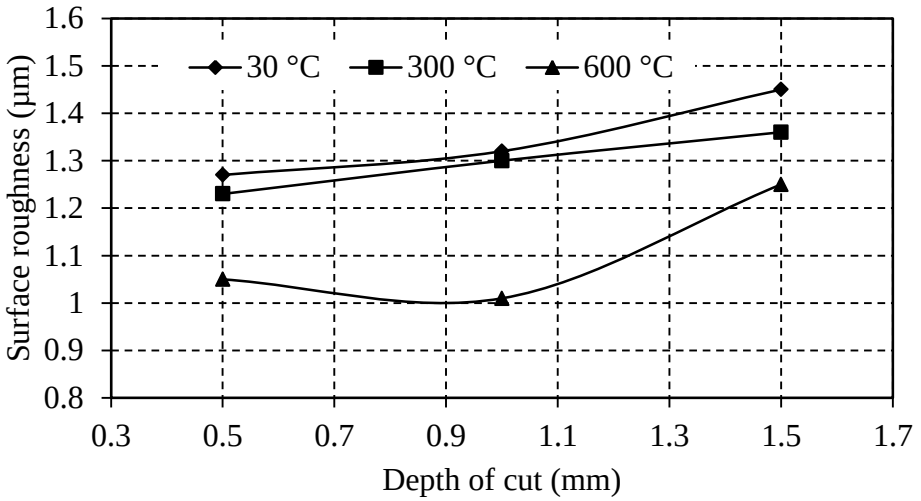

Figure 4.6 Variation of surface roughness with respect to depth of cut and workpiece temperature at cutting speed 100 m/min and feed rate 0.13 mm/min

Measurement of microhardness

A similar method has been adopted for measurement of microhardness of machined subsurface sample of Inconel 625 as carried out for Inconel 718 before. The microhardness below machined subsurface (up to 60 µm from the machined surface) decreased with increase of workpiece temperature and called heat affected zone (HAZ). After moving some distance (from 60 µm to 160 µm), the annealing decreased and strain hardening zone formed due to plastic deformation of thematerial. The microhardness value became higher in the strain hardening zone (SHZ). When moving towards center (160 µm to 200 µm), the shearing and plastic deformation decreased and the hardness value reached to its parent material zone (PMZ) as shown in Fig. 4.7.

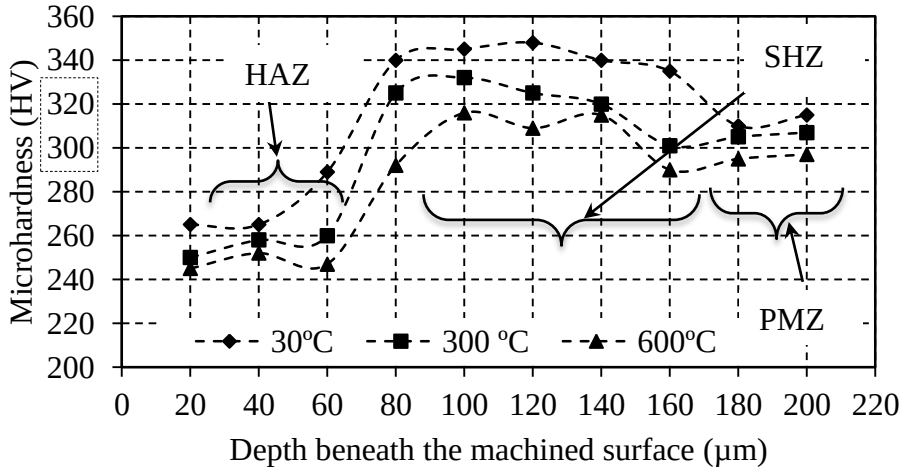

Figure 4.7 Effect of workpiece temperature on microhardness below the machined surface

4.2.3 Tool life and tool wear

The effect of cutting parameters like cutting speed, feed rate and depth of cut with workpiece temperature on tool life has been studied.

Effect of cutting speed on tool life

The effect of workpiece temperature and cutting speed on tool life and corresponding flank wear has been presented (Fig 4.8(a-b)). It was observed that,increase of 209, 161 and 238% of tool life at 600°C compared to room temperature at cutting speed of 40, 60 and 100 m/min respectively. But with increase of cutting speed from 40 to 100 m/min, there was reduction of tool life (38, 10 and 32%) at 30, 300 and 600ºC temperature respectively.

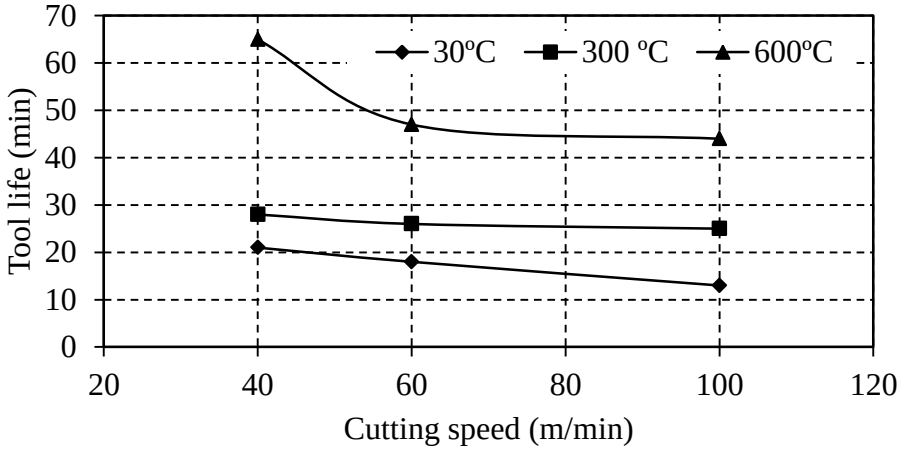

(a)

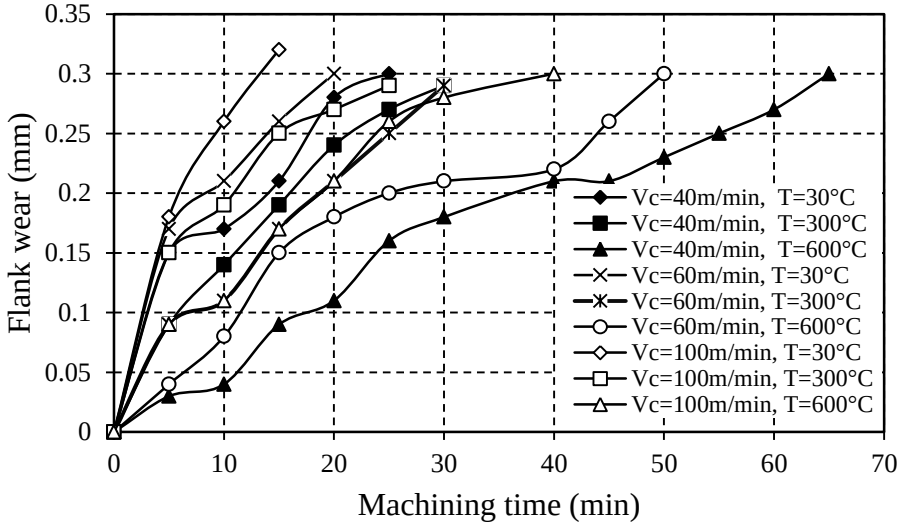

(b)

Figure 4.8 Variation of (a) Tool life (b) Flank wear with respect to cutting speed and workpiece temperature at feed rate 0.13 mm/rev and depth of cut 0.5 mm

Effect of feed rate on tool life

The effect of feed rate on tool life and flank wear was studied at different temperature of the workpiece as presented (Fig 4.9 (a-b)). The tool life increased (80, 76 and 62%) at 0.1, 0.13 and 0.15 mm/rev feed rate respectively, when workpiece was heated at 600ºC compared to room temperature. It was observed that the tool life decreased by (23, 33 and 31%) at 30, 300 and 600°C respectively, when feed rate increase from 0.1 to 0.15 mm/rev.

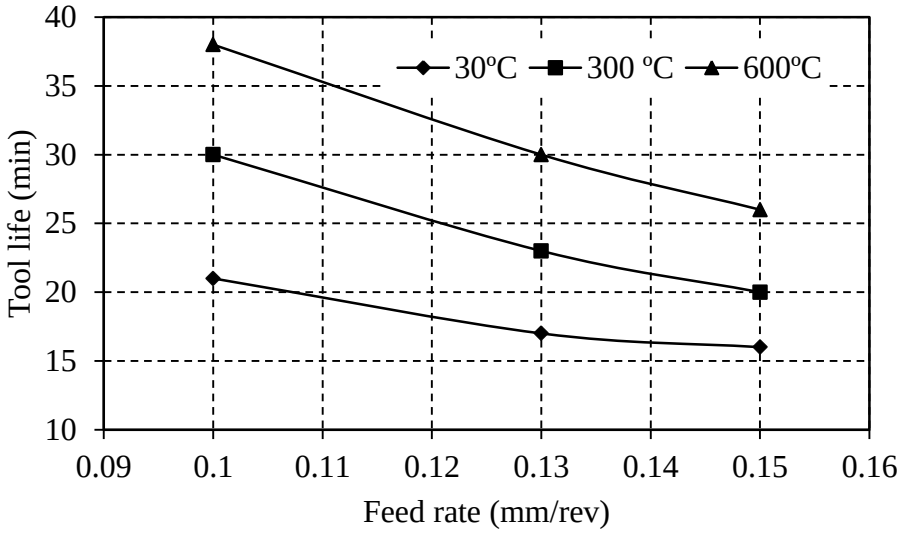

(a)

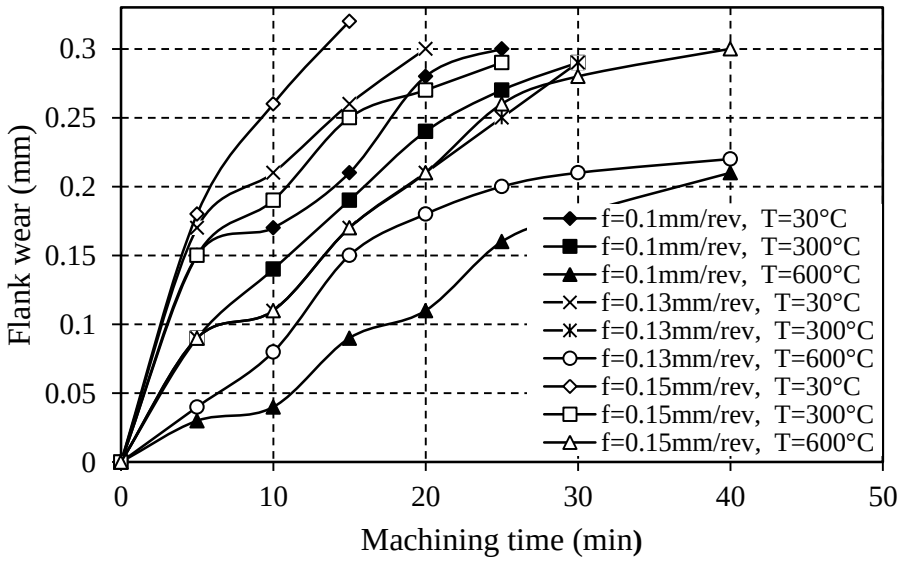

(b)

Figure 4.9 Variation of (a) Tool life (b) Flank wear with respect to feed rate and workpiece temperature at cutting speed 100 m/min and depth of cut 0.5 mm

Effect of depth of cut on tool life

The effect of depth of cut on tool life and flank wear in theroom and hot machining operation as demonstrated in (Fig 4.10 (a-b)). Machining Inconel 625 from room temperature to 600ºC, the tool life increased (120, 107 and 75%) at 0.5, 1 and 1.5 mm depth of cut respectively. But with increase in the depth of cut from 0.5 to 1.5 mm, there was a reduction of (20, 17 and 36%) tool life at 30, 300 and 600ºC temperature respectively. The variation of flank wear with respect to time is shown in Fig. 4.10 (b).

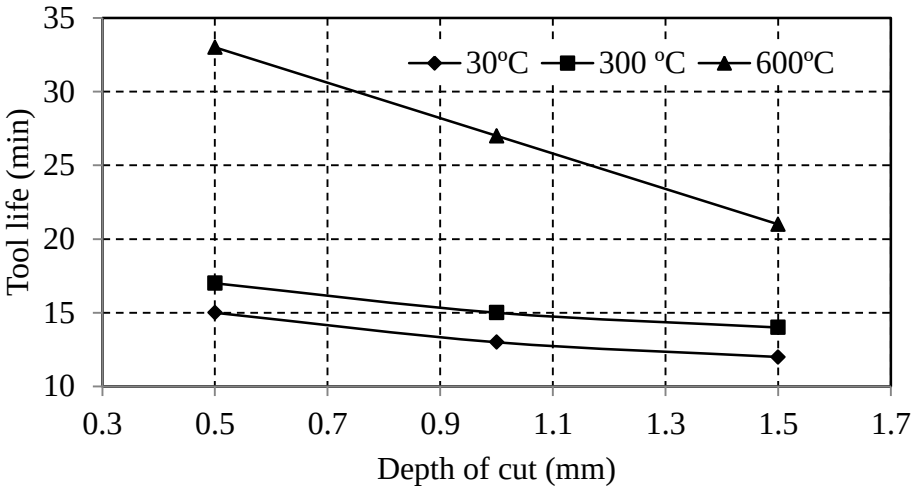

(a)

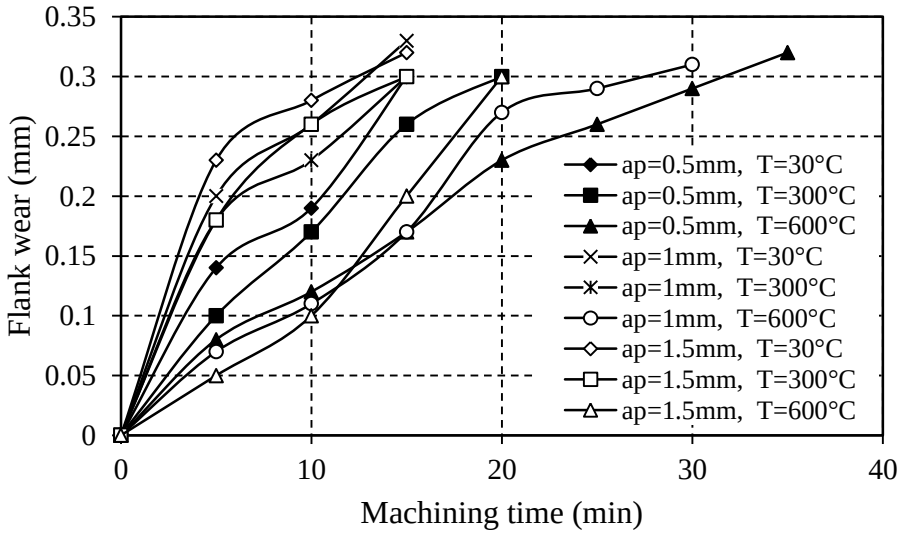

(b)

Figure 4.10 Variation of (a) Tool life (b) Flank wear with respect to depth of cut and workpiece temperature at cutting speed 100 m/min and feed rate 0.13 mm/rev

4.2.4 Analysis of tool wear

Variation of tool life and chip reduction coefficient with respect to workpiece temperature at different cutting speed is shown in Fig. 4.11 (a-b). Wear formation in different conditions in 30ºC and 600ºC is shown in Fig 4.12. This figure indicates that at room temperature (30ºC), there was severe tool wear formation. At low cutting speed built-up-edge (BUE) and chipping, formation occurred. When workpiece temperature increased to 300ºC, there was notch wear formation and again increased to 600ºC, diffusion wear was the main tool wear. The tool wear at heated conditions was low compared to room temperature. So at optimum temperature (600ºC), the stress on the rake face of the tool was lower, as a result tool wear formation was less. It was observed that at room and high temperature, notch wear and the built-up-edge formation took place. With the increase of cutting speed, the tool wear decreased and with increase of feed rate, tool wear increased in both room and heating conditions.

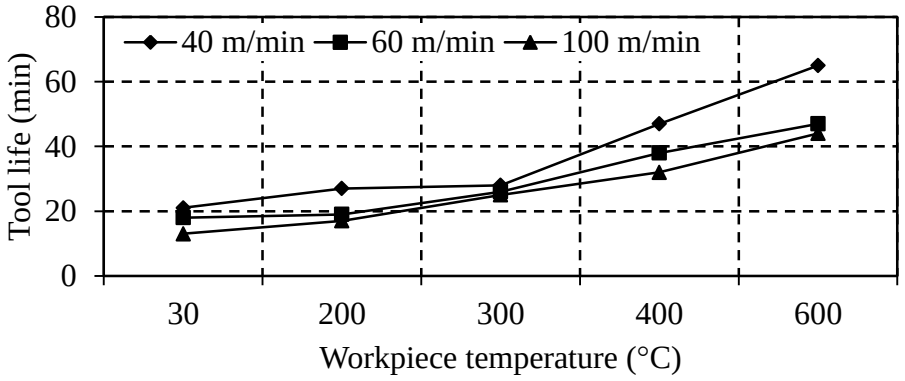

(a)

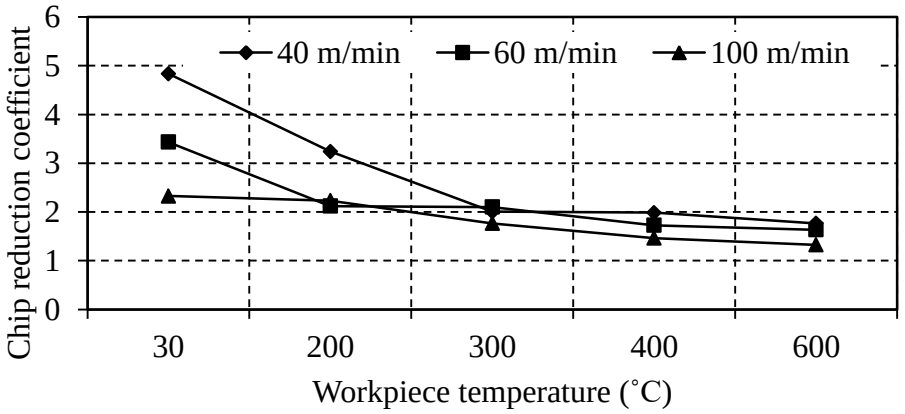

(b)

Figure 4.11 (a) Effect of workpiece temperature on (a) tool life (b) chip reduction coefficient at feed rate 0.13 mm/rev and depth of cut 0.5 mm

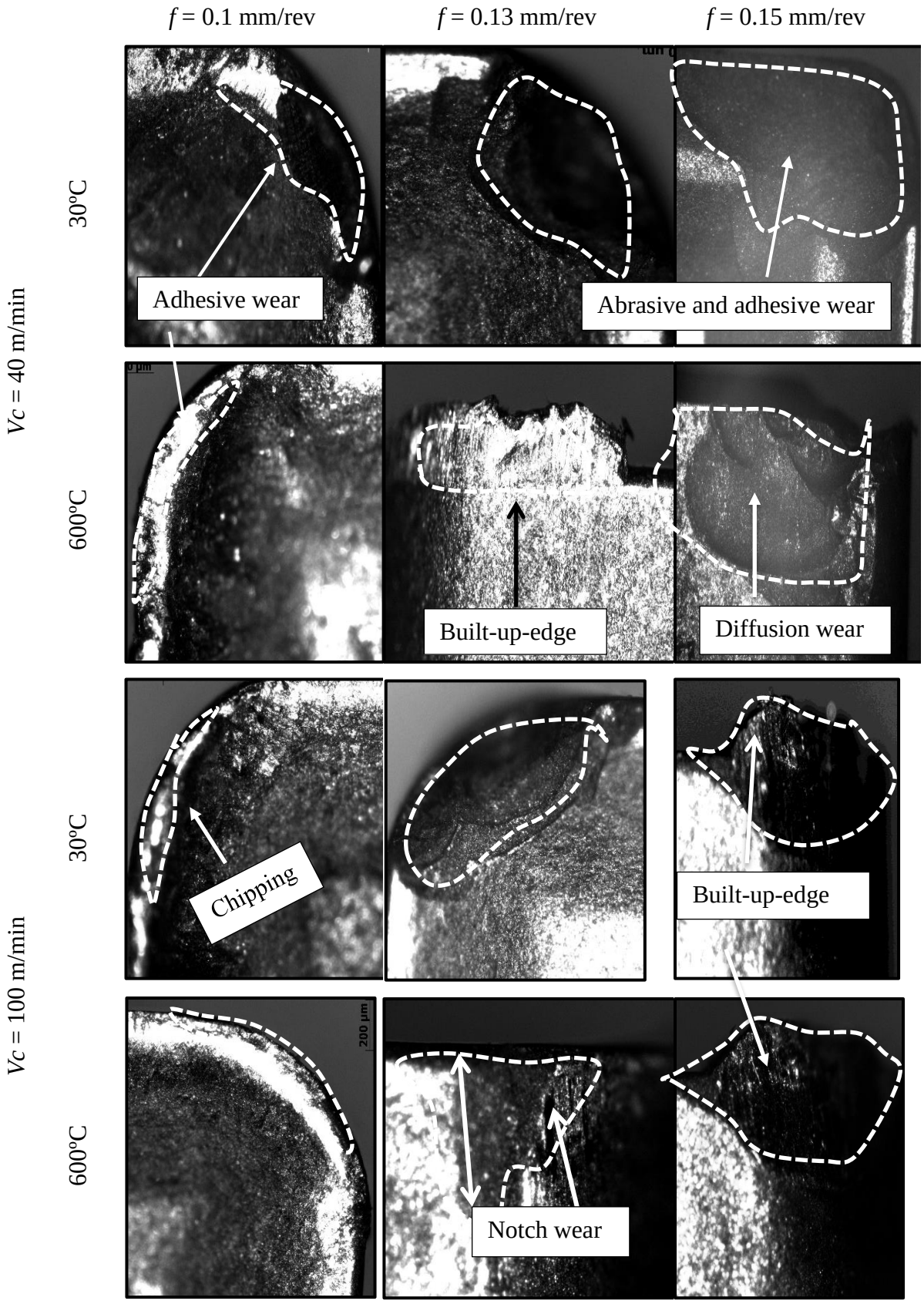

Figure 4.12 Tool wear at different cutting condition in machining Inconel 625

4.2.5 Chip morphology

Figure 4.13 Formation of different types of chips with respect to cutting speed and workpiece temperature at feed rate 0.13 mm/rev and depth of cut 0.5 mm

Machining Inconel 625 with uncoated carbide inserts at different cutting conditions, the chips produced were collected. It was observed that chips produced during room temperature were quite discontinuous. With increase in workpiece temperature, the chips were spiral and continuous and with further increased in workpiece temperature to 600ºC,

there was the formation of continuous chips due to an increase of ductility of the workpiece (Fig.4.13).

4.2.6 Analysis on chip-tool contact length

Chip-tool contact length was also studied in machining of Inconel 625 alloy with uncoated carbide insert using scanning electron microscope. It was found that, with the application of heating, the chip-tool contact length increased compared to room temperature conditions. It was observed that chip tool contact length increased by 64.1% (from 201 µm to 560 µm) at 600°C temperature compared to room temperature. The variation of chip-tool contact length at different workpiece temperature is plotted in (Fig 4.14 (a-b)).

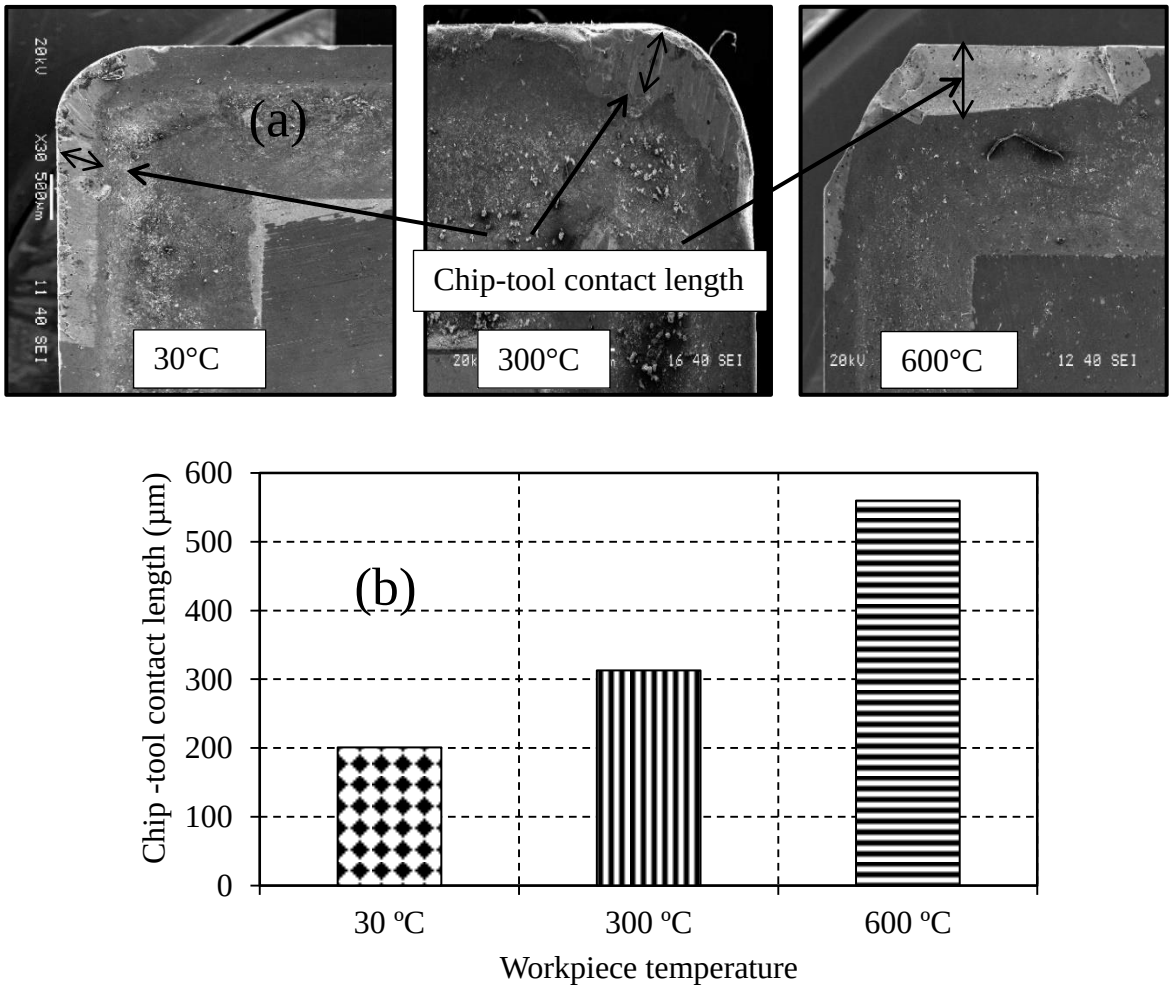

Figure 4.14 (a) SEM images of worn cutting tools (b) Graphical plot chip-tool contact length vs workpiece temperature at cutting speed of 100 m/min, feed rate 0.13 mm/rev, and depth of cut 0.5 mm

4.3 Modeling of hot machining of Inconel 625 using surface response methodology

The same machining input parameters and along with workpiece temperature (Parameters are same as for Inconel 718) were taken for modeling of Inconel 625 using response surface methodology and the flank wear and surface roughness obtained is presented in Table 4.4.The fitted quadratic model for the responses which were calculated from the F-test is tabulated in Table 4.5.

Table 4.4 Design layout and experiment results

Run	Coded factors				Actual factors				Response variables	
	X_1	X_2	X_3	X_4	V_c	f	a_p	T	VB_{max}, mm	R_a, μm
1	0	0	0	0	70	0.125	1	315	0.229	2.291
2	-1	+1	-1	+1	40	0.15	0.5	600	0.229	2.693
3	-1	-1	-1	-1	40	0.1	0.5	30	0.228	2.420
4	0	-1	0	0	70	0.1	1	1	0.253	2.455
5	+1	0	0	0	100	0.125	1	315	0.232	2.248
6	-1	0	0	0	40	0.125	1	315	0.206	2.902
7	0	0	0	0	70	0.125	1	315	0.224	2.291
8	+1	-1	+1	+1	100	0.1	1.5	600	0.323	2.236
9	+1	-1	+1	-1	100	0.1	1.5	30	0.286	2.301
10	+1	-1	-1	-1	100	0.1	0.5	30	0.232	2.203
11	0	0	+1	0	70	0.125	1.5	315	0.255	2.501
12	0	0	0	0	70	0.125	1	315	0.225	2.298
13	-1	+1	-1	-1	40	0.15	0.5	30	0.255	2.542
14	0	+1	0	0	70	0.15	1	315	0.259	2.479
15	+1	+1	+1	-1	100	0.15	1.5	30	0.316	2.370
16	0	0	0	+1	70	0.125	1	600	0.257	2.537
17	+1	+1	-1	-1	100	0.15	0.5	30	0.288	2.259
18	-1	-1	+1	+1	40	0.1	1.5	600	0.273	2.616
19	0	0	0	0	70	0.125	1	315	0.214	2.291
20	0	0	0	0	70	0.125	1	315	0.237	2.297
21	0	0	0	-1	70	0.125	1	30	0.236	2.387
22	-1	-1	+1	+1	40	0.1	1.5	600	0.246	2.539
23	-1	+1	+1	+1	40	0.15	1.5	600	0.250	2.795
24	+1	+1	+1	+1	100	0.15	1.5	600	0.314	2.234

25	+1	-1	-1	+1	100	0.1	0.5	600	0.287	2.259
26	+1	+1	-1	+1	100	0.15	0.5	600	0.322	2.300
27	-1	-1	-1	+1	40	0.1	0.5	600	0.263	2.801
28	0	0	-1	0	70	0.125	0.5	315	0.219	2.358
29	-1	+1	+1	-1	40	0.15	1.5	30	0.267	2.643
30	0	0	0	0	70	0.125	1	315	0.227	2.296

Table 4.5 ANOVA table for the fitted models

Source	DoF	SS	MS	*F*-Value	*P*-Value
Flank wear					
Model	14	0.031186	0.002228	18.12	0
Error	15	0.001844	0.000123		
Lack-of-fit	9	0.001079	0.000120	0.94	0.552
Pure error	6	0.000765	0.00127		
Total	29	0.033030			
R^2-94.42					
R^2 Adjusted-89.21					
Prediction R^2-69.15					
Surface roughness					
Model	14	0.902560	0.064469	11.60	0
Error	15	0.083399	0.005560		
Lack-of-fit	9	0.030279	0.003364	0.38	0.907
Pure error	6	0.053120	0.008853		
Total	29	0.985959			
R^2-91.54					
R^2Adjusted-83.65					
Prediction R^2-77.65					

The significant parameters which affects the responses whose *P* values are less than 0.05.

When R^2 approaches to unity, the predicted value fit the experimental data.

For flank wear, the parameters viz. V_c, f, a_p, T,T^2,V_cT, *and* fT can be regarded as significant as the corresponding *P*-value was observed to be less than 0.05. Similarly, for surface roughness the following parameters i.e.V_c, f, a_p, *and* V_c^2 can be regarded as significant as shown in Table 4.6 and Table 4.7 respectively. The final quadratic models of response equation for flank wear and surface roughness in coded form using backward elimination process can be represented as follows in Eq.(4-1) and Eq. (4-2) respectively.

$$Flank\ wear = 0.33190+0.02263\ X_1+0.00631\ X_2+0.01026\ X_3+0.00604\ X_4-0.00471\ X_1\ X_1+0.01615X_2X_2+0.00529X_3X_3+0.03002X_4X_4+0.00598X_1X_2+0.00589X_1X3+0.00323X_1X_4-0.00954X_2X_4-0.00585X_3X_4 \quad (4\text{-}1)$$

$$Surface\ Roughness = 2.4576-0.1891X_1+0.0497\ X_2+0.0497\ X_3+0.0374\ X_4+0.1703\ X_1\ X_1-0.0638\ X_2\ X_2-0.0702\ X_3\ X_3-0.0219\ X_4\ X_4+0.00598\ X_1\ X_2-0.0050\ X_1\ X_3-0.0230\ X_1\ X_4+0.0373X_2\ X_3+0.0180\ X_2\ X_4-0.0187\ X_3\ X_4 \quad (4\text{-}2)$$

Table 4.6 Results of the analysis of variance (ANOVA) for the flank wear

Symbol	DoF	SS	MS	*F*-Value	*P*-Value	Remarks
V_c	14	0.008521	0.008521	69.33	**0.000***	Significant
f	1	0.000658	0.000658	5.36	**0.035***	Significant
a_p	1	0.001753	0.001753	14.27	**0.002***	Significant
T	1	0.000613	0.000613	4.99	**0.041***	Significant
V_c^2	1	0.000061	0.000061	0.50	0.492	
f^2	1	0.000483	0.000483	3.93	0.066	
a_p^2	1	0.000061	0.000061	0.62	0.442	
T^2	1	0.002265	0.002265	18.43	**0.001***	Significant
V_cf	1	0.000061	0.000061	4.27	0.057	
V_ca_p	1	0.000509	0.000509	4.14	0.060	
V_cT	1	0.001696	0.001696	13.80	**0.002***	Significant
$f\,a_p$	1	0.000153	0.000153	1.25	0.282	
$f\,T$	1	0.001351	0.001351	10.99	**0.005***	Significant
a_pT	1	0.000471	0.000471	3.83	0.069	

Table 4.7 Results of the analysis of variance (ANOVA) for the surface roughness

Symbol	DoF	SS	MS	*F*-Value	*P*-Value	Remarks
V_c	14	0.595183	0.595183	107.05	**0.000***	Significant
f	1	0.040858	0.040858	7.35	**0.016***	Significant
a_p	1	0.037352	0.037352	6.72	**0.020***	Significant
T	1	0.023503	0.023503	4.23	0.058	
V_c^2	1	0.079479	0.079479	14.29	**0.002***	Significant
f^2	1	0.007539	0.007539	1.36	0.262	
a_p^2	1	0.013528	0.013528	0.013528	2.43	

T^2	1	0.001202	0.001202	0.22	0.649
$V_c f$	1	0.000467	0.000467	0.08	0.776
$V_c a_p$	1	0.000363	0.000363	0.07	0.802
$V_c T$	1	0.007257	0.007257	1.31	0.271
$f\, a_p$	1	0.020362	0.020362	3.66	0.075
$f\, T$	1	0.004797	0.004797	0.87	0.367
$a_p T$	1	0.004797	0.004797	0.86	0.907

The regression equation, in terms of actual factors, the final quadratic models of response equation are expressed in Eq. (4-3) and Eq. (4-4)

$$\textit{Flank wear} = 0.684-0.00031* V_c-6.08*f-0.004*a_p -0.000094*T-0.000005*V_c *V_c +25.8* f * f +0.0211* a_p * a_p+0.00798*V_c * f +0.000393*V_c * a_p +0.000001*V_c * T -0.259* f * a_p - 0.00134* f * T -0.000041*a_p*T \quad (4\text{-}3)$$

$$\textit{Surface roughness} = 1.82-0.03067*V_c +24.3* f +0.348* a_p +0.000304* T +0.000189*V_c *V_c -102.1* f * f -0.281* a_p * a_p -0.0075*V_c * f -0.281* a_p * a_p -0.0075*V_c * f -0.00033*V_c * a_p -0.000003*V_c * T +2.98* f* T-0.000131*a_p *T \quad (4\text{-}4)$$

Eq. (4-3) and Eq. (4-4) can be utilized for predicting the flank wear and surface roughness and difference between predicted and measured are shown in Fig.4.15 and Fig.4.16 respectively. There was good agreement between the experiment and predicted result and an average 4% error of flank wear and 4% of surface roughness was observed between experimental and predicted value.

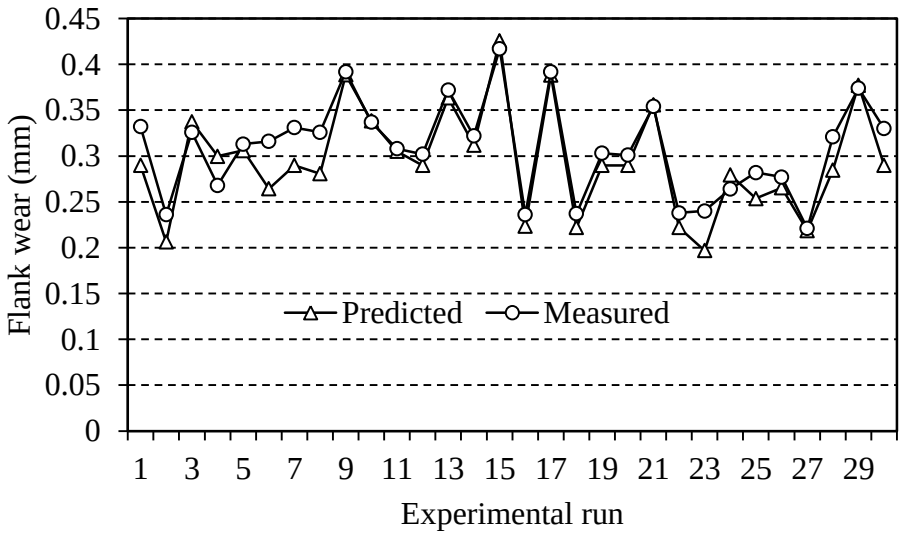

Figure 4.15 Comparison between the predicted and measured flank wear

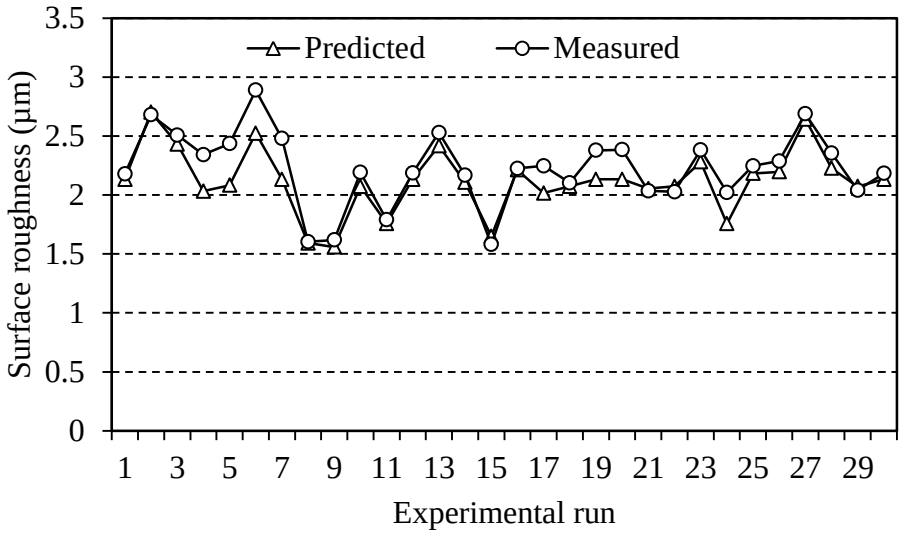

Figure 4.16 Comparison between the predicted and measured surface roughness

surface and corresponding contour plots were plotted in Fig. 4.17 and Fig.4.18 for surface roughness and flank wear respectively in order to investigate the effect of machining parameters. Fig.4.17 (a) shows the effect of cutting speed and feed rate on surface roughness where the depth of cut and temperature are kept at the middle level. Fig. 4.17 (b) presents the effect of depth of cut and temperature on surface roughness, kept cutting speed and feed at the middle level. The surface roughness value increases with the increase of feed rate, temperature, and depth of cut, whereas there isdecrease of surface roughness with an increase of cutting speed.

Similarly, response surface for variation flank wear with respect to cutting speed and feed rate, where the depth of cut and temperature is kept at the middle value. Fig.4.18 (a) shows the flank wear increase with the increase of cutting speed, feed rate and depth of cut. Fig. 4.18 (b) shows the effect of depth of cut and temperature on flank wear, where cutting speed and feed rate is kept at the middle value. With the increase of temperature up to certain level, the flank wear decreases, with further increase of the workpiece temperature increases. This is due to the diffusion wear of the cutting tool at higher temperature.

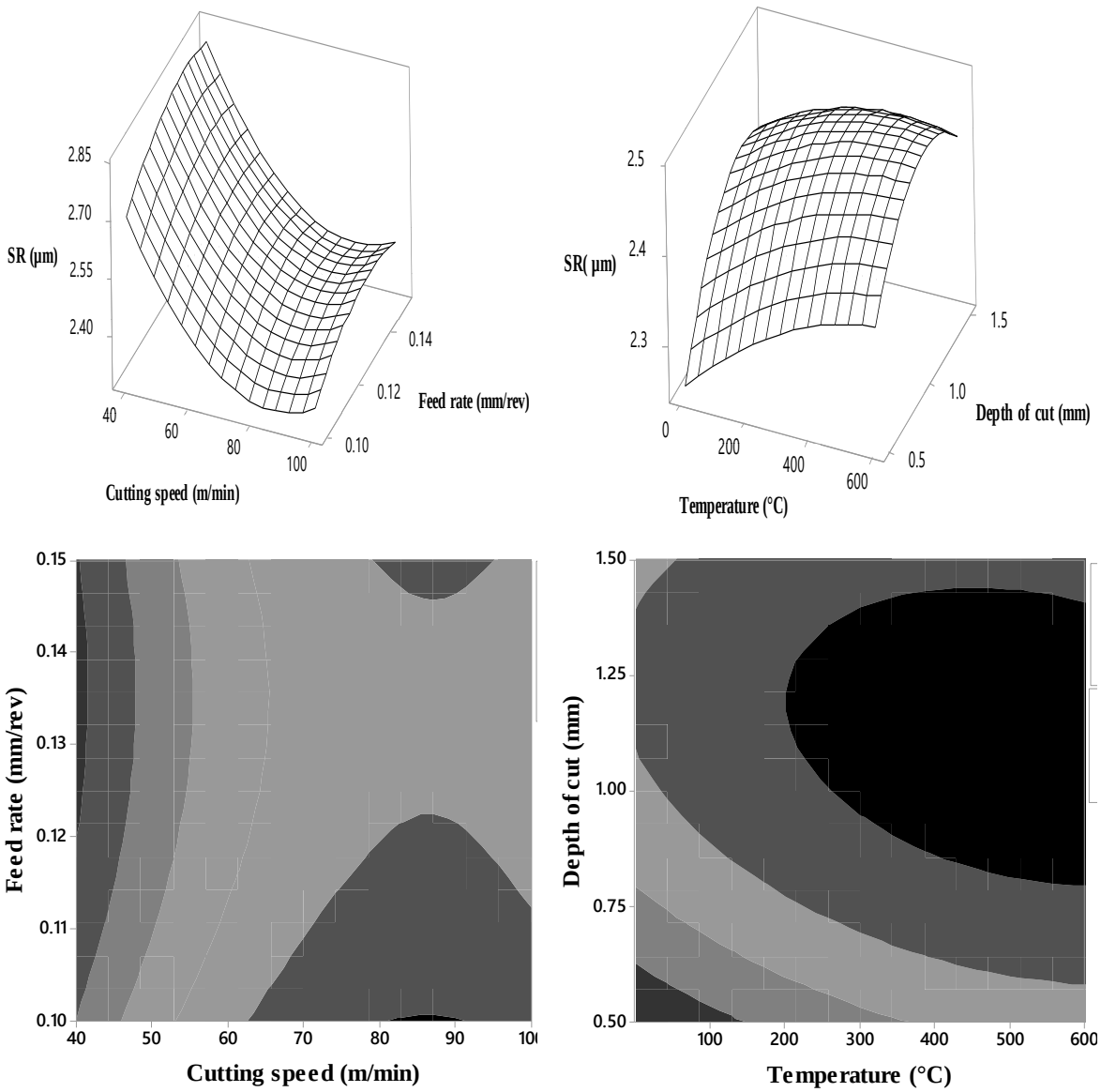

(a) (b)

Figure 4.17 Surface and contour plot for surface roughness with respect to (a) Cutting speed and feed rate (b) Temperature and depth of cut

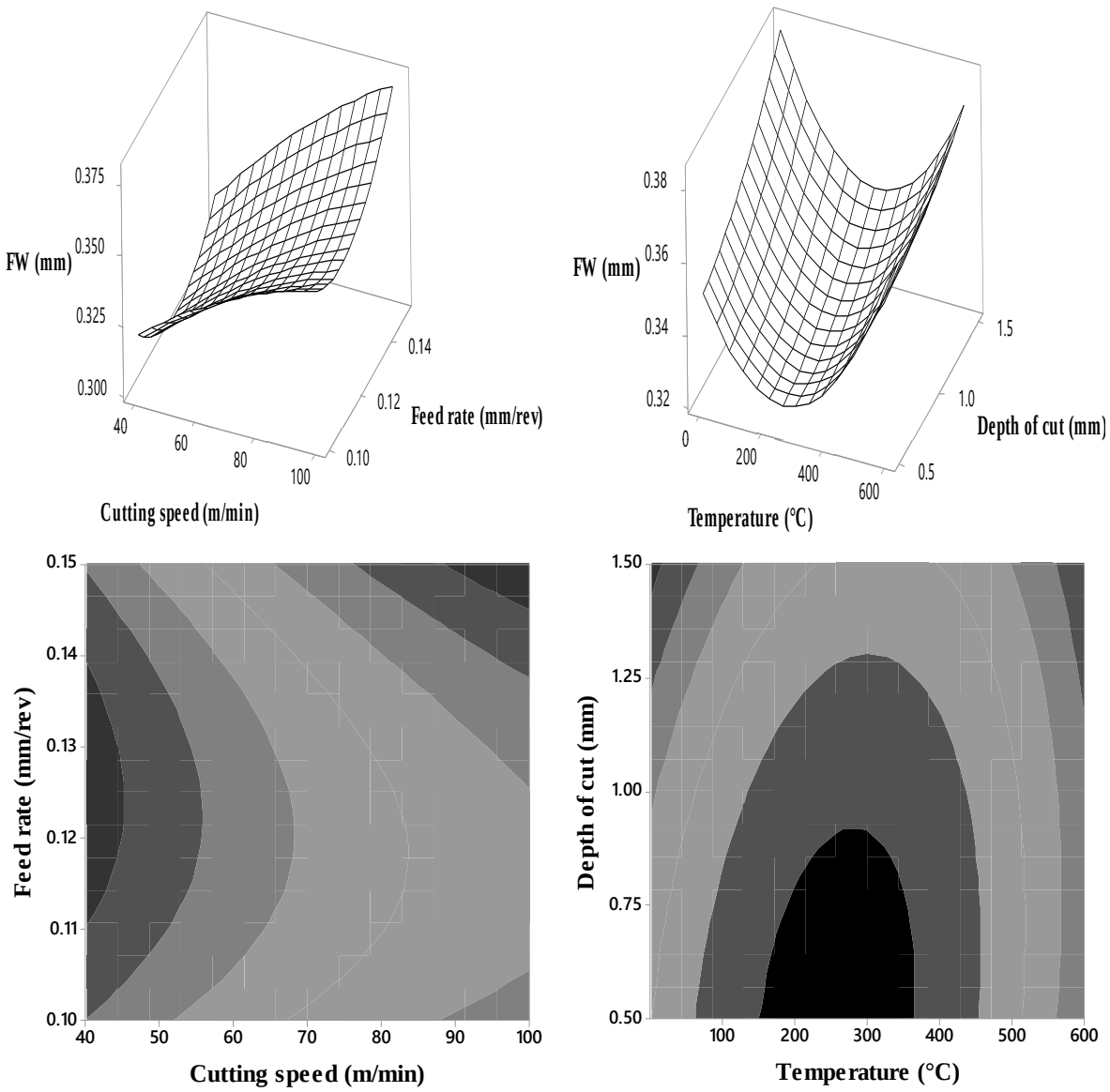

(a) (b)

Figure 4.18 Surface and contour plot for flank wear with respect to (a) Cutting speed and feed rate (b) Temperature and depth of cut

The analysis of machining parameters such as cutting speed, feed rate, depth of cut and temperature using response surface methodology allows the effect of each one on the responses such as flank wear and surface roughness. Cutting speed and temperature mostly affect the flank wear and surface roughness compared to feed rate and depth of cut. The predicted results of surface roughness and flank wear show good agreement with the experimental results.

4.4 Optimization of multi-response parameter of machining of Inconel 625 using PCA-taguchi and desirability method

4.4.1 Principal component analysis

For optimization of hot machining parameters of Inconel 625, the machining experiments were carried out with same as Inconel 718 and tabulated in Table 4.8. In this chapter, surface roughness, power and chip reduction coefficient are taken as theoutput. The power was measured by power logger and chip reduction coefficient was calculated from the ratio between the chip thickness and uncut chip thickness values. The chip thickness was measured with the help of tool maker microscope. The responses are normalized according to lower the better criteria, tabulated in Table 4.9. The eigen analysis for covariance matrix was calculated similarly same as Inconel 718 as shown Table 4.10. Principal components computed using L_9 OA (Orthogonal array) experimental observations shown in Table 4.11.

Table 4.8 Experiment layout and responses

Run order	Speed (m/min)	Feed rate (mm/rev)	Depth of cut (mm)	Temp.(°C)	Surface roughness (μm)	Power (kW)	Chip reduction ratio(ξ)
1	40	0.1	0.5	30	2.86	0.258	2.826
2	40	0.13	1	300	0.86	0.26	2.82
3	40	0.15	1.5	600	1.85	0.325	2.705
4	60	0.1	1	600	1.04	0.295	2.812
5	60	0.13	1.5	30	1.36	0.324	3.435
6	60	0.15	0.5	300	1.83	0.699	4.442
7	100	0.1	1.5	300	1.02	0.451	1.133
8	100	0.13	0.5	600	1.06	0.574	1.465
9	100	0.15	1	30	0.77	0.353	4.327

Table 4.9 Calculation of normalization data

Run	Surface roughness	Power	Chip reduction ratio (CRC)
1	0	1	0.488365
2	0.956938	0.995465	0.490178
3	0.483254	0.848073	0.494711
4	0.870813	0.9161	0.492596
5	0.717703	0.85034	0.304322
6	0.492823	0	0
7	0.880383	0.562358	1
8	0.861244	0.78458	0.899668
9	1	0.283447	0.034754

Table 4.10 Eigen value and eigen vector of the covariance matrix

Eigen value	1.4925	1.0813	0.4261
	0.02	0.936	0.353
Eigen vector	-0.704	-0.263	-0.66
	0.71	-0.235	-0.664
Proportion	0.498	0.36	0.142
Cumulative	0.498	0.858	1

Table 4.11 Principal components in all L_9 OA experimental observations

Run	Principal component1	Principal component 2	Principal component 3
1	1.050739	-0.14823	0.335726
2	1.722518	0.749078	0.669327
3	1.291398	0.345539	0.401828
4	0.994677	0.689907	0.584939
5	0.814708	0.519646	0.612504
6	0	0.461282	0.173967
7	1.1059	0.911138	0.017932
8	1.191109	0.811202	0.224463
9	0.224222	0.869621	0.516998

The multiple performance characteristics index value is tabulated in Table 4.12. It was observed thatfeed rate was the most effective parameter for influencing the responses followed by cutting speed, temperature, and depth of cut respectively as shown in Table

4.13. Fig 4.19 shows the main effect graph for SN ratio and theoptimal setting is lie at 100 m/min cutting speed, 0.1 mm/rev feed rate, 1 mm depth of cut and 600°C temperature respectively to minimize the surface roughness, power and chip reduction ratio.

Table 4.12 Multiple performance characteristics of index (MPCI)

Expt. Run	MPCI	SN ratio
1	0.614	-4.23349
2	0.748	-2.52693
3	0.665	-3.54614
4	0.894	-0.97346
5	0.646	-3.79073
6	0.19	-14.4083
7	0.883	-1.08058
8	0.924	-0.69027
9	0.606	-4.35722

Table 4.13 Response table for SN ratio

Level	Cutting speed	Feed rate	Depth of cut	Temperature
1	0.6755	0.7955	0.5761	0.6220
2	0.5769	0.7725	0.7595	0.6070
3	0.8007	0.4869	0.7314	0.8183
Max-Min	0.2239	0.3086	0.1834	0.2113
Rank	2	1	4	3

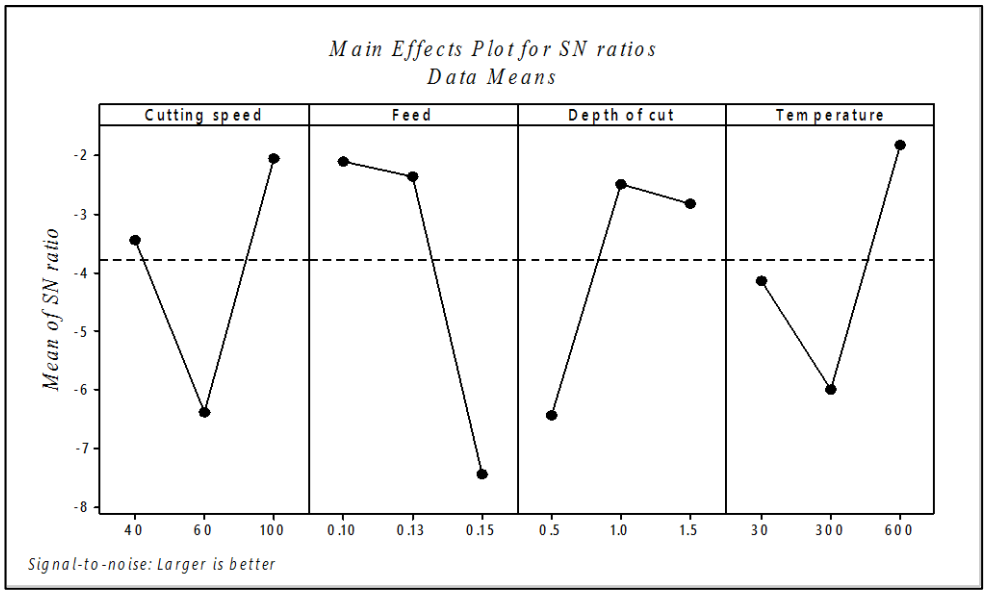

Figure 4.19 Main effect plot for SN ratio

4.4.2 Optimization using desirability function analysis

Theresponses obtained were normalized for calculation of individual desirability index and corresponding composite desirability index is calculated using Eq. (3-15) and Eq. (3-16) respectively and tabulated in Table 4.14. The value of composite desirability index closer to one is regarded as an optimal setting for machining responses.

Table 4.14 Calculation of individual desirability index and composite desirability index

Expt. Run	Individual desirability Index (d_i)			Composite desirability d_G
	Surface roughness	Power	Chip reduction ratio	
1	0.014151	1	0.488365	0.209283
2	0.957547	0.995465	0.490178	0.741135
3	0.490566	0.848073	0.494711	0.580069
4	0.872642	0.9161	0.492596	0.704417
5	0.721698	0.85034	0.304322	0.536683
6	0.5	0	0	0
7	0.882075	0.562358	1	0.810318
8	0.863208	0.78458	0.899668	**0.852822**
9	1	0.283447	0.034754	0.178707

The experimental run versus composite desirability index is shown in Fig.4.20. The optimal setting lies at cutting speed of 100 m/min, feed rate 0.13 mm/rev, 0.5 mm depth of cut and 600°C temperature respectively. In order to check the best optimal setting out of two optimization technique, a confirmation test was conducted using the optimal setting and better result obtained is considered as the best optimal setting for this machining operation as shown in Table 4.15.

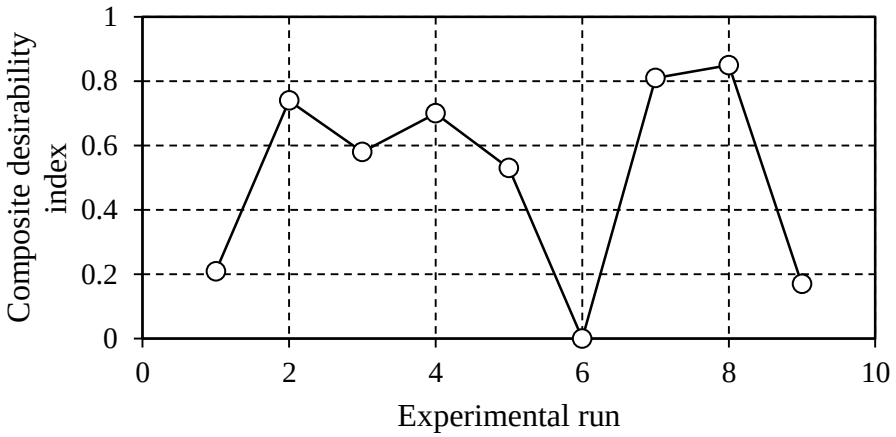

Figure 4.20 Composite desirability index vs Experimental run

Table 4.15 Comparison of obtained results between two optimization techniques

Methods	*Vc*	*f*	a_p	*T*	*SR*	*Power*	*CRC(ξ)*
PCA	100	0.1	1	600	1.02	0.347	1.345
DFA	100	0.13	0.5	600	1.06	0.353	1.465

4.5 Conclusion

In this chapter, hot machining of Inconel 625 alloy was carried out to describe the advantages in in machinability criteria. The experimental trials were carried out at varying cutting parameters same as Inconel 718. Response surface methodology has been used to predict the experimental data such as flank wear and surface roughness. Principal component and desirability function analysis have been used to optimize the machining parameters to achieve multi-response criteria. Following conclusions was derived from this chapter.

- There was maximum reduction of 35%, 29% and 50% of cutting, feed, and radial force respectively was observed in the hot turning (600°C) of Inconel 625 compared to room temperature.
- Compared to room temperature conditions, there was improvement of 40% surface finish and increase 209% of tool life in hot machining (600°C).
- There was an increase of chip tool contact length and decrease of chip thickness with the increase of workpiece temperature

- The predicted flank wear and surface roughness using surface response methodology were good correlation with the experimental results. An aveage 4 % error of flank wear and 4% of surface roughness was observed between experimental and predicted value.

- The optimal settings were obtained at 100 m/min cutting speed, 0.1 mm/rev feed rate, 1 mm depth of cut and 600°C temperature using principal component analysis to minimize the surface roughness, power and chip reduction coefficient.

Chapter 5

Experimental Investigation and Modeling of Hot Machining of Monel 400

5.1 Introduction

In this chapter, another type of nickel and copper base alloys called Monel 400 is used for machining investigation. Monel is nickel-base alloys having 23-33% copper and initially created by metallurgist David H. Browne in 1906. It is having high corrosion resistance to acids and alkali, high mechanical strength, good ductility and low coefficient of thermal expansions. It is generally used in valve systems, springs, heat exchangers, wind instruments, fuel tank, piping systems, screw machined product, brass strings, trolling wire etc. [128]. Monel 400 is a high corrosion resistant, high strength and high-temperature nickel base material and different from other alloys, has been widely used in aerospace, marine sectors due to above characteristics. Monel 400 has the ability to retain its physical properties at high temperature over 700°C. Like Inconel 718, Monel 400 is considered as difficult to cut material due to high strength, work hardening characteristics and presence of an abrasive particle in the microstructure. Cutting force and temperature at the tool edge have the biggest problem during machining of nickel base alloy as it directly affects the tool life of the cutting tool. One approach to machine these hard materials is to soften the workpiece surface layer by using the external heat source in order to reduce the shear strength and strain hardening [10].

Sarkar and Mitra [155] used Monel 400 as workpiece material in electro discharge machining process to investigate the die corner accuracy. They used pulse on time, pulse frequency, peak current, servo voltage and wire tension as input parameters and machining were performed using L_{18} OA. It was observed that pulse on time and peak current influenced the material removal rate and surface roughness compared to other parameters. Similarly, modeling of machining rate and surface quality characteristics using RSM method in wire electro discharge machining was studied by Vinod et al. [127].

Desirability function analysis was utilized for optimization of surface roughness and machining rate.

It is observed from literature that, a few works have been carried out on machining of Monel 400 using EDM or WEDM and no work has not studied for bulk machining of Monel 400 using hot machining yet. In this chapter Monel 400 was used as workpiece material and machining was performed for both room and heated conditions in order to analyses the machinability. The cutting force, feed force, radial force, tool wear, tool life, surface roughness, chip tool contact length and chip morphology etc., have been analyzed in both room temperature and at heated conditions. Similar to Inconel 718 and Inconel 625, the modeling of hot turning of Monel 400 using response surface methodology has been carried out. Desirability function analysis, theprincipal component along with Taguchi's method was used to optimize the machining parameters in thehot turning of Monel 400 alloys. A similar experimental setup and cutting variables were used for carrying out hot machining of Monel 400 as that of for Inconel 718 and Inconel 625. Tool life, cutting force, feed force, radial force, surface finish, tool wear, and chip morphology, were investigated at both room temperature and heated conditions. The chemical composition and mechanical properties of Monel 400 are tabulated in Table 5.1 and Table 5.2 respectively.

Table 5.1 Chemical composition of Monel 400 (weight %) [156]

Ni	Cu	Fe	C	Si	Mn
63 min	28	2.5 max	2	5	2

Table 5.2 Physical properties of Monel 400 [156]

Properties	Values
Density	8.8 g/cm^3
Melting point	1350 ºC
Hardness	172HV
Coefficient of expansion	13.9 µm/m ºC
Modulus of rigidity	65.3 kN/mm^2
Modulus of elasticity	173 kN/mm^2

5.2 Results and discussion

The variation of different responses with respect to different cutting variables (cutting speed, feed rate, depth of cut and workpiece temperature) are tabulated in Table 5.3 and has been discussed below.

Table 5.3 Responses obtained at various cutting conditions in room and heated conditions

Cutting conditions			Force (N)									Tool life (min)			Surface roughness (μm)		
			30°C			300°C			600°C			30°C	300°C	600°C	30°C	300°C	600°C
V_c(m/min)	f(mm/rev)	a_p(mm)	Feed	Radial	Cutting	Feed	Radial	Cutting	Feed	Radial	Cutting						
40	0.13	0.5	178	12	203	162	8	195	147	5	143	28	45	52	3.1	2.7	1.6
60			169	11	192	157	8	177	127	4	135	22	34	38	2.5	1.9	1.2
100			155	9	175	144	6	160	85	4	128	14	27	29	2.2	1.9	1.09
100	0.1	0.5	181	6	317	154	4	281	146	3	268	24	33	42	2	1.6	1.2
	0.13		217	7	342	211	6	332	209	4	323	21	25	37	2.2	1.7	1.3
	0.15		243	9	363	226	6	358	208	4	339	18	20	28	2.5	1.9	1.6
100	0.13	0.5	163	7	225	145	6	206	132	4	186	17	18	19	2.1	1.9	1.8
		1	151	9	196	139	7	182	121	5	173	16	17	19	2	1.8	1.6
		1.5	142	10	178	126	8	169	109	5	145	14	15	17	2	1.7	1.6

5.2.1 Force

Variation of cutting, feed and radial force with respect to cutting speed and workpiece temperature

The variation of cutting, feed and radial force with respect to cutting speed and workpiece temperature is shown in Fig.5.1(a-c). Reduction of (29, 29 and 26%) cutting force (Fig. 5.2 (a)), (17, 24 and 45%) feed force (Fig. 5.2 (b)) and (56, 63 and 55%) radial force

(Fig. 5.2 (c)) was obtained at 40, 60, and 100 m/min cutting speed respectively, when workpiece heated to 600°C compared to room temperature. But with increase in the cutting speed from 40 to 100 m/min, there was reduction of (13, 17, and 10%) cutting force, (12, 11 and 42%) feed force and (25, 25, and 20%) radial force at 30, 300 and 600°C temperature respectively.

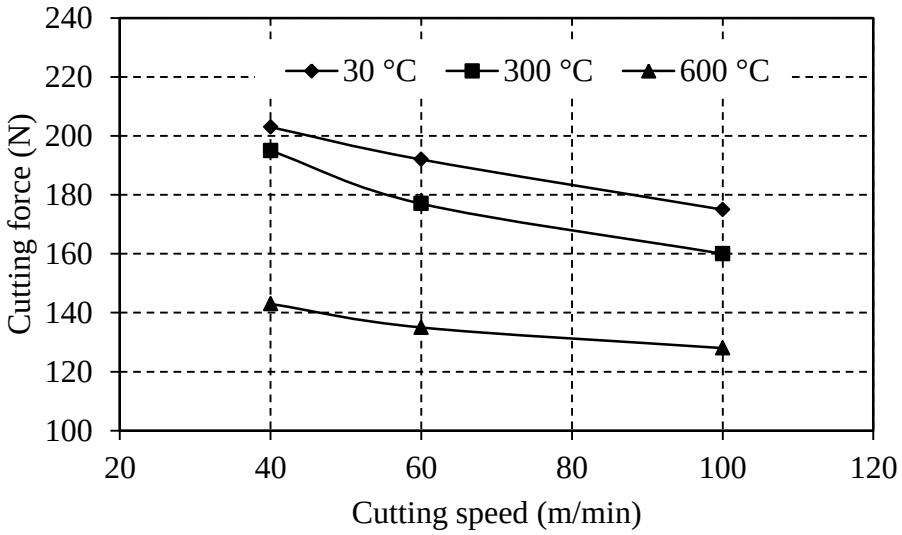

(a)

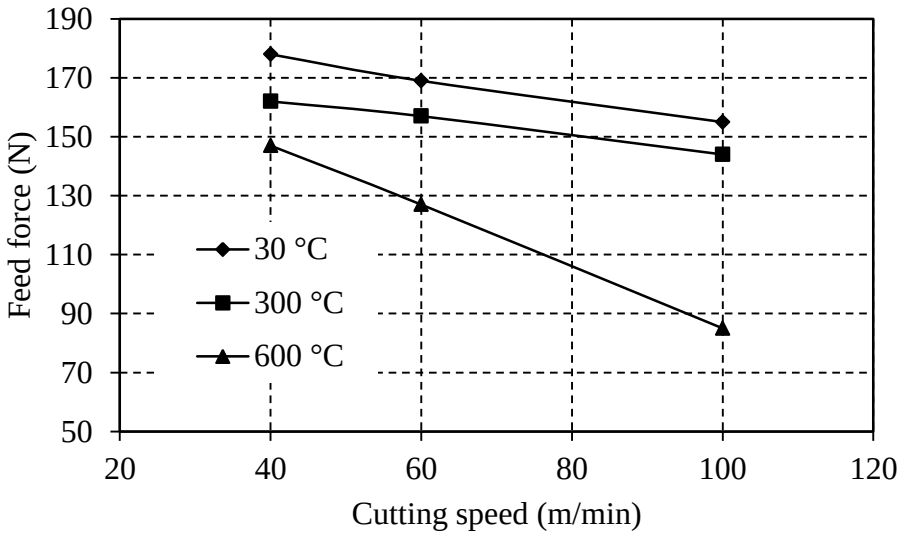

(b)

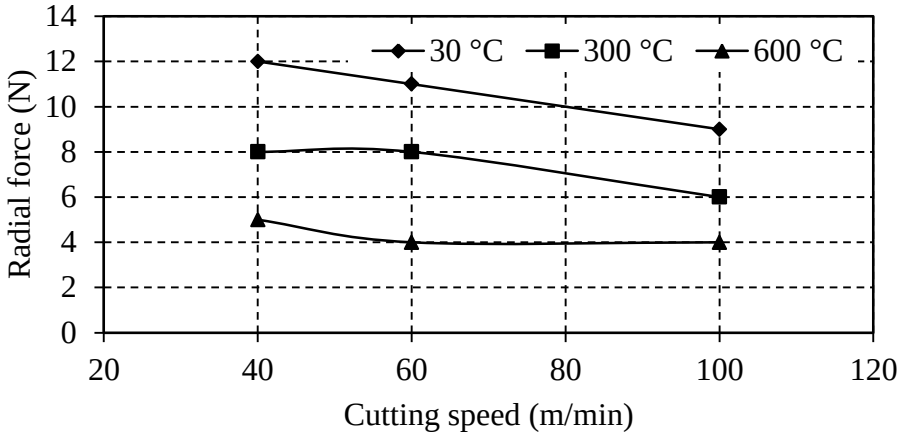

(c)

Figure 5.1 Variation of (a) Cutting force (b) Feed force (c) Radial force with respect to cutting speed and workpiece temperature at feed rate 0.13mm/rev and depth of cut 0.5 mm

Variation of cutting, feed force and radial force with respect to feed rate and workpiece temperature

Variation of cutting, feed and radial force with respect to feed rate and workpiece temperature is shown in Fig. 5-2 (a-c). There was reduction of (15, 5 and 6%) cutting force (Fig. 5.2 (a)), (19, 3, and 14%) feed force (Fig. 5.2 (b)) and (42, 44 and 50%) radial force (Fig. 5.2 (c)) at feed rate of 0.1, 0.13, and 0.15 mm respectively, when machining was carried out at 600°C compared to room temperature. But with the increase of feed rate from 0.1 to 0.15 mm/rev, there was increase of (14, 27, and 26%) cutting force, (34, 46 and 42%) feed force and (42, 33 and 25%) radial force at 30, 300 and 600°C temperature respectively.

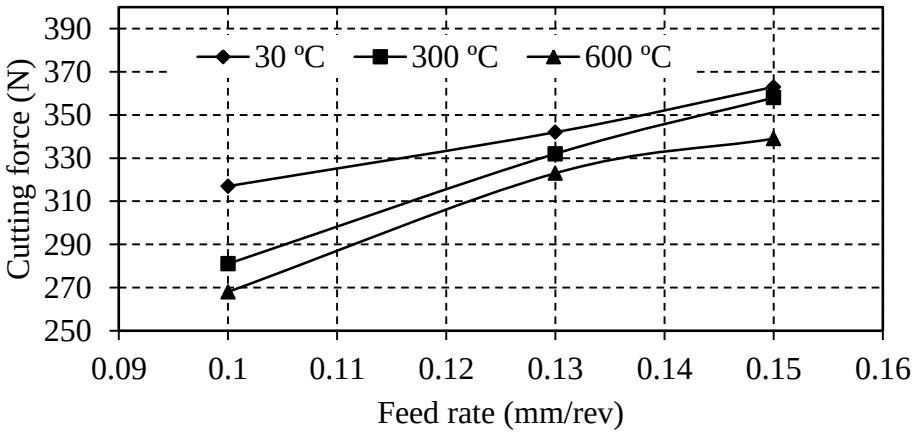

(a)

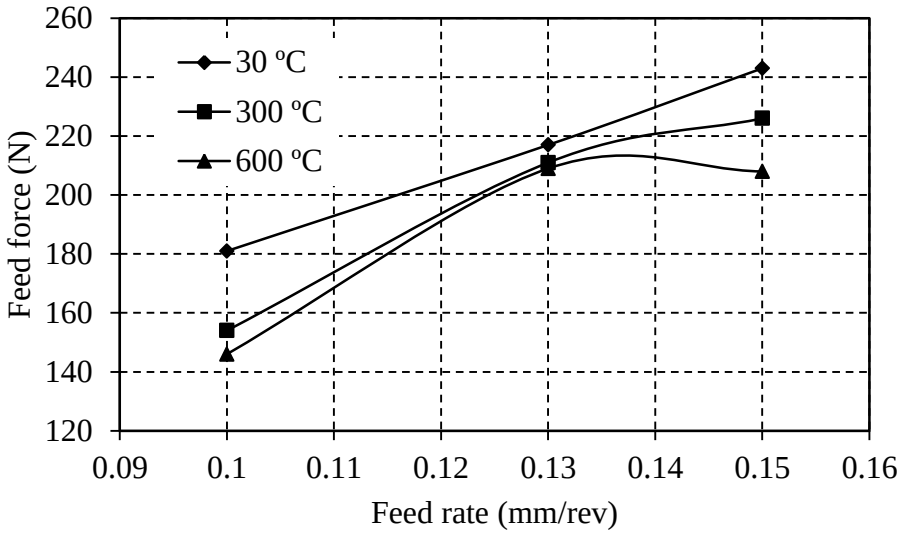

(b)

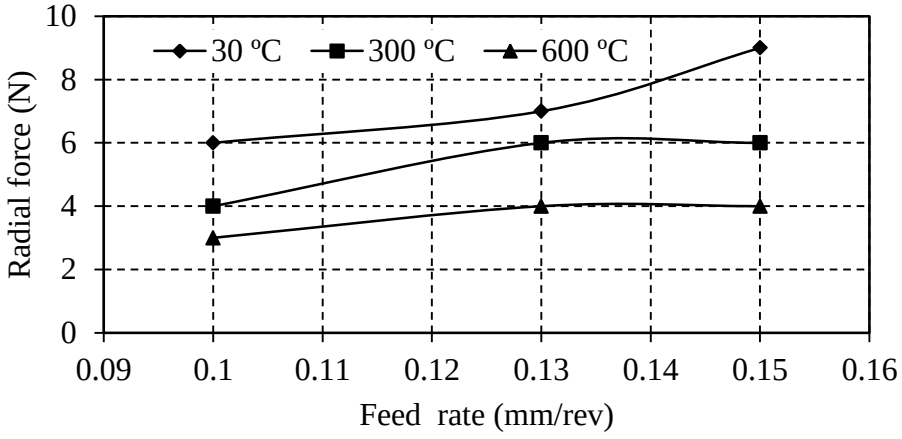

(c)

Figure 5.2 Variation of (a) Cutting force (b) Feed force and (c) Radial force with respect to feed rate and workpiece temperature at cutting speed of 100 m/min and depth of cut 0.5 mm

Variation of cutting, feed and radial force with respect to depth of cut and workpiece temperature

The variation of cutting, feed and radial force with respect to the depth of cut and workpiece temperature is shown in Fig. 5.3 (a-c). With increase ofworkpiece temperature from room temperature to 600ºC, there was decrease of (17, 11 and 18%) cutting force (Fig. 5.3 (a)), (19, 19 and 23%) feed force (Fig. 5.2 (b)), and (40, 44 and 50%) radial force (Fig. 5.2 (c)), at depth of cut 0.5, 1 and 0.1 mm respectively. With increase of depth of cut from 0.5 to 1.5 mm, there was reduction of (20, 17 and 22%) cutting force, (12, 13 and

17%) feed force and (20, 25 and 33%) radial force at 30, 300 and 600ºC workpiece temperature respectively.

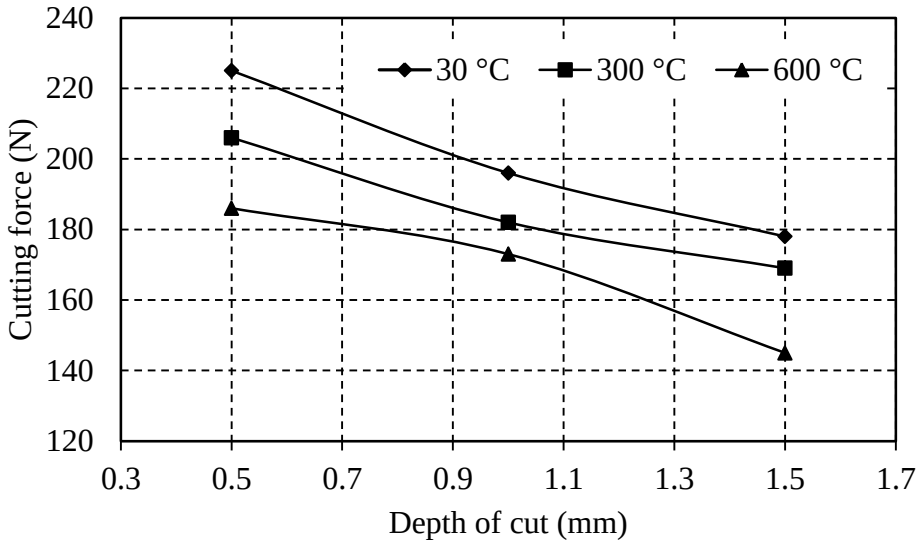

(a)

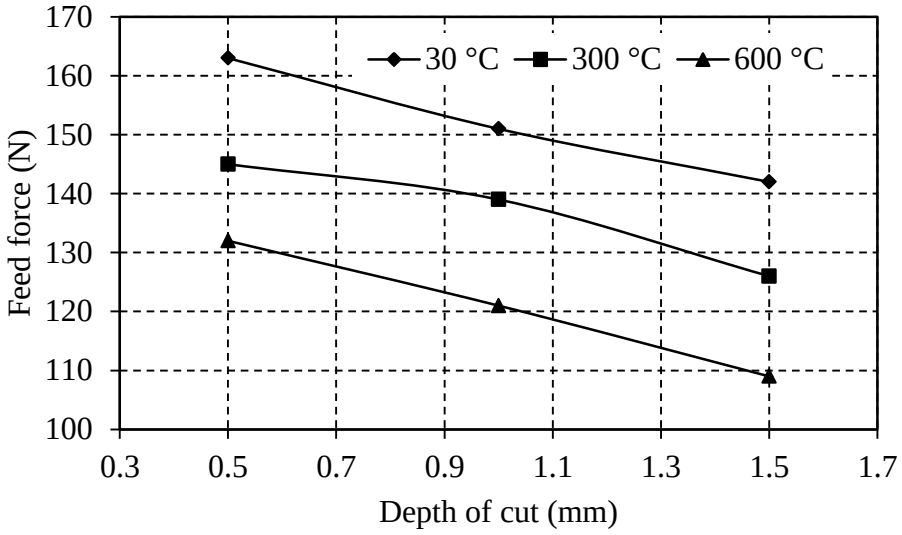

(b)

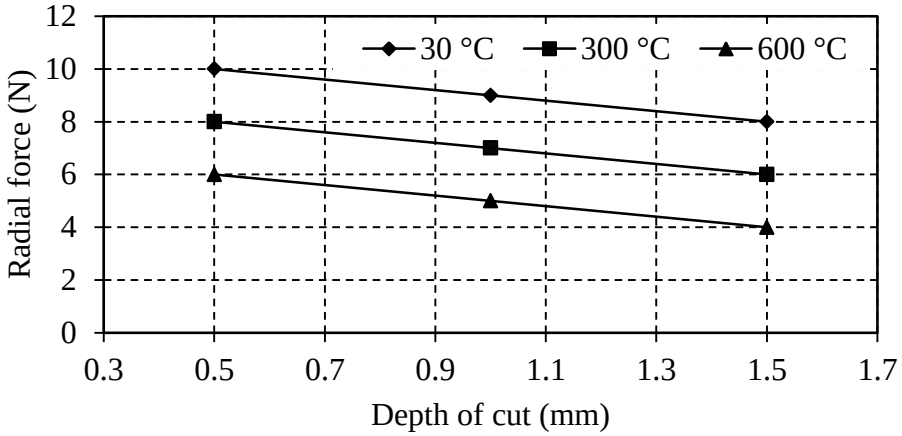

(c)

Figure 5.3 Variation of (a) Cutting force, (b) Feed force (c) Radial force with respect to depth of cut and workpiece temperature at cutting speed of 100 m/min and feed rate of 0.13 mm/rev

5.2.2 Surface roughness and microhardness

Effect of cutting speed on surface finish

Variation of surface roughness with respect to cutting speed and workpiece temperature has been presented in Fig 5.4. There was a reduction of 48, 52 and 50% surface roughness at cutting speed 40, 60 and 100 m/min respectively, at 600°C workpiece temperature compared to room temperature. With increase of the cutting speed from 40 to 100 m/min, there was improvement surface finish by reducing surface roughness (29, 29 and 31%) at 30, 300 and 600°C temperature respectively.

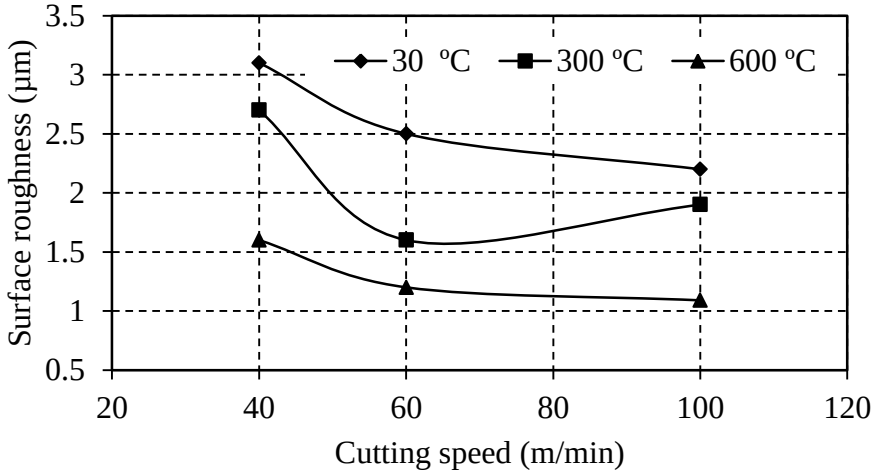

Figure 5.4 Variation of surface roughness with respect to cutting speed and workpiece temperature at feed rate 0.13 mm/rev and depth of cut 0.5 mm

Effect of feed rate with workpiece temperature on surface roughness

Variation of surface roughness with respect to feed rate and workpiece temperature is shown in Fig.5.5. The surface roughness reduced 40, 40, and 36% at feed rate 0.1, 0.13 and 0.15 mm/rev respectively, when workpiece temperature was 600°C compared to room temperature. There was increase of (20, 15 and 25%) surface roughness at 30, 300, and 600°C temperature respectively, when feed rate increased from 0.1 to 0.15 mm/rev.

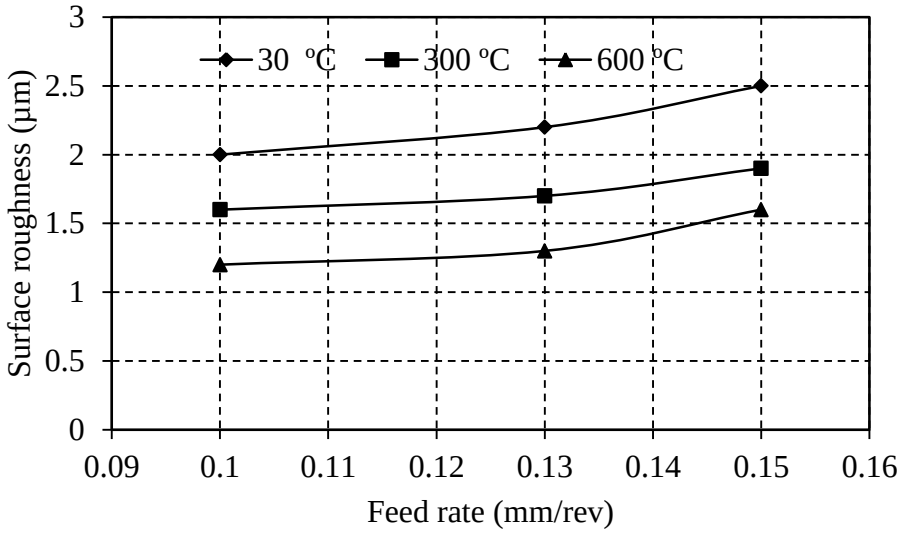

Figure 5.5 Variation of surface roughness with respect to feed rate and workpiece temperature at cutting speed 100 m/min and depth of cut 0.5 mm

Effect of depth of cut on surface finish

There was decrease of surface roughness 14, 20 and 20% at 0.5, 1 and 1.5 mm depth of cut respectively, machining at 600°C compared to room temperature. With increase of the depth of cut from 0.5 to 1.5 mm, there was an improvement of surface finish by reducing surface roughness 4, 10, and 11% at 30, 300 and 600°C temperature respectively as shown in Fig.5.6.

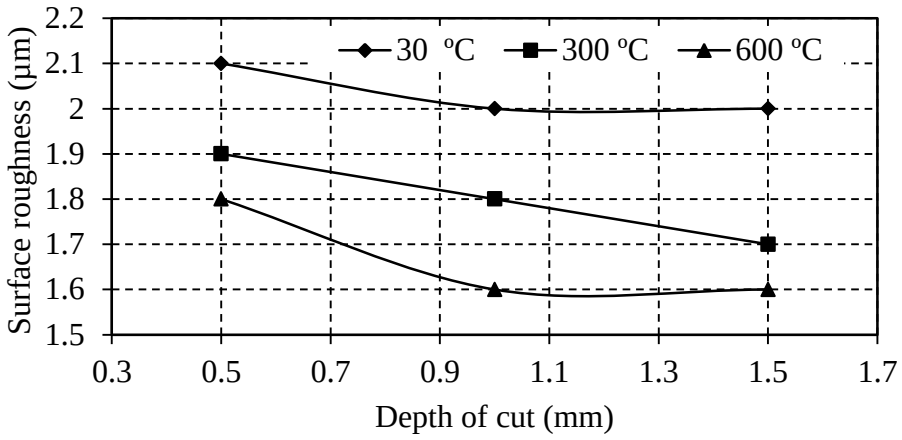

Figure 5.6 Variation of surface roughness with respect to depth of cut and workpiece temperature at cutting speed 100 m/min and feed rate 0.13 mm/rev

Effect of heating on microhardness beneath the machined surface

Due to heating on the surface of the workpiece, the microhardness distribution below the machined surface decreased due to annealing up to 60 µm from the machined surface (heat affected zone) as shown in Fig. 5.7. But after some distance, the heating effect decreased, and strain hardening formation started, hence increased microhardness value due to plastic deformation (strain hardening zone (70-170 µm)).

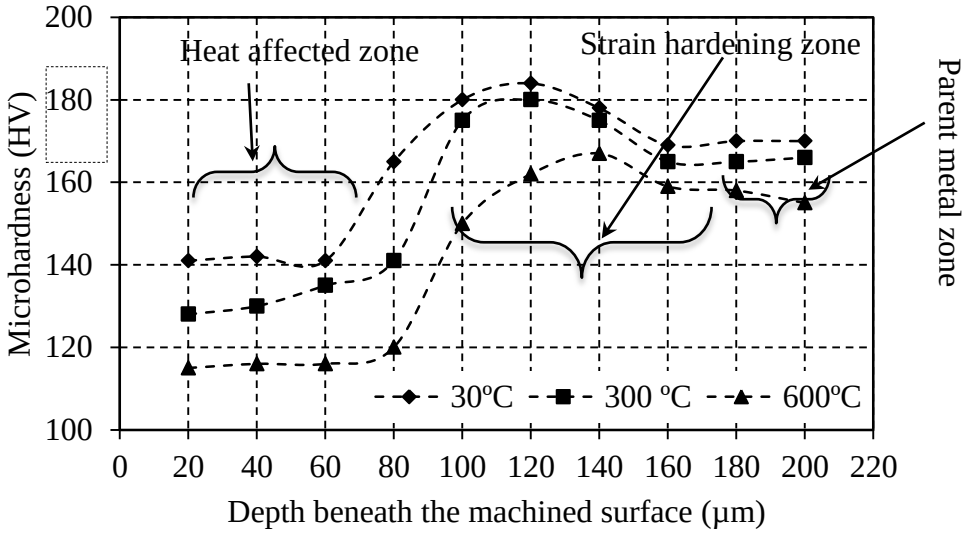

Figure 5.7 Effect of heating on microhardness beneath the machined surface

After moving some distance (170-190 µm) towards thecenter, the strain hardening decreased due decreased of shearing and plastic deformation and microhardness value becomes same as that of parent material (Monel 400).

5.2.3 Tool life

Effect of cutting speed on tool life

The variation of tool life and corresponding flank wear with respect to cutting speed and workpiece temperature is shown in Fig 5.8 (a-b). The height of flank wear is taken 0.3 mm in order to determine tool life. Variation of flank wear with respect to time is shown in Fig. 5.9 (a).

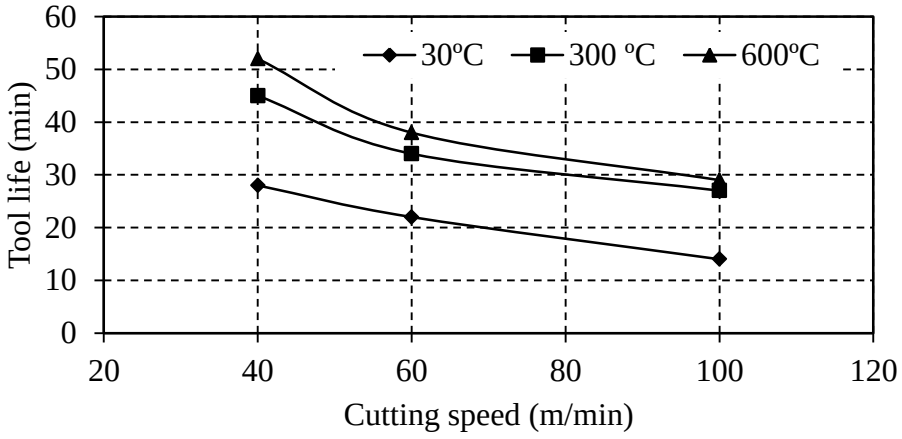

(a)

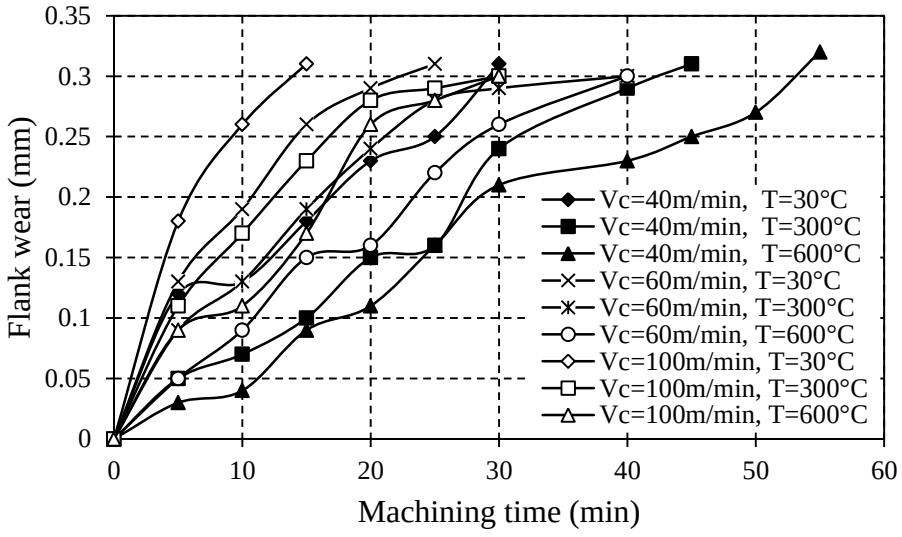

(b)

Figure 5.8 Effect of cutting speed on (a) Tool life (b) Flank wear at different workpiece temperature at feed rate of 0.13 mm/rev and depth of cut 0.5 mm

It was observed that there was increase of 85, 72, 107% of tool life at cutting speed 40, 60 and 100 m/min respectively, at workpiece temperature 600°C compared to room

temperature. But with increase of the cutting speed from 40 to 100 m/min, there was decrease in tool life 50, 40 and 44% at 30, 300 and 600°C workpiece temperature respectively.

Effect of feed rate on tool life

Referring to Fig 5.9 (a-b) there was anincrease of tool life 75, 76 and 55% at feed rate 0.1, 0.13 and 0.15 mm/rev respectively, machining at 600°C compared to room temperature. With increase of the feed rate from 0.1 to 0.15 mm/rev, there was decrease of tool life by 25, 39 and 33% at 30, 300 and 600°C workpiece temperature respectively. Variation of flank wear with respect to time is shown in Fig. 5.9 (b).

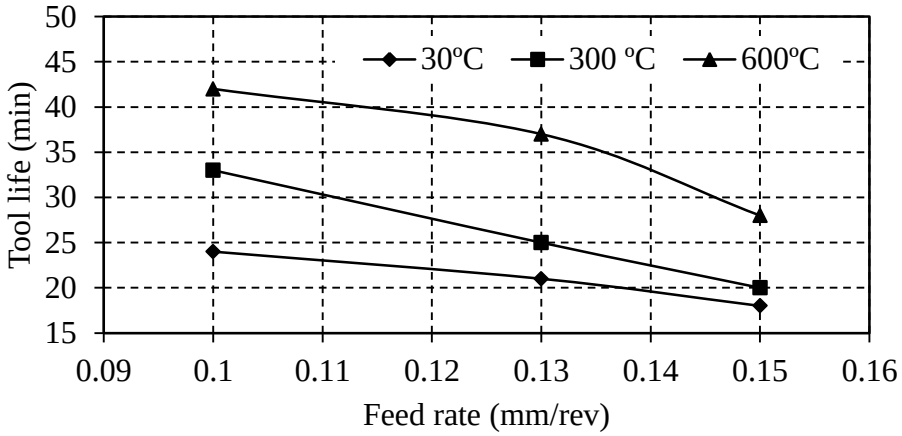

(a)

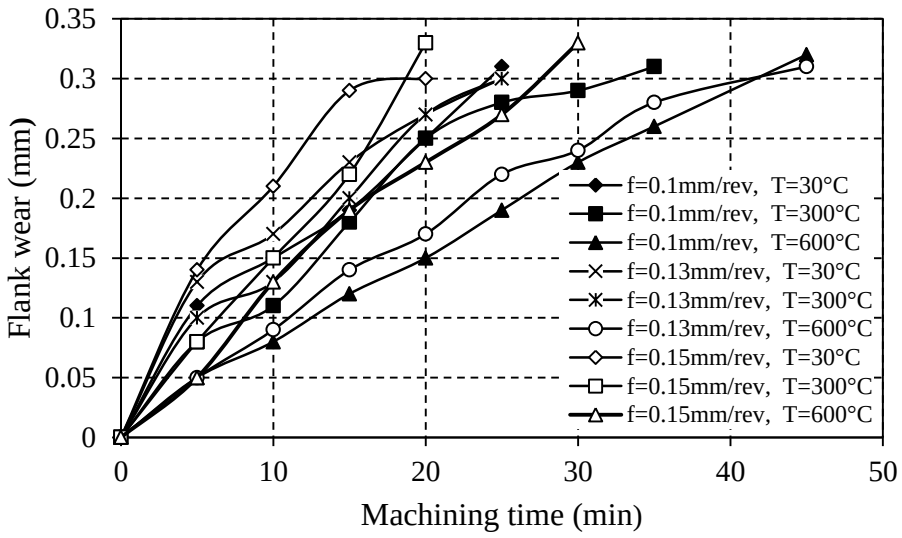

(b)

Figure 5.9 Effect of feed rate on (a) Tool life (b) Flank wear at different workpiece temperature at cutting speed 100 m/min and depth of cut 0.5 mm

Effect of depth of cut on tool life

The effect of depth of cut on flank wear and tool life was studied as shown in Fig 5.10 (a-b). During hot machining at 600°C temperature, there was increase of 11, 18 and 21% tool life, at 0.5, 1 and 1.5 mm depth of cut respectively compared to room temperature. When the depth of cut increased from 0.5 to 1.5 mm, there was decrease of tool life 17, 16 and 10% at 30, 300 and 600°C workpiece temperatures respectively. Variation of flank wear with respect to time is shown in Fig. 5. 10 (b).

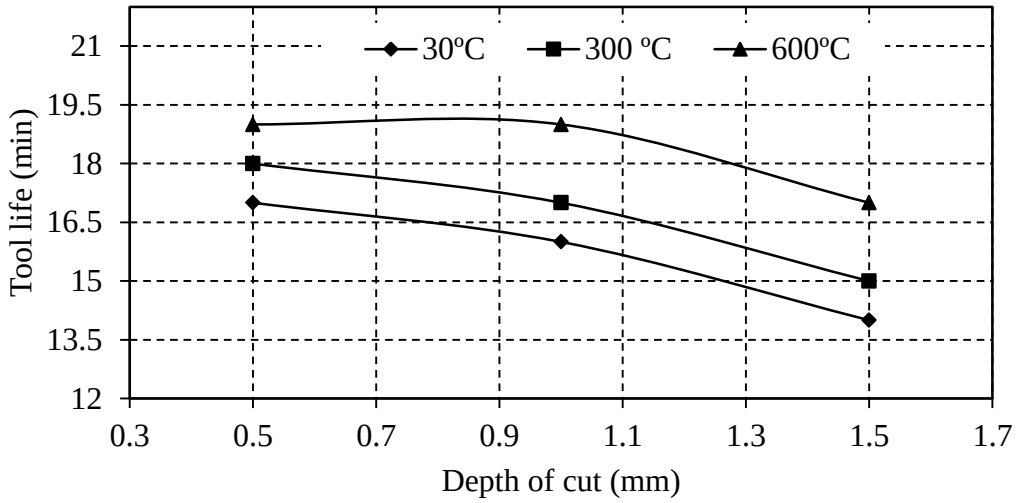

(a)

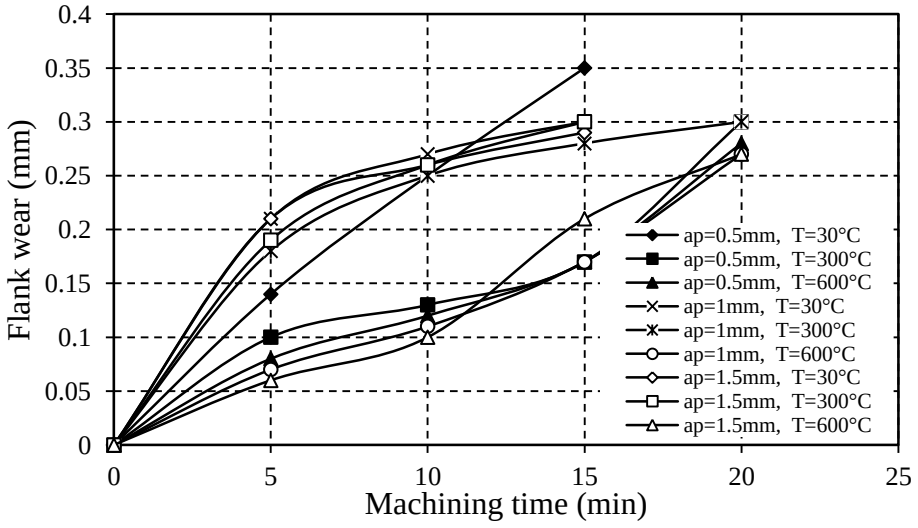

(b)

Figure 5.10 Effect of depth of cut on (a) Tool life (b) Flank wear at different workpiece temperature at cutting speed 100 m/min and feed rate 0.13 mm/rev

Effect of heating on tool wear

Monel 400 being a high resistant material, machining with carbide insert leads to wear formation easily. The flank wear is the main dominant wear in machining of Monel 400 alloys (Fig. 5.11(a-b)). After machining Monel 400 at cutting speed of 60 m/min, the tool wear reached 0.3 mm at room temperature, whereas, the same wear was 0.16 mm at 600°C temperature of the workpiece for 9 min cutting time operation. In hot machining, diffusion wear is dominant because during heating not only workpiece is subjected to ahigh temperature but also inserts too. So, at elevated temperature, the material from the cutting tool diffused from the rake face and formed crater wear. Built-up-edge and notch wear were formed during machining as shown in Fig 5.12 (a-b).

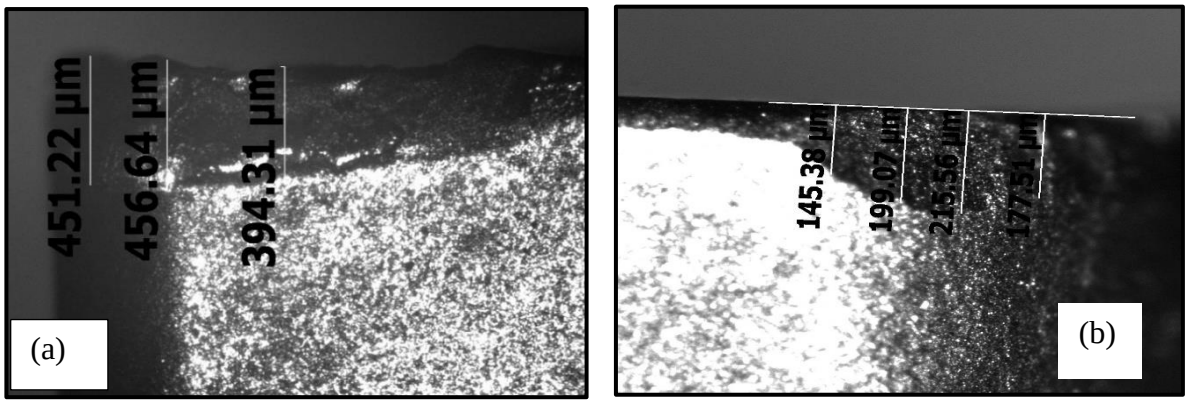

Figure 5.11 Tool wear observed after machining 9 min, at (a) 30°C (b) 600°C

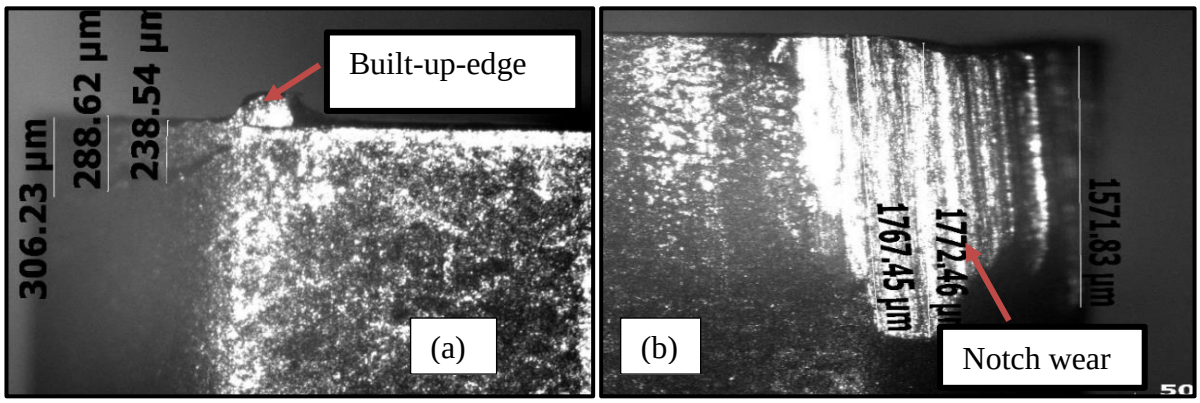

Figure 5.12 (a) Built-up-edge (b) Notch wear formation

The close up view of tool wear at different cutting speed (40 and 100 m/min) and different depth of cut (0.5, 1 and 1.5 mm) with respect to workpiece temperature is shown in Fig 5.13.

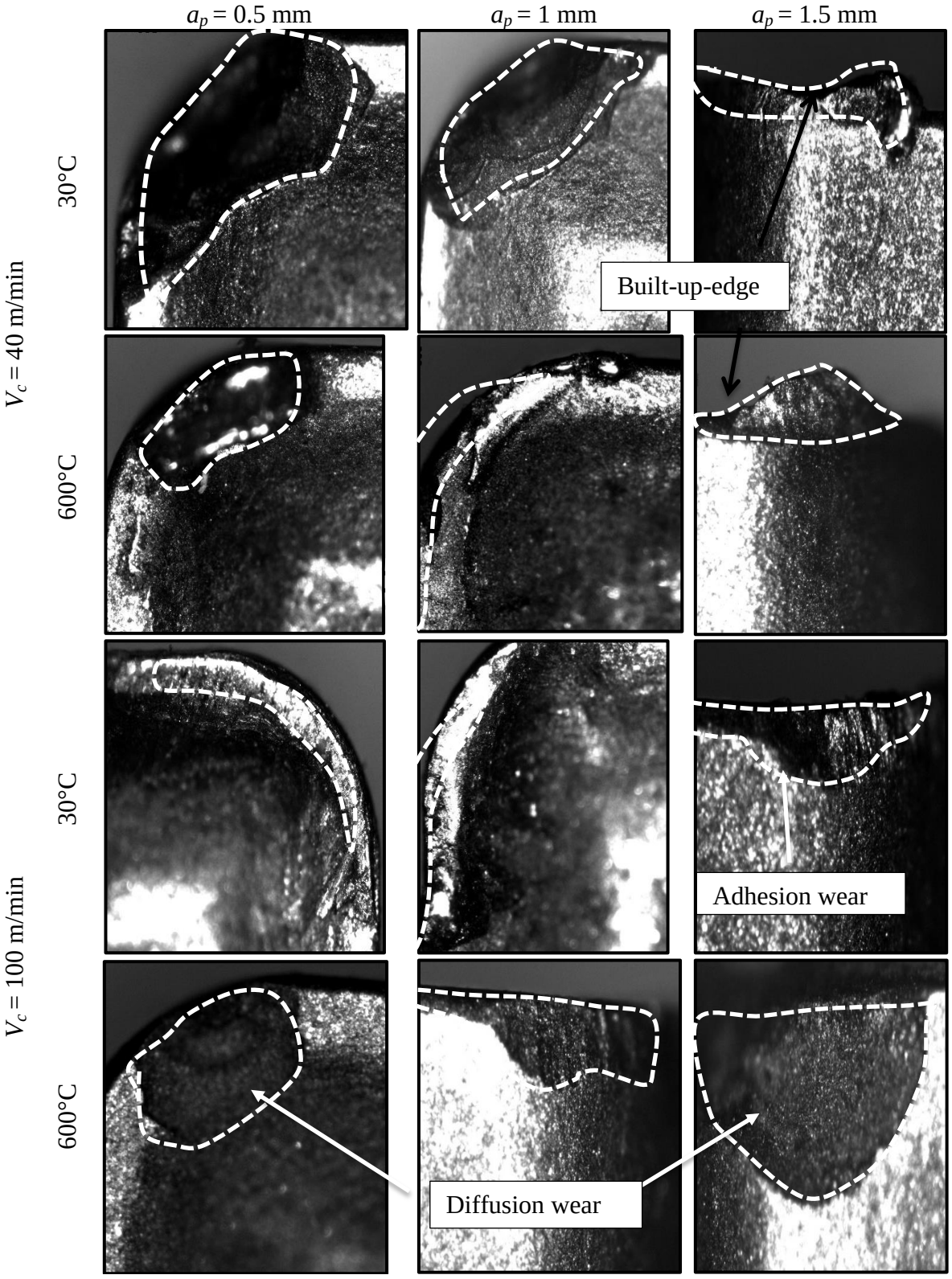

Figure 5.13 Tool wear at different cutting velocity and depth of cut in room and heated conditions

5.2.4 Chip morphology

The chip characteristics and morphology on hot machining of Monel 400 with uncoated carbide tool as shown in Fig. 5.14. Two types of chips are observed. Machining under room temperature produces the short and discontinuous chip (spiral type).

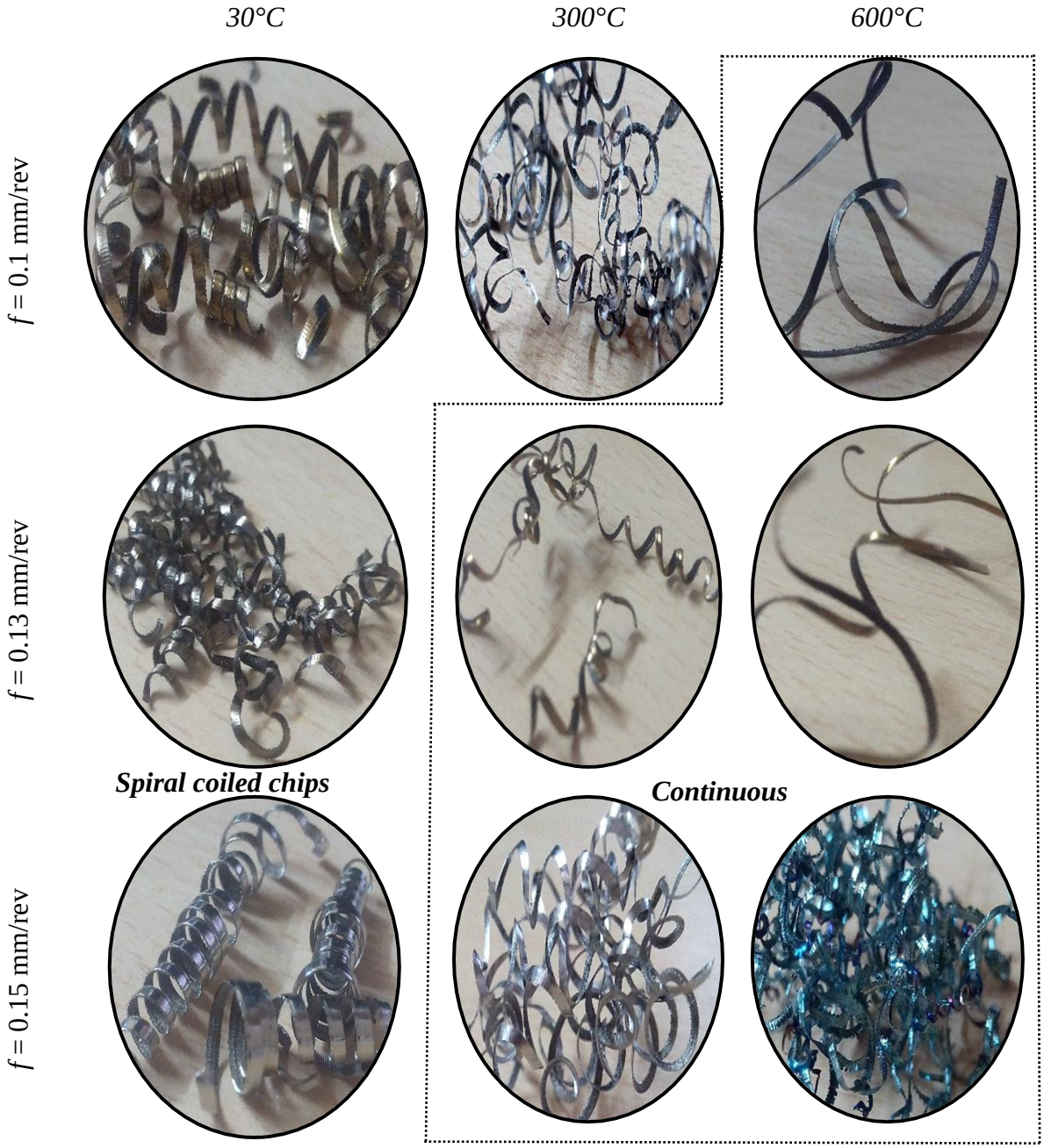

Figure 5.14 Chips formation at cutting speed 100 m/min, depth of cut 0.5 mm

The continuous chips are produced at a high temperature of workpiece, since the ductility of the material increases. The chip thickness was measured at three different locations on

the chip with the help of optical microscope as shown in Fig. 5.15 and average was taken. It was observed that, the chip thickness decreased with the increase of workpiece temperature. The variation of chip thickness with respect to workpiece temperature has been plotted in Fig.5.16.

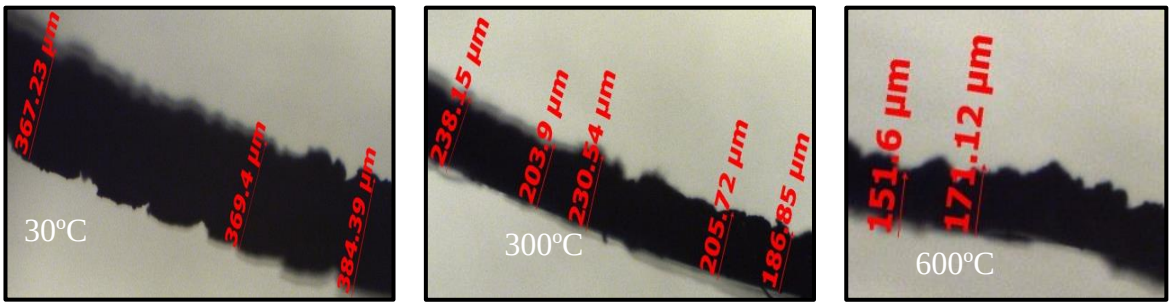

Figure 5.15 Optical microscope view of chip thickness at different workpiece temperature

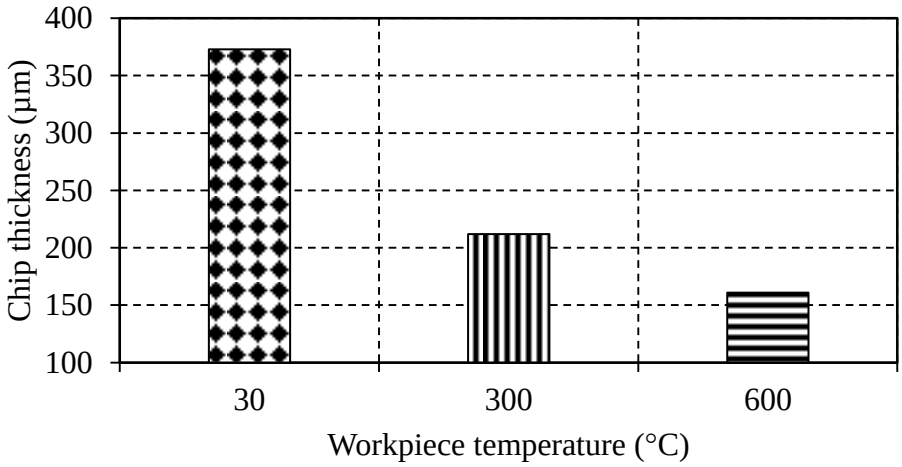

Figure 5.16 Variation of chip thickness with respect to workpiece temperature at cutting speed 100 m/min, feed 0.13 mm/rev and depth of cut 0.5 mm

5.2.5 Chip-tool contact length

The optical view of chip-tool contact length is shown in Fig.5.17. The variation of chip tool contact length with temperature is shown in Fig 5.18. It is clearly seen that chip-tool contact length increased from 141.11 µm (at room temperature) to 570.406 µm (600°C workpiece temperature).

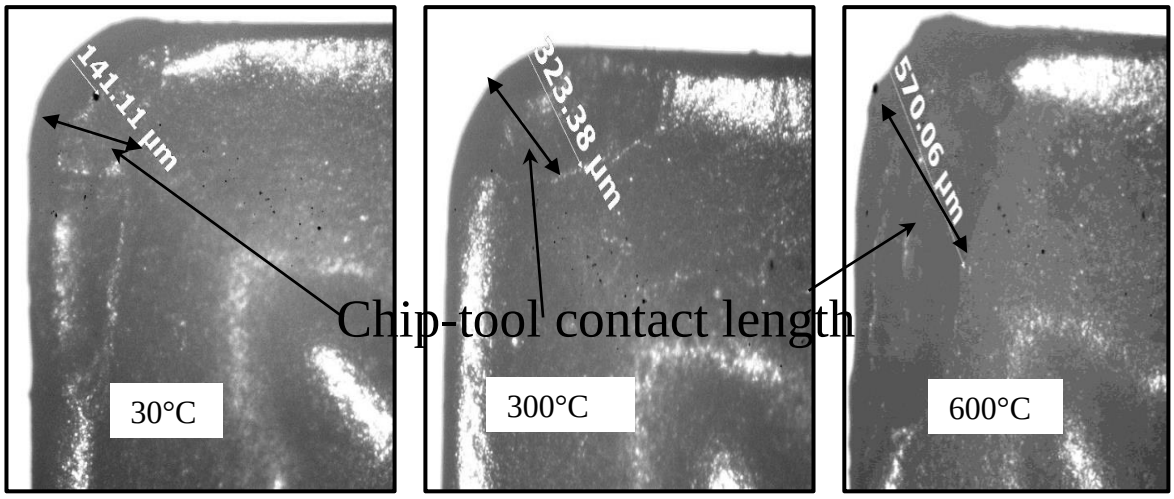

Figure 5.17 Optical microscope view of chip-tool contact length (cutting speed=100 m/min, feed=0.13 mm/rev and depth of cut=0.5 mm)

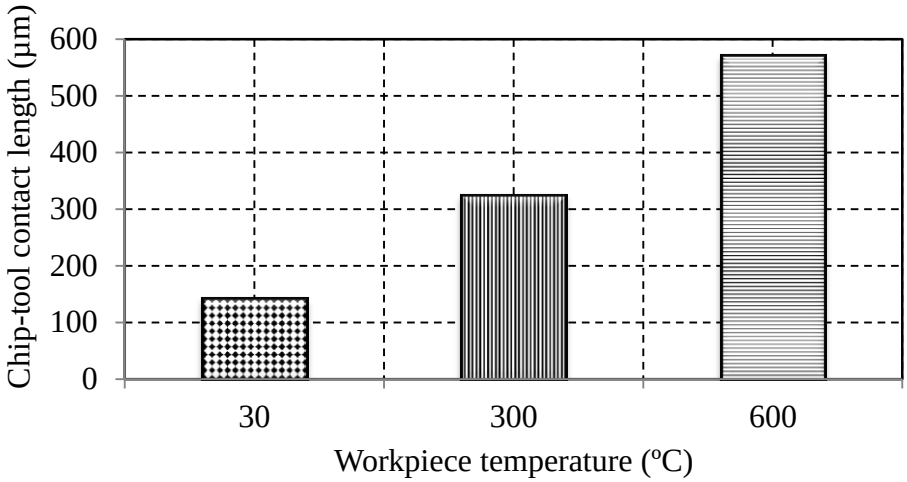

Figure 5.18 Chip-tool contact length vs workpiece temperature (cutting speed =100 m/min, feed = 0.13 mm/rev and depth of cut = 0.5 mm)

5.3 Modeling of hot turning of Monel 400 using response surface methodology

Experimental investigation of hot machining of Monel 400 was carried out as per response surface methodology as given in Table 5.4. The fitted ANOVA table for surface roughness and flank wear are tabulated in Table 5.5.

Table 5.4 Design layout and experimental results

Run	Coded factors				Actual factors				Response variables	
	X_1	X_2	X_3	X_4	V_c	f	a_p	T	$VB_{max,}$ mm	R_a, μm
1	0	0	0	0	70	0.125	1	315	0.229	2.295
2	-1	+1	-1	+1	40	0.15	0.5	600	0.229	2.697
3	-1	-1	-1	-1	40	0.1	0.5	30	0.228	2.432
4	0	-1	0	0	70	0.1	1	1	0.253	2.443
5	+1	0	0	0	100	0.125	1	315	0.232	2.245
6	-1	0	0	0	40	0.125	1	315	0.206	2.905
7	0	0	0	0	70	0.125	1	315	0.224	2.232
8	+1	-1	+1	+1	100	0.1	1.5	600	0.323	2.323
9	+1	-1	+1	-1	100	0.1	1.5	30	0.286	2.184
10	+1	-1	-1	-1	100	0.1	0.5	30	0.232	2.184
11	0	0	+1	0	70	0.125	1.5	315	0.255	2.501
12	0	0	0	0	70	0.125	1	315	0.225	2.293
13	-1	+1	-1	-1	40	0.15	0.5	30	0.255	2.542
14	0	+1	0	0	70	0.15	1	315	0.259	2.480
15	+1	+1	+1	-1	100	0.15	1.5	30	0.316	2.368
16	0	0	0	+1	70	0.125	1	600	0.257	2.531
17	+1	+1	-1	-1	100	0.15	0.5	30	0.288	2.259
18	-1	-1	+1	+1	40	0.1	1.5	600	0.273	2.616
19	0	0	0	0	70	0.125	1	315	0.214	2.291
20	0	0	0	0	70	0.125	1	315	0.237	2.295
21	0	0	0	-1	70	0.125	1	30	0.236	2.387
22	-1	-1	+1	+1	40	0.1	1.5	600	0.246	2.539
23	-1	+1	+1	+1	40	0.15	1.5	600	0.250	2.795
24	+1	+1	+1	+1	100	0.15	1.5	600	0.314	2.234
25	+1	-1	-1	+1	100	0.1	0.5	600	0.287	2.259
26	+1	+1	-1	+1	100	0.15	0.5	600	0.322	2.294
27	-1	-1	-1	+1	40	0.1	0.5	600	0.263	2.776

28	0	0	-1	0	70	0.125	0.5	315	0.219	2.354
29	-1	+1	+1	-1	40	0.15	1.5	30	0.267	2.643
30	0	0	0	0	70	0.125	1	315	0.227	2.296

Table 5.5 ANOVA table for the fitted models

Source	DoF	SS	MS	*F*-value	*P*-value
Flank wear					
Model	14	0.030213	0.002158	19.21	0
Error	15	0.001685	0.000112		
Lack-of-fit	9	0.001041	0.000116	1.08	0.482
Pure error	6	0.000645	0.000107		
Total	29	0.031898			
vR^2-94.72					
R^2 Adjusted-89.79					
Prediction R^2-68.26					
Surface roughness					
Model	14	0.847618	0.060544	6.68	0
Error	15	0.136008	0.009067		
Lack-of-fit	9	0.0100854	0.011206	1.92	0.222
Pure error	6	0.053120	0.008853		
Total	29	0.983626			
R^2-86.17					
R^2 Adjusted-73.27					
Prediction R^2-55.67					

Table 5.6 and Table 5.7 show the ANOVA table for flank wear and surface roughness. Backward elimination process was utilized to reduce quadratic model by eliminating the insignificant process (*P*-value > 0.05). The coefficient of determination R^2 which determined the ratio of explained variation to the total variation. The R^2-value 94.72%, R^2-adjusted value 89.79% and R^2-prediction value 68.26% for flank wear were obtained. Similarly, for surface roughness R^2 value 86.17%, R^2 adjusted value 73.27% and prediction R^2 value 55.67% were obtained. The cutting speed, feed, depth of cut, temperature, square of feed and temperature, aproduct of speed and feed, a product of speed and temperature, a product of feed and temperature were the most significant parameter affecting flank wear.

Table 5.6 Analysis of variance (ANOVA) for the flank wear

Source	DoF	SS	MS	*F*-Value	*P*-Value	Remarks
Model	14	0.030213	0.002158	19.21	0	
V_c	1	0.007415	0.007415	66	**0.000**	Significant
f	1	0.000589	0.000589	5.24	**0.037***	Significant
a_p	1	0.002214	0.002214	19.70	**0.000***	Significant
T	1	0.000713	0.000713	6.34	**0.024***	Significant
Vc^2	1	0.000204	0.000204	1.82	0.197	
f^2	1	0.002045	0.002045	18.20	**0.001***	Significant
a_p^2	1	0.000215	0.000215	1.91	0.187	
T^2	1	0.000896	0.000896	7.98	**0.013***	Significant
$V_c * f$	1	0.000851	0.000851	7.57	**0.015***	Significant
$V_c * a_p$	1	0.000128	0.000128	1.14	0.302	
$V_c * T$	1	0.001155	0.001155	10.28	**0.006***	Significant
$f * a_p$	1	0.000250	0.000250	2.23	0.156	
$f * T$	1	0.000801	0.000801	7.13	**0.017***	Significant
$a_p * T$	1	0.000483	0.000483	4.30	0.056	
Residual	15	0.001685	0.000112			
Total	29	0.031898				

Table 5.7 Analysis of variance (ANOVA) for the surface roughness

Source	DoF	SS	MS	*F*-Value	*P*-Value	Remarks
Model	14	0.847618	0.060544	6.68	0	
V_c	1	0.589081	0.589081	64.97	**0.000***	Significant
f	1	0.005392	0.005392	0.59	0.453	
a_p	1	0.001298	0.001298	0.14	0.710	
T	1	0.010754	0.010754	1.19	0.293	
Vc^2	1	0.048623	0.048623	5.36	**0.035***	Significant
f^2	1	0.001132	0.001132	0.12	0.729	
a_p^2	1	0.008831	0.008831	0.97	0.339	
T^2	1	0.001738	0.001738	0.19	0.668	
$V_c * f$	1	0.007906	0.007906	0.87	0.365	
$V_c * a_p$	1	0.002829	0.002829	0.31	0.585	
$V_c * T$	1	0.046114	0.046114	5.09	**0.039***	Significant
$f * a_p$	1	0.026176	0.026176	2.89	0.110	
$f * T$	1	0.000607	0.000607	0.07	0.799	
$a_p * T$	1	0.005979	0.005979	0.66	0.429	
Residual	15	0.001685	0.000112			
Total	29	0.983626				

Similarly, cutting speed, square of cutting speed and product of speed and temperature was affecting the surface roughness. The final quadratic models of response equation in terms of coded factors for flank wear and surface roughness are presented as follows in Eq. (5-1) and Eq. (5-2) respectively.

$$Flank\ Wear = 0.22694+0.02120X_1+0.00597X_2+0.01158X_3+0.00676X_4-0.00889\ X_1^2+0.02811\ X_2^2+0.00911\ X_3^2+0.01861\ X_4^2+0.00765\ X_1\ X_2+0.00297\ X_1\ X_3+0.00921\ X_1\ X_4-0.00415\ X_2\ X_3-0.00767\ X_2\ X_4-0.00596\ X_3\ X_4 \quad (5\text{-}1)$$

$$Surface\ Roughness = 2.4243-0.18889\ V_c+0.0181\ f+0.0089\ a_p+0.0263\ T+0.1371\ Vc^2-0.0209\ f^2-0.0584\ a_p^2-0.0259\ T^2-0.0233\ V_c*\ f+0.0140\ V_c*\ a_p-0.0582\ V_c*\ T+0.0425\ f*\ a_p-0.0067\ f*\ T-0.0209\ a_p*T \quad (5\text{-}2)$$

The final quadratic models of response equation in terms of uncoded factors for flank wear and surface roughness are presented as follows Eq. (5-3), Eq. (5-4) respectively.

$$Flank\ wear = 0.860 + 0.00028\ Vc - 11.05\ f - 0.0089\ a_p - 0.000020\ T - 0.000010\ Vc*Vc + 45.0\ f*f + 0.0365\ a_p*a_p + 0.000000\ T*T + 0.01020\ Vc*f + 0.000198\ Vc*a_p + 0.000001\ Vc*T - 0.332\ f*a_p - 0.001076\ f*T - 0.000042\ a_p*T \quad (5\text{-}3)$$

$$Surfaceroughness=2.67\ 0.0225\ Vc+ 8.2\ f+ 0.042\ a_p+ 0.001034\ T+ 0.000152\ Vc*Vc\ 33.5\ f*f\ 0.234\ a_p*a_p 0.000000\ T*T\ 0.0311\ Vc*f+ 0.00093\ Vc*a_p\ 0.000007\ Vc*T+ 3.40\ f*a_p - 0.00094\ f*T - 0.000147\ a_p*T \quad (5\text{-}4)$$

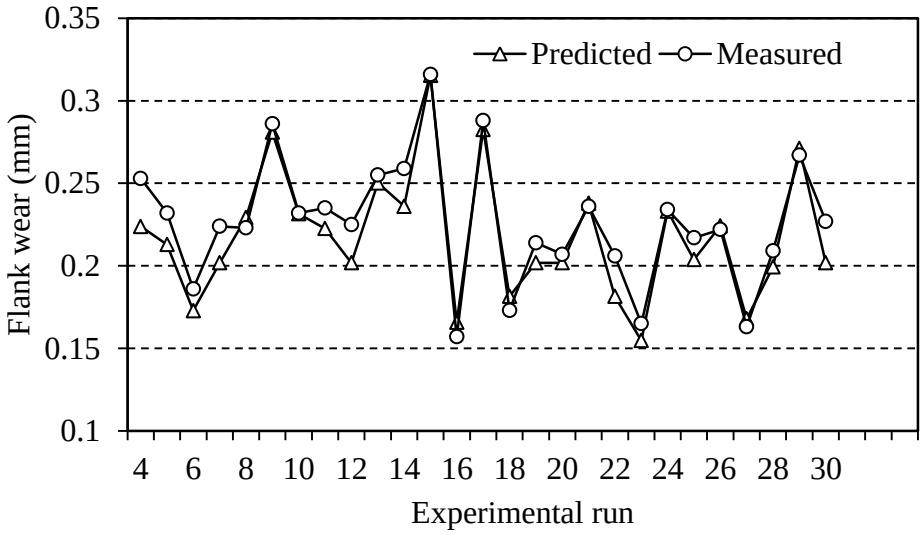

(a)

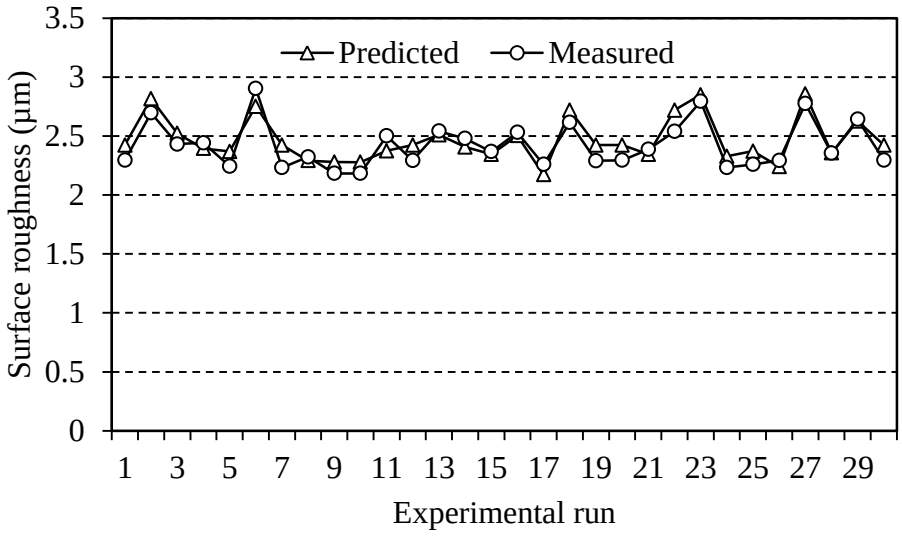

(b)

Figure 5.19 Comparison between measured and predicted value for (a) Flank wear (b) Surface roughness

The comparison between the measured and predicted value for flank wear and surface roughness is shown in Fig. 5.19 (a-b) respectively. It was observed that, an average error 4% for flank wear and 2% for surface roughness was observed between the predicted and experimental results. In order to better understand the interaction effect of machining parameters on responses, surface plots and corresponding contour plots were created. Surface and contour plots have been plotted to analyze the influence of hot turning parameters on surface roughness and flank wear as shown in Fig. 5.20 (a-b) and Fig.5.21 (a-b) respectively.

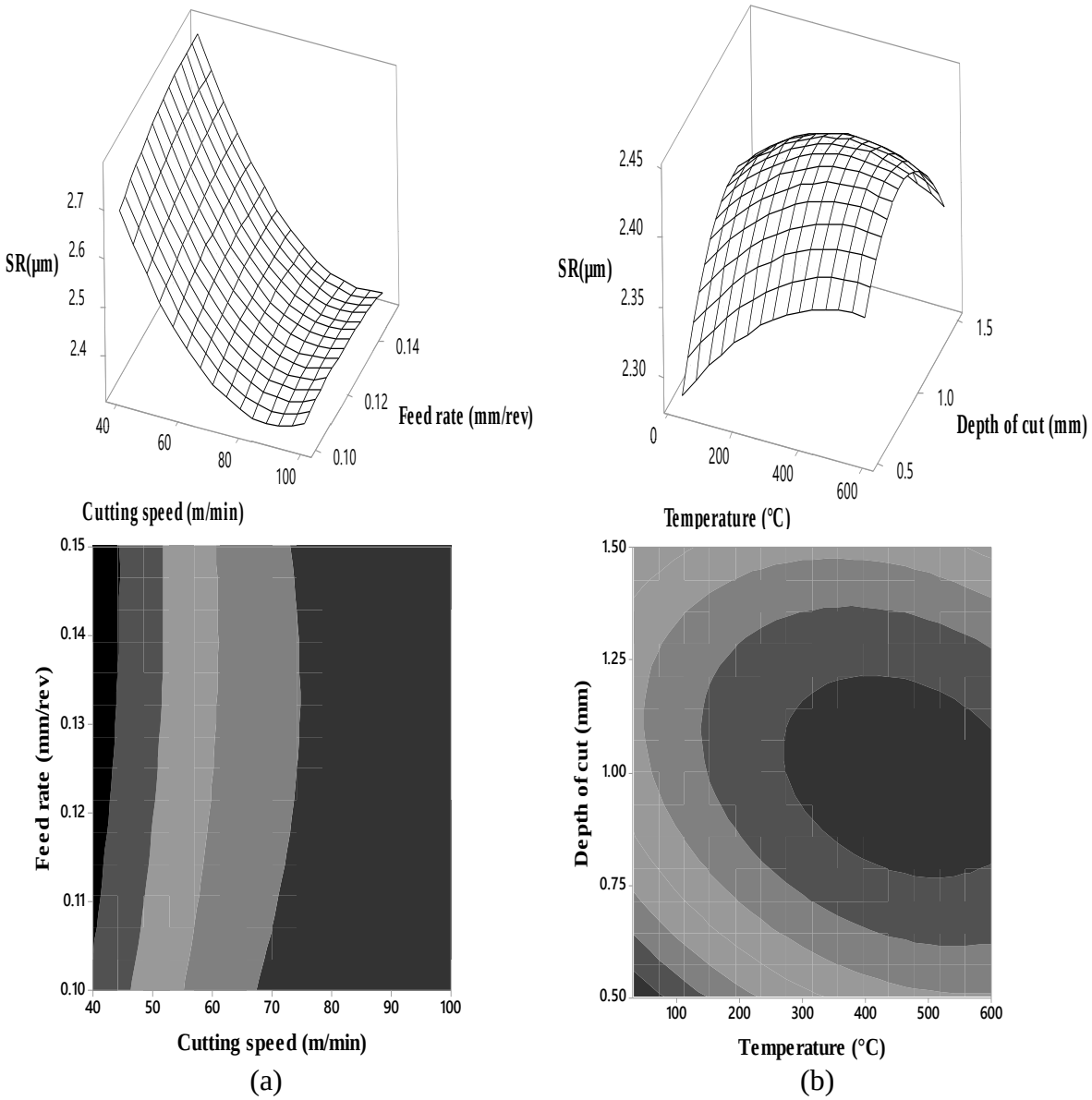

(a) (b)

Figure 5.20 Surface and contour plot for surface roughness with respect to (a) Cutting speed and feed (b) Temperature and depth of cut

Response graph shows that with the increase of temperature, depth of cut and feed rate the surface roughness value increases. While, with increase of cutting speed surface roughness reduces. Similarly, the flank wear increased with the increase of cutting speed, depth of cut, but with the increase of feed rate and temperature up to certain value it decreased initially then increased.

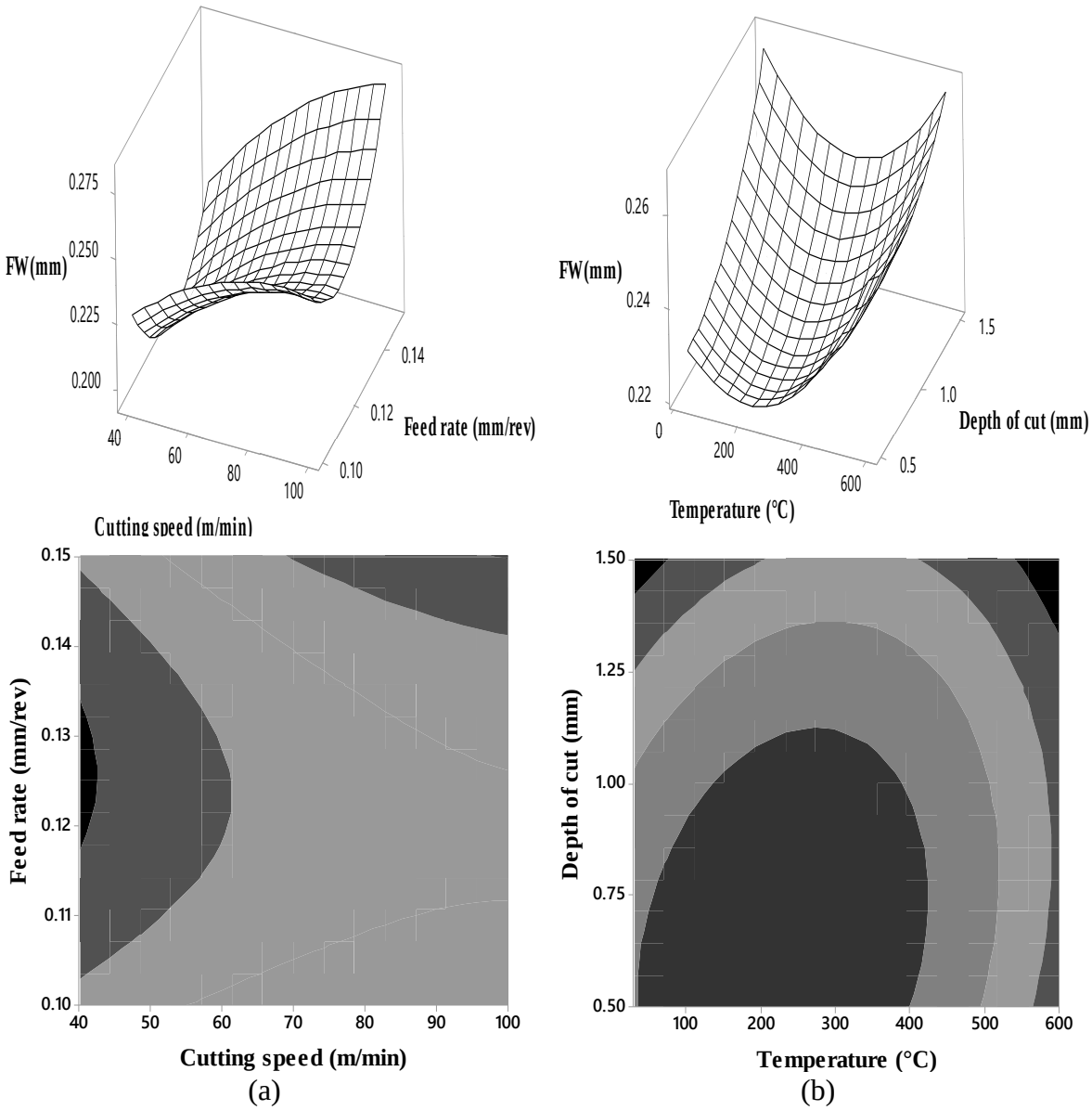

Figure 5.21 Surface and contour plot for flank wear with respect to (a) Cutting speed and feed rate (b) Temperature and depth of cut

The mathematical models of flank wear and surface roughness obtained from the surface response methodology technique in the hot turning of Monel 400 have been discussed in this article. Temperature is the most significant factor which affects flank wear, whereas cutting speed is the significant factor influencing the surface roughness. The predicted results agree with the experimental results. An average error of 4% for flank wear and 2% for surface roughness was observed between the predicted and experimental results respectively.

5.4 Optimization of hot turning of Monel 400 using principal component analysis, desirability function analysis, and taguchi's method

5.4.1 Introduction

In this section, the optimizations were carried out with same input parameters as taken for Inconel 718 and Inconel 625 for machining. Material removal rate, power, and flank wear were chosen as responses in machining Monel 400 and tabulated in Table 5.8. It was observed that, temperature was the most significant parameter which was affecting the responses followed by the depth of cut, feed and cutting speed.

5.4.2 Principal component analysis

The responses are initially normalized according criterion. In this case, the material removal rate was considered for higher the better, and power and flank wear were chosen for lower the better criteria and tabulated in Table 5.9. The eigen values and eigen vectors were calculated (Eq. 3-12) and tabulated in Table 5.10.

Table 5.8 Design table and obtained responses

Run order	Speed (m/min)	Feed rate (mm/rev)	Depth of Cut (mm)	Temperature (°C)	MRR (mm^3/min)	Power (W)	Flank wear (mm)
1	40	0.1	0.5	30	2000	566	0.365
2	40	0.13	1	300	5200	536	0.289
3	40	0.15	1.5	600	9000	579	0.212
4	60	0.1	1	600	6000	647	0.238
5	60	0.13	1.5	30	11700	638	0.275
6	60	0.15	0.5	300	4500	643	0.301
7	100	0.1	1.5	300	15000	701	0.21
8	100	0.13	0.5	600	6500	719	0.203
9	100	0.15	1	30	15000	698	0.236

Table 5.9 Calculation of normalized data

Run Order	MRR	Power	Flank wear
1	0.6	0.836065574	0
2	0.17333	1	0.49032258
3	1	0.765027322	0.98709677
4	0.06667	0.393442623	0.81935484
5	0.64	0.442622951	0.58064516
6	0.26667	0.415300546	0.41290323
7	0.2	0.098360656	1
8	0	0	1.04516129
9	0.2	0.114754098	0.83225806

Table 5.10 Eigen value and eigen vectors of the covariance matrix

Eigen value	2.1991	0.4320	0.3688
Eigen vector	0.573	0.688	0.445
	-0.572	0.725	-0.384
	0.587	0.034	-0.809
Proportion	0.733	0.144	0.123
Cumulative	0.733	0.877	1

Table 5.11 Principal components in all L_9 OA experimental observations

Run	Principal 1	Principal 2	Principal 3
1	0.478232	0.606151	-0.32105
2	-0.15557	0.910305	-0.654
3	0.425328	1.113098	-0.81821
4	0.411438	0.52359	-0.64837
5	0.500481	0.853142	-0.28738
6	0.100986	0.446832	-0.84794
7	1.078374	0.791842	-0.36681
8	0.785346	0.272154	-0.65496
9	0.974791	0.798268	-0.24327

Table 5.12 Multiple performance characteristics of index (MPCI)

Expt. Run	MPCI	SN ratio
1	0.146	-16.7042
2	0.608	-4.32369
3	0.173	-15.2353
4	0.247	-12.137
5	0.090	-20.9026
6	0.510	-5.84148
7	0.315	-10.0374
8	0.010	-39.8288
9	0.255	-11.8672

Table 5.13 Response table for signal to noise ratio

Level	Cutting speed	Feed rate	Depth of cut	Temperature
1	-10.952	-12.960	-20.792	-16.491
2	-12.960	-21.685	-8.968	-6.937
3	-20.578	-10.122	-15.392	-22.400
Max-Min	9.6262	11.563	11.823	15.464
Rank	4	3	2	1

From the Fig.5.22, it shows that the optimization of machining parameters lies at cutting speed 40 m/min, feed rate 0.15 mm/rev, depth of cut 1 mm and temperature at 300°C to maximize the MRR, and to minimize the power and flank wear.

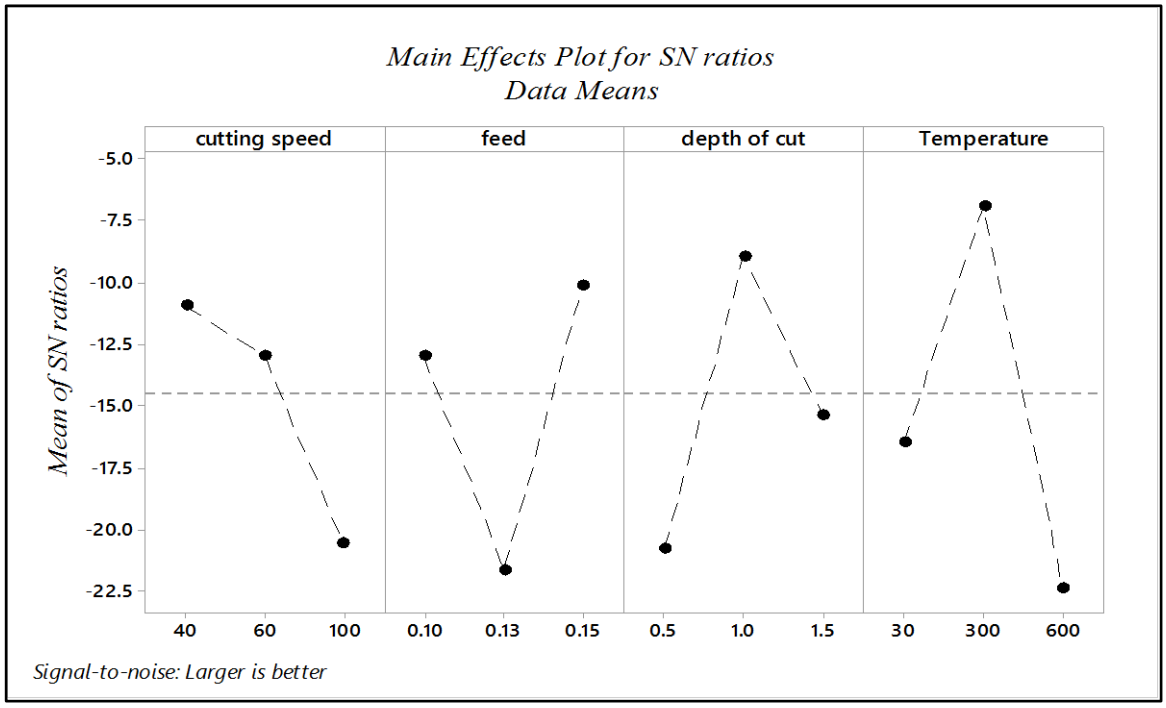

Figure 5.22 Main effect plot for SN ratio

5.5 Optimization of machining parameters using desirability analysis

The assigned weight to responses will be such that sum of weight will one. The individual and composite desirability are shown in Table 5.14. In this case, the material removal rate, power, and flank wear are assigned weighted value of 0.3, 0.4 and 0.3 respectively. The highest value of composite desirability is the close to optimal value. The composite desirability index vs experimental run is shown in Fig. 5.23.The optimal combination of hot turning of Monel 400 lies at 40 m/min cutting speed; 0.15 mm/rev feed rate, temperature (600°C) and 1.5 mm depth of cut.

In order to check the adequacy and acceptability of the proposed above two optimization methodology, a confirmation test has been performed and best result obtained is considered as best optimal setting for machining operation as tabulated in Table 5.15. The best result for MRR was obtained using DFA, whereas for power and flank wear the optimal setting for this machining operation was obtained using PCA.

Table 5.14 Calculation of individual and composite desirability index

Expt. Run	Individual desirability Index (d_i) MRR	Power	Flank wear	Composite desirability d_G
1	0	0.836066	0	0
2	0.246154	1	0.469136	0.454
3	0.538462	0.765027	0.944444	**0.780**
4	0.307692	0.393443	0.783951	0.438
5	0.746154	0.442623	0.555556	0.583
6	0.192308	0.415301	0.395062	0.3
7	1	0.098361	0.95679	0.492
8	0.346154	0	1	0
9	1	0.114754	0.796296	0.487

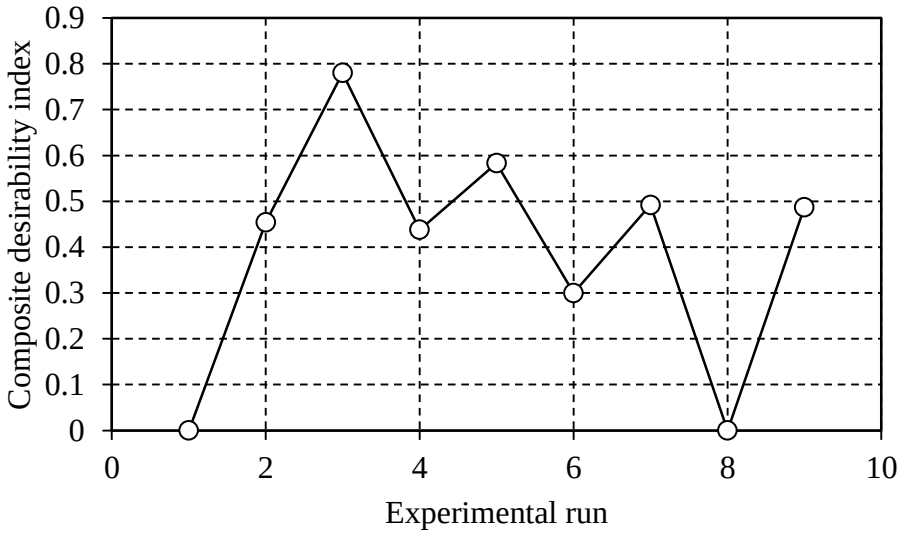

Figure 5.23Composite desirability index vs Experimental run

Table 5.15 Comparison of obtained results between two optimization techniques

Method	*Vc*	*f*	a_p	*T*	*MRR*	*Power*	*Flank wear*
PCA	40	0.15	1	300	6000	557	0.210
DFA	40	0.15	1.5	600	9000	579	0.212

5.6 Conclusion

In this chapter, hot machining of another nickel base alloy i.e. Monel 400 wasused to study the machinability criteria such as tool life, forces, surface roughness, tool wear, and chip morphology etc. The experimental trials were carried out at varying cutting speed, feed rate, depth of cut and different workpiece temperature and results obtained were compared with the room temperature conditions. Response surface methodology has been used to predict the experimental data such as flank wear and surface roughness. Principal component and desirability function analysis have been used to optimize the machining parameters to achieve multi-response criteria. Following conclusions was derived from this chapter.

- There was a reduction of 29%, 45% and 55% cutting, feed, and radial force at heated conditions (600°C) compared to room temperature.
- There was an 50% improvement of surface finish and 107% of tool life in hot machining (600°C) compared to room temperature conditions.
- Increase of chip tool contact length and decrease of chip thickness was observed with the increase of workpiece temperature.
- The predicted flank wear and surface roughness using surface response methodology was a good correlation with the experimental results. An average error of 4% and 2% for flank wear and surface roughness was observed between the predicted and experimental results.
- The optimal settings were obtained by cutting speed 40m/min, feed 0.15 mm/rev, depth of cut 1.5 mm and temperature at 600°C using principal component analysis to minimize the power and flank wear and maximize the material removal rate.

Chapter 6

Finite Element Modeling in Machining Process

6.1 Introduction

FE Modeling is a tool to analyse the machining process for determining different machinability criteria for given set of process variables. It is possible to draw important conclusions about the machining process to achieve better machinability criteria from the modeling. A number of investigations have carried out FEM modeling for different types of heat assisted machining processes.

Zaeh et al. [157] simulated laser assisted machining of two different materials. They observed that titanium machined better in LAM compared to steel. Numerical and experimental investigation of laser assisted machining of high strength materials were studied by [139,158,159] using DEFORM software. With the help of heating, there was reduction in force, stress and increase the process zone temperature. They used heat exchange window to define heat exchange in the local area, which was available in the software. Muhammad et al. [160] studied finite element analysis of forces in the drilling of titanium alloys at elevated temperature using FEM software. FE simulations for conventional drilling and hot drilling was performed and found that cutting forces and torque were reduced in hot drilling as compared to conventional drilling. Numerical modeling of vibration-assisted turning of Ti-base alloys was reported [100,161] using MSC Marc/Mentat. Duan et al. [162] investigated the cutting temperature field of machining of hardened steel using FEM based ABAQUS software and observed, the highest tool tip temperature was located at a certain distance from the tip and simulation results were partially validated with the experiment. Mottaghizadeh and Bagheri [163] studied 3D modeling of temperature by finite element modeling in machining using ABAQUS. It was observed that cutting speed and feed rate were more effective parameters compared to the depth of cut that influenced the tool temperature distribution. Woon and Rahman [164] used finite element simulation to study the effect of edge radius on chip formation, shear stress distribution, and effective rake angle in micromachining of

AISI 4340 steel using different cutting tool edge radius. Lotfi et al. [148] studied the wear mechanism of nickel base alloys using two different cutting tool in finite element analysis. The effect of cutting depth significantly affecting the tool wear and selection of usui's parameters was necessary for a better result. Ozel et al. [165] discussed the effect of different micro-geometry of PCBN cutting tool on cutting forces, stresses, tool wear on machining of AISI 4340 using finite element analysis. With the variation of the microgeometry, the tool wears depth and predicted wear depth rate were decreased. Ducobu et al. [166] predicted the tool wear of Ti6Al4V using DEFORM software. The flank wear, crater wear, and plastic deformation were the modes of failure during theturning operation. Yen et al. [167] investigated the tool wear modeling in finite element analysis using Usui's model. The predicted data was having some error with the experiment data due to theselection of in appropriate usui's constant. A numerical modeling was reported by Wu et al. [168] in micro turning operation using different cutting edge radius. The cutting force and specific cutting force were greatly affected by the grain size. Higher cutting force and specific cutting energy were obtained on the smaller variation of grain size. Ahn et al. [169] studied the cutting force and specific cutting energy in laser assisted machining using the different cutting parameter. The numerical results revealed that laser assisted machining reduced the cutting force and specific cutting energy compared to room temperature machining process. Pervaiz et al. [170,171] studied DEFORM-2D analysis for energy consumption on machining processes. The obtained cutting forces during simulation were used to determine the power consumption in machining simulation. The cutting energy calculated by multiplying the power and time interval, which was taken carefully as these affected directly the machining energy consumption. It was found that with the increase of cutting force the energy consumption increased but decreased with the increased of feed rate.

In this chapter, experimental and numerical analysis results obtained in conventional and hot turning operation are discussed. Different variables like temperature, cutting forces, stress, in the cutting zone were recorded at various cutting conditions for both room and high temperature. It is very difficult to find out these values experimentally. So finite element modeling was used to different responses. There are many types of FE software for simulation of machining problem. In the present study, DEFORM software was used in 2D and 3D with adaptive remeshing technique to reduce the mesh distortion, when the chip formation took place. FE models were used to determine cutting force, process zone

temperature, stress, chip thickness, tool wear and chip tool contact length in hot machining of Inconel 718.

6.2 Basic Concepts of the FEM

Finite element simulation is preferred in manufacturing industries due to following reasons

- Can solved non-linear problems
- Thermo-mechanical analysis
- Reduce the time and cost

In any finite element methods, certain assumptions are taken. The assumptions are

1) The cutting tool is considered as rigid
2) The workpiece is considered to be homogenous, isotropic, and incompressible solid.
3) The value of friction at tool-chip interface and tool-workpiece interaction taken to be constant

6.2.1 Mesh

The mesh of the workpiece material and tool is significant for the accuracy of the result. Along with the mesh size, number and types of elements used in the mesh are significant during the simulation. For this, the cutting edge of the tool and workpiece are densely meshed. 2D and 3D mesh for tool and workpiece are shown in Fig 6.1. The chip separation in finite element simulation is due to plastic deformation of the initial mesh. In remeshing technique, the initial distorted mesh again remesh in refinement way and the deformation node. The workpiece is modeled as a plastic body with 30,000 elements and the tool is defined as a rigid body with 20,000 elements. In newer mesh improves the accuracy of the result, but only the demerit is that it takes more computational time. Adaptive remeshing of machining simulation is shown in Fig 6.2.

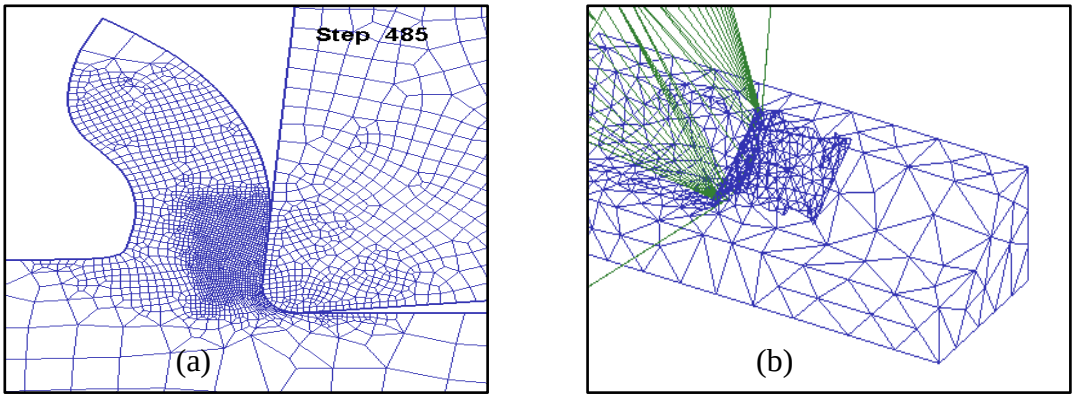

Figure 6.1 Illustration of mesh models for (a) 2D and (b) 3D machining process

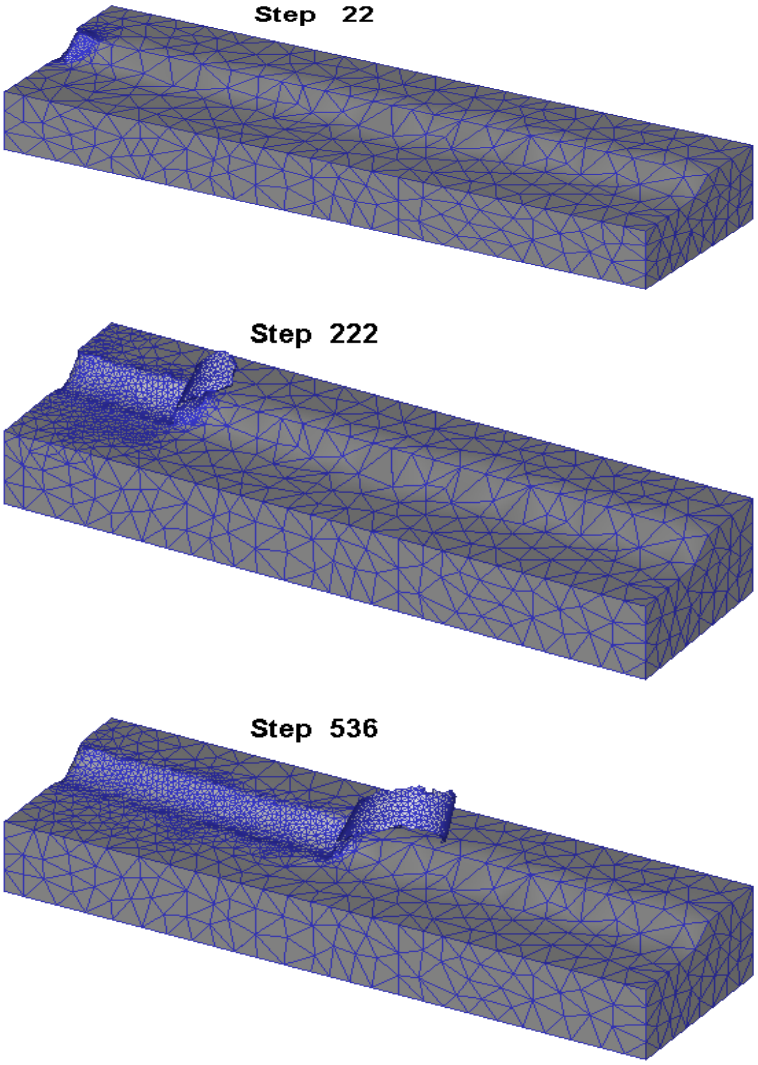

Figure 6.2 Remeshing at different steps

6.2.2 Boundary conditions

Mechanical and thermal boundary conditions have to be coupled in order to account for the thermal process during a large deformation analysis because, in the machining process, dissipation of plastic and frictional work leads to achange of temperature field within tool and workpiece.

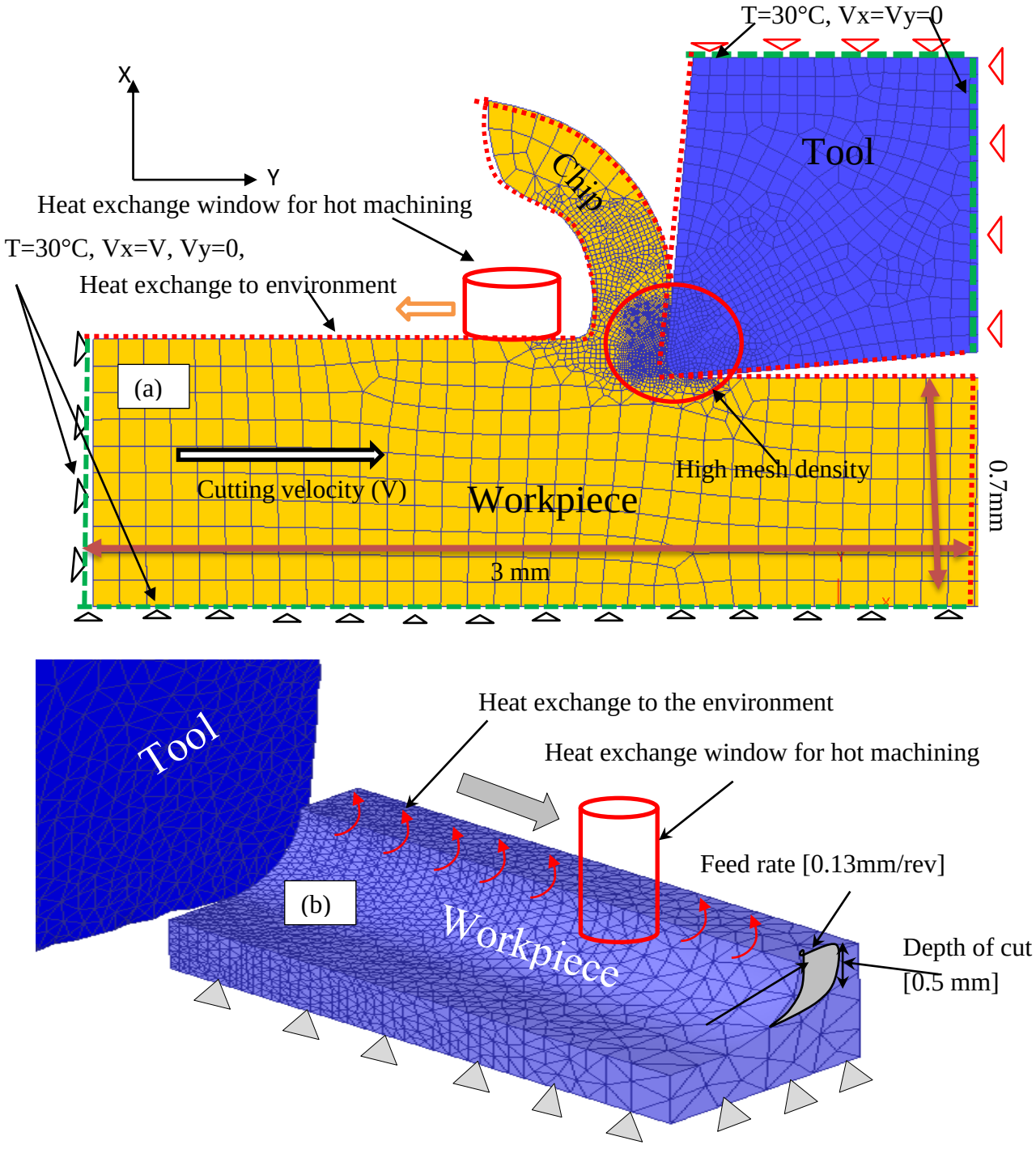

Figure 6.3 Displacement and thermal boundary conditions (a) 2D (b) 3D

The relative movement of thetool and the workpiece and heat generation in theprimary and secondary zone along with boundary condition is shown in Fig 6.3. There are two boundary conditions are given to the workpiece and tool. i.e. Displacement and thermal boundary conditions. Contact boundaries are defined using element edges in 2D and faces in 3D machining simulation.

6.2.3 Modeling of the workpiece material

For accurate result in FEM, the properties of material need to be defined. Mechanical and thermal properties are the main properties need to be defined and other properties can be added like thermal emissivity, hardness, and grain size. The flow stress data of any materials can be determined by using constitutive equation. Strain, strain rate, and temperature are afunction of the flow stress data. Various constitutive models have been modeled for simulation of material behavior in machining simulation. Among of all, the Johnson-Cook model is mostly used by the investigators in thermally assisted machining [55,144,159] and has been used in the present study. The flow stress using Johnson-cook modeling is consisting of three effects. The first term is called strain hardening effect, second is called viscosity effect, and the third term is called thermal softening effect as represented in Eq.(6-2).

$$\sigma = \underbrace{\left(A + B\bar{\varepsilon}^{n}\right)}_{Hardening}\underbrace{\left(1 + C\ln\left(\frac{\dot{\bar{\varepsilon}}}{\dot{\bar{\varepsilon}}_0}\right)\right)}_{Viscosity}\underbrace{\left(1 - \left(\frac{T - T_{room}}{T_{melt} - T_{room}}\right)^{m}\right)}_{Thermal\ softening} \tag{6-2}$$

where σ is flow stress, $\bar{\varepsilon}$, $\dot{\bar{\varepsilon}}$, $\dot{\bar{\varepsilon}}_0$ are the equivalent plastic strain, plastic strain rate and reference equivalent plastic strain rate (s^{-1}). T, T_{melt} and T_{room} are temperature, melting temperature of the material and room temperature (ºC). A, B, C, m and n are the Johnson-cook material constants.

6.2.4 Contact or friction modeling

The accurate and reasonable result in machining simulation depends upon the friction modeling. Tangential force which is generated between two surfaces is consider as friction force. Friction force depends on different aspects, contact geometry, relative motion of the

contact bodies and material properties of the contact surfaces. In metal cutting, friction at chip/tool interface complicated as it depends on variable factors, like cutting speed, feed rate, and tool geometry. So it is necessary to define proper friction characteristics and present study focus on shear friction was considered throughout the simulation.

$$\tau = \mu\sigma_n \tag{6-3}$$

where, τ is the shear stress, μ =0.6 is the friction factor and σ_n is the normal stress.

6.2.5 Fracture modeling

In FEM, the highest damage values were found along the primary shear zone [172–174] and Cockcroft Latham damage model was used for chip separation in the present study, which is the fracture energy represented by the area under the stress strain curve. So, it is necessary to define a fracture or damage criteria. According to chip separation criteria, material falls when the equivalent plastic strain reaches a critical value with the cumulative damage *D* given by Eq. (6-4).

$$D = \sum \frac{\Delta\varepsilon^p}{\varepsilon_f} \tag{6-4}$$

where, $\Delta\varepsilon^p$ the increment of the equivalent plastic is strain and ε_f is the equivalent strain at failure. $\Delta\varepsilon^p$ is updated at every load and ε_f is expressed by in Eq.(6-5).

$$\varepsilon_f = \left[D_1 + D_2 \exp D_3 \left(\frac{p}{\sigma} \right) \right] \left[1 + D_4 \ln \left(\frac{\dot{\varepsilon}^p}{\dot{\varepsilon}_0} \right) \right] \left(1 + D_5 \frac{\theta - \theta_0}{\theta_{melt} - \theta_0} \right) \tag{6-5}$$

where, p/σ is the ratio of the hydrostatic pressure to the equivalent stress.

6.2.6 Usui's tool wear model

This model considers abrasion wear of the tool [148]. In the present study this tool wear model was implemented for calculation of tool wear as shown in Eq. (6-6).

$$w = \int a.p.V.e^{-b/T} dt \tag{6-6}$$

where, *P* is the stress contact surface, *V* is the relative slip velocity, *T* is the absolute temperature of the contact surface and *a, b* is calibration coefficient. In the present study the value of *a* and *b* are taken as $1*10^{-5}$ and 1000 respectively in DEFORM software.

In order to simulate the effect of hot machining, a heat exchange window is available in DEFORM software to define heat exchange in the local area and moves along the workpiece (Fig.6.3). The environment temperature was set at 30ºC, except for a spot (called the nozzle radius), which is kept at the workpiece temperature 600ºC. The total heat input, *Q*, through the window can be defined in Eq.(6-7) [139,175].

$$Q = hA(T_{wd} - T_w) \qquad (6-7)$$

where, *A* is the surface area of heat exchange window, h is the convention coefficient, T_{wd} and T_w are the temperature of the window and workpiece respectively. Within the aforementioned window, both tool and workpiece might exchange heat to the environment. The overall FE modeling is illustrated in Fig. 6.4.

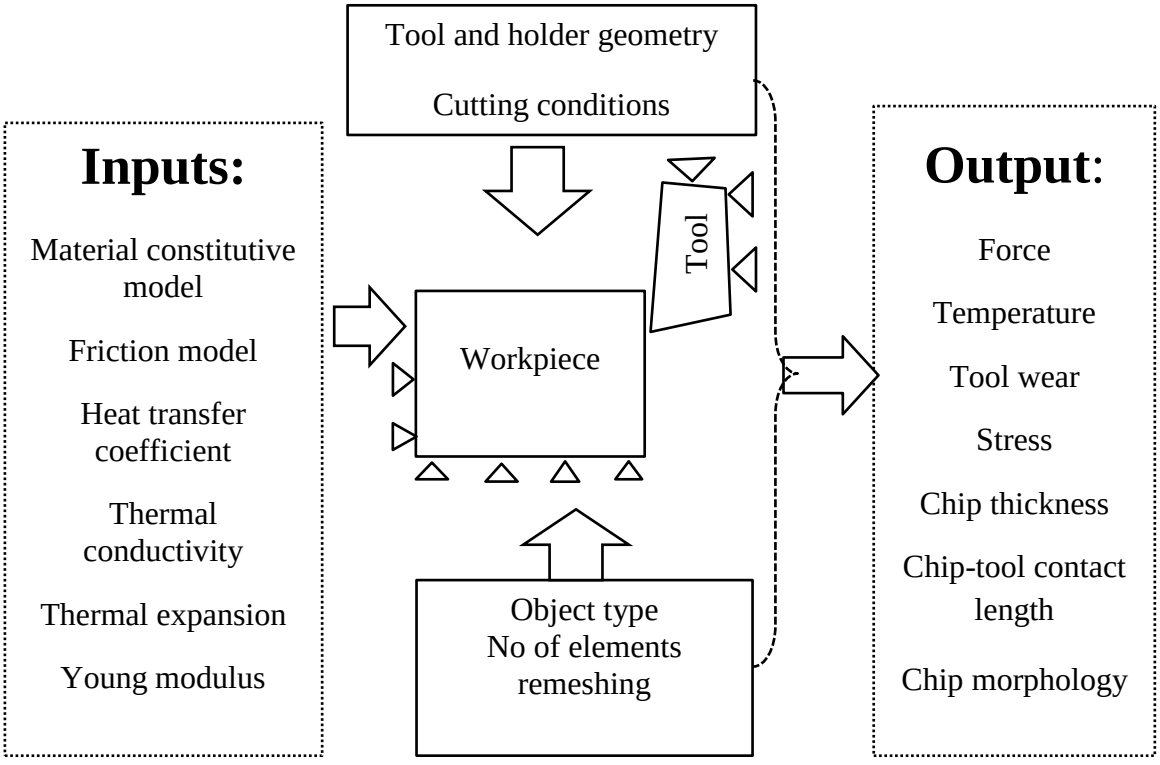

Figure 6.4 Overall machining modeling used in DEFORM software

The number of simulation steps was kept at 10000. The simulations were carried out on core i7 processor, 3 GB RAM computer. For one simulation it takes almost 24 hours to complete. The objectives of this study are as follows

1. To validate the simulation results like cutting force, thrust force, chip temperature, stress and chip shape with the experimental results at different cutting conditions.
2. Study the chip thickness and chip tool contact length
3. Chip morphology and tool wear

6.3 Results and discussion

The simulation results have been evaluated based on the forces, temperature, chip thickness, chip tool contact length, tool wear and chip morphology.

6.3.1 Effect of machining variables on forces at different workpiece temperature

At the initial contact of the tool, the cutting force increased and in this study, the steady state level of forces was considered. With the application of heating on surface of the workpiece, a significant reduction of cutting force was observed. At room temperature, as the cutting tool experiences much stress, so cutting force fluctuates, but after heating the material at 300ºC, cutting force decreased from 428 N to 421 N. As 300ºC is not sufficient to reduce the shear strength of Inconel 718, again temperature of the workpiece increased up to 600ºC, the cutting force decreased significantly from 721 N to 364 N. At room temperature, there was discontinuous or segmented type chip formation, which was sign of fluctuation of cutting and thrust force. When workpiece temperature increased to 600°C, the chip formation became continuous type which is sign of smooth force (No fluctuation). Increase of cutting speed from (40 m/min to 100 m/min), the cutting and thrust force decreased. The comparison between the cutting and thrust forces between simulation and experiment was carried out as shown in Fig 6.6 and good agreement (95% consistency) was noticed. Similarly, simulated cutting force and thrust force with high temperature was performed and compared with the experimental forces as shown in Fig 6.7 (a-b) respectively. There was 95% consistency between the simulated and experimental forces was observed.

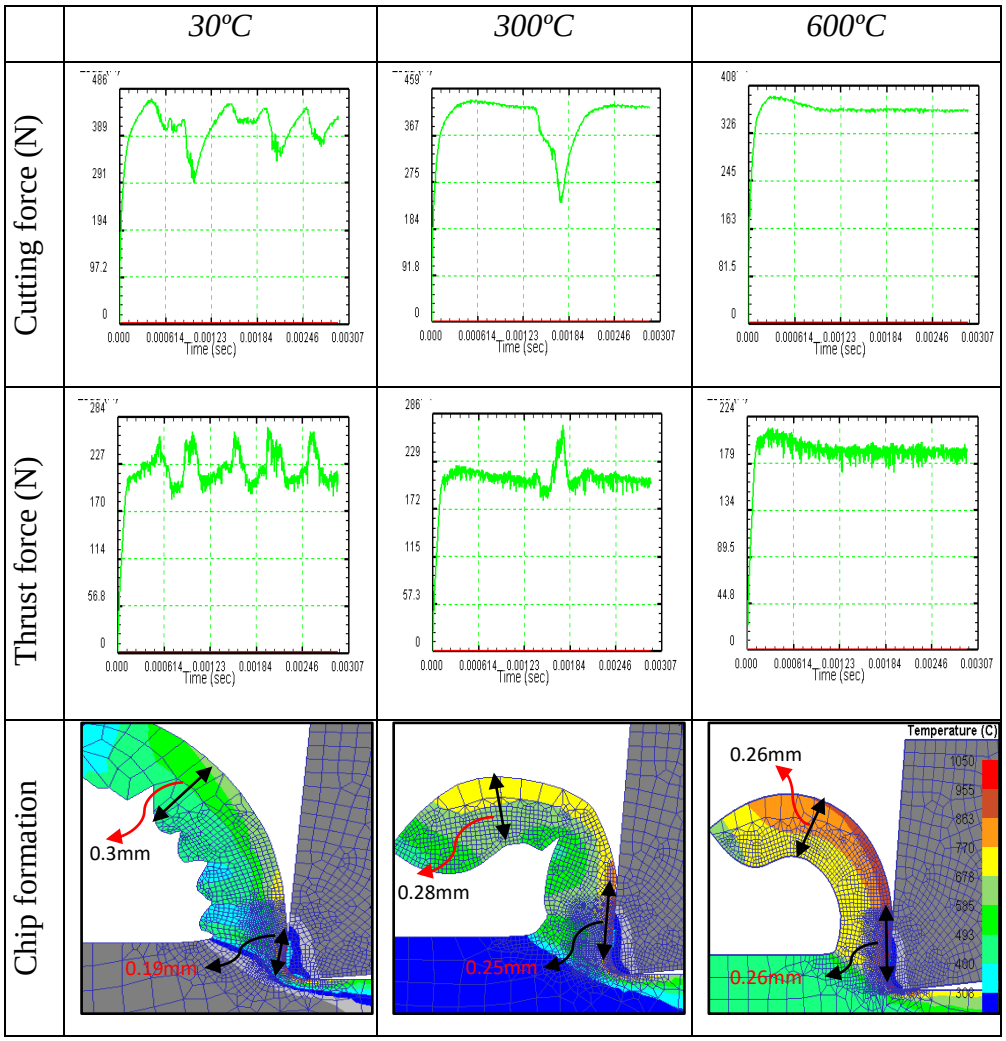

Figure 6.5 Simulated cutting and thrust force and chip formation at *Vc* =100 m/min, *f* = *0.13* mm/rev, a_p = 0.5 mm and at different workpiece temperature

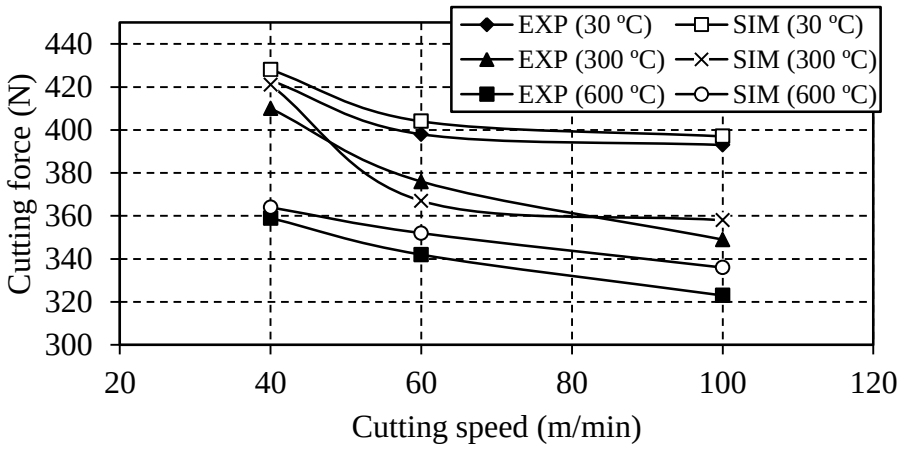

(a)

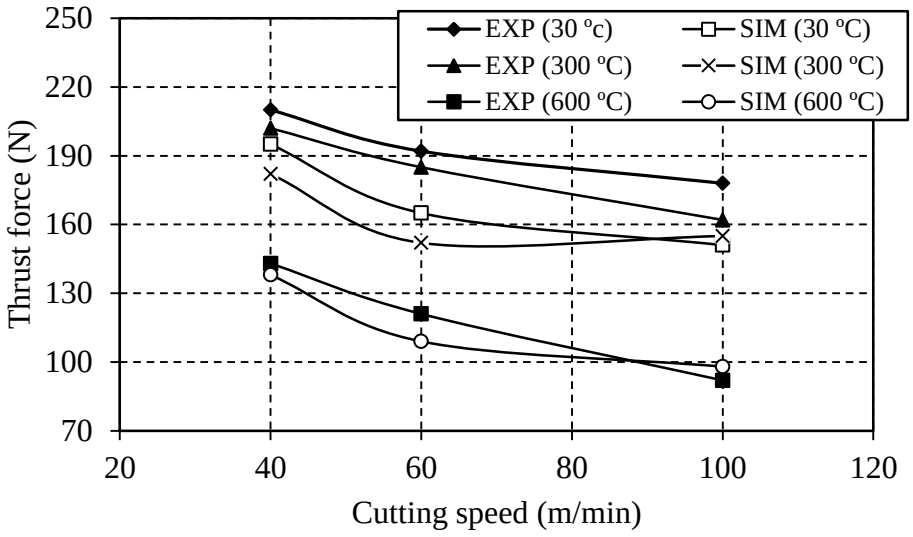

(b)

Figure 6.6 Comparison between the simulated and experimental (a) Cutting force (b) Thrust force with respect cutting speed and workpiece temperature

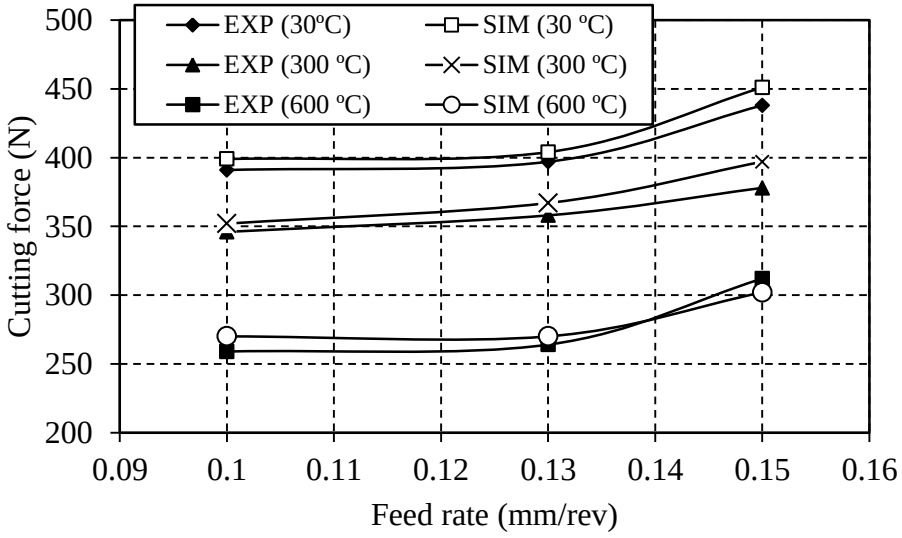

(a)

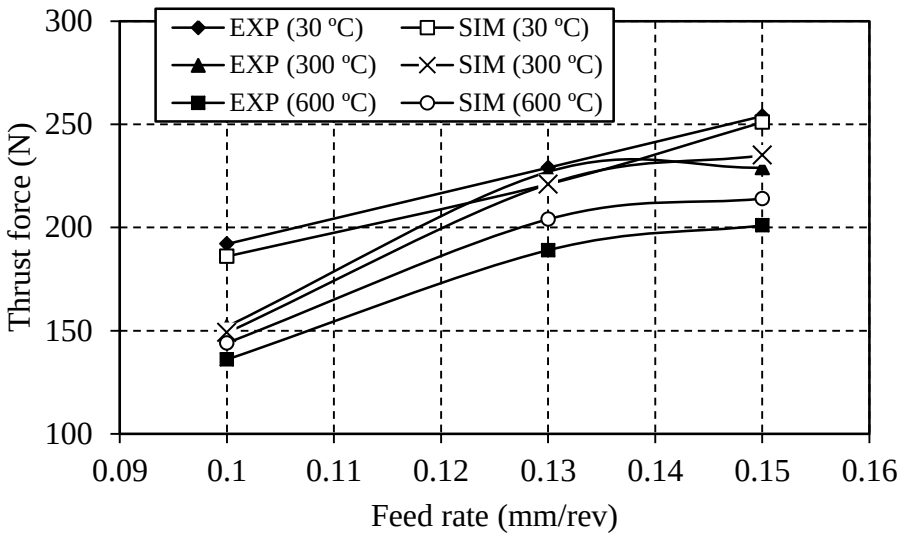

(b)

Figure 6.7 Comparison between experimental and simulated (a) Cutting force (b) Thrust force with respect to feed rate and workpiece temperature

6.3.2 Temperature distribution on the tool, chip and stress distribution on workpiece at different workpiece temperature

It was noted that relatively high temperature in the process zone during hot machining compared to room temperature machining. Due to high process zone temperature at heated conditions, the flow stress of the workpiece reduced compared to room temperature. From Fig. 6.8 (a) it is clearly seen that the maximum process zone temperature at room temperature was 895°C, whereas at 600°C heating temperature, the maximum process zone temperature increased to 1040°C. The increase of process zone temperature also reduced the heat generation due to plastic deformation during machining. It was observed that, effective stress at room temperature reduced from 1690 MPa to 1610 MPa at 600°C (Fig. 6.8 (b)). The decrease in workpiece stress reduces flow stress, tool wear and tool temperature. The tool temperature reduced from 197°C at room temperature to 123°C at 600°C heating temperature (Fig. 6.8 (c)). Fig 6.5 shows how workpiece temperature affects the chip formation mechanism of chip segment. At 30°C, chip segments are formed by fracture and it is in the form of crack propagating over the chip. With the increase of heating, the chip shape changes and formed by the combination of thermal softening and fracture [145]. It shows that temperature distribution in the chip increased with increase of workpiece temperature. At 30°C the chip temperature was 758°C,

whereas increasing the workpiece temperature up to 600°C, the chip temperature increased up to 975°C for 40 m/min cutting speed. The chip temperature was higher when the cutting speed increased from 40 m/min to 100 m/min. At low cutting speed (40 m/min), and in room temperature, the chip temperature was low. The chip temperature was validated with the experiment, where infrared pyrometer was used for temperature measurement of chips. The comparison between the simulated and numerical chip temperature is shown in Fig.6.9.

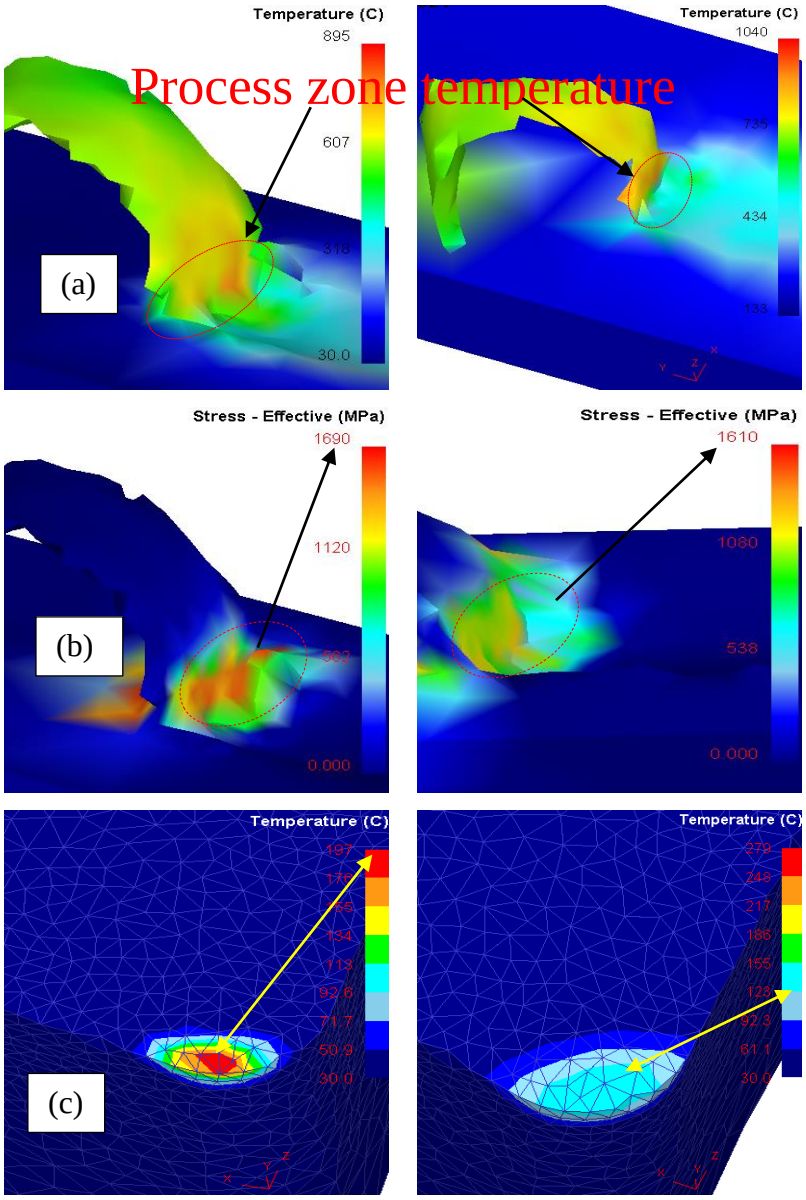

30°C 600°C

Figure 6.8 Temperature distribution at process zone (a) Effective stress at room and heated conditions (b) Temperature distribution on the tool (c)

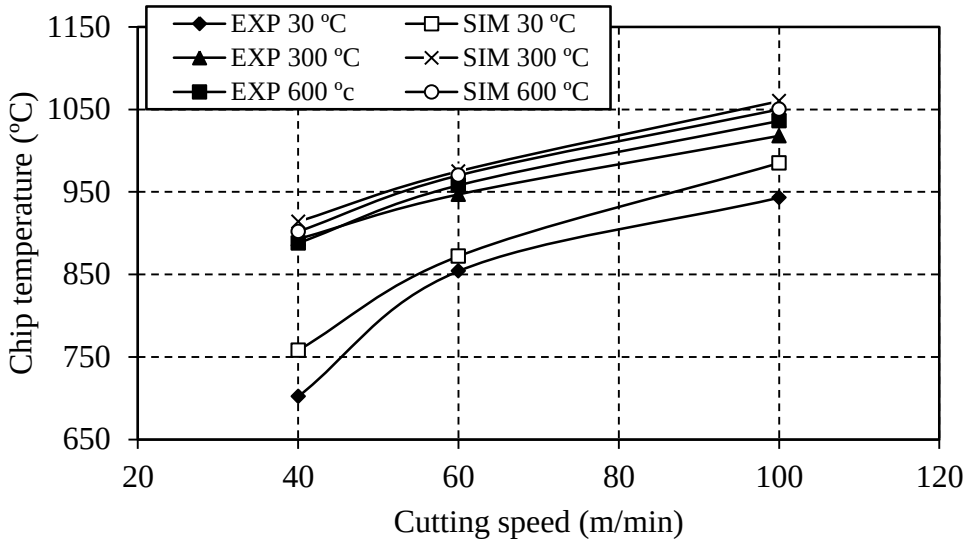

Figure 6.9 Comparison of simulated and experimental chip temperature

6.3.3 Effect of workpiece temperature on Chip morphology and chip tool contact length and tool wear

The variation of chip thickness and chip-tool contact length has been studied numerically. The numerical sample chip thickness and chip-tool contact length obtained has been extracted from the Fig.6.5. Fig. 6.10 shows the 3D simulated chip tool contact length and tool wear. There was positive coherence between simulated and experimental chip tool contact length and tool wear. It was observed that chip thickness decreased and chip tool contact length increased with the increased of workpiece temperature. The simulated chip thickness and chip tool contact length are compared with experimental chip thickness and chip-tool contact length, which were measured by optical microscope and positive coherence between them was found as shown in Fig 6.11 (a-b). It was observed that maximum 11% error in chip thickness and 10% error in chip tool contact length between the experiment and simulation results.

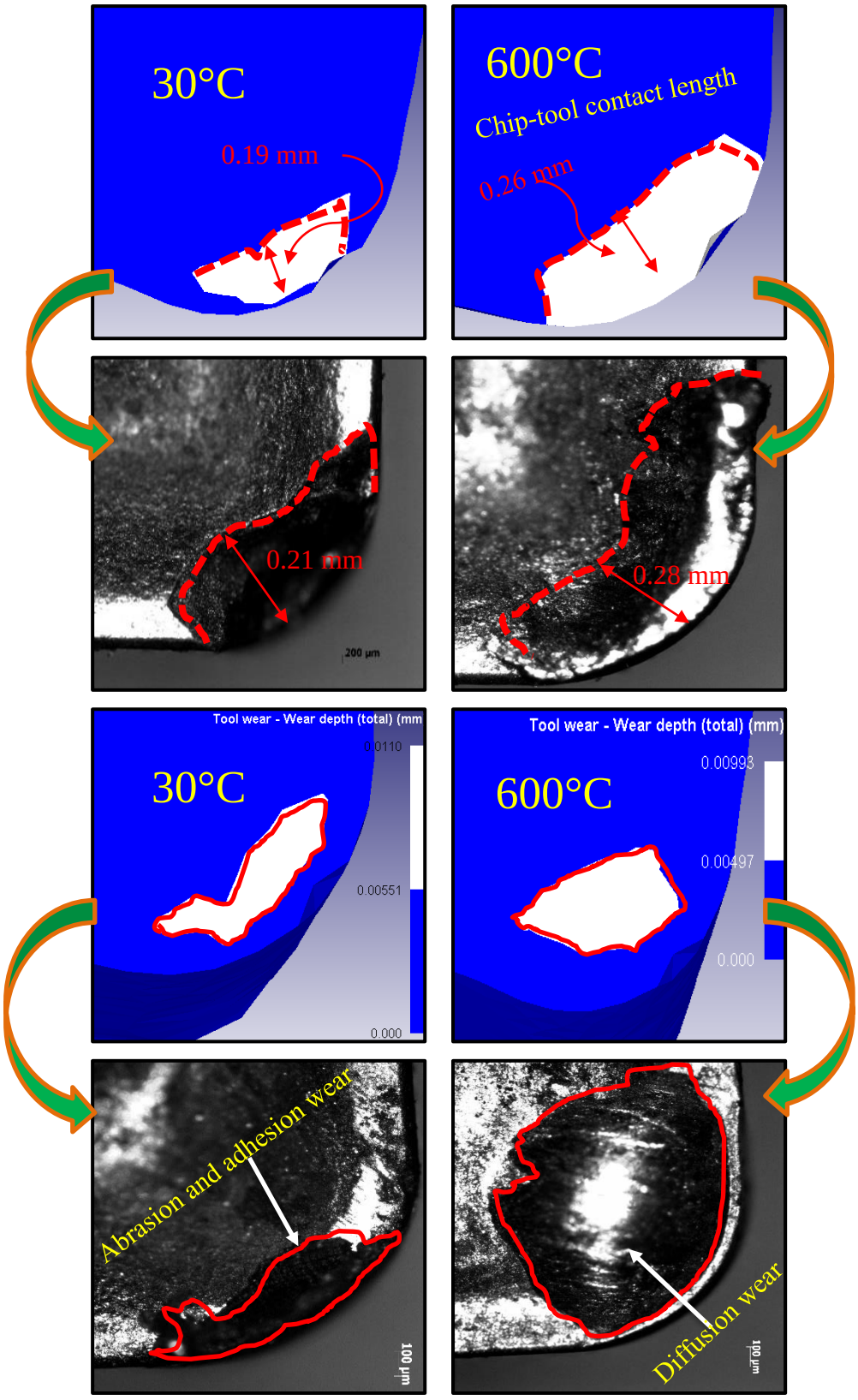

Figure 6.10 Comparison between 3D simulated and experimental chip tool contact length and tool wear in different workpiece temperature at steady state condition

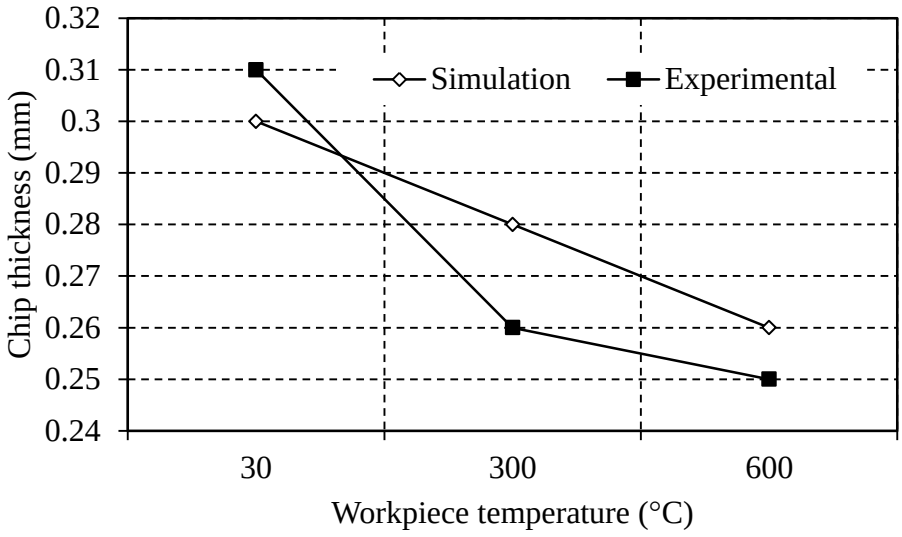

(a)

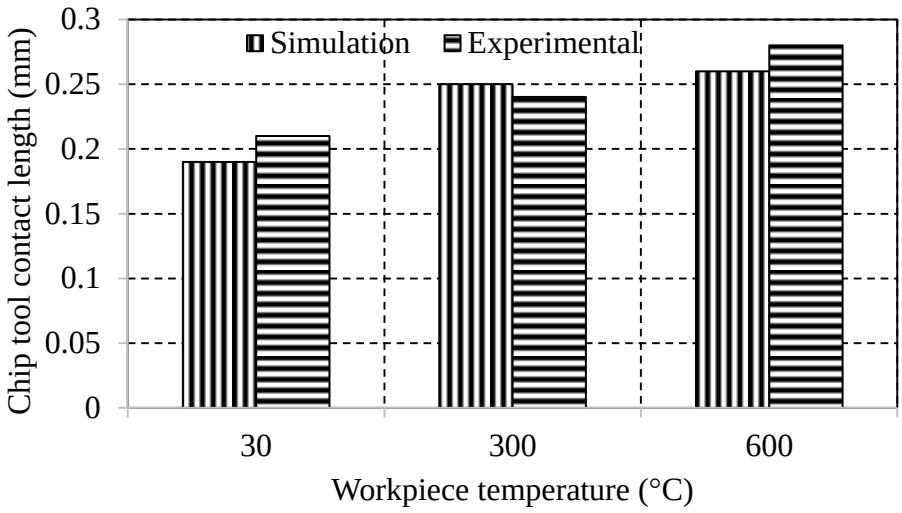

(b)

Figure 6.11 Graphical plot between simulated and experimental (a) Chip thickness (b) Chip-tool contact length at cutting speed 100 m/min, feed rate 0.13 mm/rev and depth of cut 0.5 mm

3D simulation was carried out for better understanding of chip formation at different environment conditions (room and heated conditions). The chip produced in 3D simulation during room temperature was segmented type, whereas increasing the workpiece temperature to 600°C, it became longer and continuous as shown in Fig.6.12. This is due to increase of ductility property of workpiece due to thermal softening.

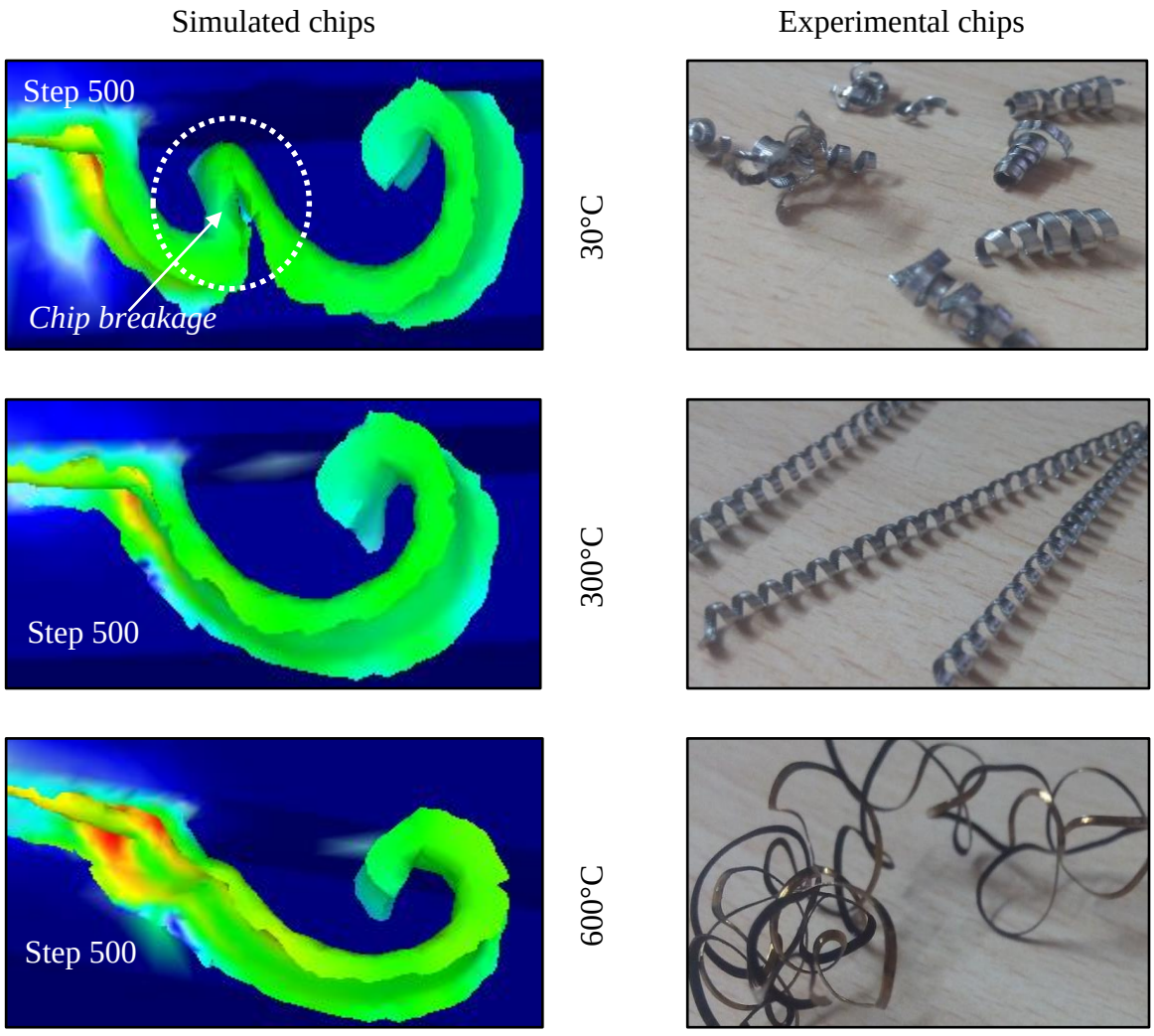

Figure 6.12 Simulated and experimental chip morphologies obtained in room and high temperatureat steady state conditions

6.4 Conclusion

A finite element model was developed to simulate room temperature and hot machining of Inconel 718. The model was used to simulate the cutting process such as cutting force, thrust force, chip thickness and chip tool contact length for various input parameters such as cutting speed, feed rate. The following conclusion can be drawn from this chapter.

- The cutting and thrust force reduced with the increase of workpiece temperature and good agreement with the experimental result. 5-10% of error was observed between simulated and experimental results.

- There was rise in process zone temperature at heated condition, hence reduction of effective stress compared to room temperature conditions.
- The chip temperature increased with the increase of workpiece temperature.
- There was maximum error of 11% and 10% between simulated and experimental chip tool contact length and chip thickness.

Chapter 7

Comparison of Machinability of Inconel 718, 625 and Monel 400 in Hot Turning Operation

7.1 Introduction

In this section, machinability of three nickel base alloys is compared in heated and room temperature conditions. The comparison between the machinability of three materials in terms of tool life, cutting force, feed force, radial force, surface finish, tool wear, chip morphology, chip-tool contact length etc. has been discussed.

7.2 Results and discussion

7.2.1 Effect of workpiece temperature on tool life

The effect of heating on tool life on three materials was given in (Fig 7.1). The tool life of Inconel 718, Inconel 625 and Monel 400 has been compared for different range of temperature. It was observed that the tool life of Inconel 718 was lower in both room and heating conditions, whereas highest tool life was achieved for Inconel 625.

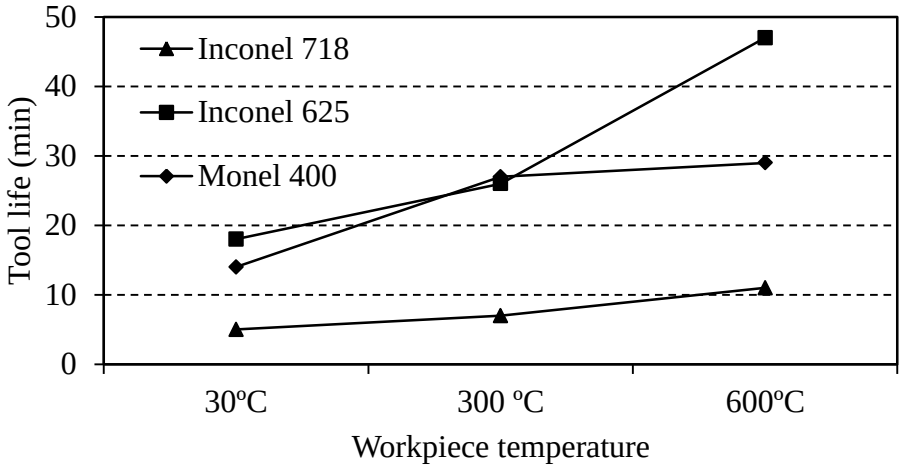

Figure 7.1 Comparisons between the tool life on machining three nickel base alloys with different workpiece temperature at *Vc* = 100 m/min, *f* = 0.13 mm/rev and a_p= 0.5 mm

Machining Inconel 718 enhanced tool life 160% (from 5 min to 13 min), whereas Inconel 625 enhanced 238% (13 min to 44 min) and Monel 400 enhanced 107% (from 14 min to 29 min) tool life at 600°C compared to room temperature machining conditions. The reason behind was, Inconel 718 have lower thermal conductivity and high tensile strength among all three materials.

7.2.2 Effect of workpiece temperature on cutting, feed and radial forces

The variation of cutting, feed and radial force with workpiece temperature was studied for three materials as shown in Fig 7.2 (a-c). Though cutting force is more for Inconel 718 compared to Inconel 625 and Monel 400. There is reduction of 17% (from 393 N to 323 N) for Inconel 718, 29% (from 235 N to 166 N) for Inconel 625 and 26% (from 175 N to 128 N) for Monel 400, when workpiece temperature is heated 600°C compared to room temperature. Similarly, there is reduction of feed force 10% (from 231 N to 166 N), 28% (from 184 N to 132 N) for Inconel 625 and 45% (from 155 N to 85 N) for Monel 400 respectively. Similarly, reduction of the radial force 46% (from 13 N to 7 N), 36% (11N to 7 N) and 55% (from 9 N to 4 N) for Inconel 718 and for Inconel 625 and Monel 400 respectively.

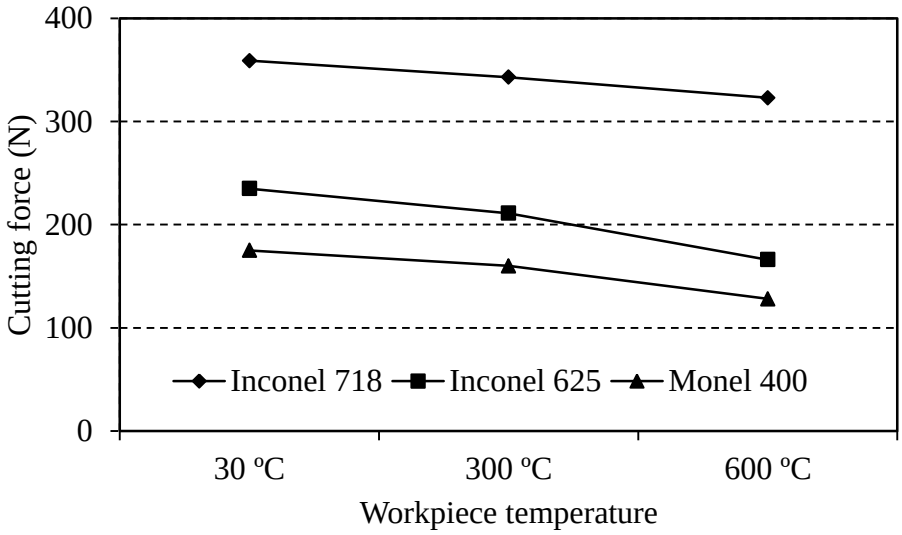

(a)

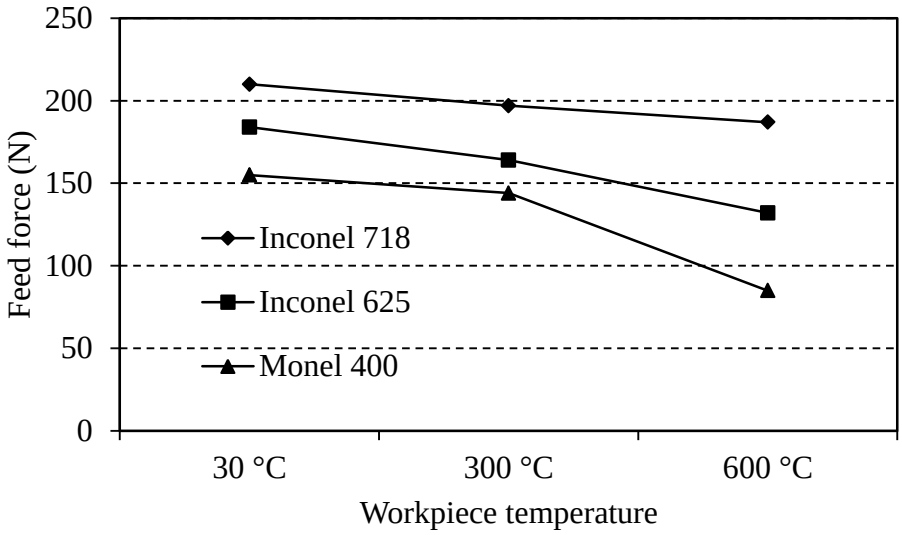

(b)

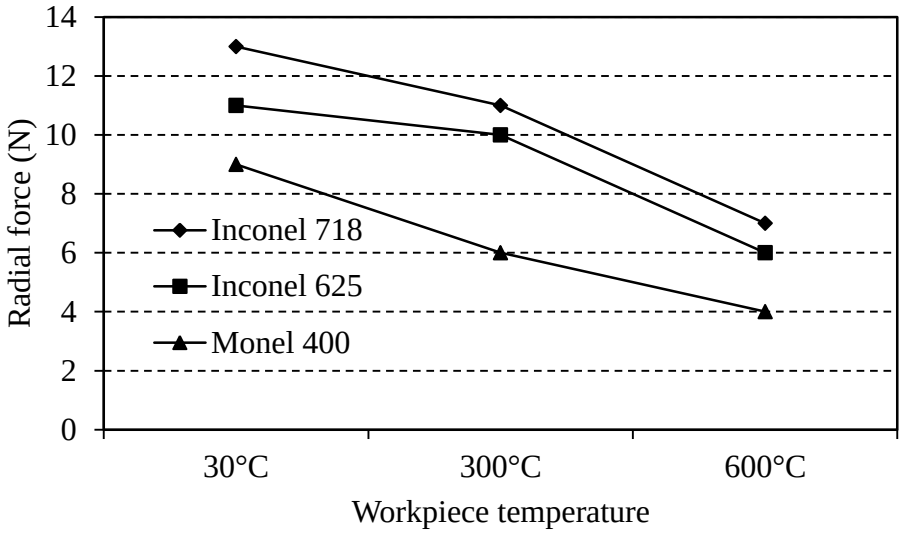

(c)

Figure 7.2 Variation of Cutting force (a) Feed force (b) Radial force (c) in different workpiece materials with respect to workpiece temperature on machining of three nickel base alloys at *Vc* =100 m/min, *f* = 0.13 mm/rev and a_p = 0.5 mm

7.2.3 Effect of heating on surface roughness on three different materials

Referring to Fig 7.3 it is observed that the surface finish of Inconel 625 is better compared to other two materials i.e. Inconel 718 and Monel 400. On machining Inconel 718 at 600°C, the surface roughness reduced 23% (from 1.7 µm to 1.3 µm) compared to room temperature. Similarly, the reduction of surface roughness 42% (from 1.12 to 0.64 µm)

for Inconel 625 and 50% (from 2.2 µm to 1.09 µm) for Monel 400 from room temperature to workpiece temperature of 600ºC.

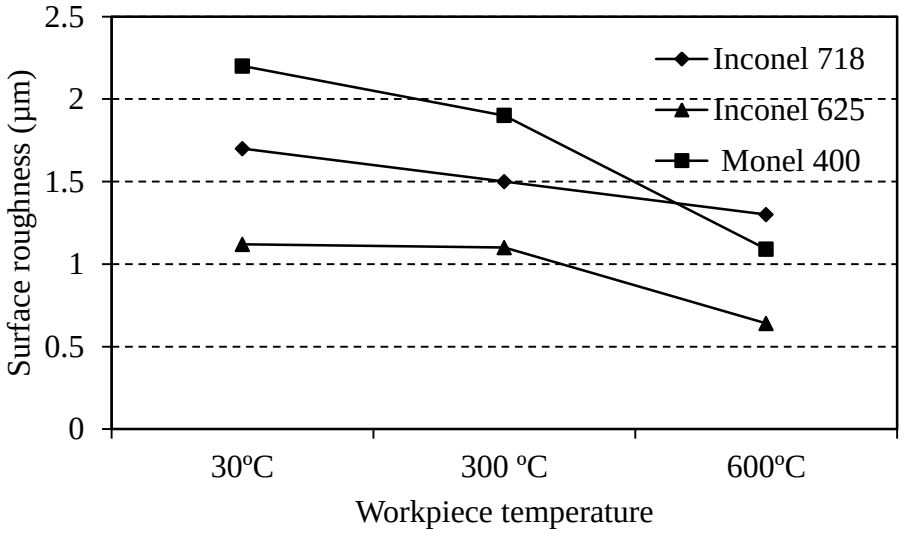

Figure 7.3 Variation of surface roughness on machining three nickel base alloys with different workpiece temperature at Vc = 100 m/min, f = 0.13 mm/rev and a_p = 0.5 mm

7.2.4 Effect of heating on chip morphology

The effect of heating on chip morphology of three materials was studied and shown in Fig 7.4. The chips formed during machining of Inconel 718 was quite continuous and spiral, but bent with a radius of curvature continuous, whereas chip produced on Inconel 625 was spiral form with straight line.

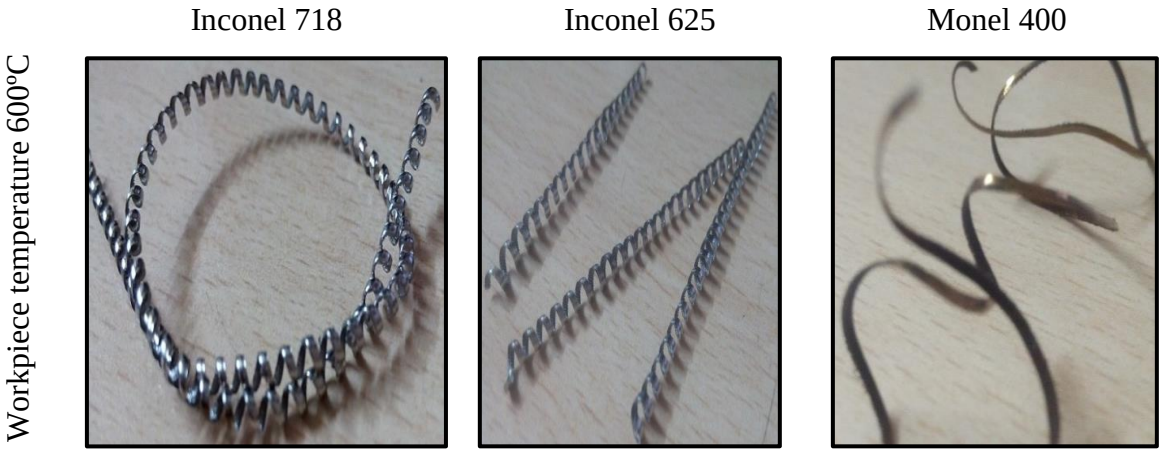

Figure 7.4 Chip formation on different workpiece material at Vc = 100 m/min, f = 0.13 mm/rev and a_p = 0.5 mm

The chips produced from machining of Monel 400 was continuous and not spiral. Thermal conductivity difference and other mechanical properties may affect the formation of chips in three different nickel base alloys along with cutting variables.

7.2.5 Effect of heating on tool wear in three materials

The tool wear formation on the cutting tool during hot machining is shown in Fig 7.5. It was observed that diffusion wear is the main dominant wear mechanism for Inconel 718, whereas for Inconel 625 notch wear and abrasion wear for Monel were the main dominant tool wear mechanism during hot machining at 600°C.

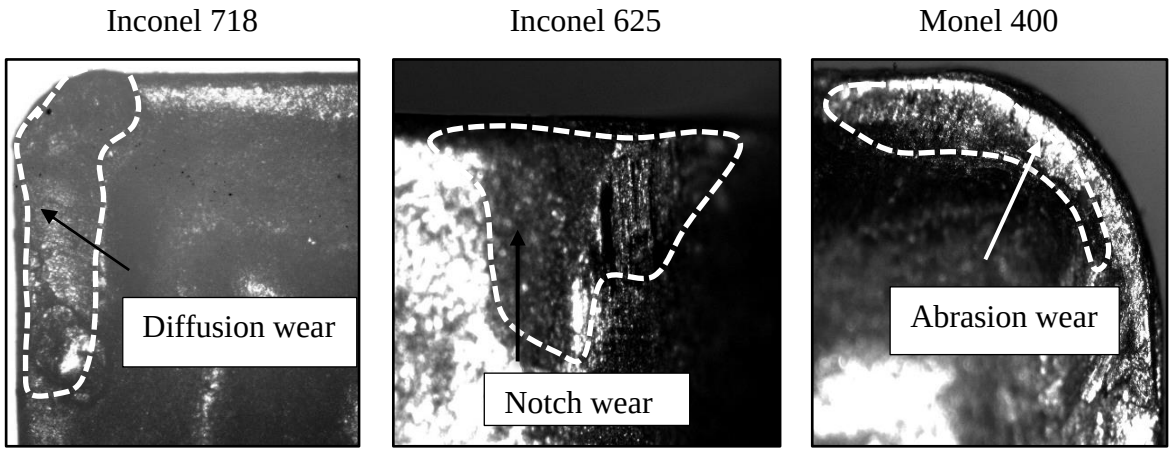

Figure 7.5 Tool wear on machining different materials at Vc = 100 m/min, f = 0.13 mm/rev, a_p = 0.5 mm and T = 600°C

7.2.6 Effect of heating on chip-tool contact length.

The effect of workpiece temperature on chip-tool contact length of three alloys is shown in Fig 7.6. It is clearly observed that chip-tool contact length of Inconel 718 is the lowest in room and high temperature. The lower chip tool contact indicates that normal stress (forces) on the tool is more in machining of Inconel 718 compared to other two materials. Chip-tool contact length increases with increase of temperature of workpiece in all materials.

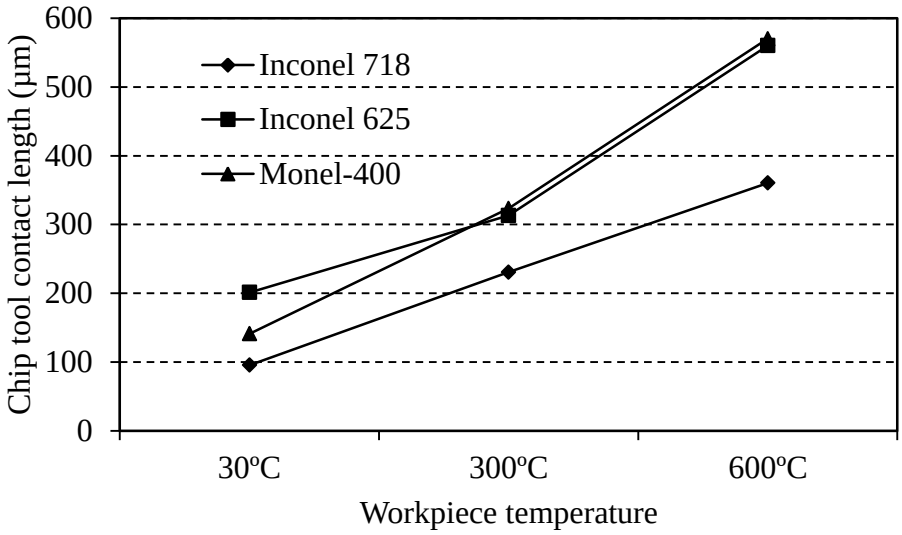

Figure 7.6 Effect of workpiece temperature on chip-tool contact length of three alloys at cutting speed 100 m/min, feed rate 0.13 mm/rev and depth of cut 0.5 mm

7.2.7 Effect of heating on microhardness below the machined surface

In all three materials the microhardness decreased with increase of workpiece temperature due to annealing. But when distance increased, the hardness value increased due to strain hardening and after zone of strain hardening and plastic deformation, the hardness value reduced to base metal hardness. The microhardness value in three materials at 600ºC is shown in Fig 7.7.

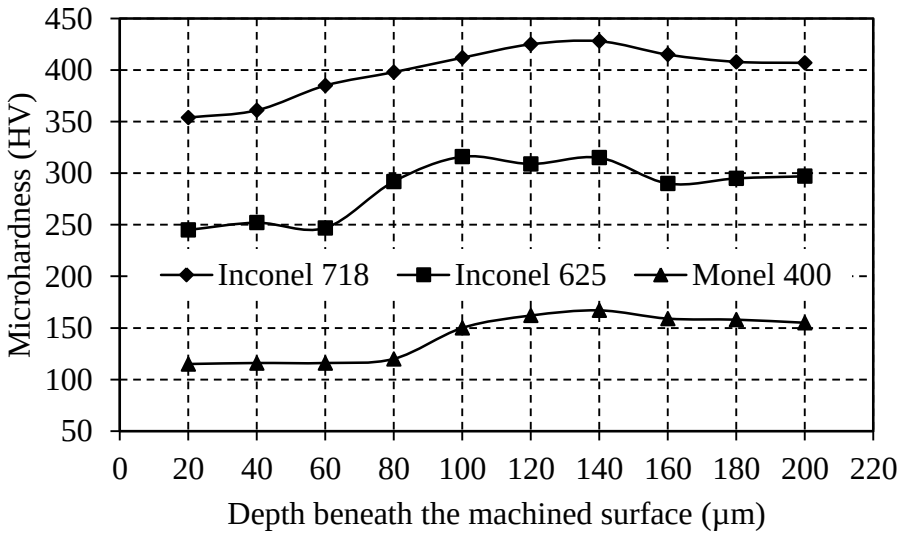

Figure 7.7 Comparison of microhardness values of three materials below the machined surface at Vc = 100 m/min, f = 0.13 mm/rev, a_p = 0.5 mm and T = 600°C

7.3 Conclucsion

In this chapter, comparison of machinability of three nickel base alloy i.e. Inconel 718, Inconel 625 and Monel 400 was presented in hot machining operation. The following conclusion was derived from this chapter.

- Tool life obtained in hot machining (600°C) of Inconel 718 was lowest and best surface finish was achieved compared to other two alloys.
- Higher cutting force was observed in hot machining (600°C) of Inconel 718 compared to Inconel 625 and Monel 400.
- The tool chip contact length value was lowest in machining of Inconel 718 compared to Inconel 625 and Monel 400 at (600°C) heating temperature.
- The wear formed was diffusion wear in hot machining (600°C) of Inconel 718 and Monel 400, whereas there was formation of notch wear in case of Inconel 625.

Chapter 8

Conclusions and Future Work

8.1 Conclusions remarks

The present work was mainly focused on machining of high strength materials like nickel-alloys, such as Inconel 718, Inconel 625 and Monel 400 using hot machining. Due to some inherent properties like high corrosion resistance, ability to withstand atelevated temperature, high wear resistance, and excellent fatigue characteristics, etc. These materials are widely used in turbine, aerospace, nuclear sector etc. Machining nickel base alloys in conventional ways possess a lot of problems due to low thermal conductivity and high chemical reaction to any cutting tools. Hot machining is an alternative technique to machining such materials, where the application of heat is imposed on the surface of the workpiece during or before machining operation. The application of heat reduced the shear strength by increasing the thermal softening in the workpiece surface and reduced tool wear, cutting forces, and improved the material removal rate and surface finish.

Additionally, FEM analysis was carried out for better understanding of chip formation between the experiment and simulation results. Process variables like stress, temperature, chip thickness, chip tool contact length and tool wear etc., have been studied well. Finally, hot machining input parameters was optimized in hot machining using principal component and desirability function analysis. Optimization of machining parameters gives an idea about the optimum combination of process parameters to improve machinability.

8.2 Conclusions

A considerable reduction of forces, tool wear and increase of surface finish, material removal rate was noticed in 600°C workpiece temperature compared to room temperature machining for same cutting conditions in three different nickel base alloys. It was observed that, there was maximum 43% improvement in surface finish and 150% increase in tool life in hot machining of Inconel 718 compared to 30°C machining conditions. Similarly, 40% improvement in surface finish and 209% in tool life for Inconel 625

and 50% improvement of surface finish and 107% increase in tool life for Monel 400 was observed.

The effect of heating on chip formation was analyzed at different cutting speed in machining of Inconel 718. With the increase of heating, the degree of segmentation of chips reduced to 57% compared to room temperature machining at cutting velocity of 100 m/min. Similarly, there was reduction of frequency of serration and chip tooth spacing with the increase of workpiece temperature compared to room temperature. The chip temperature produced during hot machining was higher compared to conventional turning process and the surface roughness reduced with the workpiece temperature in machining all three materials. In machining three materials the chip thickness decreased and chip tool contact length increased with increase of workpiece temperature. Hence, hot machining process resulted in a significant reduction of cutting forces, surface roughness without altering the properties of the machined surface, resulted high material removal rate and tool life compred to room temperature machiing.

FE modeling was carried out with the help of DEFORM software in both room and high temperature of the workpiece. The developed FE models for conventional and hot turning processes have the added advantage of elucidating the temperature characterstics in regions of the workpiece which is not impossible in experiment. A considerable reduction of forces was observed at high temperature 600˚C compared to room temperature with cutting speed, but with an increase of feed rate there was an increase of cutting and thrust force in both room and workpiece temperature. A good prediction of the effect of cutting conditions and workpiece temperature on cutting forces, chip morphology, tool wear,chip tool contact length and chip thickness were observed with the experimental result.

Response surface methodology was used to model the hot machining of three materials. In all case same input parameters and responses (flank wear and surface roughness) were used for analysis. It was observed that the predictive models showed good agreement with the experimental data. An average 4% error for flank wear and 3% for surface roughness were observed between the predicted and measured values in machining of Inconel 718, whereas average 4% error of flank wear and 4% of surface roughness for Inconel 625, and 4% error of flank wear and 2% of surface roughness for Monel 400 were observed.

Optimization methods were used to optimize the machining input parameters in three nickel base alloys. Principal component analysis (PCA) and desirability function analysis,

along with taguchi's method were used to determine the optimal setting for multi-objective optimization techniques. The optimal settings were obtained at 100 m/min cutting speed, 0.1 mm/rev feed rate, 1.5 mm depth of cut and 300°C temperature using desirability function analysis to minimize flank wear, surface roughness and chip reduction ratio in machining of Inconel 718, whereas the best optimal settings were obtained at 100 m/min cutting speed, 0.1 mm/rev feed rate, 1 mm depth of cut and 600°C temperature using principal component analysis to minimize the surface roughness, power and chip reduction coefficient in machining of Inconel 625. Similarly, the optimal setting was obtained at cutting speed 40 m/min, feed 0.15 mm/rev, depth of cut 1.5 mm and temperature at 600°C using principal component analysis to minimize the power and flank wear and maximize the material removal rate in machining of Monel 400.

Comparison of machinability of three nickel base alloys also has been studied. It was found that machining of Inconel 718 was having lower tool life in both room and high temperature compared to Inconel 625 and Monel 400. Tool life was enhanced to 160% (from 5 min to 13 min) in machining of Inconel 718, whereas for Inconel 625 enhanced to 238% (13 min to 44 min) and 107% (from 14 min to 29 min) enhanced for Monel 400 at 600˚C compared to room temperature at cutting speed 100 m/min, feed 0.13 mm/rev and depth of cut 0.5 mm machining conditions. It was observed that the maximum increase in tool life was obtained for Inconel 625 using flame heating. This technique is more suitable for Inconel 625 compared to Inconel 718 and Monel 400, when tool life is considered as machinability criteria. Similarly, maximum reduction of cutting force was observed in machining of Inconel 615 followed by Monel 400 and Inconel 718. Better surface finish was obtained in machining of Inconel 625 followed by Inconel 718 and Monel 400. Thus, the overall experimental and numerical results obtained for room and hot machining processes will pose an interesting case for machining of nickel base alloys and eventual widespread adoption of this technology in the industry.

8.3 Contribution

In the present study, conventional and hot conventional turning operation were used to analyze the forces, temperature, tool wear and tool life, surface roughness, the temperature in the cutting zone and chip morphology in experimentally. Numerical simulation was also employed to validate the parameters like cutting force, thrust force, tool wear, and chip morphology etc. The process variables which are difficult to determine experimentally

was determined in simulation like stress, and process zone temperature. Further, the machining input parameters are optimized by utilizing different optimization method.

- Heating with gas flame along with conventional turning nickel base alloys like Inconel 718, Inconel 625 and Monel 400 was investigated first time for forces, tool life, tool wear, cutting zone temperature, chip morphology etc.
- A considerable reduction of tool wear, cutting force, feed force and radial force
- Improvement of surface finish was achieved compared to conventional turning process.
- The finite element was utilized for analyzing process variables like process zone temperature, cutting forces, stress, temperature, chip tool contact length, chip morphology and tool wear in both room and elevated temperature conditions.
- Optimization methods were used to choose best input parameters for better outputs in hot turning processes.

8.4 Future work

During the research work, although some challenges were carried out successfully, but there are few issues can be resolved in order to extend the current study.

- To investigate the influence of heating on the microstructural changes of the workpiece using different theories and model.
- Use of different coated tool and performing experimental investigation in room and heating conditions.
- Analysis of residual stress in the machined surface during conventional and hot conventional turning operation.
- Study of white layer formation on the machined surface in conventional and hot conventional turning operation.
- Development of FEM model to validate the residual stress, surface finish for the machining of moderns alloys (Inconel 625 and Monel 400).
- Different non-traditional or naturally inspired algorithm can be applied to the machining processes to optimize the machining parameters.

References

[1] J. R. Davis, *Nickel, Cobalt, and Their Alloys*. *ASM international*, 2000.

[2] E. O. Ezugwu, Z. M. Wang, and A. R. Machado, "The machinability of nickel-based alloys: a review," *J. Mater. Process. Technol.*, vol. 86, pp. 1–16, 1999.

[3] S. Sikder, "Analytical model for force prediction when machining metal matrix," *Master Thesis, University of Ontario*, 2010.

[4] R. Muhammad,"Hot ultrasonically assisted turning of Ti-15V3Al3Cr3Sn: experimental and numerical analysis". *Ph.D. Thesis, Loughborough University*, 2013.

[5] N. A. Abukhshim, P. T. Mativenga, and M. A. Sheikh, "Heat generation and temperature prediction in metal cutting: A review and implications for high speed machining," *Int. J. Mach. Tools Manuf.*, vol. 46, pp. 782–800, 2006.

[6] A. O. Tay, M. G. Stevenson, G. D. V. Davis, and P. L. B. Oxley, "A numerical method for calculating temperature distributions in machining, from force and shear angle measurements," *Int. J. Mach. Tool Des. Res.*, vol. 16, pp. 335–349, 1976.

[7] T. Childs, K. Maekawa, T. Obikawa, and Y. Yamane, "Metal machining–theory and applications," *Elsevier*, London, 2000.

[8] M. Sumer, A. F. Misir, N. T. Telcioglu, A. U. Guler, and M. Yenisey, "Comparison of heat generation during implant drilling using stainless steel and ceramic drills," *J. Oral Maxillofac. Surg.*, vol. 69, pp. 1350–1354, 2011.

[9] G. Boothroyd, "Temperatures in orthogonal metal cutting," *Proc. Inst. Mech. Eng.*, vol. 177, pp. 789–810, 1963.

[10] E. O. Ezugwu, "High speed machining of aero-engine alloys," *J. Brazilian Soc. Mech. Sci. Eng.*, vol. 26, pp. 1–11, 2004.

[11] E. O. Ezugwu, "Key improvements in the machining of difficult-to-cut aerospace superalloys," *Int. J. Mach. Tools Manuf.*, vol. 45, pp. 1353–1367, 2005.

[12] R. S. Joshi and H. Singh, "An investigation on flank wear mechanism of tungsten carbide drills during conventional and modulation assisted drilling," *Mach. Sci. Technol.*, vol. 18, pp. 99–119, 2014.

[13] E. Kuljanic, M. Sortino, and G. Totis, "Machinability of difficult machining materials," *14th Int. Res. Conf.*, pp. 11–18, 2010.

[14] Z. Y. Wang, K. P. Rajurkar, J. Fan, S. Lei, Y. C. Shin, and G. Petrescu, "Hybrid machining of Inconel 718,"*Int. J. Mach. Tools Manuf.*,vol. 43, pp.1391–1396, 2003.

[15] A. A. Khan and M. I. Ahmed, "Improving tool life using cryogenic cooling," *J. Mater. Process. Technol.*, vol. 196, pp. 149–154, 2008.

[16] D. Fernández, V. García Navas, A. Sandá, and I. Bengoetxea, "Comparison of machining inconel 718 with conventional and sustainable coolant," *mmsciece*, pp. 506–510, 2014.

[17] F. Pusavec, C. Courbon, J. Rech, J. Kopac, and I. S. Jawahir, “An Investigation of the effect of nitrogen phase on cryogenic machining performance and a case study on machining of Inconel 718 Alloy,” *Asme Msec*, pp. 1–10, 2014.

[18] C. Raval,“Machining of titanium under cryogenic condirions". Ph.D Thesis, Indian Institute of Technology Kanpur.

[19] M. Ay, U. Caydas and A. Hasçal, “Optimization of micro-EDM drilling of inconel 718 superalloy,” *Int. J. Adv. Manuf. Technol*, pp. 1015–1023, 2013.

[20] G. Talla and S. Gangopadhayay, “State of the art in powder-mixed electric discharge machining : A review,” *Proc. Inst. Mech. Eng. Part B J. Eng. Manuf.*, 2016.

[21] L. Tang, C. Gao, J. Huang, H. Shen, and X. Lin, “Experimental investigation of surface integrity in finish dry hard turning of hardened tool steel at different hardness levels,” *Int. J. Adv. Manuf. Technol.*, vol. 77, pp. 1655–1669, 2015.

[22] H. Aouici, H. Bouchelaghem, M. A. Yallese, M. Elbah, and B. Fnides, “Machinability investigation in hard turning of AISI D3 cold work steel with ceramic tool using response surface methodology,” *Int. J. Adv. Manuf. Technol.*, vol. 73, pp. 1775–1788, 2014.

[23] Y. Karpat and A. Srivastava, “Hard turning with variable micro-geometry PCBN tools,”*CIRP Annals - Manufacturing Technology*, vol. 57, pp. 73–76, 2008.

[24] A. Pal, S. K. Choudhury, and S. Chinchanikar, “Machinability assessment through experimental investigation during hard and soft turning of hardened steel,” *Procedia Mater. Sci.*, vol. 6, pp. 80–91, 2014.

[25] T. Tamizharasan, T. Selvaraj, and A. N. Haq, “Analysis of tool wear and surface finish in hard turning,” *Int. J. Adv. Manuf. Technol.*, vol. 28, pp. 671–679, 2006.

[26] A. W. Warren and Y. B. Guo, “Characteristics of residual stress profiles in hard turned vs Ground surfaces with and without a white layer,” *J. Manuf. Sci. Eng*, pp. 616–623, 2009.

[27] M. Neslusan, M. Faktor, M. Cillikova, and S. Republic, “Analysis of surface integrity after hard turning”, *mmscience*, pp. 481–484, 2014.

[28] Y. B. Guo and C. R. Liu, “3D FEA modeling of hard turning,” *J. Manuf. Sci. Eng.*, *J. Manuf. Sci. Eng*, vol. 124, pp. 189, 2002.

[29] D. M. Kim, “Finite element simulation of the hard turning process with patterned tool inserts.” *Master Thesis, UNIST*, 2013

[30] C. Zhenzhen, X. Jiuhua, D. Wenfeng, and M. Changyu, “Grinding performance evaluation of porous composite-bonded CBN wheels for Inconel 718,” *Chinese J. Aeronaut.*, vol. 27, pp. 1022–1029, 2014.

[31] R. B. Pavan, G. B. Kiran, R. R. Srikant, and A. V. Gopal, “Investigations on grinding of Inconel 718 using newly developed graphene nanoplatelets impregnated grinding wheels,” *AIMTDR*, pp. 3–8, 2014.

[32] Z. Zhong, K. Ramesh, and S. H. Yeo, “Grinding of nickel-based super-alloys and advanced ceramics,” *Mater. Manuf. Process.*, vol. 16, pp. 195–207, 2001.

[33] T. Tecelli, “Simulation of grinding surface creation – A single grit approach", *University of Huddersfield repository*, 2010.

[34] P. L. Tso, “Study on the grinding of Inconel 718,” *J. Mater. Process. Tech.*, vol. 55, pp. 421–426, 1995.

[35] K. Kadirgama, M. M. Noor, H. H. Habeeb, M. M. Rahman, and B. Mohamad, “Effect of dry cutting on force and tool life when machining aerospace material,” *Ijmme*, vol. 4, pp. 93–97, 2010.

[36] L. Fusova, P. Rokicki, Z. Spotz, K. Saksl and C. Siemers, "Tool wear mechanisms in tools used for high-speed cutting of difficult- to-machine metals,” *Roznov Pod Radhostem, Czech Repulic.* EU, 2010.

[37] T. Kivak, K. Habali, and U. Seker, “The effect of cutting paramaters on the hole quality and tool wear during the drilling of inconel 718,” *Gazi Univ. J. Sci.*, vol. 25, pp. 533–540, 2012.

[38] V. Bushlya, J. Zhou, and J. E. Ståhl, “Effect of cutting conditions on machinability of superalloy inconel 718 during high speed turning with coated and uncoated PCBN tools,” *Procedia CIRP*, vol. 3, pp. 370–375, 2012.

[39] W. Akhtar, J. Sun, P. Sun, W. Chen, and Z. Saleem, “Tool wear mechanisms in the machining of nickel based super-alloys: A review,” *Front. Mech. Eng.*, vol. 9, pp. 106–119, 2014.

[40] Y. Qiao, X. Ai, and Z. Liu, “Machining performance and tool wear of coated carbide inserts in high speed turning powder metallurgy nickel-base superalloy,” *Proc. - 2010 WASE Int. Conf. Inf. Eng. ICIE 2010*, vol. 3, pp. 71–74, 2010.

[41] F. Zemzemi, J. Rech, W. B. Salem, A. Dogui, and P. Kapsa, " Identification of friction and heat partition model at the tool-chip-workpiece interfaces in dry cutting of an inconel 718 alloy with CBN and coated carbide tools", *Advances in Manufacturing science and Technology*, vol. 38. 2014.

[42] H. R. Krain, A. R. C. Sharman, and K. Ridgway, “Optimisation of tool life and productivity when end milling Inconel 718TM,” *J. Mater. Process. Technol.*, vol. 189, pp. 153–161, 2007.

[43] S. Olovsjo, A. Wretland, and G. Sjberg, “The effect of grain size and hardness of wrought alloy 718 on the wear of cemented carbide tools,” *Wear*, vol. 268, pp. 1045–1052, 2010.

[44] I. Ucun, K. Aslantas, and F. Bedir, “An experimental investigation of the effect of coating material on tool wear in micro milling of Inconel 718 super alloy,” *Wear*, vol. 300, pp. 8–19, 2013.

[45] M. J. Bermingham, S. Palanisamy, and M. S. Dargusch, “Understanding the tool wear mechanism during thermally assisted machining Ti-6Al-4V,” *Int. J. Mach. Tools Manuf.*, vol. 62, pp. 76–87, 2012.

[46] K. A. Venugopal, S. Paul, and A. B. Chattopadhyay, "Tool wear in cryogenic turning of Ti-6Al-4V alloy," *Cryogenics*, vol. 47, pp. 12–18, 2007.

[47] S. Bahi, G. List, and G. Sutter, "Analysis of adhered contacts and boundary conditions of the secondary shear zone," *Wear*, vol. 330–331, pp. 608–617, 2015.

[48] M. Armendia, A. Garay, L. M. Iriarte, and P. J. Arrazola, "Comparison of the machinabilities of Ti6Al4V and Ti-metal using uncoated WC-Co tools," *J. Mater. Process. Technol.*, vol. 210, no. 2, pp. 197–203, 2010.

[49] J. Kramar, D. and J. Kopac, "High performance manufacturing aspect of hard-to-machine materials," *conference articles*,vol. 4, pp. 3–14, 2009.

[50] E. O. Ezugwu, J. Bonney, and Y. Yamane, "An overview of the machinability of aeroengine alloys," *J. Mater. Process. Technol.*, vol. 134, pp. 233–253, 2003.

[51] H. G. Prengel, P. C. Jindal, K. H. Wendt, A. T. Santhanam, P. L. Hegde, and R. M. Penich, "A new class of high performance PVD coatings for carbide cutting tools," *Surf. Coatings Technol.*, vol. 139, pp. 25–34, 2001.

[52] I. G. Euan, E. Ozturk, and N. D. Sims, "Modeling static and dynamic cutting forces and vibrations for inserted ceramic milling tools," *Procedia CIRP*, vol. 8, pp. 564–569, 2013.

[53] M. Bakkal, A. J. Shih, and R. O. Scattergood, "Chip formation, cutting forces, and tool wear in turning of Zr-based bulk metallic glass," *Int. J. Mach. Tools Manuf.*, vol. 44, pp. 915–925, 2004.

[54] Y. Shi, C. Zhao, M. Qi, Y. Liu, and P. Deng, "Research on the cutting force of nickel-based superalloy," *Proc. - 2013 4th Int. Conf. Intell. Syst. Des. Eng. Appl. ISDEA 2013*, pp. 527–530, 2013.

[55] Y. Xi, M. Bermingham, G. Wang, and M. Dargusch, "FEA modelling of cutting force and chip formation in thermally assisted machining of Ti6Al4V Alloy," *Mater. Sci. Forum*, vol. 765, pp. 343–347, 2013.

[56] D. Zhu, X. Zhang, and H. Ding, "Tool wear characteristics in machining of nickel-based superalloys," *Int. J. Mach. Tools Manuf.*, vol. 64, pp. 60–77, 2013.

[57] B. A. Khidhir and B. Mohamed, "Study of cutting speed on surface roughness and chip formation when machining nickel-based alloy," *J. Mech. Sci. Technol.*, vol. 24, pp. 1053–1059, 2010.

[58] F. Pušavec, A. Stoić, and J. Kopač, "The role of cryogenics in machining processes," *Teh. Vjesn.*, vol. 16, pp.3-9, 2009.

[59] D. Ulutan, M. Sima, and T. Özel, "Prediction of machining induced surface integrity using elastic-viscoplastic simulations and temperature-dependent flow softening material models in titanium and nickel-based alloys," *Adv. Mater. Res.*, vol. 223, pp. 401–410, 2011.

[60] D. Jin and Z. Liu, "Effect of cutting speed on surface integrity and chip morphology in high-speed machining of PM nickel-based superalloy FGH95," *Int. J. Adv. Manuf. Technol.*, vol. 60, pp. 893–899, 2012.

[61] X. Cai, S. Qin, J. Li, Q. An, and M. Chen, “Experimental investigation on surface integrity of end milling nickel-based alloy inconel 718,” *Mach. Sci. Technol. Int. J.*, vol. 18 , pp. 37–41, 2014.

[62] R. L. Peng, J. Zhou, S. Johansson, A. Billenius, V. Bushlya, and J. Stahl, “Surface integrity and the influence of tool wear in high speed machining of inconel 718,” pp. 1–10, *Confrence article*. Linkoping University, 2013.

[63] D. Umbrello, “Investigation of surface integrity in dry machining of Inconel 718,” *Int. J. Adv. Manuf. Technol.*, vol. 69, pp. 2183–2190, 2013.

[64] R. M’Saoubi, D. Axinte, C. Herbert, M. Hardy, and P. Salmon, “Surface integrity of nickel-based alloys subjected to severe plastic deformation by abusive drilling,” *CIRP Ann. - Manuf. Technol.*, vol. 63, pp. 61–64, 2014.

[65] H. EI-Hofy, *Advanced machining processes*. CRC publication 2005.

[66] N. N. S. Chen and K. C. Lo, “Factors affecting tool life in hot machining of alloy steels,” *Int. J. Mach. Tool Des. Res.*, vol. 14, pp. 161–173, 1974.

[67] N. N. S. Chen and K. C. Lo, “Factors affecting tool life in hot machining of alloy steels,” *Int. J. Mach. Tool Des. Res.*, vol. 14, pp. 161–173, 1974.

[68] G. S. Kainth and M. N. Chaturvedi, “Theroetical investigation of temperature in hot machining,” vol. 156, pp. 241–256, 1975.

[69] K. C. Lo and N. N. S. Chen, “Prediction of tool life in hot machining of alloy steels,” *Int. J. Prod. Res.*, pp. 47–63, 1977.

[70] V. Raghuram and M. K. Muju, “Improving tool life by magnetisation in hot machining,” *Int. J. Mach. Tool Des. Res.*, vol. 20, pp. 87–96, 1980.

[71] W. Xu, X. Liu, J. Sun, and L. Zhang, “Finite element simulation and experimental research on electric hot machining,” *Int. J. Adv. Manuf. Technol.*, vol. 66, pp. 407–415, 2013.

[72] D. Ulutan, A. Pleta, and L. Mears, “Electrically-assisted machining of titanium alloy Ti-6Al-4V and nickel-based alloy IN-738: An Investigation,” *Proc. ASME 2015 Int. Manuf. Sci. Eng. Conf.*, pp. 1–5, 2015.

[73] E. A. Rahim, N. Warap, and Z. Mohid, “Thermal-assisted machining of nickel-based alloy,” *Superalloys*, pp. 3–29, 2015.

[74] M. Baili, V. Wagner, G. Dessein, J. Sallaberry, and D. Lallement, “An Experimental investigation of hot machining with induction to improve Ti-5553 machinability,” *Appl. Mech. Mater.*, vol. 62, pp. 67–76, 2011.

[75] M. I. Hossain, A. K. M. N. Amin, A. U. Patwari, and A. Karim, “Enhancement of machinability by workpiece preheating in end milling of Ti-6Al-4V,” *J. Achiev. Mater. Manuf. Eng.* vol. 31, pp. 320–326, 2008.

[76] T. L. Ginta, A. K. M. N. Amin, M. A. Lajis, A. N. M. Karim, and H. C. D. M. Radzi, “Improved tool life in end milling Ti-6Al-4V through workpiece

Preheating," *Eur. J. Sci. Res. ISSN 1450-216X Vol.27 No.3 (2009), pp.384-391*, vol. 27, pp. 384–391, 2009.

[77] M. A. Lajis, A. K. M. Nurul Amin, and A. N. M. Karim, "Surface integrity in hot machining of AISI D2 hardened steel," *Adv. Mater. Res.*, vol. 500, pp. 44–50, 2012.

[78] J. Luo, H. Ding, and A. J. Shih, "Induction-heated tool machining of elastomers—Part 2: chip morphology, cutting forces, and machined surfaces," *Mach. Sci. Technol.*, vol. 9, pp. 567–588, 2005.

[79] A. K. M. Nurul Amin and T. L. Ginta, *Heat-Assisted Machining*, vol. 11, *Comprehensive of material processing*, Elsevier, 2014.

[80] B. K. Hinds and S. M. De Almeida, "Plasma arc heating for hot machining," *Int. J. Mach. Tool Des. Res.*, vol. 21, pp. 143–152, 1981.

[81] G. Madhavulu and B. Ahmed, "Hot machining process for improved metal removal rates in turning operations," *J. Mater. Process. Technol.*, vol. 44, pp. 199–206, 1994.

[82] C. E. Leshock, J. N. Kim, and Y. C. Shin, "Plasma enhanced machining of inconel 718: Modeling of workpiece temperature with plasma heating and experimental results," *Int. J. Mach. Tools Manuf.*, vol. 41, pp. 877–897, 2001.

[83] T. Kittagawa and K. Maekawa, "Plasma hot machining for new engineering materials," *Wear*, vol. 139, pp. 251–267, 1990.

[84] L. Popa, "Complex study of plasma hot machining". *university politehnica of Bucharest* pp. 26–33, 2012.

[85] L. N. L. Lacalle, J. A. Sánchez, A. Lamikiz, and A. Celaya, "Plasma assisted milling of heat-resistant superalloys," *J. Manuf. Sci. Eng.*, vol. 126, pp. 274, 2004.

[86] J. W. Novak, Y. C. Shin, and F. P. Incropera, "Assessment of plasma enhanced machining for improved machinability of Inconel 718," *J. Manuf. Sci. Eng.*, vol. 119, pp. 125, 1997.

[87] R. Bejjani, B. Shi, H. Attia, and M. Balazinski, "Laser assisted turning of titanium metal matrix composite," *CIRP Ann. - Manuf. Technol.*, vol. 60, pp. 61–64, 2011.

[88] O. Abdulghani, M. Sobih, A. Youssef, and E. T. Al, "Modeling and simulation of laser assisted turning of hard steels," *Scienfic research publishing*, vol. pp. 106–113, 2013.

[89] P. Dumitrescu, P. Koshy, J. Stenekes, and M. A. Elbestawi, "High-power diode laser assisted hard turning of AISI D2 tool steel," *Int. J. Mach. Tools Manuf.*, vol. 46, pp. 2009–2016, 2006.

[90] R. Bejjani and M. Balazinski, "Machinability and chip formation of titanium metal matrix composites," *Technology*, vol. 13, 2011.

[91] K. Zhuang, X. Zhang, D. Zhu, and H. Ding, "Employing preheating- and cooling-assisted technologies in machining of Inconel 718 with ceramic cutting tools: towards

reducing tool wear and improving surface integrity," *Int. J. Adv. Manuf. Technol.*, vol. 80, pp. 1815–1822, 2015.

[92] D. H. Kim and C. M. Lee, "A study of cutting force and preheating-temperature prediction for laser-assisted milling of Inconel 718 and AISI 1045 steel," *Int. J. Heat Mass Transf.*, vol. 71, pp. 264–274, 2014.

[93] W. S. Woo and C. M. Lee, "A study of the machining characteristics of AISI 1045 steel and Inconel 718 with a cylindrical shape in laser-assisted milling," *Appl. Therm. Eng.*, vol. 91, pp. 33–42, 2015.

[94] S. Sun, M. Brandt, J. E. Barnes, and M. S. Dargusch, "Experimental investigation of cutting forces and tool wear during laser-assisted milling of Ti-6Al-4V alloy," *Proc. Inst. Mech. Eng. Part B J. Eng. Manuf.*, vol. 225, pp. 1512–1527, 2011.

[95] H. Ding and Y. C. Shin, "Laser-assisted machining of hardened steel parts with surface integrity analysis," *Int. J. Mach. Tools Manuf.*, vol. 50, pp. 106–114, 2010.

[96] J. Yang, S. Sun, M. Brandt, and W. Yan, "Experimental investigation and 3D finite element prediction of the heat affected zone during laser assisted machining of Ti6Al4V alloy," *J. Mater. Process. Technol.*, vol. 210, pp. 2215–2222, 2010.

[97] F. E. Pfefferkorn, F. P. Incropera, and Y. C. Shin, "Heat transfer model of semi-transparent ceramics undergoing laser-assisted machining," *Int. J. Heat Mass Transf.*, vol. 48, pp. 1999–2012, 2005.

[98] R. A. Rahman Rashid, S. Sun, G. Wang, and M. S. Dargusch, "The effect of laser power on the machinability of the Ti-6Cr-5Mo-5V-4Al beta titanium alloy during laser assisted machining," *Int. J. Mach. Tools Manuf.*, vol. 63, pp. 41–43, 2012.

[99] M. C. Anderson and Y. C. Shin, "Laser-assisted machining of an austenitic stainless steel: P550," *Proc. Inst. Mech. Eng. Part B-Journal Eng. Manuf.*, vol. 220, pp. 2055–2067, 2006.

[100] R. Muhammad, A. Maurotto, A. Roy, and V. Silberschmidt, "Hot ultrasonically assisted turning of β -Ti alloy," Loughborough university, vol.1, pp.336–341, 2012.

[101] D. K. Pal and S. K. Basu, "Hot machining of austenitic manganese steel by shaping," *Int. J. Mach. Tools Res.*, vol. 11, pp. 45–61, 1971.

[102] M. Davami and M. Zadshakoyan, "Investigation of tool temperature and surface quality in hot machining of hard-to-cut materials," *World Acad. Sci. Eng. Technol.*, vol. 46, pp. 672–676, 2008.

[103] K. P. Maity and P. K. Swain, "An experimental investigation of hot-machining to predict tool life," *J of mater. process. Technol*, vol. 8, pp. 344–349, 2007.

[104] S. K. Thandra and S. K. Choudhury, "Effect of cutting parameters on cutting force, surface finish and tool wear in hot machining," *Int. J. Mach. Mach. Mater.*, vol. 7, pp. 278, 2010.

[105] N. Tosun and L. Ozler, "Optimisation for hot turning operations with multiple performance characteristics," *Int. J. Adv. Manuf. Technol* pp. 777–782, 2004.

[106] A. M. Ravi, S. M. Murigendrappa, and P. G. Mukunda, “Experimental investigation on thermally enhanced machining of high-chrome white cast iron and to study its machinability characteristics using Taguchi method and artificial neural network,” *Int. J. Adv. Manuf. Technol.*, vol. 72, pp. 1439–1454, 2014.

[107] V. Upadhyay, P. K. Jain, and N. K. Mehta, “Machinability studies in hot Machining of Ti-6Al-4V Alloy,” *Adv. Mater. Res.*, vol.622–623, pp.361–365, 2012.

[108] N. M. Kamdar and P. V. K. Patel, “Experimental investigation of machining parameters of EN 36 steel using tungsten carbide cutting tool during hot machining,” *Int. J. Eng. Res. Appl.*, vol. 2, pp. 1833–1838, 2012.

[109] S. Ranganathan and T. Senthilvelan, “Multi-response optimization of machining parameters in hot turning using grey analysis,” *Int. J. Adv. Manuf. Technol.*, vol. 56, pp. 455–462, 2011.

[110] S. Ranganathan, T. Senthilvelan, and G. Sriram, “Evaluation of machining parameters of hot turning of stainless steel by applying ANN and RSM,” *Mater. Manuf. Process.*, vol. 25, pp. 1131–1141, 2010.

[111] N. Tosun and L. Özler, “A study of tool life in hot machining using artificial neural networks and regression analysis method,” *J. Mater. Process. Technol.*, vol. 124, pp. 99–104, 2002.

[112] R. Muhammad, N. Ahmed, A. Roy, and V. Silberschmidt, “Turning of advanced alloys with vibrating cutting tool,” vol. 188, pp. 277–284, 2012.

[113] R. Muhammad, A. Maurotto, M. Demiral, A. Roy, and V. Silberschmidt, “Thermally enhanced ultrasonically assisted machining of Ti alloy,” *CIRP J. Manuf. Sci. Technol.*, vol. 7, pp. 159–167, 2014.

[114] R. Muhammad, N. Ahmed, M. Demiral, A. Roy, and V. V. Silberschmidt, “Computational study of ultrasonically-assisted turning of Ti Alloys,” *Adv. Mater. Res.*, vol. 223, pp. 30–36, 2011.

[115] W. Grzesik, J. Rech, and T. Wanat, “Surface integrity of hardened steel parts in hybrid machining operations,” vol. 18, pp. 367–370, 2006.

[116] T. Nath and D. P. Singh, “Hybrid machining process assessment and improvement,” *conference article*, 2013.

[117] B. Lauwers, “Surface integrity in hybrid machining processes,” *Procedia Eng.*, vol. 19, pp. 241–251, 2011.

[118] D. R. Unune and H. S. Mali, “Current status and applications of hybrid micro-machining processes: A review,” *Proc. Inst. Mech. Eng. Part B J. Eng. Manuf.*, vol. 229, pp. 1681–1693, 2015.

[119] J. Kozak and K. P. Rajurkar, “Hybrid machining process evaluation and development,” *Proceedings of the 35th international MATADOR conference*, pp. 1–25, 2010.

[120] E. Rahim, N. Warap, and Z. Mohid, “Thermal assisted machining of nickel-based alloy,” Superalloy, *Intech publication*, pp. 3–30, 2015.

[121] N. Tosun and L. Ozler, "A study of tool life in hot machining using artificial neural networks and regression analysis method," *J. Mater. Process. Technol.* vol. 124, pp. 99–104, 2002.

[122] N. Tosun and L. Ozler, "Optimisation for hot turning operations with multiple performance characteristics," *Int. J. Adv. Manuf. Technol.*, vol. 23, pp. 777–782, 2004.

[123] S. Ranganathan and T. Senthilvelan, "Optimizing the process parameters on tool wear of WC insert when hot turning of AISI 316 stainless steel," *ARPN J. Eng. Appl. Sci.*, vol. 5, pp. 24–35, 2010.

[124] S. Patil, N.K. Kamble and S. S. Sarnobat, "Multi-response optimization of hot machining Process using GRA," *Indian Journal of Applied Research*, pp.3–8, 2013.

[125] N. R. Modh, G. D. Mistry, and K. B. Rathod, "An experimental investigation to optimize the process parameters of AISI 52100 steel in hot machining," *Int. J. Eng. Res. and app*, vol. 1, pp. 483–489, 2011.

[126] M. P. Jenarthanan and R. Jeyapaul, "Optimisation of machining parameters on milling of GFRP composites by desirability function analysis using Taguchi method," *Int. J. Eng. Sci. Technol.*, vol. 5, pp. 23–36, 2013.

[127] V. Kumar, V. Kumar, and K. K. Jangra, "An experimental analysis and optimization of machining rate and surface characteristics in WEDM of Monel-400 using RSM and desirability approach," *J. Ind. Eng. Int.*, vol. 11, pp. 297–307, 2015.

[128] N. Kribes, Z. Hessainia, and M. A. Yallese, "Optimisation of machining parameters in hard turning by desirability function analysis using response surface methodology," *Design and Modeling of Mechanical System-II*, 2016.

[129] S. A. Hussain, V. Pandurangadu, and K. P. Kumar, "Machinability of glass fiber reinforced plastic (GFRP) composite materials," *International Journal of Engineering, Science and Technology*, vol. 3, pp. 103–118, 2011.

[130] B. John, "Application of desirability function for optimizing the performance characteristics of carbonitrided bushes," *Int. J. Ind. Eng. Comput.*, vol. 4, pp. 305–314, 2013.

[131] I. Hanafi, F. M. Cabrera, F. Dimane, and J. T. Manzanares, "Application of particle swarm optimization for optimizing the process parameters in turning of PEEK CF30 composites," *Procedia Technol.*, vol. 22, pp. 195–202, 2016.

[132] E. Kilickap and M. Huseyinoglu, "Selection of optimum drilling parameters on burr height using response surface methodology and genetic algorithm in drilling of AISI 304 stainless steel," *Mater. Manuf. Process.*, vol. 25, pp. 1068–1076, 2010.

[133] M. . Noordin, V. . Venkatesh, S. Sharif, S. Elting, and A. Abdullah, "Application of response surface methodology in describing the performance of coated carbide tools when turning AISI 1045 steel," *J. Mater. Process. Technol.*, vol. 145, pp. 46–58, 2004.

[134] P. Thangavel, V. Selladurai, and R. Shanmugam, "Application of response surface methodology for predicting flank wear in turning operation," *Proc. Inst. Mech. Eng.*

Part B J. Eng. Manuf., vol. 220, pp. 997–1003, 2006.

[135] I. Asilturk, S. Neseli and M. A. Ince, "Optimisation of parameters affecting surface roughness of Co28Cr6Mo medical material during CNC lathe machining by using the Taguchi and RSM methods," *Measurement*, vol. 78, pp. 120–128, 2016.

[136] B. Yang and S. Lei, "Laser assisted milling of silicon nitride ceramic: a machinability study," *Int. J. Mechatronics Manuf. Syst.*, vol. 1, pp. 116–130, 2008.

[137] Y. Tian, B. Wu, M. Anderson, and Y. C. Shin, "Laser assisted milling of silicon nitride ceramics and inconel 718," *J. Manuf. Sci. Eng.*, vol. 130, no. 3 , 2008.

[138] G. Germain, J. L. Lebrun, T. Braham-Bouchnak, D. Bellett, and S. Auger, "Laser-assisted machining of Inconel 718 with carbide and ceramic inserts," *Int. J. Mater. Form.*, vol. 1, pp. 523–526, 2008.

[139] B. Shi, H. Attia, R. Vargas, and S. Tavakoli, "Numerical and experimental investigation of laser assisted machining of inconel 718," *Maching Science and. Technology*, vol. 12, no. 4, pp. 498–513, 2008.

[140] H. Attia, S. Tavakoli, R. Vargas, and V. Thomson, "Laser-assisted high-speed finish turning of superalloy Inconel 718 under dry conditions," *CIRP Ann. - Manuf. Technol.*, vol. 59, pp. 83–88, 2010.

[141] B. Shi, H. Attia, R. Vargas and S. Tavakoli, "Numerical and experimental investigation of laser-assisted machining of inconel 718," *Machining Science and Technology* , vol.12, pp. 498-513,2008.

[142] F. Pušavec and J. Kopač, "Sustainability assessment: Cryogenic machining of inconel 718," *Stroj. Vestnik/Journal Mech. Eng.*, vol. 57, pp. 637–647, 2011.

[143] R. Arunachalam, and M. A. Mannan, "Machinability of nickel-based high temperature alloys," *Machining Science and Technology*, vol.4, pp. 127–168, 2007.

[144] S. Joshi, A. Tewari, and S. S. Joshi, "Microstructural characterization of chip segmentation under different machining environments in orthogonal machining of Ti6Al4V," *J. Eng. Mater. Technol.*, vol. 137 pp. , 2015.

[145] S. Joshi, A. Tewari, and S. Joshi, "Influence of preheating on chip segmentation and microstructure in orthogonal machining of Ti6Al4V," *J. Manuf. Sci. Eng.*, vol. 135, pp. 1–11, 2014.

[146] T. Leemet, "The characterization and modeling of the dynamic behavior of hard-to-machine alloys". *EPJ web of conference*, 2012.

[147] R. Ramanujam, K. Venkatesan, V. Saxena, R. Pandey, T. Harsha, and G. Kumar, "Optimization of machining parameters using fuzzy based principal component analysis during dry turning operation of inconel 625 - A hybrid approach," *Procedia Eng.*, vol. 97, pp. 668–676, 2014.

[148] M. Lotfi, M. Jahanbakhsh, and A. Akhavan Farid, "Wear estimation of ceramic and coated carbide tools in turning of Inconel 625: 3D FE analysis," *Tribol. Int.*, vol. 99, pp. 107–116, 2016.

[149] K. Jemielniak, J. Kossakowska, and T. Urbański, "Application of wavelet transform of acoustic emission and cutting force signals for tool condition monitoring in rough turning of Inconel 625," *Proc. Inst. Mech. Eng. Part B J. Eng. Manuf.*, vol. 225, pp. 123–129, 2011.

[150] K. Jemielniak, T. Urbanski, J. Kossakowska, and S. Bombinski, "Multi-feature fusion based tool condition monitoring in rough turning of inconel 625," *Proceedings of 4th CIRP international conference of high performance cutting*, pp. 285–290, 2010.

[151] N. Kashaev, M. Horstmann, V. Ventzke, S. Riekehr, and N. Huber, "Comparative study of mechanical properties using standard and micro-specimens of base materials Inconel 625, Inconel 718 and Ti-6Al-4V," *J. Mater. Res. Technol.*, vol. 2, pp. 43–47, 2013.

[152] A. Maurotto, R. Muhammad, A. Roy, V. I. Babitsky, and V. V. Silberschmidt, "Comparing machinability of Ti-15-3-3-3 and Ni-625 alloys in UAT," *Procedia CIRP*, vol. 1, pp. 330–335, 2012.

[153] S. Dhanabalan, K. Sivakumar, C. S. Narayanan, S. Dhanabalan, K. Sivakumar, and C. S. Narayanan, "Analysis of form tolerances in electrical discharge machining process for Inconel 718 and 625 analysis of form tolerances in electrical discharge machining process for Inconel 718 and 625," *Journal of materials and manufacturing processes*, vol. 29, pp. 253-259, 2014.

[154] N. L. M. Krishna and H. P. Raju, "Acoustic emission characteristics of Inconel 718 and Inconel 625 micro finished by extrusion honing process," *International Journal of research in advent Technology*,vol. 2, pp. 81–86, 2014.

[155] S. Sarkar and S. Mitra, "Experimental investigation on die corner accuracy for wire electrical discharge machining of Monel 400 alloy" *Proceedings of the Institution of Mechanical Engineers , Part B : Journal of Engineering Manufacture* 2012.

[156] www.specialmetalswiggin.co.uk, "MONEL alloy K-500,".

[157] M. F. Zaeh, R. Wiedenmann, and R. Daub, "A thermal simulation model for laser-assisted milling," *Phys. Procedia*, vol. 5, pp. 353–362, 2010.

[158] H. Zamani, J.-P. Hermani, B. Sonderegger, and C. Sommitsch, "3D simulation and process optimization of laser assisted milling of Ti6Al4V," *Procedia CIRP*, vol. 8, pp. 75–80, 2013.

[159] G. Singh, M. Teli, A. Samanta, and R. Singh, "Finite element modeling of laser-assisted machining of AISI D2 Tool Steel," *Mater. Manuf. Process.*, vol. 28, no. 4, pp. 443–448, 2013.

[160] R. Muhammad, N. Ahmed, Y. M. Shariff, and V. Silberschmidt, "Finite element analysis of forces in drilling of Ti-Alloys at elevated temperature," *Solid State Phenom.*, vol. 188, pp. 250–255, 2012.

[161] R. Muhammad, N. Ahmed, A. Roy, and V. Silberschmidt, "Numerical modelling of vibration assisted turning of Ti-15333," *5th CIRP confrence on high performace cutting*, vol. 1, pp. 347–352, 2012.

[162] C. Z. Duan, H. Y. Yu, Y. J. Cai, and Y. Y. Li, “Finite element simulation and experiment of chip formation during high speed cutting of hardened Steel,” *Appl. Mech. Mater.*, vol. 29–32, pp. 1838–1843, 2010.

[163] P. Mottaghizadeh and M. Bagheri, “3D modeling of temperature by finite element in machining with experimental authorization,” *Int. j. of mech. aero, industrial, mechatronic and manufacturing engineering*, vol. 6, pp. 1646–1652, 2012.

[164] K. S. Woon and M. Rahman, “The effect of tool edge radius on the chip formation behavior of tool-based micromachining,” *Int. J. Adv. Manuf. Technol.*, vol. 50, no. 9–12, pp. 961–977, 2010.

[165] T. Özel, T. K. Hsu, and E. Zeren, “Effects of cutting edge geometry, workpiece hardness, feed rate and cutting speed on surface roughness and forces in finish turning of hardened AISI H13 steel,” *Int. J. Adv. Manuf. Technol.*, vol. 25, pp. 262–269, 2005.

[166] F. Ducobu, P.-J. Arrazola, E. Rivière-Lorphèvre, and E. Filippi, “Finite element prediction of the tool wear influence in Ti6Al4V machining,” *Procedia CIRP*, vol. 31, pp. 124–129, 2015.

[167] Y. C. Yen, J. Söhner, B. Lilly, and T. Altan, “Estimation of tool wear in orthogonal cutting using the finite element analysis,” *J. Mater. Process. Technol.*, vol. 146, pp. 82–91, 2004.

[168] X. Wu, L. Li, N. He, X. Hao, C. Yao, and L. Zhong, “Investigation on the ploughing force in microcutting considering the cutting edge radius,” *Int. J. Adv. Manuf. Technol.*, vol. 45, pp.1–7, 2016.

[169] J.W. Ahn, W.S. Woo, C.M. Lee, "A study on the energy efficiency of specific cutting energy in laser-assisted machining", *Appl. Therm. Eng*. vol no. 94 pp. 748–753, 2016.

[170] S. Pervaiz, I. Deiab, A. Rashid, and M. Nicolescu, “Prediction of energy consumption and environmental implications for turning operation using finite element analysis,” *Proc. Inst. Mech. Eng. Part B J. Eng. Manuf.*, pp. 1–8, 2014.

[171] S. Pervaiz, I. Deiab, and H. Kishawy, “A finite element based energy consumption analysis for machining AISI 1045 carbon steel using uncoated carbide tool,” *Adv. Mater. Process. Technol.*, vol.2, pp.83–92, 2016.

[172] J. Liu, Y. Bai, and C. Xu, “Evaluation of ductile fracture models in finite element simulation of metal cutting processes,” *J. Manuf. Sci. Eng.*, vol.136, 2013.

[173] A. B. M. Hadzley, R. Izamshah, A. S. Sarah, and M. N. Fatin, “Finite element model of machining with high pressure coolant for Ti-6Al-4V alloy,” *Procedia Eng.*, vol. 53, pp. 624–631, 2013.

[174] A. D. Prete, L. Filice, and D. Umbrello, “Numerical simulation of machining nickel-based alloys,” *Procedia CIRP*, vol. 8, pp. 540–545, 2013.

[175] G. Singh, M. Teli, A. Samanta, R. Singh, “Finite element modeling of laser-assisted machining of AISI D2 Tool Steel, *Materials and manufacturing processes*” vol. 28, pp no. 443-448, 2013.

List of Publication

1. A. K. Parida and K.P.Maity, Prediction of energy and power consumption in hot turning of Inconel-718 using DEFORM-2D, Alexandria Journal of Engineering, Elsevier, Communicated.

2. K. P. Maity andA. K. Parida, Multi-Response Optimization of Hot Machining Parameters using PCA Coupled with Taguchi Methodology, International Journal of Manufacturing Technology and Research, Nova Publisher, Communicated.

3. A. K. Parida and K.P.Maity, Study of cutting force and surface integrity in hot machining of Monel 400. International Journal of mechanical and material engineering, Springer, Communicated.

4. A. K. Parida and K.P.Maity, Experimental and Numerical Modeling of Thermal enhanced machining of Inconel 718, Engineering Science and Technology, an International Journal, Elsevier, Communicated.